1-1-2007

Investigation of crack prediction in reinforced concrete liquid containing structures

Armin Zyarishalmani
Ryerson University

INVESTIGATION OF CRACK PREDICTION IN REINFORCED CONCRETE LIQUID CONTAINING STRUCTURES

By

Armin Zyarishalmani

B.Sc., University of Tehran, Iran, 2004

A Thesis
Presented to Ryerson University
in Partial Fulfillment of the
Requirements for the Degree of
Master of Applied Science
in the Program of
Civil Engineering

Toronto, Ontario, Canada, 2007

AUTHOR'S DECLARATION

I hereby declare that I am the sole author of this thesis.

I authorize Ryerson University to lend this thesis to other institution or individuals for the purpose of scholarly research.

I further authorize Ryerson University to reproduce this thesis by photocopying or by other means, in total or in part, at the request of other institution or individuals for the purpose of scholarly research.

BORROWERS PAGE

Name	Address	Date

INVESTIGATION OF CRACK PREDICTION IN REINFORCED CONCRETE LIQUID CONTAINING STRUCTURES

Armin Zyarishalmani, Master of Applied Science, 2007

Department of Civil Engineering
Ryerson University

ABSTRACT

Cracking in liquid containing structures, if it is not properly controlled, can have serious detrimental effects on the overall system functionality. Having a consistent knowledge of concrete cracking characteristics is essential for a designer to ensure serviceability requirements of the structure. In spite of several proposed crack prediction models that have been used as the base for design codes, still a lack of certainty can be clearly felt in predicting cracking behavior of reinforced concrete. This is due to the fact that cracking is a very complex phenomenon in which numerous factors are involved, and it is always too cumbersome to take effects of all these influential aspects into account. In order to acquire more insight into this issue, a comprehensive attempt has been made both experimentally and theoretically here in this study. This research is primarily dealing with cracks that develop under monotonic increasing load which is the main cause for the formation of wide cracks among other causes such as shrinkage or temperature. In this regard, several laboratory tests were conducted on a one meter wide strip of a tank wall. These experiments covered a range of loading configuration that would enable various combinations of stresses across the reinforced concrete section. Cracking behavior and water tightness of the slab were closely monitored and reported. Fiber reinforced polymers were shown to be a suitable means of remediation in reducing water leakage or recovering structural strength. A positive role of concrete autogenous healing on water leakage was investigated during the practical test. A comparison is made between experimental results and several recent well-known crack prediction models, through which their advantages and disadvantages are revealed and discussed. Several finite element models (FEM) have been successfully built with the aid of computer program ABAQUS/6.5 to capture the post-failure stress/strain condition in concrete and

reinforcement, the results of which are perfectly matching with those obtained from experimental tests and theoretical calculations.

ACKNOWLEDGMENTS

I would like to express my sincere gratitude to my research supervisor Dr. Reza Kianoush without whom this study could not be accomplished. His persistent support and valuable suggestions have guided me through all steps from the beginning of my graduate study. My crude knowledge of the subject has learnt a lot from his wise and sophisticated understanding. I would like to thank Nidal Jaalouk for his precious help in performing physical tests in the structural lab. His kind assistance and brilliant ideas made it possible to carry out ideal experimental tests. I am also grateful to the Cement Association of Canada for their financial support of this research study and to the R.J. Watson Inc. for their free donation of the glass FRP material. My appreciation also extends to all undergraduate students who were involved in performing laboratory tests.

TABLE OF CONTENTS

LIST OF TABLES

LIST OF FIGURES

LIST OF SYMBOLS

A_{ct}	area of the concrete tension chord at any section between primary cracks
A_e	effective stretched concrete area
A_s	area of all reinforcements in the section
A_s'	area of bottom layer of reinforcements
A_{st}	area of top layer of reinforcements
a_{cr}	distance from the bar surface to the point where the crack width is calculated
b	slab section width
c	clear concrete cover
c_1	thickness of cover from tension fiber to center of closest bar
c_e	equivalent concrete cover
d	effective depth
d'	distance from the center of bottom layer of reinforcements to the compressive fiber of slab section
d^*	controlling cover distance
d_c	distance from center of bar to extreme tension fiber
E_c	modulus of elasticity of concrete
E_s	elastic modulus of steel
e	load eccentricity
f_c'	compressive strength of concrete
f_{ct}	tensile strength of concrete
f_s	stress in the steel bar
f_r	modulus of rupture of concrete
G_f^I	fracture energy which is dissipated in the formation of a crack of unit length per unit thickness
H	tank height
h	overall height of the member
I_{cr}	moment of inertia of the cracked section
I_{gt}	moment of inertia of the un-cracked section
k	compression chord depth coefficient
k_1	coefficient accounting for bar type
k_2	coefficient accounting for loading type
$l_{s,\max}$	length over which slip occurs between the steel reinforcement and the concrete
M_s	bending moment
n	modular ratio

P	eccentric load
r	tank radius
s	bar spacing
S	crack spacing
S_{rm}	average stabilized crack spacing
T	direct tensile force
T_s	tensile force in tensile reinforcement at crack section
w	crack width
w_k	characteristic crack width
x	depth of compression zone
$\bar{y}$	centroid of the cracked section
α	coefficient relating the average crack width to the design value
α_1	coefficient accounting for bond stress and bar stress relation
α_2	coefficient accounting for bond stress and load duration relation
β	ratio of distance between neutral axis and tension face to distance between neutral axis and centroid of reinforcing steel
β_1	empirical factor to assess average strain
ε_m	mean strain in the steel bar between adjacent cracks
ε_s	tensile steel strain
ε_{s2}	steel strain at location of crack under service load
ε_{sr2}	steel strain at location of crack under load that causes cracking of the effective concrete area
$\varepsilon_{s,ave}$	average strain in steel bar
ε_s'	compressive steel strain
ε_{sm}	mean tensile reinforcement strain
ε_c	concrete strain
ε_{cm}	average concrete strain within segment length
ε_{cs}	strain of concrete due to shrinkage
ρ	tensile reinforcement ratio
ρ'	bottom layer reinforcement ratio
ρ_m	modified reinforcement ratio
$\rho_{s,eff}$	effective reinforcement ratio
ρ_{te}	reinforcement ratio based on the effective area of tensile concrete
ϕ	bar diameter
ϕ_1	ratio between concrete cover and distance from neutral axis to tension face
ϕ_2	ratio between average effective concrete area around steel bar and the area of steel bar
ϕ_3	ratio between distances from neutral axis to tension face and steel bars
ψ	coefficient accounting for non-uniformity in steel strain

ψ_s	crack spacing factor
υ	coefficient accounting for bond properties of steel bars
τ_b	bond stress
γ	unit weight of material contained in tank
γ_c	unit weight of concrete
σ_{ct}	stress at the extreme tension fiber of concrete
σ_{st}	stress in tensile bars

CHAPTER 1

INTRODUCTION

1.1 Introduction

The problem of cracking in concrete stems from its low tensile strength. Whenever the tensile stress in a concrete section reaches its tensile strength crack occurs in that section. This rise in stress can happen due to numerous causes. Some of common causes of cracking are gathered in Figure 1.1. In each of these cases in order to control or prevent the occurrence of excessively wide cracks, provisions specific to that type of crack must be undertaken. Cracking in liquid containing structures (LCS) is of major importance. This is because not only it can ruin the appearance and raise aesthetic problems, but it also can degrade durability and facilitate corrosion process or even result in a serious damage to the overall serviceability with respect to liquid tightness. From all different types of cracks this study is mainly dealing with those created due to external loads, which in case of a water tank can be made by internal water pressure. One effective solution for controlling cracks that occur due to load is to provide sufficient amount of reinforcement in the concrete section. The role of reinforcement is to redistribute stresses from cracked sections to other portion of the member as a result of which the crack width will be reduced. In order for a designer to make decision on the minimum required amount of reinforcement that satisfies a certain crack width limitation, the relation between the crack width and the external load for different reinforcement ratios must be known. Since the experimental data is not always available and one specific test is not applicable to all kinds of loading conditions, the theoretical models have found their ways into engineering design procedure. Unfortunately, current available crack models are not providing a solid and unique base for predicting concrete crack width, and therefore most design codes have preferred to adopt more conservative models. This may result in heavily reinforced concrete sections which are not optimized with respect to economy and time. With the intention of providing further illumination into the subject, in this research some of widely used crack prediction models are reevaluated based on empirical data that acquired through laboratory tests. Experimental observations indicate that crack

width increases with increasing steel stress, cover thickness, and area surrounding each reinforcing bar. These factors are three main variables that are recognized and incorporated in most crack prediction models. Noting that section properties are known parameters, the accuracy of the predicted crack width which is calculated based on an authentic model lies merely on determination of stress in reinforcement. However, finding the steel stress/strain history after cracking is not always a straight forward practice and can become quite tedious at some points. Although steel stress is calculated analytically in this study for the given specimens, it is realized that this method is more cumbersome than what can be fitted into designing procedures. Additionally, not a general formulation can be applied to all loading and stress conditions and it can differ from case to case. As a result of this, a considerable attention is given to finite element modeling (FEM). Various FE models are proposed by researchers to capture highly nonlinear behavior of reinforced concrete structures and each day the importance of a nonlinear method of analysis is more acknowledged by industry. In case that an authentic FE model becomes validated based on the empirical data, it can be used to draw stress/strain history of steel which can then be used for crack width prediction.

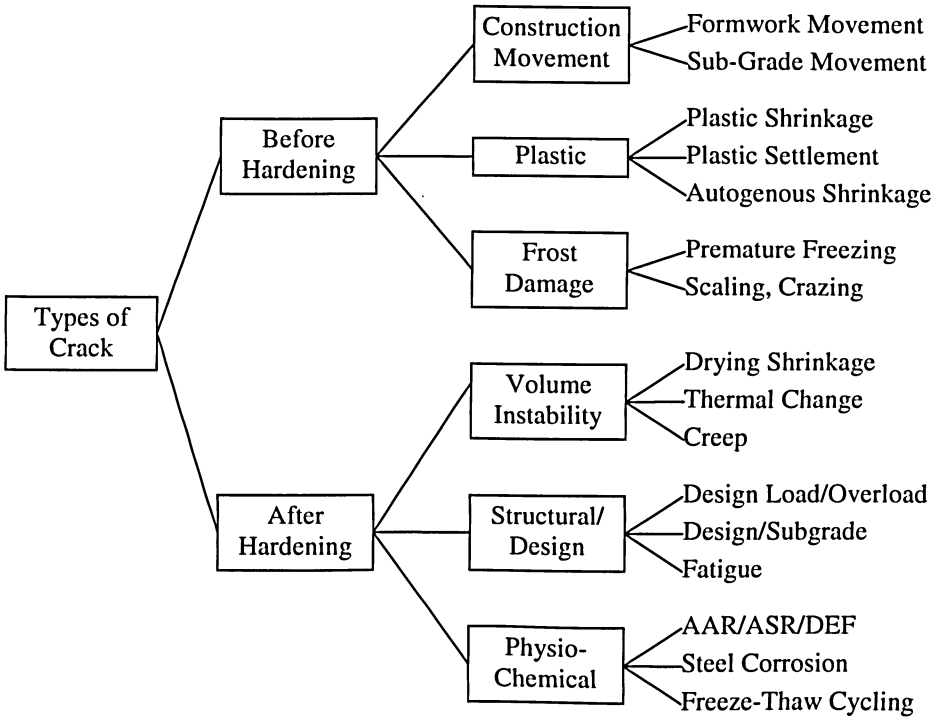

Figure 1.1 Common causes of cracking in concrete structures

1.2 Background

Cracking in reinforced concrete structures is inevitable due to the low tensile strength of concrete. Excessively wide cracks may not only destroy the aesthetics of the structure, but also weaken structure durability by exposing steel reinforcement to the environment. The maximum crack width that may be considered not to impair the appearance of a structure depends on various factors including the position, length, and surface texture of the crack as well as the illumination in the surrounding area. According to Park & Paulay (1975), crack widths in the range 0.25 to 0.38 *mm* may be acceptable for aesthetic reasons. Crack width that will not endanger the corrosion of steel reinforcement depends on the environment surrounding the structure. Table 1.1 shows the maximum allowable crack widths recommended by ACI Committee 224R (2001) for the protection of reinforcement against corrosion. These values are taken as the basis for the development of rules prescribed in ACI 318 (2002) for the distribution of tension steel to limit the crack width. According to Table 1.1, the maximum allowable crack width in water-retaining structures is 0.1 *mm*, however, it is not clear which type of crack is considered in this design guideline. Some crack width limitations are also recommended by ACI 350 (2006) specifically for flexural cracks in environmental engineering concrete structures. According to this code flexural crack widths should be limited to 0.23 *mm* (0.009 *in*) and 0.27 *mm* (0.011 *in*) for severe and normal exposure respectively.

Table 1.1 Guide to reasonable crack widths, reinforced concrete under service load (ACI 224R-01)

Exposure Condition	Crack Width	
	in.	mm
Dry air or protective membrane	0.016	0.41
Humidity, moist air, soil	0.012	0.30
Deicing chemicals	0.007	0.18
Seawater and seawater spray, wetting and drying	0.006	0.15
Water-retaining structures*	0.004	0.10

*Exclusing nonpressure pipes.

To control the crack width, designers may use the guidelines prescribed in various building codes. These guidelines are based on certain crack width prediction formulas

developed by various researchers. Inspection of crack width prediction procedures proposed by various investigators indicates that each formula contains a different set of variables. A literature review also suggests that there is no general agreement among various investigators on the relative significance of different variables affecting the crack width, despite the large number of experimental work carried out during the past few decades. This is at least partly due to the differences in the variables incorporated by different investigators in their experimental work. Taking all the parameters into account in a single experimental program is not normally feasible due to the large number of variables involved, and the interdependency of some of the variables. Analytical methods, on the other hand, can incorporate most of the variables without much difficulty. However, a literature search reveals that different investigators have concentrated on different sets of parameters in their calculation, to simplify the complex phenomenon of cracking in reinforced concrete.

1.2.1 Crack Width and Spacing Prediction Models

The development of crack spacing and crack width prediction formulas is usually based on calculated concrete stress distributions within the tensile zone of a member. Different investigators have used various simplified analytical procedures to determine the concrete tensile stress. While some analytical investigations are coupled with experimental works to verify the new prediction formulas, there are some investigations totally based on test results. In most investigations, a uniaxial tension member has been used to simulate the conditions around steel bars in the constant moment region of a member. In experimental investigations, a concrete prism with a steel bar embedded along its axis is subjected to a tensile force applied to the two protruding ends of the bar. The resulting tensile cracks are considered to represent flexural cracks in a constant moment region of a beam. In analytical investigations the axial tensile stress distribution, developed in the concrete prism resulting from the bond force transferred from the steel bar, is calculated. This stress distribution is then used to predict the formation of new cracks in between existing cracks. Important aspects of these investigations and the resulting prediction formulas are discussed below.

Chi & Kirstein method

Cylindrical uniaxial tension members were analyzed by Chi & Kirstein (1958) to determine the concrete tensile stresses within the member. The resulting average crack width was calculated as the extension of steel bar between the two ends of the member, neglecting the concrete extension. The calculated spacing and width of cracks were found to depend on the diameter of concrete cylinder analyzed. A cylinder diameter of 4 times the bar diameter was used in the development of the following prediction formulas.

$$S_{\min} = 5\lambda\phi \tag{1.1}$$

$$w_{s,ave} = \frac{5\lambda\phi}{E_s}\left(f_s - \frac{438}{\lambda\phi}\right) \tag{1.2}$$

where $S_{\min}$ = minimum crack spacing (*mm*); $w_{s,ave}$ = average crack width at the level of reinforcement (*mm*); E_s = elastic modulus of steel (*MPa*); f_s = stress in the steel bar (*MPa*); and ϕ = bar diameter (*mm*). In the above equation the coefficient λ relates to the ratio of the assumed effective concrete area in tension to the area of a single bar, which was found to vary between 0.786 and 1 for the 16 members analyzed.

Broms method

A slightly different approach was used by Broms (1965) to calculate the tensile stresses developed in concrete due to bond forces. Results of the elastic analysis have shown that high longitudinal tensile stresses are developed in the concrete within a circle inscribed between the two adjacent flexural cracks, with its centre located at reinforcement level. Broms used these findings to argue that a new crack will be formed at mid way between adjacent cracks only if the crack spacing is larger than twice the concrete cover measured from the center of the steel bar. Results of 10 beams tested by Broms have shown that the average crack spacing was close to twice the concrete cover for steel stresses ranging from 140 to 205 *MPa*. This value of the average crack spacing was multiplied by the average strain in steel bar to predict the average crack width. Thus, for steel stresses

ranging from 140 to 205 *MPa* the average crack width at the tension face of members reinforced with a single bar was expressed as:

$$w_{t,ave} = 2c_1\varepsilon_{s,ave} \tag{1.3}$$

where $w_{t,ave}$ = average crack width at the tension face; c_1 = thickness of cover from tension fiber to center of closest bar; and $\varepsilon_{s,ave}$ = average strain in steel bar.

Broms & Lutz method

To investigate the applicability of above findings to members with multiple bars, Broms & Lutz (1965) carried out uniaxial tensile tests on seven concrete specimens reinforced with four steel bars symmetrically placed within the cross section. Test results have shown that the relationships derived for members with a single bar are also applicable to members with multiple bars if the concrete cover c in Eq. 1.3 is replaced by an equivalent concrete cover c_e. Assuming that the maximum crack width is twice the average crack width, the following equation was proposed to calculate the maximum crack width for steel stresses from 140 to 205 *MPa*.

$$w_{\max} = 4c_e\varepsilon_{s,ave} \tag{1.4}$$

$$c_e = d_c\sqrt{1+\left(\frac{s}{4d_c}\right)^2} \tag{1.5}$$

where $w_{\max}$ = maximum crack width; c_e = equivalent concrete cover; d_c = distance from center of bar to extreme tension fiber; and s = bar spacing.

Venkateswarlu & Gesund method

Venkateswarlu & Gesund (1972) analyzed the portion of a beam between two successive cracks using a two-dimensional finite element method to evaluate the effects of bond force. Results have shown that the maximum concrete tensile stress across any section between the cracks occurs at reinforcement level. This maximum stress varied along the

length of the bar, with the peak value occurring at the mid-section between the two cracks. Maximum crack spacing was evaluated by comparing the calculated maximum tensile stress and tensile strength of concrete. The maximum crack width at reinforcement level was calculated as the relative difference in extensions of steel and concrete for the length between the two cracks. The following formulas were proposed to calculate the spacing and width of cracks.

$$S_{\max} = \frac{14.5\phi}{1+n\rho_m} \tag{1.6}$$

$$w_{t,\max} = \frac{2.4\times10^{-5}\phi(1462-f_s)f_s}{(1+n\rho_m)(662-f_s)} \tag{1.7}$$

where $S_{\max}$ = maximum crack spacing; $n = E_s/E_c$ = modular ratio in which E_s and E_c are the elastic moduli of steel and concrete respectively, and ρ_m = modified reinforcement ratio, which relates to the concrete cover. $w_{t,\max}$ and ϕ are in millimeters and f_s is in *MPa*.

Bazant & Oh method

Bazant & Oh (1983) carried out a theoretical study on the spacing and width of cracks, using the energy criterion of fracture mechanics as well as the strength criterion. The study suggested that the crack spacing depends mainly on the axial strain of steel bars, bar spacing, bar diameter, fracture energy of concrete and its elastic modulus. Based on the study, Oh & Kang (1987) proposed the following equations for the prediction of average crack spacing and maximum crack width in reinforced concrete members.

$$\frac{S_{ave}}{\phi} = 25.7(\phi_1)^{4.5} + 1.66(\phi_2)^{1/3} + \frac{0.236\times10^{-6}}{\varepsilon_s^2} \tag{1.8}$$

$$\frac{w_{t,\max}}{\phi} = \left[159(\phi_1)^{4.5} + 2.83(\phi_2)^{1/3}\right](\varepsilon_s - 0.0002)\phi_3 \tag{1.9}$$

where ε_s = steel strain; ϕ_1 = ratio between concrete cover and distance from neutral axis to tension face; ϕ_2 = ratio between average effective concrete area around steel bar and the area of steel bar; and ϕ_3 = ratio between distances from neutral axis to tension face and steel bars.

Beeby method

A theoretical investigation into the cracking of reinforced concrete members was carried out by Beeby (1970, 1971). A simplified version of his proposed formula for the crack width in a flexural member is as follow:

$$w = \frac{3a_{cr}\varepsilon_m}{\left(1+2\frac{(a_{cr}-c)}{(h-x)}\right)} \tag{1.10}$$

where a_{cr} = distance from the bar surface to the point where the crack width is calculated; ε_m = mean strain in the steel bar between adjacent cracks; h = overall height of the member; and x = depth of compression zone.

The above equation has been recommended in BS 8110 : Part 1 (1997) for the calculation of crack width in flexural members.

Watstein, Parsons & Clark method

Watstein & Parsons (1943) carried out uniaxial tensile tests on axially reinforced concrete cylinders to investigate the formation of cracks. Based on the results, an expression was developed to predict the average crack width of a tension member. To make this prediction procedure applicable to flexural members, Clark (1956) modified two coefficients of the expression based on test results of 56 beams and one-way slabs. Assuming a value of modular ratio n = 8, the following formula was proposed by Clark (1956):

$$w_{t,ave} = 1.29\times10^{-6}\left(\frac{h-d}{d}\right)\frac{\phi}{\rho}\left[2.56f_s - \left(\frac{1}{\rho}+8\right)\right] \tag{1.11}$$

where d = effective depth (mm). h and ϕ are in millimeters and f_s is in MPa.

Kaar & Mattock method

Based on test results of 48 beams, Kaar & Mattock (1963) developed the following equation to predict the maximum crack width:

$$w_{s,\max} = 1.57\times10^{-5} f_s \sqrt[4]{A_e} \tag{1.12}$$

where $w_{s,\max}$ = maximum crack width at reinforcement level (mm); and A_e = effective stretched concrete area (area of concrete symmetric with reinforcing steel divided by number of bars) (mm^2).

Gergely & Lutz method

Gergely & Lutz (1968) proposed a crack width prediction formula based on a computer statistical analysis of a large number of test results from different sources. A simplified version of this equation is

$$w_{t,\max} = 0.011\beta f_s \sqrt[3]{cA_e}\times10^{-3} \tag{1.13}$$

in which β = ratio of distance between neutral axis and tension face to distance between neutral axis and centroid of reinforcing steel (taken as approximately 1.20 for typical beams in buildings). $w_{t,\max}$ and c are in mm, A_e is in mm^2 and f_s is in MPa.

The above equation has been used by ACI 318 (1995) in prescribing the rules for the distribution of tension reinforcement for controlling the crack width.

Lan & Ding method

Lan and Ding (1992) developed an equation to predict the maximum crack spacing based on test results of a large number of reinforced concrete flexural members. Maximum crack spacing was then multiplied by the steel strain ε_s at the cracked section, together with two other coefficients to evaluate the maximum crack width. These two coefficients ψ and υ represent the non-uniformity in steel strain and the bond properties of steel bars, respectively. The proposed prediction formula for the average crack spacing and maximum crack width are as follows:

$$S_{ave} = (2.7c + 0.11\phi/\rho_{te})\upsilon \tag{1.14}$$

$$w_{t,\max} = 1.41 S_{ave}\varepsilon_s\psi \tag{1.15}$$

where ρ_{te} = reinforcement ratio based on the effective area of tensile concrete.

Chowdhury & Loo method

Based on test results of 18 reinforced and 12 partially prestressed concrete beams, Chowdhury & Loo (2001) developed an equation for predicting the average crack spacing in terms of the concrete cover, bar spacing, bar diameter and the reinforcement ratio. The average crack spacing was then multiplied by the steel strain at the cracked section to determine the average crack width. The resulting maximum crack width was taken as 1.5 times the average crack width. The proposed formulas are as follows:

$$S_{ave} = 0.6(c - s) + 0.1(\phi/\rho) \tag{1.16}$$

$$w_{t,\max} = 1.5\varepsilon_s S_{ave} \tag{1.17}$$

in which c = clear concrete cover.

Frosch method

According to the physical model proposed by Frosch (1999), the crack width at the level of reinforcement can be calculated as follows:

$$S_c = \psi_s d^* \tag{1.18}$$

$$w_s = \varepsilon_s S_c \tag{1.19}$$

where S_c = crack spacing; d^* = controlling cover distance; and ψ_s = crack spacing factor: 1.0 for minimum crack spacing; 1.5 for average crack spacing; and 2.0 for maximum crack spacing.

In order to estimate the crack width at the tension face of the section the value of Eq. 1.19 must be multiplied by the same β that is used in Eq. 1.13. Crack control in ACI 318 (2002) is achieved through the spacing criterion for reinforcing steel which is drawn based on the Eq. 1.19.

Gilbert method

Gilbert (2005) proposed an analytical model to predict the width of flexural cracks. His model was based on the tension chord model developed by Marti et al. (1998). He considered a reduced value of bond stress for higher reinforcement stresses to extract the following formulation:

$$w_i = \frac{S}{E_s}\left[\frac{T_s}{A_{st}} - \frac{\tau_b S}{\phi}(1 + n\rho_{te})\right] \tag{1.20}$$

where w_i = instantaneous crack width; T_s = tensile force in tensile reinforcement at crack section; A_{st} = area of tensile reinforcement; and τ_b = bond stress.

This model is explained in more detail in Chapter 3. Gilbert also proposed a model for predicting long-term crack width. He stated that the bond stress decreases with time, probably as a result of shrinkage induced slip and tensile creep. As a result of this, stress in concrete between cracks, and hence, the concrete elongation reduces. By taking into account the effect of this, as well as, concrete shortening between cracks due to shrinkage itself, the resultant crack width increases over time.

1.2.2 Finite Element Models for RC Structures

The earliest publication on the application of the finite element method on the analysis of RC structures was presented by Ngo and Scordelis (1967). In their study, simple beams were analyzed with a model in which concrete and reinforcing steel were represented by constant strain triangular elements, and a special bond link element was used to connect the steel to the concrete which describe the bond-slip effect. A linear elastic analysis was performed on beams with predefined crack patterns to determine principal stresses in concrete, stresses in steel reinforcement and bond stresses. Scordelis et al. (1974) used the same approach to study the effect of shear in beams with diagonal tension cracks and accounted for the effect of stirrups, dowel shear, aggregate interlock and horizontal splitting along the reinforcing bars near the support.

Nilson (1972) introduced nonlinear material properties for concrete and steel and a nonlinear bond-slip relationship into the analysis and used an incremental load method of nonlinear analysis. Cracking was accounted for by stopping the solution when an element reached the tensile strength, and reloading incrementally after redefining a new cracked structure. Franklin (1970) advanced the capabilities of the analytical method by developing a nonlinear analysis which automatically accounted for cracking within finite elements and the redistribution of stresses in the structure. This made it possible to trace the response of two dimensional systems from initial loading to failure in one continuous analysis. Incremental loading with iterations within each increment was used to account for cracking in the finite elements and for the nonlinear material behavior.

Plane stress elements were used by numerous investigators to study the behavior of reinforced concrete frame and wall systems. Nayak and Zienkiewicz (1972) conducted two dimensional stress studies which include the tensile cracking and the elasto-plastic behavior of concrete in compression using an initial stress approach. Cervenka (1970) analyzed shear walls and spandrel beams using an initial stress approach in which the elastic stiffness matrix at the beginning of the entire analysis is used in all iterations.

Cervenka proposed a constitutive relationship for the composite concrete-steel material through the un-cracked, cracked and plastic stages of behavior.

For the analysis of RC beams with material and geometric nonlinearities, Rajagopal (1976) developed a layered rectangular plate element with axial and bending stiffness in which concrete was treated as an orthotropic material. Selna (1969) analyzed beams and frames made up of one-dimensional elements with layered cross sections which accounted for progressive cracking and changing material properties through the depth of the cross section as a function of load and time. Significant advances and extensions of the finite element analysis of reinforced concrete beams and frames to include the effects of heat transfer due to fire, as well as the time-dependent effects of creep and shrinkage, were made by Becker and Bresler (1974).

Two basically different approaches have been used so far for the analysis of RC slabs by the finite element method: the modified stiffness approach and the layer approach. The former is based on an average moment-curvature relationship which reflects the various stages of material behavior, while the latter subdivides the finite element into imaginary concrete and steel layers with idealized stress-strain relations for concrete and reinforcing steel.

Experimental and analytical studies of RC slabs were conducted by Joffriet and McNeice (1971). The analyses were based on a bilinear moment-curvature relation which was derived from an empirically determined effective moment of inertia of the cracked slab section including the effect of tension stiffening. The change in bending stiffness of the elements due to cracking normal to the principal moment direction is accounted for by reducing the flexural stiffness of the corresponding element. Dotroppe et al. (1973) used a layered finite element procedure in which slab elements were divided into layers to account for the progressive cracking through the slab thickness. Scanlon and Murray (1974) have developed a method of incorporating both cracking and time-dependent effects of creep and shrinkage in slabs. They used layered rectangular slab elements which could be cracked progressively layer by layer, and assumed that cracks propagate

only parallel and perpendicular to orthogonal reinforcement. Lin and Scordelis (1975) utilized layered triangular finite elements in RC shell analysis and included the coupling between membrane and bending effects, as well as the tension stiffening effect of concrete between cracks in the model. Bresler and Bertero (1968) used an axisymmetric model to study the stress distribution in a cylindrical concrete specimen reinforced with a single plain reinforcing bar. The specimen was loaded by applying tensile loads at the ends of the bar.

In one of the pioneering early studies, Rashid (1968) introduced the concept of a "smeared" crack in the study of the axisymmetric response of prestressed concrete reactor structures. Rashid took into account cracking and the effects of temperature, creep and load history in his analyses. Today the smeared crack approach of modeling the cracking behavior of concrete is almost exclusively used by investigators in the nonlinear analysis of RC structures, since its implementation in a finite element analysis program is more straightforward than that of the discrete crack model. Computer time considerations also favor the smeared crack model in analyses which are concerned with the global response of structures. At the same time the concerted effort of many investigators in the last 20 years has removed many of the limitations of the smeared crack model.

Gilbert and Warner (1978) used the smeared crack model and investigated the effect of the slope of the descending branch of the concrete stress-strain relation on the behavior of RC slabs. They were among the first to point out that analytical results of the response of reinforced concrete structures are greatly influenced by the size of the finite element mesh and by the amount of tension stiffening of concrete. Several studies followed which corroborated these findings and showed the effect of mesh size and tension stiffening on the accuracy of finite element analyses of RC structures with the smeared crack model. In order to better account for the tension stiffening effect of concrete between cracks some investigators have artificially increased the stiffness of reinforcing steel by modifying its stress-strain relationship. Others have chosen to modify the tensile stress-strain curve of concrete by including a descending post-peak branch.

In the context of the smeared crack model, two different representations have emerged: the fixed crack and the rotating crack model. In the fixed crack model a crack forms perpendicular to the principal tensile stress direction when the principal stress exceeds the concrete tensile strength and the crack orientation does not change during subsequent loading. The ease of formulating and implementing this model has led to its wide-spread used in early studies. Subsequent studies, however, showed that the model is associated with numerical problems caused by the singularity of the material stiffness matrix. Moreover, the crack pattern predicted by the finite element analysis often shows considerable deviations from that observed in experiments.

The problems of the fixed crack model can be overcome by introducing a cracked shear modulus, which eliminates most numerical difficulties of the model and considerably improves the accuracy of the crack pattern predictions. The results do not seem to be very sensitive to the value of the cracked shear modulus (Barzegar and Schnobrich 1986), as long as a value which is greater than zero is used, so as to eliminate the singularity of the material stiffness matrix and the associated numerical instability. Some recent models use a variable cracked shear modulus to represent the change in shear stiffness, as the principal stresses in the concrete vary from tension to compression.

In the rotating crack model proposed by Cope et al. (1980) the crack direction is not fixed during the subsequent load history. Several tests by Vecchio and Collins (1982) have shown that the crack orientation changes with loading history and that the response of the specimen depends on the current rather than the original crack direction. In the rotating crack model the crack direction is kept perpendicular to the direction of principal tensile strain and, consequently, no shear strain occurs in the crack plane. This eliminates the need for a cracked shear modulus. A disadvantage of this approach is the difficulty of correlating the analytical results with experimental fracture mechanics research, which is at odds with the rotating crack concept. This model has, nonetheless, been successfully used in analytical studies of RC structures whose purpose is to study the global structural behavior, rather than the local effects in the vicinity of a crack.

While the response of lightly reinforced beams in bending is very sensitive to the effect of tension stiffening of concrete, the response of RC structures in which shear plays an important role, such as over-reinforced beams and shear walls, is much more affected by the bond-slip of reinforcing steel than the tension stiffening of concrete. To account for the bond-slip of reinforcing steel two different approaches are common in the finite element analysis of RC structures. The first approach makes use of the bond link element proposed by Ngo and Scordelis (1967). This element connects a node of a concrete finite element with a node of an adjacent steel element. The link element has no physical dimensions, i.e. the two connected nodes have the same coordinates.

The second approach makes use of the bond-zone element developed by de Groot et al. (1981). In this element the behavior of the contact surface between steel and concrete and of the concrete in the immediate vicinity of the reinforcing bar is described by a material law which considers the special properties of the bond zone. The contact element provides a continuous connection between reinforcing steel and concrete, if a linear or higher order displacement field is used in the discretization scheme. A simpler but similar element was proposed by Keuser and Mehlhorn (1987), who showed that the bond link element cannot represent adequately the stiffness of the steel-concrete interface.

Even though many studies of the bond stress-slip relationship between reinforcing steel and concrete have been conducted, considerable uncertainty about this complex phenomenon still exists, because of the many parameters which are involved. As a result, most finite element studies of RC structures do not account for bond-slip of reinforcing steel and many researchers express the opinion that this effect is included in the tension-stiffening model.

Very little work has been done, so far, on the three-dimensional behavior of reinforced concrete systems using solid finite elements, because of the computational effort involved and the lack of knowledge of the material behavior of concrete under three-dimensional stress states. Suidan and Schnobrich (1973) were the first to study the behavior of beams with 20-node three-dimensional isoparametric finite elements. The behavior of concrete

in compression was assumed elasto-plastic based on the von-Mises yield criterion. A coarse finite element mesh was used in these analyses for cost reasons.

1.3 Objectives

This study is dedicated to provide more insight into cracking behavior of reinforced concrete and its significance in liquid containing structures. A particular attention is given to the assessment of current code's design guidelines regarding the crack control. Several primary goals of this research can be pointed out as follows:

- To gain a better understanding of the concrete cracking behavior under different combination of stresses through several experimental investigations.
- To investigate the problem of leakage in a simulated tank wall cracked under different loading configurations.
- To evaluate the application of glass fiber reinforced polymers (FRP) in remediation of cracked RC structures with intention of both recovering strength and reducing leakage.
- To evaluate the role of concrete self healing process commonly known as autogenous healing in reducing water leakage.
- To assess the accuracy of several proposed crack width prediction models by comparing their results with those collected from experimental data.
- To develop a reliable reinforced concrete FE model with the aid of a computer program ABAQUS/6.5 (Hibbitt et al., 2004) and validate it by comparing the model responses with experimental observations.

1.4 Organization

The entire work of this thesis is presented in five chapters. An introduction to the subject of this research study is given in Chapter 1. A comprehensive literature review on previously proposed crack and FE models is provided in Background section of Chapter 1. Also explained in this chapter are the objectives sought throughout this study.

All experimental tests performed during experimental investigation phase of this research work are reported in Chapter 2. These tests consist of four different loading configurations. The application of glass FRP in remediation of cracked members is examined and explained in direct tension and high eccentricity tests. Also a phenomenon known as autogenous healing in concrete is discussed in the third phase of direct tension test. At the end of Chapter 2 the overall results obtained from experiments are used to make a recommendation for controlling the maximum probable crack width.

Chapter 3 is mainly concentrating on the analytical calculation of crack width and crack spacing. The results of various crack prediction models are compared with each other and with experimental observations as well. A design guide is recommended based on the results of the most appropriate models.

Several FE models are introduced in Chapter 4 to capture the post-cracking behavior of reinforced concrete. The performance of these models is examined by making comparison with experimental results and analytical calculations. Finally, all materials presented in this thesis are summarized in Chapter 5. The main conclusions reached in this study are highlighted and some suggestions are recommended for future research.

CHAPTER 2

CONCRETE CRACKING EXPERIMENTAL INVESTIGATION

2.1 General

Since the invention of reinforced concrete, the applications of this composite material have grown extensively. Nowadays, reinforced concrete has become the most attractive material choice for civil and architectural engineers. This composite material has multiple advantages against any other construction material, some of which are ideal design versatility, excellent shape flexibility, environmentally friendly production, high compressive strength, less producing cost, adequate durability in moisturized area, etc. Numerous dramatic improvements and progresses in engineering structures could not be made without the use of this efficient material. Larger capacity circular water tanks, nuclear power plants, bridge decks and piers, eye-catching skyscrapers, tall communication towers, tunnels, etc. are some instances that verify the excellent performance and adaptability of this composite material. Despite its wide range of applications, reinforced concrete has its own flaws and deficiencies. Although it is very efficient in compression, concrete is very weak in tension. Cracking is an undesirable phenomenon that occurs due to this fact. Cracks are undesirable in a sense that they can facilitate corrosion process in reinforcements, which in turn can affect durability. They also may result in gas or liquid seepage into or out of the system which in both cases it can be hazardous or disapproving. The structures that engage liquid preservation, transmission or obstruction are more vulnerable to adverse effects of crack formation. In these types of structures any water tightness defect may result in a serious failure of the entire system functionality. According to the available relevant research sources, the need of a more in-depth investigation is felt to address the cracking issue. Although, several attempts have been made by others toward crack prediction and control, still the argument has remained questionable. Therefore, a number of empirical investigations pertaining cracking behavior of reinforced concrete under monotonic increasing load and its correlation with water leakage are performed in this study in hopes of acquiring further knowledge of the subject. The outcome of this investigation can be used as a base

to evaluate the current codes requirements for crack control. In all tests, the practical aspects were given a particular attention without compromising the theoretical aspects. Therefore, all specimens were designed in scale and pattern comparable to the real structure. In this project, four different load settings were considered to enable the stress conditions similar to that exist in the actual structure. In the following, all tests are described individually and their results are presented and discussed.

2.2 Direct Tension

There are some occasions in which reinforced concrete section is under purely tensile force. For instance, a vertical section of a circular tank must carry the tensile ring force produced by internal pressure. Members such as floor and roof slabs, walls and tunnel linings may also be subjected to direct tension as a result of the restraint of volume change. In these situations crack formation in concrete appears to be an inevitable fact, however, in order to ensure an adequate durability and functionality of the structure the crack width must be kept in a certain limit. This can be achieved in various ways, the main of which is providing sufficient reinforcement throughout the section. In a simple manner, reinforcement is binding the concrete together. By redistributing stresses from cracked sections to adjacent areas, reinforcement induces several narrow cracks instead of few wide cracks. In addition to the reinforcement ratio, its layout across the section can be quite influential. For instance, for the same reinforcement cross sectional area, using higher number of thin reinforcements will result in a better distribution of stresses throughout the section, and hence a narrower crack will form. Furthermore, the bonding condition between reinforcement and concrete is of a major importance, considering that an excessive bond slip may result in an unduly increased crack width.

Creating a purely tensile stress condition throughout the reinforced concrete section is always a challenging task. Besides, equipments available in the structural lab stipulate a particular design of specimen that perfectly makes the use of existing tools. Figure 2.1 shows the schematic of the specimen built for direct tension test. This element simulated a one meter wide horizontal strip of a tank wall. Hydraulic jacks placed on both sides of

specimen were exerting equal expanding forces to the adjacent I-beam and through the steel rod to the other I-beam. This set-up would enable a uniform level of tensile stresses all across the length of slab. The specimen was placed on rolling pipes at both ends to provide a completely free to slide condition. The primary intention of this test was to obtain a relation between tensile load and the maximum crack width. In addition to that, water leakage could be examined by exposing a major crack to water pressure and monitoring water flow across the crack at different loading levels. Direct tensile cracks are through cracks that can grow in full depth of the section and must be taken more seriously than other types of cracks. ACI 224R (2001) has limited the allowable crack width to 0.1 *mm* for water-retaining structures, however, nothing has been mentioned about the type of crack.

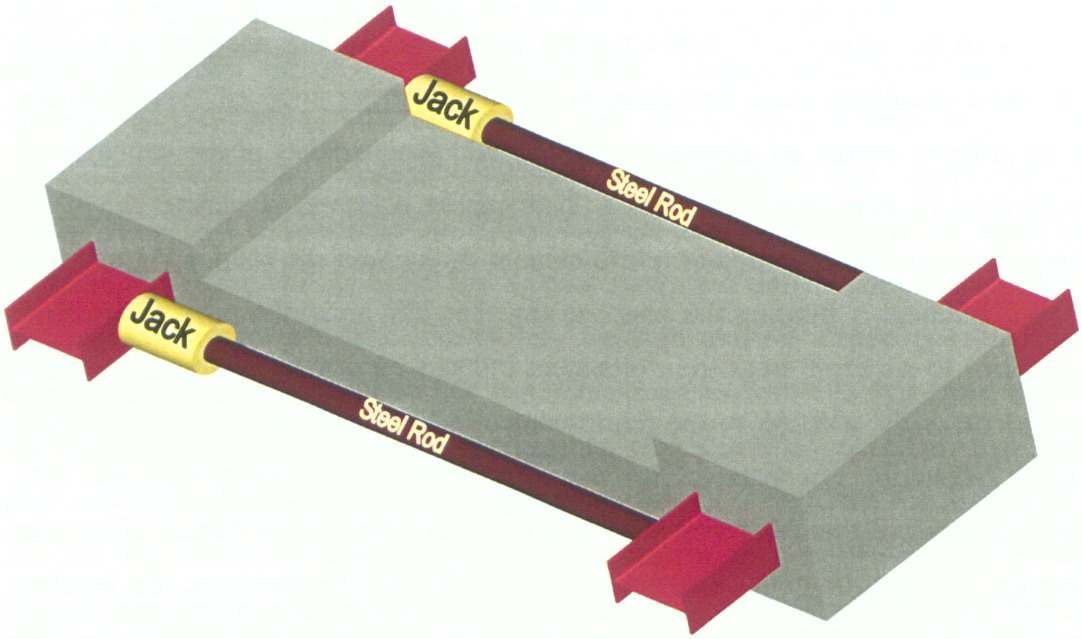

Figure 2.1 Direct tension specimen and hydraulic jacks configuration

Reinforcement layout and the location of strain gauges are shown in Figure 2.2. A longitudinal reinforcement ratio of 0.96% was provided by 8 No.20 bars which were tied and hold in place by 6 No.15 stirrups. All reinforcing bars were Grade 400 steel conforming to Canadian Standards Association (CSA) standards with yield stress of 400 *MPa* and modulus of elasticity of 200 *GPa*. Two ends of the slab were made more rigid by means of extra ties and larger slab thickness to ensure a perfect bond and load

transmission between I-beams and the middle part of the slab. In this fashion, all cracks were expected to develop in the thin middle portion of the slab. As it can be seen in Figure 2.2 ten strain sensors were distributed evenly between longitudinal bars. These sensors are coded and their corresponding numbers are also shown in Figure 2.2. These numbers will be specified on each of diagrams drawn based on the collected data from that specific strain sensor. The use of strain sensors is essential in order to obtain stress/strain history of reinforcements which has been proved to have a close link with the crack width. Always, there are some potential for errors in the strain readings whether due to imperfect installation or improper physical calibration. Even though a careful attempt was taken to perform as perfect as possible installation of sensors, still some of strain readings were not showing a reasonable accuracy and were eliminated from final report based on engineering judgment. Longitudinal reinforcements were completely fixed into I-beams to provide a complete coherence and unity of the entire structure.

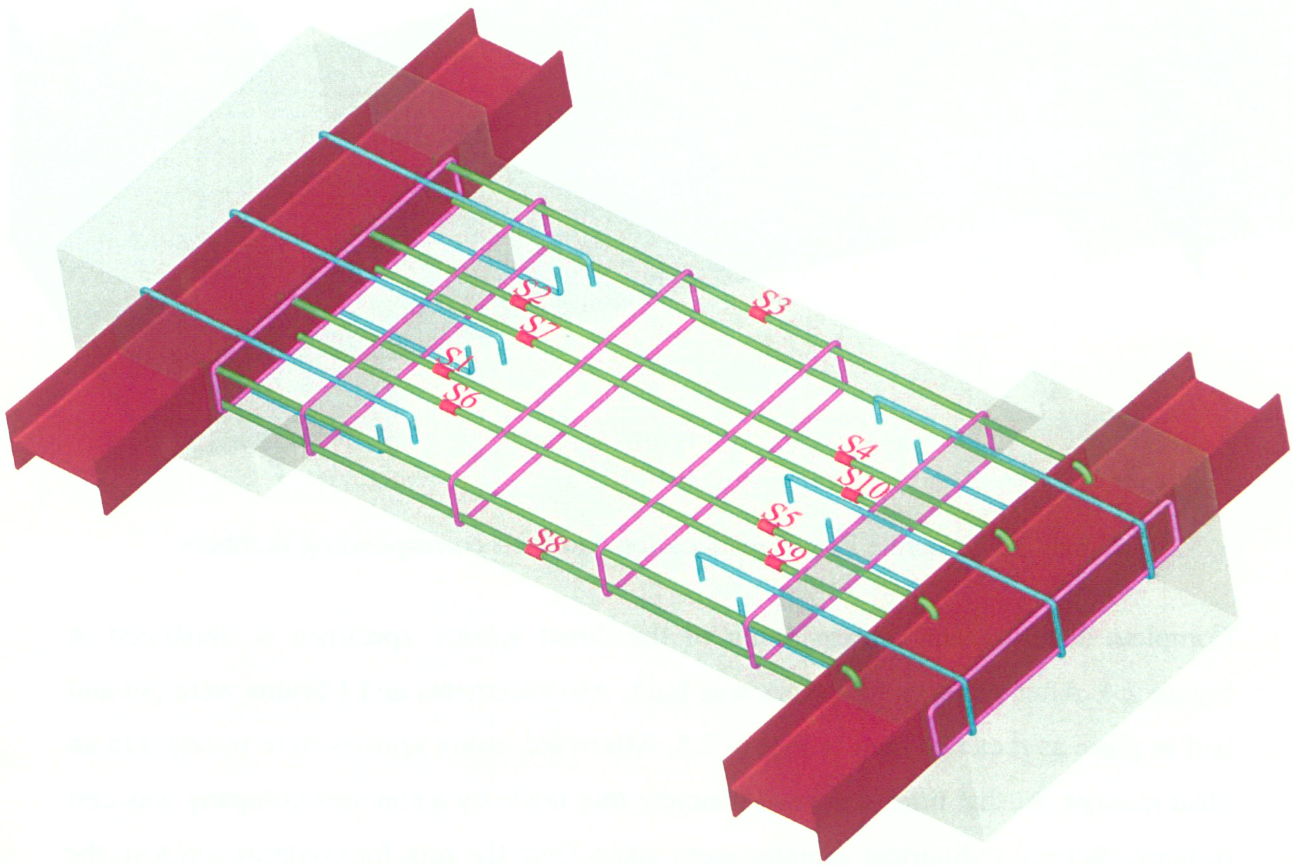

Figure 2.2 Reinforcement layout in direct tension specimen, strain sensors location and their corresponding numbers

Six concrete PI-gauges were installed on the concrete surface as shown in Figure 2.3. They were attached to both top and bottom faces of the concrete slab, and were carefully aligned with the longitudinal direction of the slab. Collected data from these gauges would help to determine the time of crack initiation and the concrete surface stress/strain condition. Concrete may crack at tensile strain as low as 100 *micro strain* $(\mu\varepsilon)$. Cracking is so brittle and whenever a crack passes through one of these PI-gauges a sudden increase in the output strain reading can be expected. The corresponding numbers of each of these PI-gauges are shown in Figure 2.3. These codes will be used to designate strain/load diagrams that will be drawn based on these PI-gauges outputs.

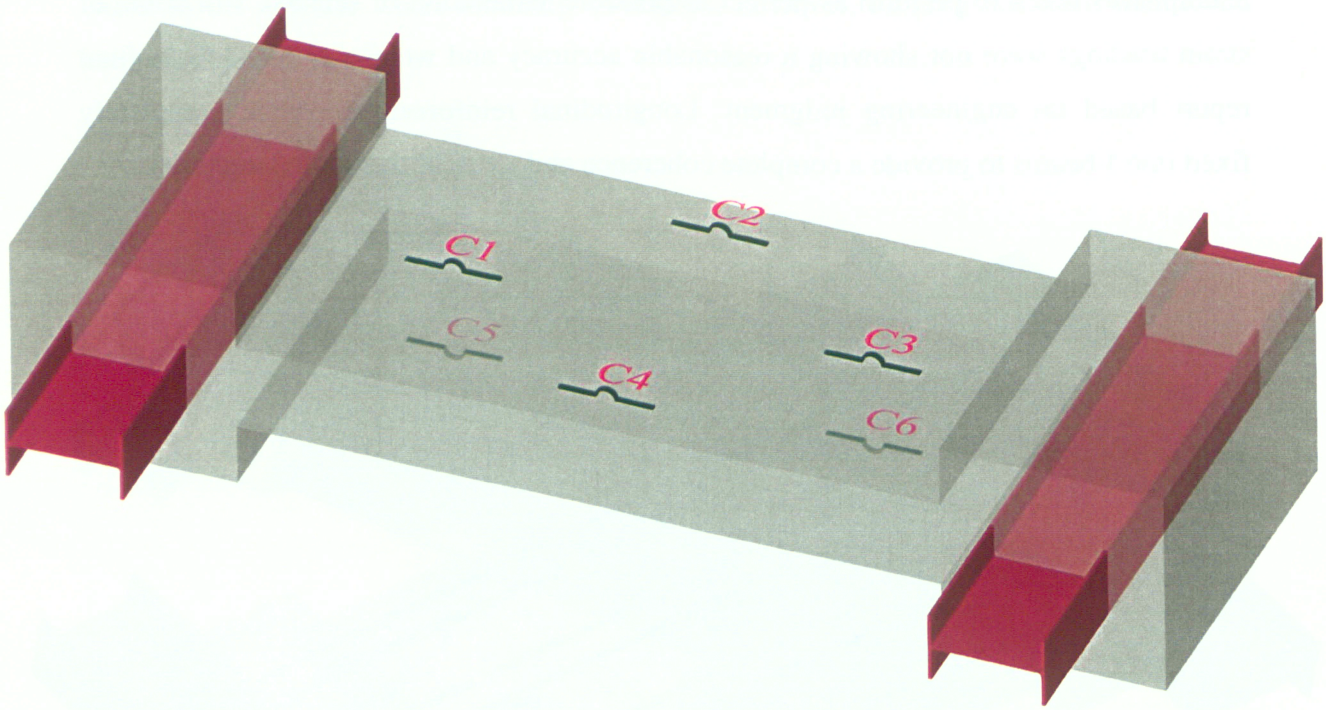

Figure 2.3 Concrete PI-gauges location and their corresponding numbers

Complete detailing and dimensioning of the direct tension specimen is illustrated in Figure 2.4. After a proper formwork was built, reinforcements and I-beams were put and tied in place as it can be seen in Figure 2.5. Afterward, strain sensors were installed in an ideal manner. At that time, a normal concrete mix made by a concrete company was cast in place. Several cylindrical samples were taken from the mix for compression test, the results of which are shown in Table 2.1.

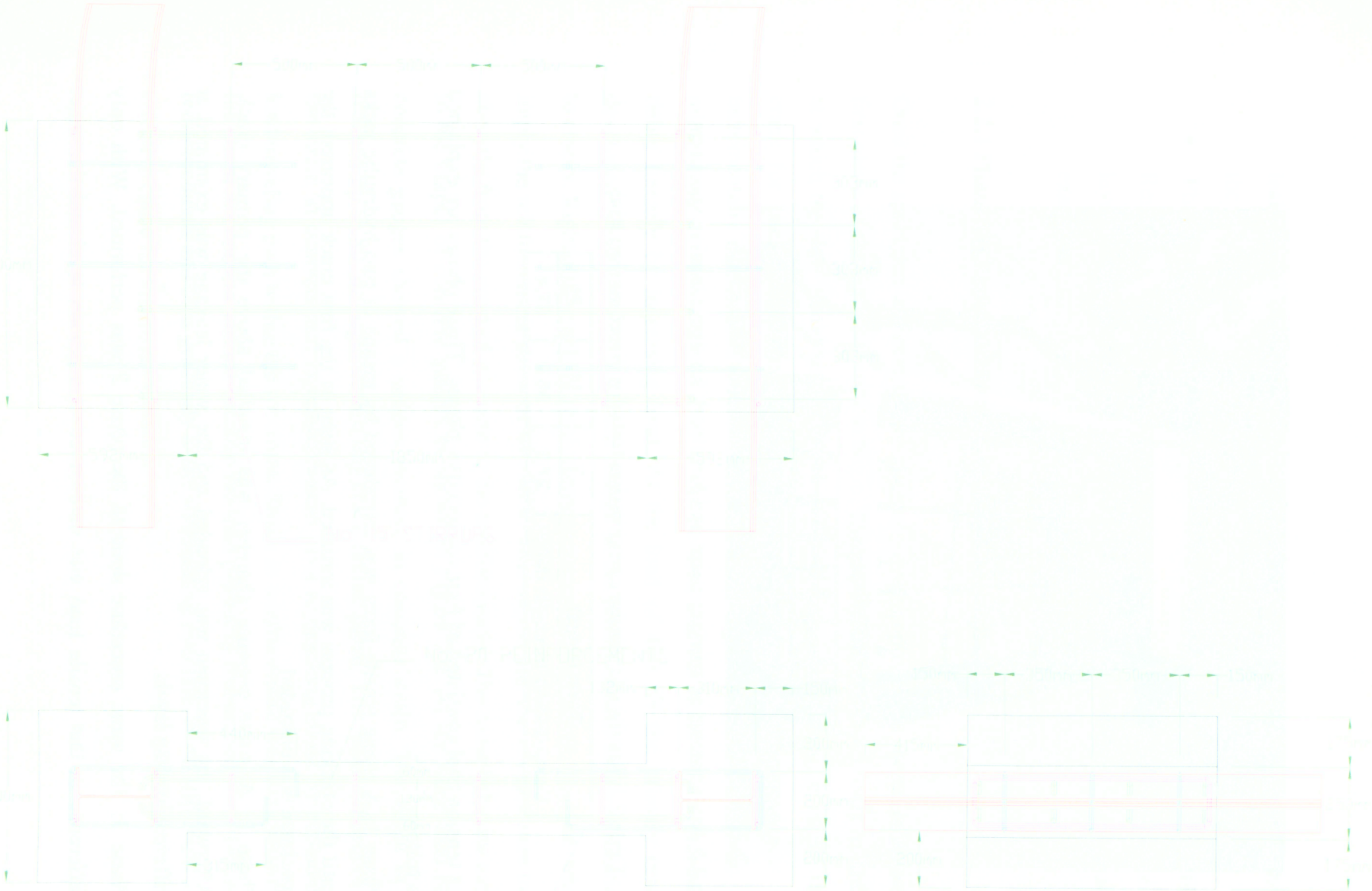

Figure 2.4 Direct tension specimen detailing and dimensioning

Figure 2.5 Arrangement of reinforcement and formwork for direct tension specimen

Table 2.1 Results of cylinder compression tests for direct tension trial

Time (Days)	7	14	28
Compressive strength (MPa)	27.3	35.9	37.4

The direct tension trial consisted of four consecutive phases. These phases are explained briefly as follows:

- Phase 1: A rising tensile force was introduced by means of two hydraulic jacks until the cracking process was initiated. As soon as the first crack appeared, the specimen was unloaded.
- Phase 2: A water pressure chamber was installed above the primary crack. Afterward, the specimen was reloaded and the water leakage was examined at different loading levels.
- Phase 3: The same procedure done in the phase 2 was performed. With only difference in that tensile load was maintained at a certain level and the water

leakage was monitored over a period of 30 hours in hopes of a possible drop in the seeping water flow rate.

- Phase 4: The top face of the slab was retrofitted with a layer of glass FRP (Fiber Reinforced Polymer). Water pressure chamber was placed on top of the FRP layer. Subsequently, the specimen was reloaded and the water leakage was examined.

2.2.1 Phase 1 (Crack Initiation)

Once the specimen was prepared and its set-up accomplished as shown in Figure 2.6, the first phase of the test was ready to begin. The goal of this phase was only to find the load at which the slab would start to crack and to determine the location of the first major crack for later installation of the water pressure chamber. The load was increased incrementally up to the first crack formation. Figure 2.7 illustrates the strain in reinforcements versus tensile load. It can be seen that the strain in reinforcements were rising linearly by increasing load. At the load of 480 kN the primary cracks were developed which induced a sudden change in the reinforcement strain at locations close to cracks. Right after cracking reinforcement strain was read about 1000 $\mu\varepsilon$ which could imply the reinforcement stress of 200 MPa. This means that the stresses were transferred abruptly from the cracked concrete to the reinforcement. The same behavior can be seen in the output of concrete gauges as shown in Figure 2.8. At the same load of 480 kN concrete gauges showed a sudden increase in concrete strain. The strain in concrete reached up to 80 $\mu\varepsilon$ right before any crack taking place. The small difference between the strain in concrete and in reinforcement prior to cracking could be explained by the load traveling path within the specimen. Strain in reinforcement was somewhat more than the strain at concrete surface because the load primarily transmitted from I-beams to the reinforcements and then gradually to the surrounding concrete. Bond slip could also be an effective cause for this strain variation.

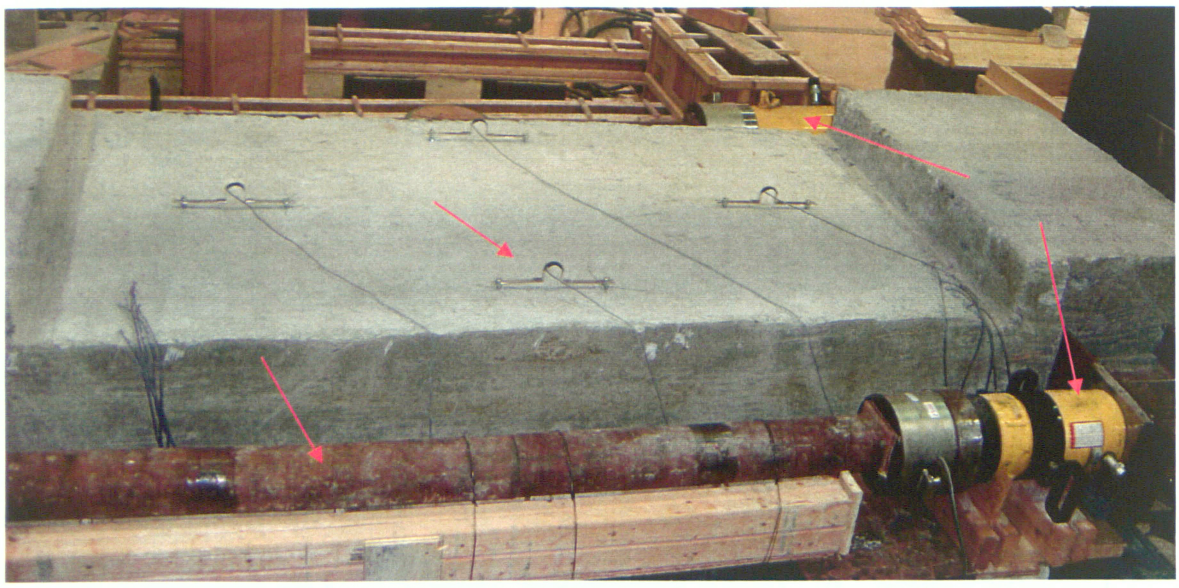

Figure 2.6 Direct tension test set-up (first phase)

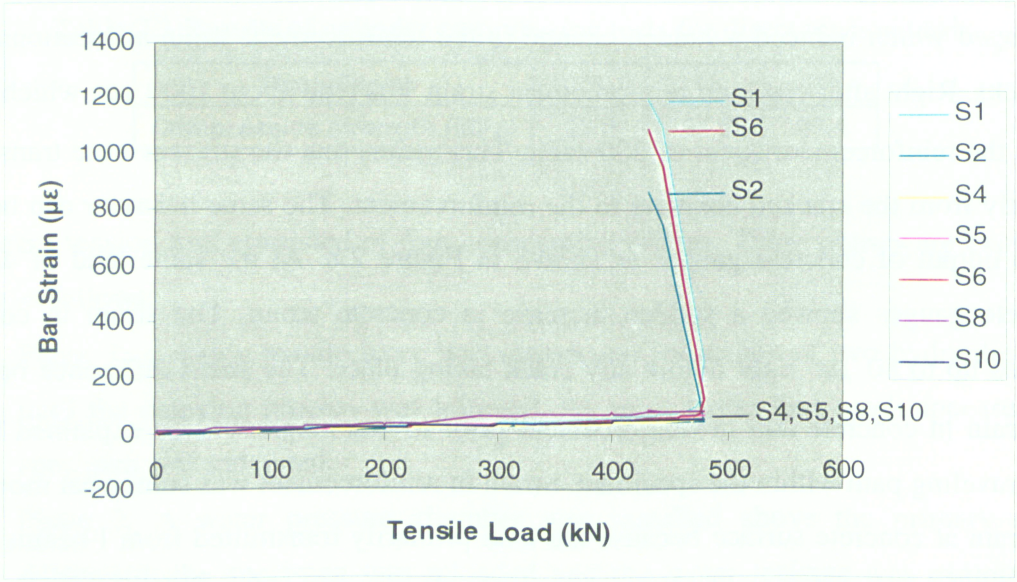

Figure 2.7 Bar strain versus tensile load for the first phase of direct tension test

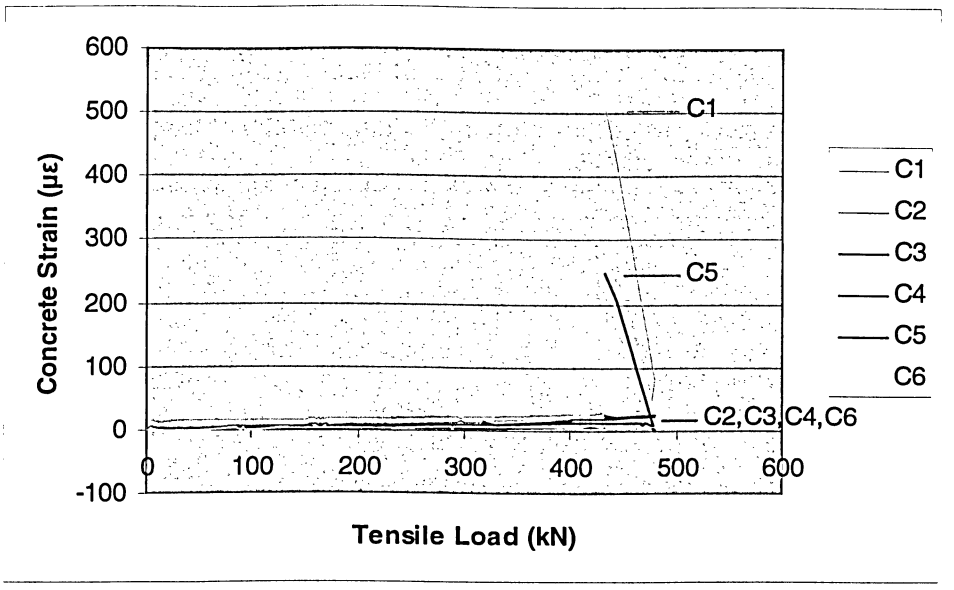

Figure 2.8 Concrete strain versus tensile load for the first phase of direct tension test

The crack initiation tensile load has been successfully estimated in the next chapter by means of analytical method. For the sake of comparison, this crack initiation tensile load (480 *kN*) can develop at the base of a circular water tank with 6 meters height, 18 meters diameter and free to slide base, as shown in the following calculation:

Ring Force (at the base of a water tank) $F = \gamma \times H \times r = 9810 \times 6 \times 9 = 529740 \qquad N/m$

where, γ = unit weight of material contained in tank; H = tank height; and r = tank radius.

Therefore, cracking at the base of this typical water tank is inevitable if a tank wall with section properties similar to those of the tested specimen is used. Noting that most water tanks are of dimensions much bigger than that of the above typical water tank, it is obvious how commonly they are exposed to the cracking problem. Besides, this is not specific to tanks and can exist in other circumstances. Concrete members and structures that transmit loads primarily by direct tension rather than bending, such as, bins and silos, shells, ties of arches, roof and bridge trusses, and braced frames and towers are experiencing the same condition.

2.2.2 Phase 2 (Water Leakage)

Once initial cracks were observed, specimen was completely unloaded and at that point the first phase of the direct tension test was accomplished. Subsequently, the second phase commenced by mounting a water pressure chamber on top of a major primary crack. The water pressure chamber is depicted in Figure 2.9. This fully confined chamber was designed to create a constant amount of water pressure over a specific region above the crack. When it was being bolted on the slab, chamber was completely sealed to the concrete surface by using a layer of rubber band and water resistant silicon in-between the concrete surface and the chamber. A hose connected to the city water system was attached to the chamber inlet and the chamber outlet was closed when water overflowed. A pressure gauge assembled on the chamber could show the amount of internal water pressure. The water pressure could be kept constant during the test by adjusting a water valve located on the chamber inlet. During the test, water pressure was kept steady at the level of 0.5 *bar* $\left(5\times10^{4}\,Pa\right)$ to ensure a condition analogous to that might exist in the real structure. This could resemble the water pressure at the base of a 5 *meters* high water tank.

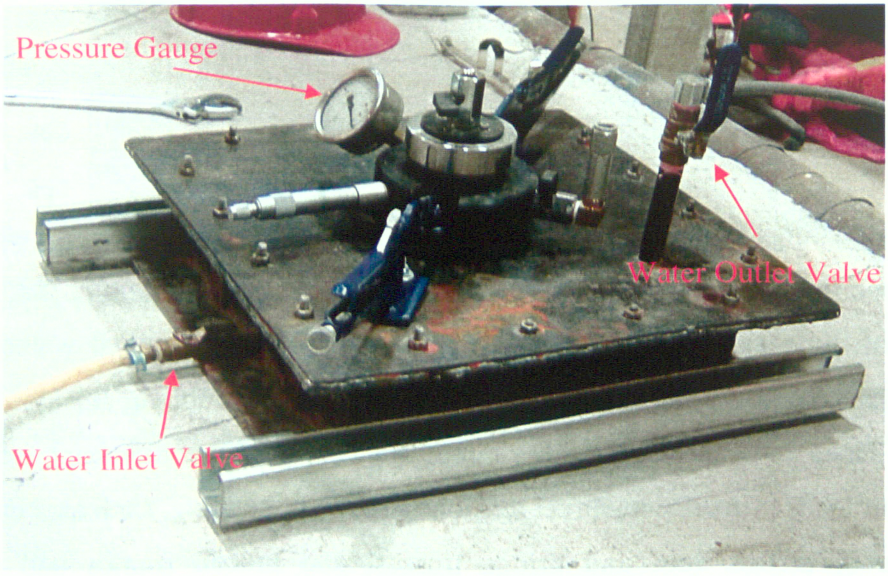

Figure 2.9 Water pressure chamber

The entire set-up of the test at this stage is shown in Figure 2.10. As it can be seen the water pressure chamber was mounted on the primary crack that was developed in previous phase of direct tension test.

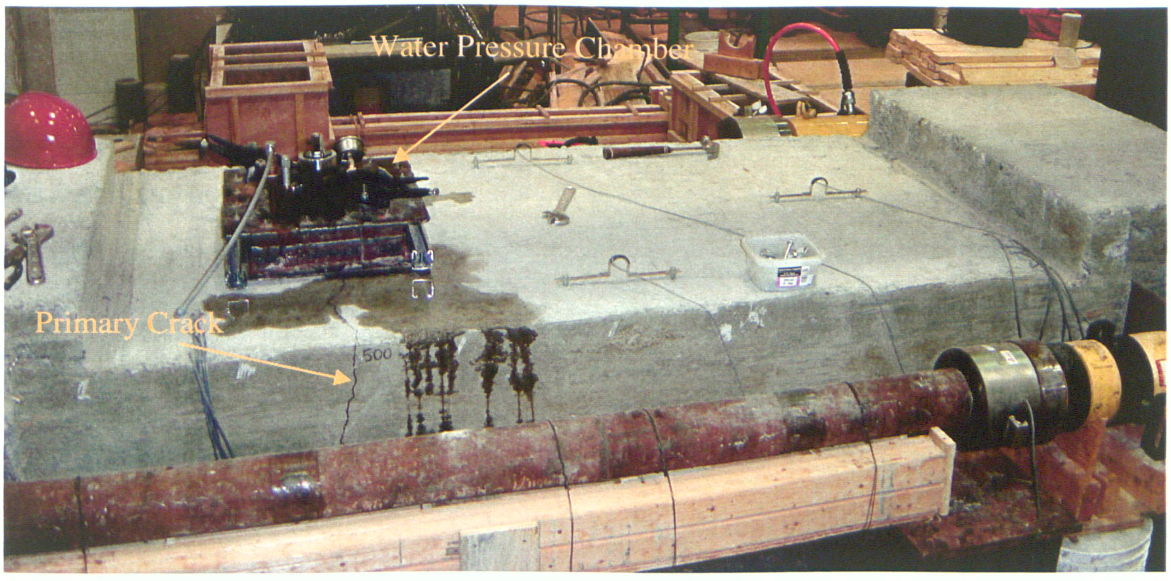

Figure 2.10 Direct tension test set-up (second phase)

Immediately after reapplying tensile load the bottom face of the slab started to become wet and soon after a slight leakage began at the load of 20 *kN*, as is illustrated in Figure 2.11. A crackscope with a precision of 0.05 *mm* and a magnification of 25X was used for measuring the width of cracks, which is depicted in Figure 2.12. The crack width at the start of leakage was measured 0.04 *mm* under a load of 20 *kN*. This indicates that direct tensile induced cracks are active problems for water retaining structures even when their width is as low as 0.04 *mm*. Therefore, in contrary to the current practice in design codes which is generalizing one allowable crack width to all types of cracks, more restrict limitations must be defined for direct tensile induced cracks which are commonly through cracks.

Subsequently, tensile load was raised incrementally, and the crack width was inspected at the end of each loading step, the results of which are gathered in Table 2.2 and drawn in Figure 2.13. In all experimental tests only the maximum crack widths corresponding the major crack underneath the water pressure chamber were reported. Therefore, crack

widths provided here in all charts and tables can be implied as the maximum observed crack widths. The consistency of some crack prediction models with these experimental results is examined in the next chapter. Strain data collected from concrete and steel strain gauges are drawn versus tensile load in Figures 2.14 and 2.15 respectively. As expected, the strains were increasing with a linear ascending trend to a load of 540 *kN*, upon which an abrupt change happened. This was because new cracks developed across or close to some of strain gauges. In fact, not all cracks formed at the same stress level due to the variability in tensile strength along the length of the tension member. But rather they occurred in a span of 90 to 110 percent of tensile strength. During this test four cracks were formed along the slab with respective spacings of 320, 700 and 300 *mm*.

Figure 2.11 Bottom view of the specimen (leakage all across the primary crack)

Figure 2.12 Crackscope

Table 2.2 Crack width versus tensile load for the second phase of direct tension test

Tensile Load (kN)	20	100	120	160	200	240	280	320	360	400	440	480	540
Crack Width (mm)	0.04	0.18	0.18	0.20	0.24	0.30	0.33	0.36	0.38	0.40	0.40	0.40	0.40

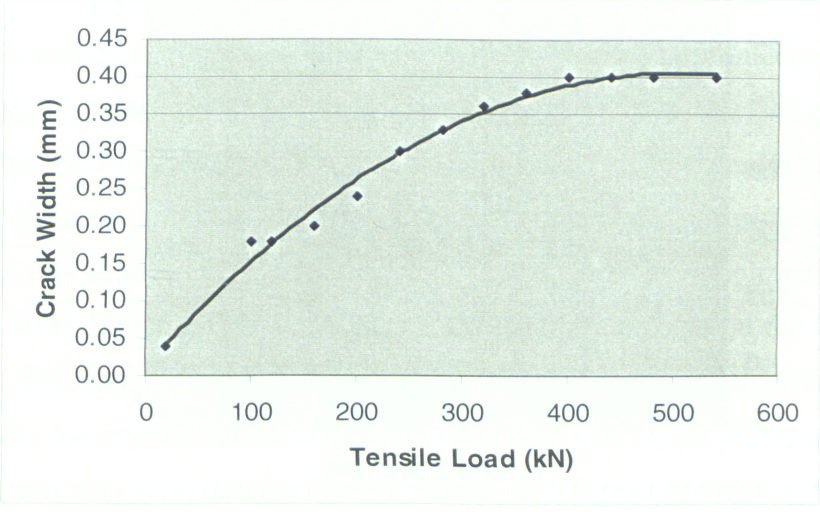

Figure 2.13 Crack width versus tensile load for the second phase of direct tension test

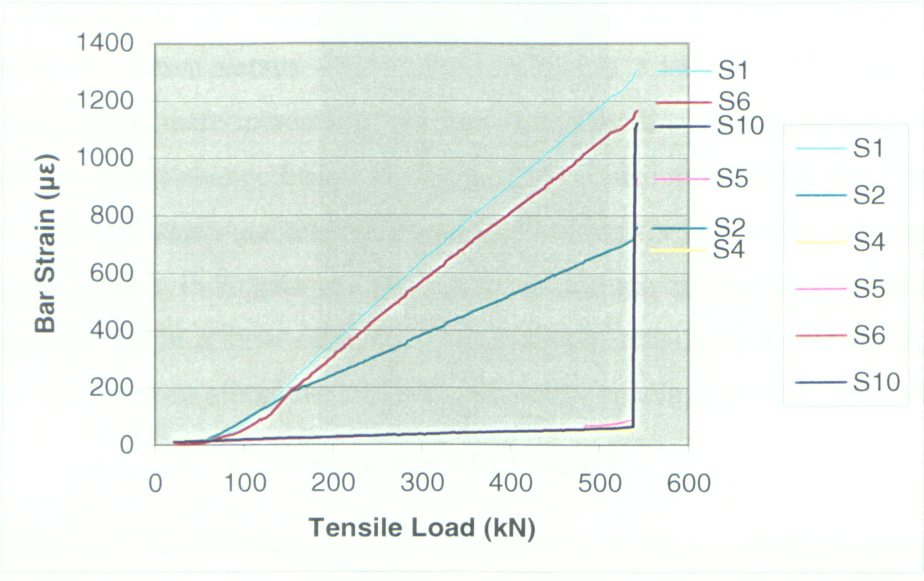

Figure 2.14 Bar strain versus tensile load for the second phase of direct tension test

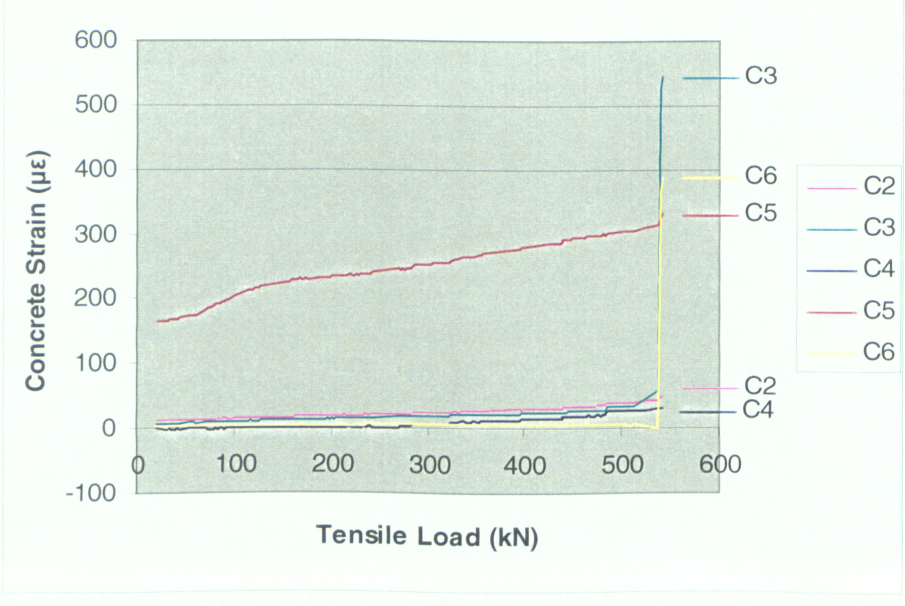

Figure 2.15 Concrete strain versus tensile load for the second phase of direct tension test

2.2.3 Phase 3 (Crack Self Healing)

2.2.3.1 An Introduction to Concrete Autogenous Healing

The presence of cracks, due to mechanical stresses or time dependent effects, such as shrinkage and creep, is one of the major factors which can influence durability and serviceability of concrete structures. Fortunately, self healing of cracks, also known as autogenous healing, is one phenomenon acting positively in durability problems of concrete. This process can take place only in presence of water and consists of chemical reactions of compounds exposed at the cracked surfaces. These reactions produce crystals, and the accretion of these from the opposite surfaces of a crack can re-establish the continuity of the material eventually. There are two major assumptions regarding the reactions of healing: the hydration of un-hydrated clinker available in the microstructure of hardened concrete, or the precipitation of calcium carbonate $CaCO_3$. The first hypothesis requires the presence of water, and the second one the presence of dissolved CO_2 in addition. Mechanical blocking, obstruction of narrow crack areas with ultra-fine material, swelling, silting up of cracks and deposition of debris can also contribute to healing.

Most studies carried out until now highlight the self healing phenomenon by means of water permeability tests. A diminution of the flow rate through cracked concrete is the main technique used to characterise self healing of cracks. Edvardsen (1999) performed such tests, conducted on small concrete specimens, with a single tensile crack in each. The typical results demonstrate that leakage of water through the specimen quickly drops to a reduced level. These results show the reaction of compounds on the crack surface, followed by diffusion through the newly formed crystals. Edvardsen explains the phenomenon by the crystallization of calcium carbonate $CaCO_3$, as the main element. He also shows that cracks with initial effective widths of 200 *microns* after sufficiently long water exposure can completely seal after five to seven weeks. The dependency of the healing rate on the initial effective crack width is also shown by Clear (1985). For example, cracks with an initial effective width less than 50 *microns* reduce to 20 *microns*

within 24 hours, and cracks with an initial effective width between 50 and 100 *microns* reduce to an effective width of 20 *microns* within seven days.

In a study by Reinhardt and Joos (2003), it has been shown that the decrease of the flow rate depends on crack width and temperature. Smaller cracks do heal faster than greater ones and a higher temperature favours a faster self-healing process. It continues that in high performance concrete (HPC) under certain condition, cracks of the width less than 0.10 *mm* can be regarded as smooth and can be closed by self-healing processes.

Hearn (1997, 1998) carried out also permeability tests on mortar (with 78 % of hydrated clinker), and water cured concrete with insignificant amount of un-hydrated clinker. The author investigates the chemical effects, like continuing hydration, dissolution and deposition of soluble species. Chemical analysis of water, inflow and outflow, points out a significant increase in Ca^{2+} ions concentration in outflow, which indicates a phenomenon of dissolution-deposition, especially of calcium carbonate $CaCO_3$.

The above experiments show that the phenomenon is of particular importance for water tightness and transfer properties of concrete structures. Additionally, some tests have been performed in order to investigate the role of self healing on mechanical properties. Jacobsen et al. (1996) performed some experiments which consisted of damaging concrete cubes by rapid freeze/thaw cycles, and then storing them in water. Deterioration and healing are measured through the evolutions of the compressive strength and the resonance frequencies giving the dynamic modulus of elasticity. Freeze/thaw cycles lead to a decrease of both resonance frequencies and compressive strengths, and self healing gives a substantial recovery of the frequency but only a small recovery of the compressive strength. The author explains this small recovery by the fact that cracks are not fully filled with the newly formed crystals. SEM (scanning electron microscope) observations by Jacobsen et al. (1995) confirm that and show that most of the crystals seen in the cracks are newly formed C-S-H.

In addition to Jacobsen's experiments, data from Pimienta and Chanvillard (2004) presents some mechanical results of concrete specimens damaged under three points bending and then healed, and point out a resonance frequency recovery especially. Ter Heide (2005) also provides some mechanical results on the behaviour of cracked concrete at early age. The tests include cracking of prismatic specimens, and mechanical characterization after ageing, by means of three points bending tests. The mechanical behaviour of healed concrete specimens for several periods of ageing is presented. Acoustic emission analysis is also performed with the aim of providing some additional, qualitative, information on the microcracking process of healed specimens.

A variety of methods have been used to investigate the healing of cracks. Most of the studies focus on observing deposition of hydration products between the crack lips using an optical microscope, a scanning electron microscope (SEM), x-ray diffraction analysis, or chemical and mineralogical studies. Besides mechanical tests, nondestructive evaluation techniques based on ultrasonic pulse velocity (UPV) measurement have been used to assess crack healing (Munday et al. 1974). Although UPV measurements can detect the occurrence of crack healing, it has been shown that this method cannot accurately determine the extent of crack healing.

In a study by Aldea et al. (1999, 2000) a nondestructive evaluation technique, which uses stress wave transmission measurement, was used to quantify the extent of healing of cracked concrete. Results of the research suggest that, in the considered cracking range, water flow through cracked samples tends to become comparable to that of un-cracked ones. Long-term permeability showed a decrease due to the ability of concrete to seal itself over time. One-sided stress wave transmission measurement proved to be a useful method to quantify autogenous healing of cracks.

ACI 224.1R (2007) states that healing will not occur if the crack is active and is subjected to movement during the healing period. Healing will also not occur if there is a positive flow of water through the crack, which dissolves and washes away the lime deposit, unless the flow of water is so slow that complete evaporation occurs at the exposed face

causing redeposition of the dissolved salts. However, this statement can be doubted according to the experimental observations in this study. It was observed during the test that the concrete self healing process could take place even when positive flow of water existed through cracks. ACI224.1R continues that saturation of the crack and the adjacent concrete with water during the healing process is essential for developing any substantial strength. The saturation must be continuous for the entire period of healing. A single cycle of drying and reimmersion will produce a drastic reduction in the amount of healing strength. Healing should be commenced as soon as possible after the crack appears. Delayed healing results in less restoration of strength than does immediate correction.

2.2.3.2 Test Procedure and Results

Third phase of direct tension test was planned with the intention of monitoring the self healing capacity of cracks under a constant amount of tensile load and a certain crack width. Roughly, a six month interruption occurred between the beginning of this stage and the end of direct tension second phase. A set-up, exactly similar to that of second phase, was arranged with the use of earlier cracked specimen, as shown in Figure 2.16.

Figure 2.16 Direct tension third phase test set-up (self healing)

The tensile load was raised in 10 or 20 *kN* increments and related crack widths were measured, the results of which are gathered in Table 2.3. Accordingly, load versus crack width curve is drawn in Figure 2.17. Almost the same crack width results were obtained in this test as that observed in the similar first part of the previous phase. The very minute difference could be due to possible human or equipment errors. Although water leakage was observed from the very beginning of the test, the loading was continued to achieve wider cracks upon which noticeably continuous flow of water could happen. This was achieved at the crack width of 0.25 *mm*.

Table 2.3 Load versus crack width for the third phase of direct tension test (self healing)

Tensile Load (kN)	0	100	120	180	200
Width of Crack Located Beneath Water Chamber (mm)	0.10	0.15	0.20	0.25	0.25

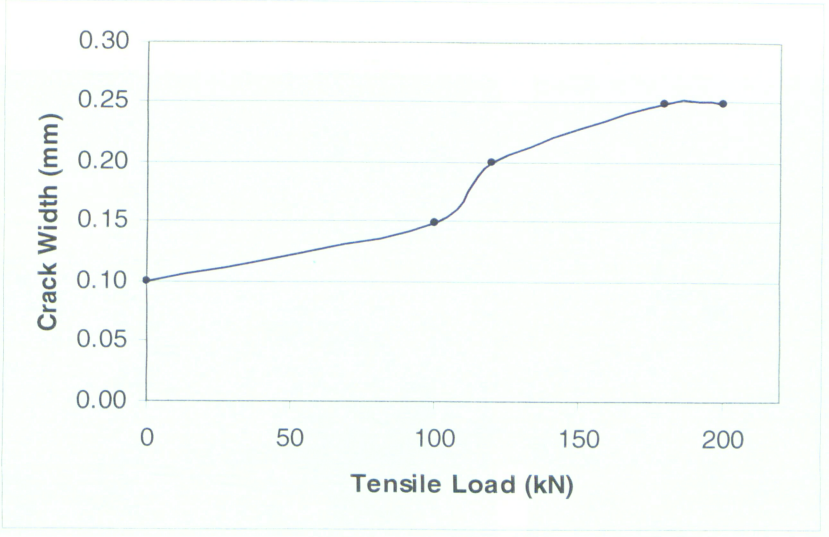

Figure 2.17 Load versus crack width for the third phase of direct tension test

The output results of bar and concrete strain are drawn versus the tensile load in Figures 2.18 and 2.19 respectively. As it can be seen the tensile load was increased up to 200 *kN*, upon which an adequately continuous leakage was observed. The tensile load was kept

steady at the level of 200 *kN* through the rest of the test. This could guarantee a passive crack, with no further movement or crack width alteration.

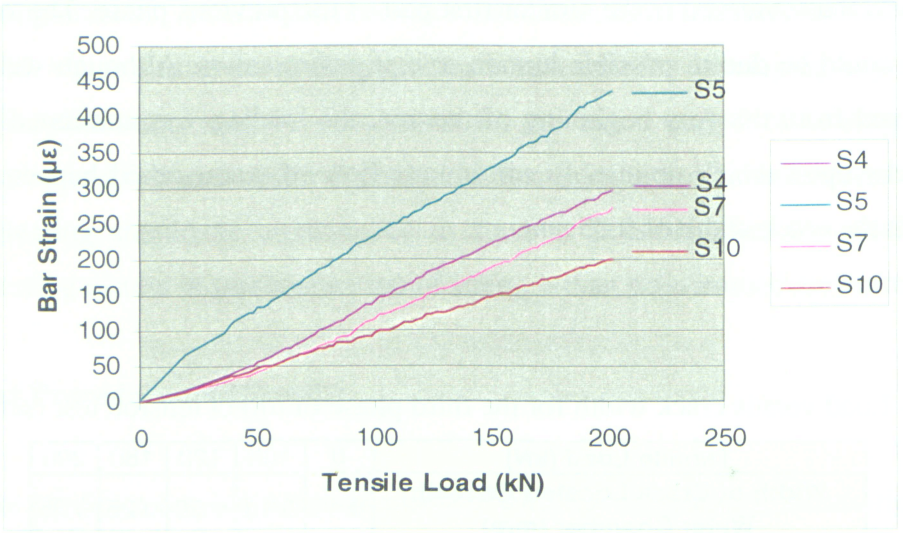

Figure 2.18 Bar strain versus tensile load for the third phase of direct tension test (self healing)

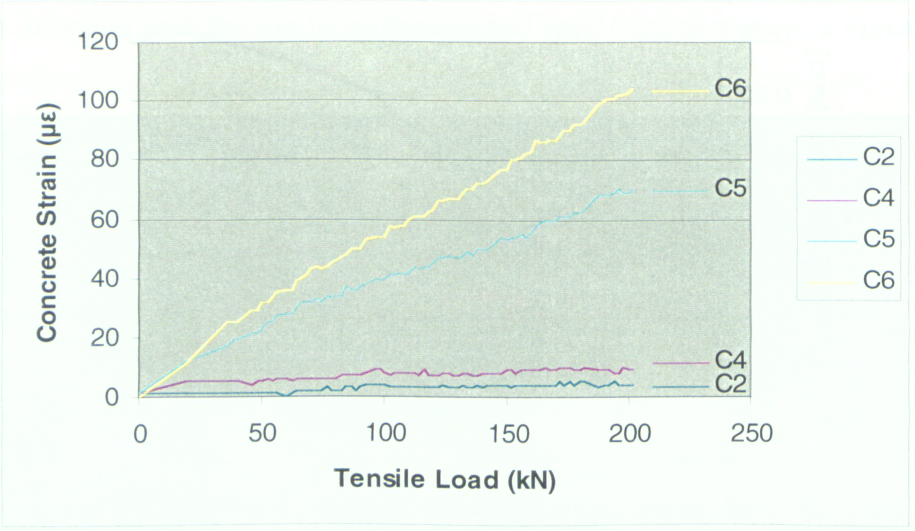

Figure 2.19 Concrete strain versus tensile load for the third phase of direct tension test (self healing)

As soon as the tensile load reached up to the satisfactory level, water flow rate monitoring was begun. Essential to produce a reliable flow rate data, a constant water pressure of 0.5 *bar* was maintained throughout the test. A wooden panel covered up in a

plastic sheet was placed beneath the crack to collect leaking water across the crack length and channel them to the measuring cup, as shown in Figures 2.20 and 2.21.

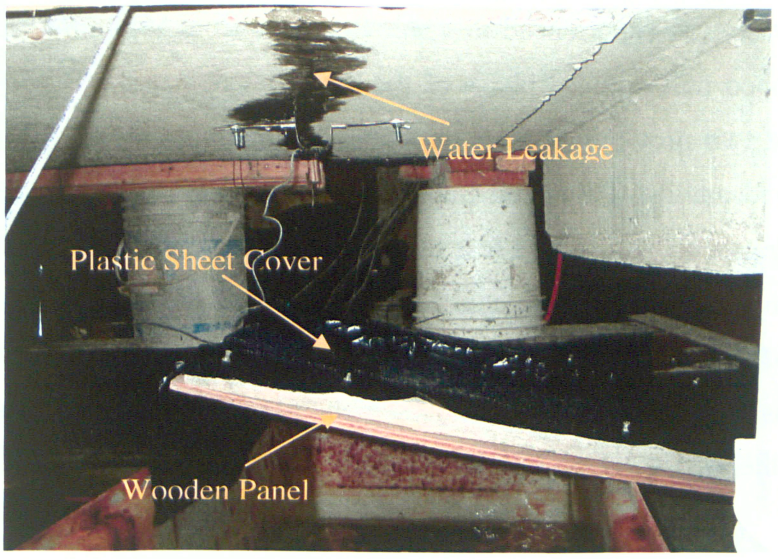

Figure 2.20 Collecting water scheme

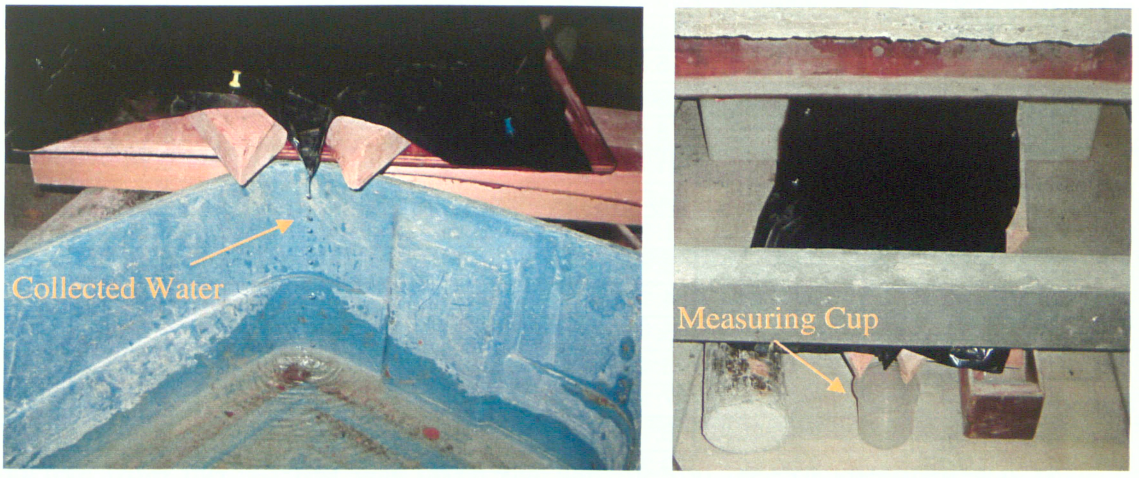

Figure2.21 Leaking water measurement

Water flow rate through the crack was recorded once every hour over a period of almost 30 hours. This was done at different stages by recording the time needed for a 1000 ml measuring cup to become completely filled up. All results are provided in Table 2.4 and the corresponding water flow rate versus time curve is drawn in Figure 2.22.

Interestingly, the water flow rate decreased significantly during the first 7 *hours*. As the test was carried on, the crack healing progress slowed down appreciably to the extent that after 20 *hours* not a considerable drop in water flow rate could be observed. An overall drop of 1.2 *ml/sec* was experienced in water flow rate from beginning to the end of the test. As mentioned before, third phase of the direct tension test was performed a while after the end of two previous phases, therefore, the healing process did not begin right after the crack formation. This is an important point to notice, as it is believed that the delayed healing process results in a less restoration capacity of cracks. This implies that a larger reduction in water flow rate could happen if no interruption was allowed between the moment of crack formation and the instant of water exposure. All in all, this experiment was another conclusive endorsement for the autogenous healing ability of cracks, even under positive flow of water and through delayed process.

Table 2.4 Flow rate versus time for the third phase of direct tension test

Time Elapsed (hr)	Time (empty cup)	Time (full cup)	Time Period (h:m:s)	Time Period (sec)	Flow Rate (ml/sec)
0	13:45:00	13:55:30	0:10:30	630	1.59
1	14:45:00	14:56:00	0:11:00	660	1.52
2	15:45:00	15:58:00	0:13:00	780	1.28
3	16:45:00	16:59:00	0:14:00	840	1.19
4	17:45:00	18:01:00	0:16:00	960	1.04
7	20:45:00	21:07:36	0:22:36	1356	0.74
10	23:45:00	0:07:32	0:22:36	1356	0.74
11	0:45:00	1:10:15	0:25:15	1515	0.66
13	2:45:00	3:10:15	0:25:15	1515	0.66
14	3:45:00	4:15:24	0:30:24	1824	0.55
15	4:45:00	5:15:27	0:30:27	1827	0.55
16	5:45:00	6:15:56	0:30:56	1856	0.54
17	6:45:00	7:16:00	0:31:00	1860	0.54
18	7:45:00	8:16:50	0:31:50	1910	0.52
19.25	9:00:00	9:34:00	0:34:00	2040	0.49
20.25	10:00:00	10:35:40	0:35:40	2140	0.47
21.25	11:00:00	11:35:45	0:35:45	2145	0.47
22.25	0:00:00	0:36:30	0:36:30	2190	0.46
23.25	13:00:00	13:40:40	0:40:40	2440	0.41
25.25	15:00:00	15:41:25	0:41:25	2485	0.40
29.35	19:06:00	19:48:15	0:42:15	2535	0.39

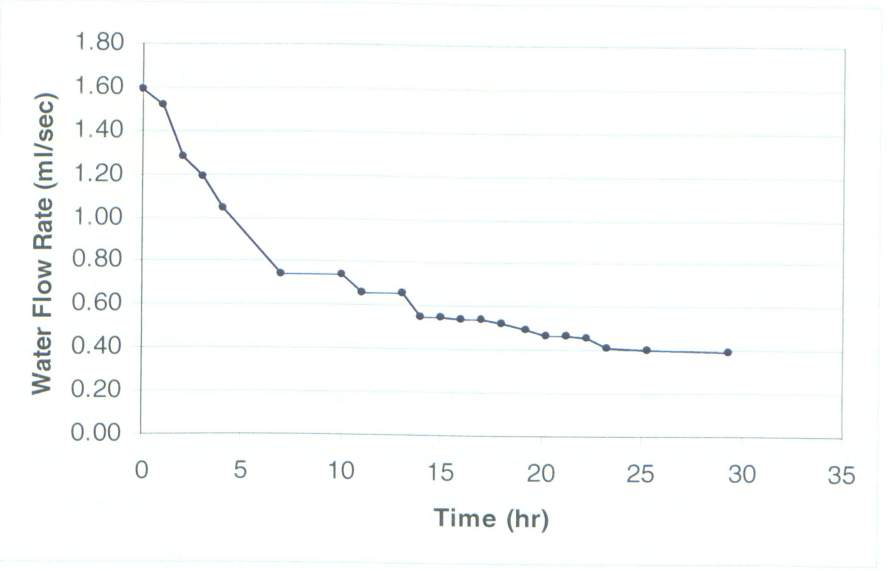

Figure 2.22 Water flow rate versus time for the third phase of direct tension test

2.2.4 Phase 4 (FRP Retrofitted)

The effectiveness of fiber reinforced polymer (FRP) in recovering the strength of damaged members is clearly recognized by engineers, however, FRP has never been thought of as a shielding layer to block the passageway of liquid through all types of cracks. This idea inspired the main purpose of investigation at this stage of direct tension test. In case that the experiment validates the authenticity of this proposal, cracks remediation in liquid containing structures may become easier, faster and much more efficient by use of FRP.

This test was launched right after the previous phase. Everything which was attached to concrete from the last test was taken out and the top face of specimen was perfectly cleaned up from any dirt. Subsequently, concrete top surface was carefully scrubbed by a steel brush to create scratch on the concrete surface for a better bonding development between glass FRP layer and the concrete surface. Once again the specimen was vacuumed from any dust made by brushing. The properties of the glass FRP used in this test are presented in Table 2.5. Two elements of epoxy (resin and hardener) were mixed up in an appropriate proportion and were thoroughly blended with a wood stick until it

turned into a single smooth liquid. Then the epoxy was applied with a soft painting brush on top surface of concrete, while the glass FRP matte was being laid and pressed on top of that simultaneously. Because it was not known from the beginning that how many glass FRP layers could stop water leakage, another layer of glass FRP was installed on top of the previous layer except beneath the water pressure chamber which left out in order to examine the effectiveness of one layer first, as seen in Figure 2.23. This would also create a plane of weakness beneath the water pressure chamber encouraging the widest crack to develop at this portion of the slab with one layer of glass FRP. If results were not satisfying, the water pressure chamber could be shifted to regions with two layers of glass FRP. Next day after that the epoxy setting process was completed, the water pressure chamber and concrete strain gauges were installed in place in the same previous manner. A small piece of the FRP layer was cut out to allow for crack width measurement at top surface of the specimen.

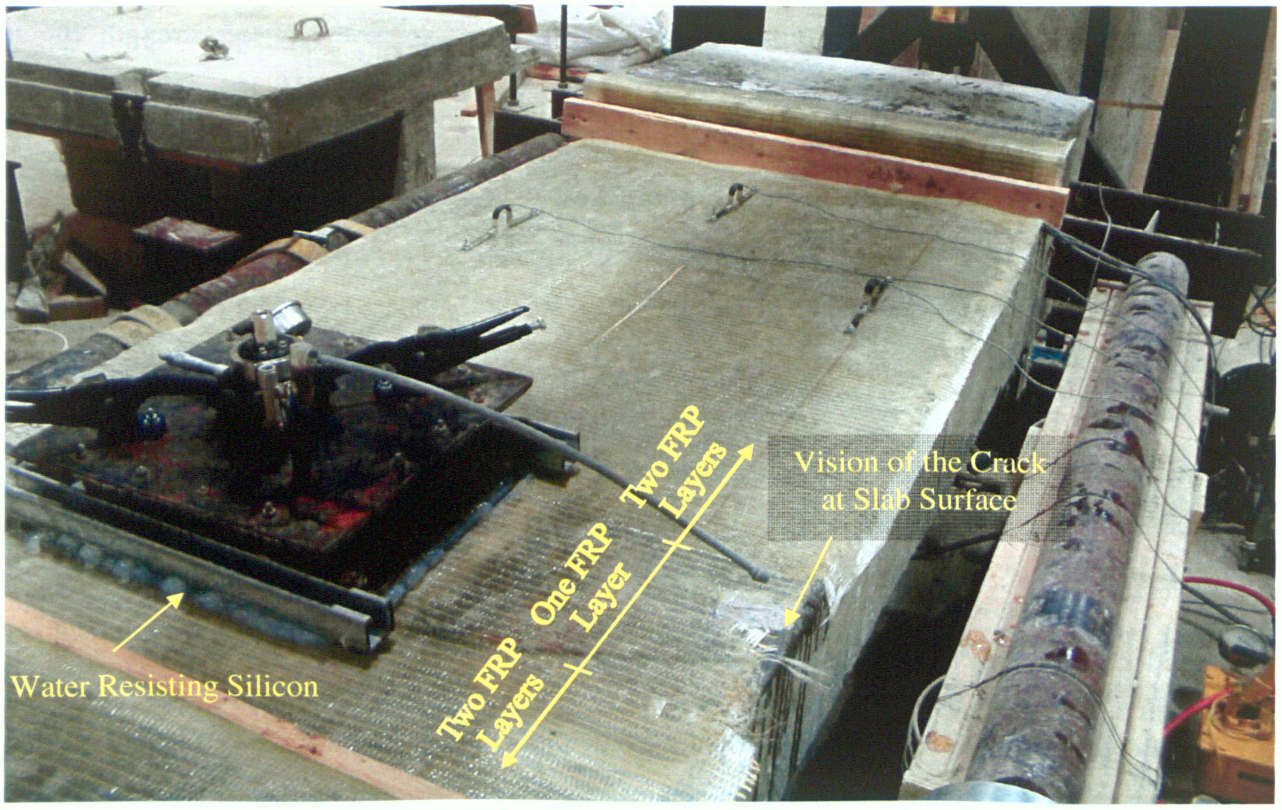

Figure 2.23 Test set-up and FRP layers for the forth phase of direct tension test

Table 2.5 Glass FRP properties
(TYFO SEH-51A Composite Laminate – R.J. Watson, Inc.)

Property	ASTM Method	Typical Test Value	Design Value
Altimate Tensile Strength in Primary Fiber Direction (Mpa)	D 3039	575	460
Elongation at Break (%)	D 3039	2.5	2.2
Tensile Modulus (Gpa)	D 3039	25.8	20.7
Design Thickness per Layer (mm)		1.3	1.3

The tensile load was increased incrementally by means of two expandable hydraulic jacks and the corresponding crack widths were measured, the results of which are shown in Table 2.6 and drawn by a trendline curve in Figure 2.24. Not a significant change was observed in the crack width to that of previous trials under loads up to 200 *kN*, which means that FRP does not have a considerable effect on the crack width at lower tensile loads. Nevertheless, as the load was increased to higher levels the influence of FRP in reducing the crack width was more noticeable.

Table 2.6 Crack width at different tensile load for the forth phase of direct tension test

Tensile Load (kN)	0	20	60	100	120	160	320	360	400	440	480	600	620	760	840	960	1060
Width of Crack Located Beneath Water Chamber (mm)	0.15	0.20	0.22	0.23	0.24	0.25	0.26	0.27	0.28	0.30	0.35	0.36	0.37	0.40	0.45	0.50	0.52

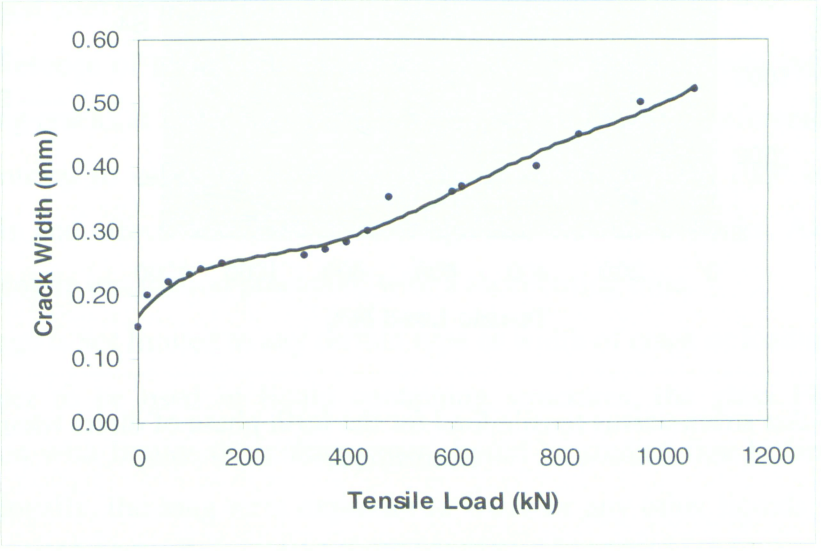

Figure 2.24 Crack width versus tensile load for the forth phase of direct tension test

The output results of bar and concrete strains are drawn versus the tensile load in Figures 2.25 and 2.26 respectively. The strain in reinforcements reached up to the yield level of 2000 $\mu\varepsilon$. Not a reasonable output was obtained from PI-gauges attached to the top face of specimen, which means that they were incapable of showing accurate strain at the FRP retrofitted surfaces, probably for the relative movement of concrete and glass FRP layer. In this case some other device would be used that could be attached on top surface of glass FRP layer and not drilled into concrete. The tensile load was raised up to 1060 *kN*, upon which no leakage was observed in any extent. The remarkable outcome of this test has proven that the glass FRP can be thought of as a potential option for remediation of damaged liquid containing structures. Glass FRP is shown to be very effective in controlling liquid leakage, and whenever economy allows, it is an excellent alternative for engineers to rehabilitate severely cracked sections of liquid containing structures. The test was accomplished at this point and the loading was stopped partly due to safety considerations.

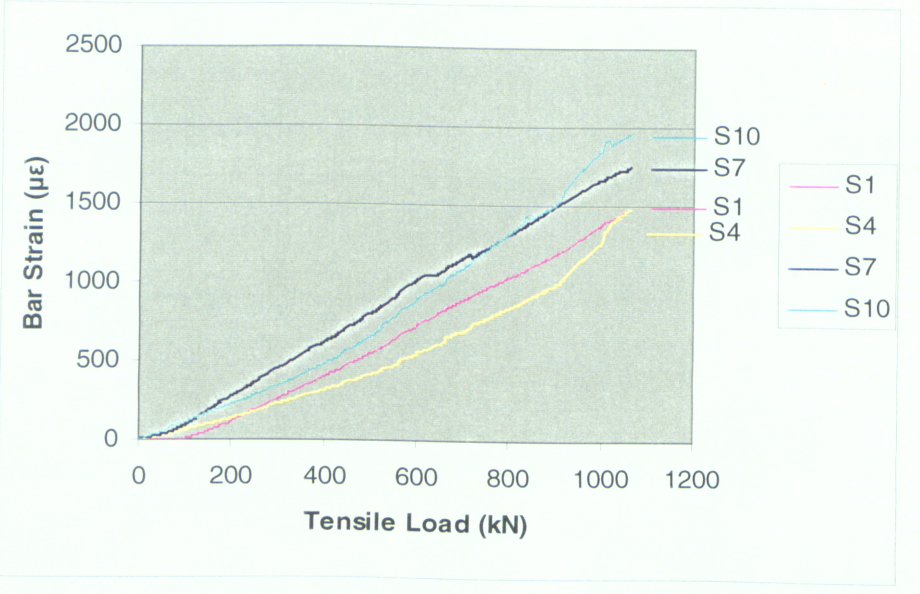

Figure 2.25 Bar strain versus tensile load for the forth phase of direct tension test (FRP Retrofitted)

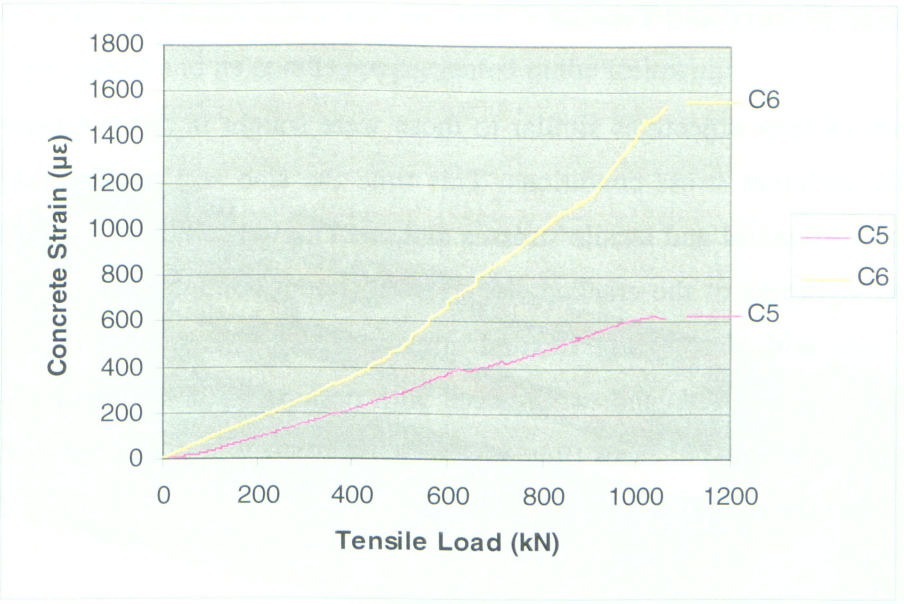

Figure 2.26 Concrete strain versus tensile load for the forth phase of direct tension test (FRP Retrofitted)

Several conclusions can be drawn according to this successful experiment about the glass FRP application:

- The application of one layer of glass FRP on the concrete cracked surface can effectively stop water leakage under at least 0.5 bar $\left(5\times10^{4}\,Pa\right)$ water pressure and even after yielding of reinforcement.
- The presence of glass FRP has no significant influence in reducing the width of existing cracks at lower loading levels prior to yielding of reinforcement.
- In contrary to other methods of crack remediation, glass FRP is much more durable and effective in case of a rising load and active cracks. Also, it needs a very simple installation procedure with a short curing time.
- Its usage is not limited to any certain type or width of crack or loading condition.
- In order to be used in liquid containing structures, the glass FRP's possible reaction with liquids other than water should be studied first before installation. Additionally, the long term exposure to water or any other liquids was not dealt with in this study and should be investigated.

2.3 Combined Flexure and Tension

In this series of tests objectives similar to those were sought in direct tension test were explored for different stress conditions. This time the slab section was subjected to a combination of flexural and tensile stresses and cracking was closely monitored, as well as the water tightness of the cracked slab. Two different combinations of stresses were examined: one with dominating flexural stresses and lesser amount of direct tensile stresses (high eccentricity), and another one with dominating direct tensile stresses and lesser amount of flexural stresses (low eccentricity). In the following, each of these tests is explained briefly and the results are discussed.

2.3.1 High Eccentricity Test

The fact that majority of structural members are usually designed to carry loads in a flexural manner has made this type of concrete behavior a center of attention for investigative studies. For instance, flexural cracking behavior of concrete walls in liquid containing structures is of major importance in regard to durability and serviceability issues. Here in order to reevaluate the flexural cracking behavior of RC walls, a specifically designed U-shape specimen was built resembling one meter wide vertical strip of a tank wall, as shown in Figure 2.27. The loads were applied with a 525 *mm* eccentricity, as a result of which a constant flexural moment and tensile force would develop throughout the length of slab. This flexural moment was created by means of two hydraulic jacks that were pushing apart the two end protruded arms of the specimen. As a result of this bending moment the maximum tensile stress would develop at top face of the slab and the maximum compression stress at bottom face. As the section was designed to fail in ductile mode, the tensile steel reinforcements were expected to yield before concrete crushing in compression. As a matter of fact the concrete compressive stresses remained in almost elastic state of stress/strain during the test. Although the formation of wide cracks at corner joints caused a premature failure of the specimen, the primary goal of this experiment which was to evaluate the flexural response of the RC

wall and its water tightness under service load was successfully achieved. The entire experiment procedure and its results are presented in the following.

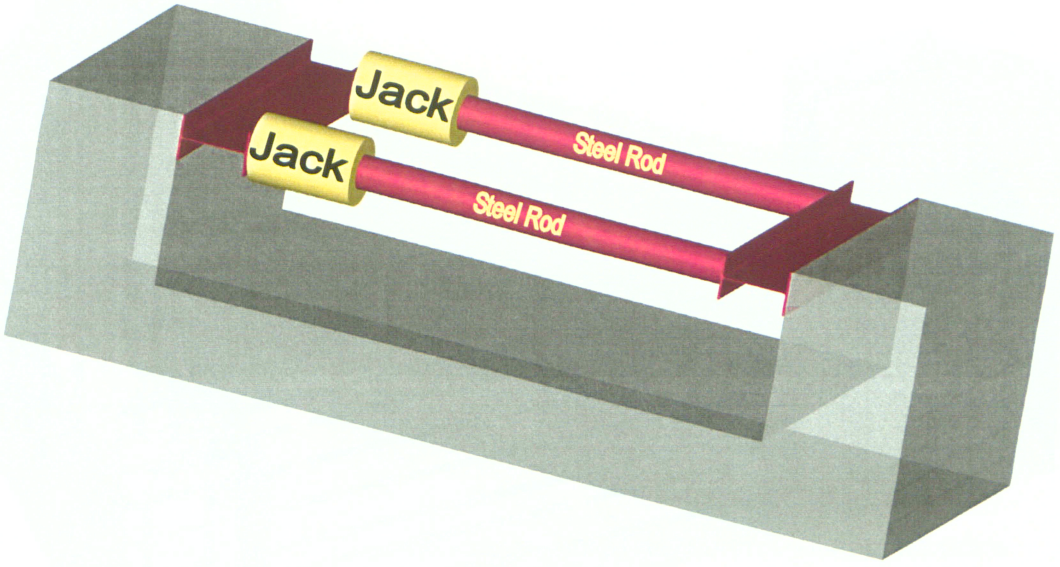

Figure 2.27 High eccentricity test specimen and hydraulic jacks positioning

The layout of reinforcements within the specimen is shown in Figure 2.28. Ten strain gauges were installed on longitudinal reinforcements to obtain the strain history during the test. The stress in reinforcement is the most important parameter with direct relation to the crack width. Theoretically, the width of crack is the difference between the elongation of steel reinforcement and the surrounding concrete. Therefore, the precision of estimated crack width extremely depends on the accuracy of the existing stress/strain data. Whenever concrete cracks at one section, all stresses will transfer from concrete to the steel reinforcement at that section, causing a sudden increase in reinforcement strain. Steel stress is reduced at sections away from the cracked section, as the stress is transmitting from steel to the surrounding concrete through the bonding stress. A certain minimum length is needed for these transmitted stresses to reach up to the tensile strength of concrete and cause the formation of a second crack. Obviously this length will increase with less bonding stress between steel and concrete. In other words, bond slip will result in formation of cracks with higher minimum spacing. Moreover, excessive bond slip can result in less concrete tension stiffening effect, and hence higher deflections can occur.

Also wider cracks can develop with higher bond slip as it reduces the stresses in concrete which in turn reduces the concrete elongation between cracks.

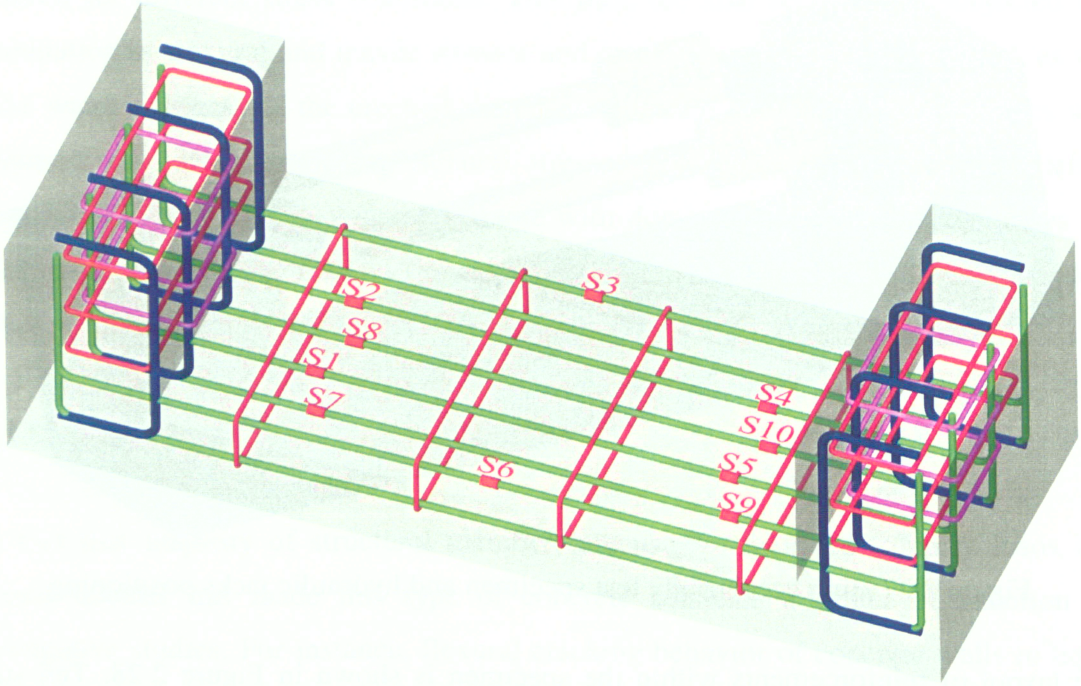

Figure 2.28 Reinforcement layout in the high eccentricity specimen, strain sensors location and their corresponding numbers

Two protruded end arms of the specimen were made more rigid than the middle slab encouraging all cracks to occur in the slab portion. Six PI-gauges were attached to the concrete surface as seen in Figure 2.29. They could record the concrete strain alterations at the surface fiber of the slab section. Although they did not have much usage in crack width prediction, the concrete strain data was useful to find out when the section was going to crack. Each time a crack occurred passing through one of these gauges, a sudden change could be detected in the output strain history. Also the collected concrete strain data could be used for comparison with those obtained from finite element analysis. The precision of these strain gauges was very dependent on their installation and physical calibration. Therefore always there was some potential for errors in the strain readings, especially when in spite of all efforts the alignment of these gauges could not be exactly lined up with the longitudinal axis of the slab.

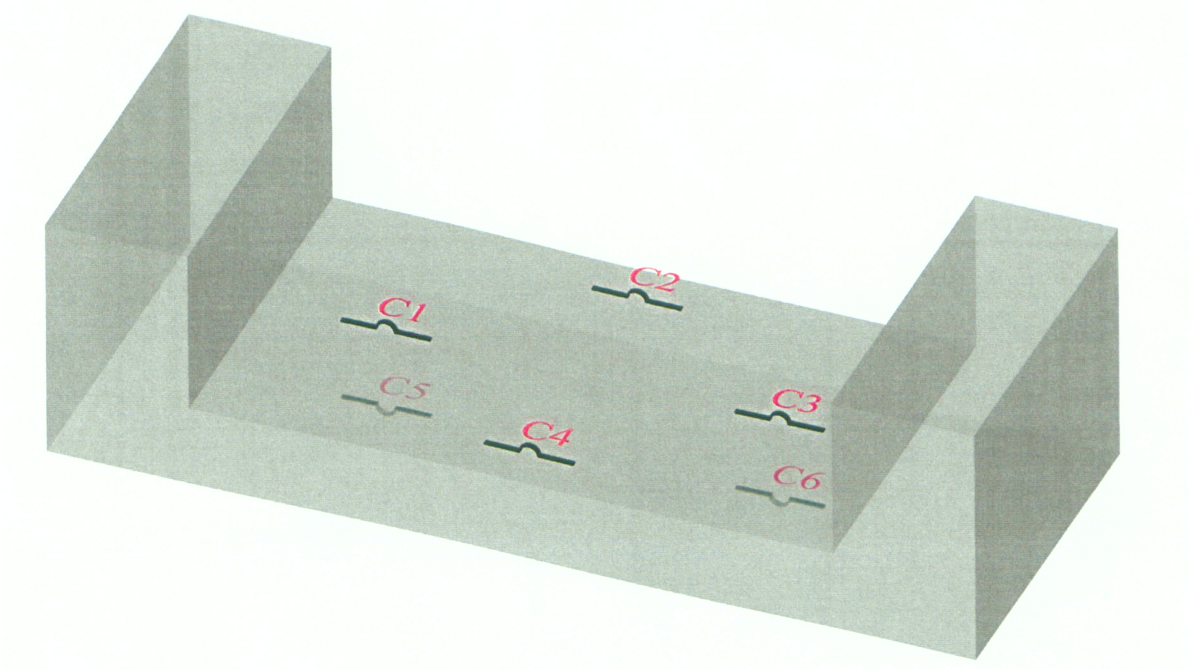

Figure 2.29 Concrete PI-gauges location and their corresponding numbers

Complete detailing and dimensioning of the combined flexure and tension specimen is illustrated in Figure 2.30. After a proper formwork was built, reinforcements were put and tied in place. Afterward, a normal concrete mix made by a concrete company was cast in place. Compressive tests were performed on several cylindrical samples, the results of which are shown in Table 2.7. The final test set-up is shown in Figure 2.31. As it can be seen two I-beams were used between hydraulic jacks and the end arms in order to provide a better distribution of the eccentric load across the specimen.

Table 2.7 Results of cylinder compression test for high eccentricity trial

Time (Days)	14	28	42
Compressive Strength (MPa)	21.1	25.6	29.9

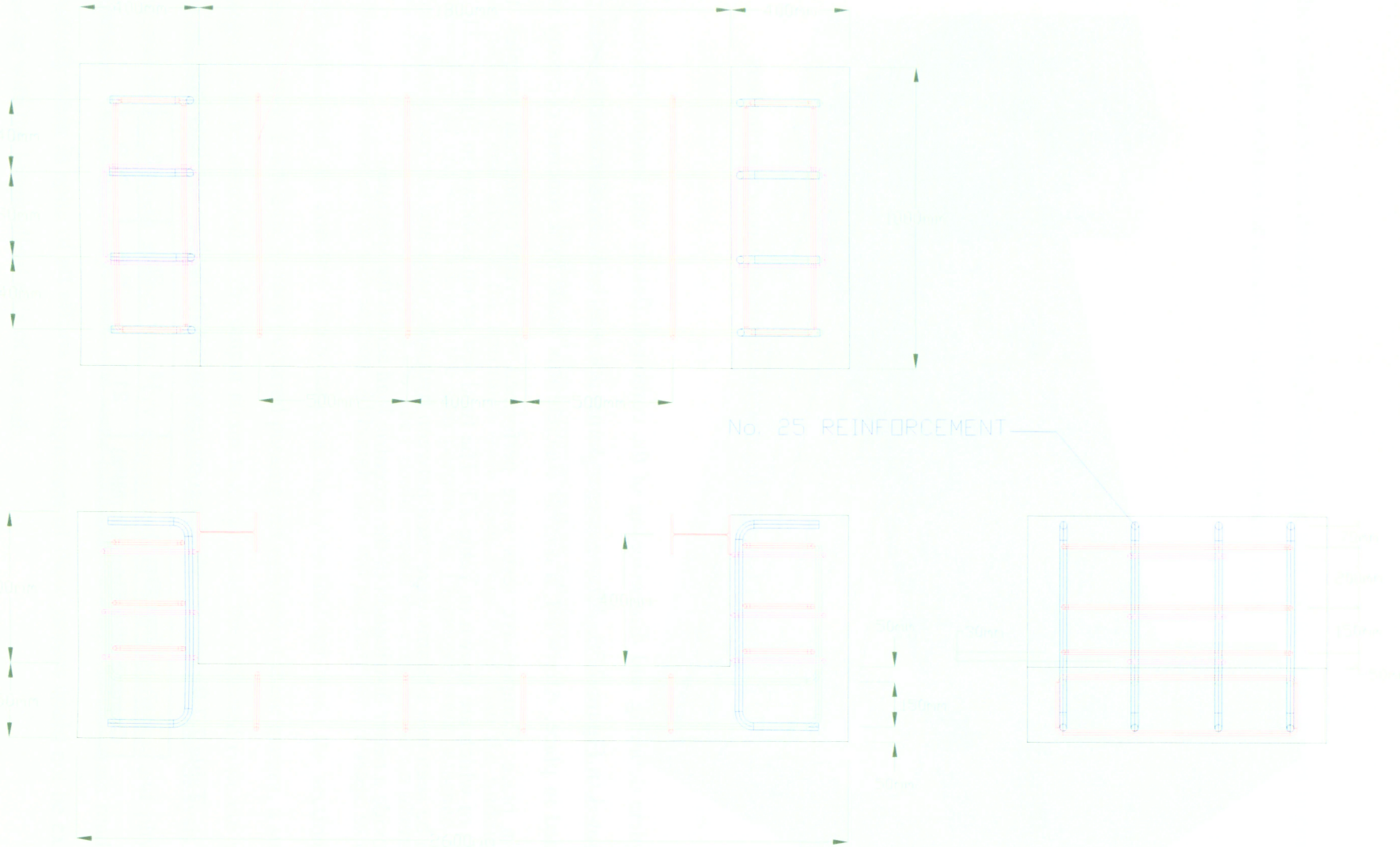

Figure 2.30 High eccentricity test specimen detailing and dimensioning

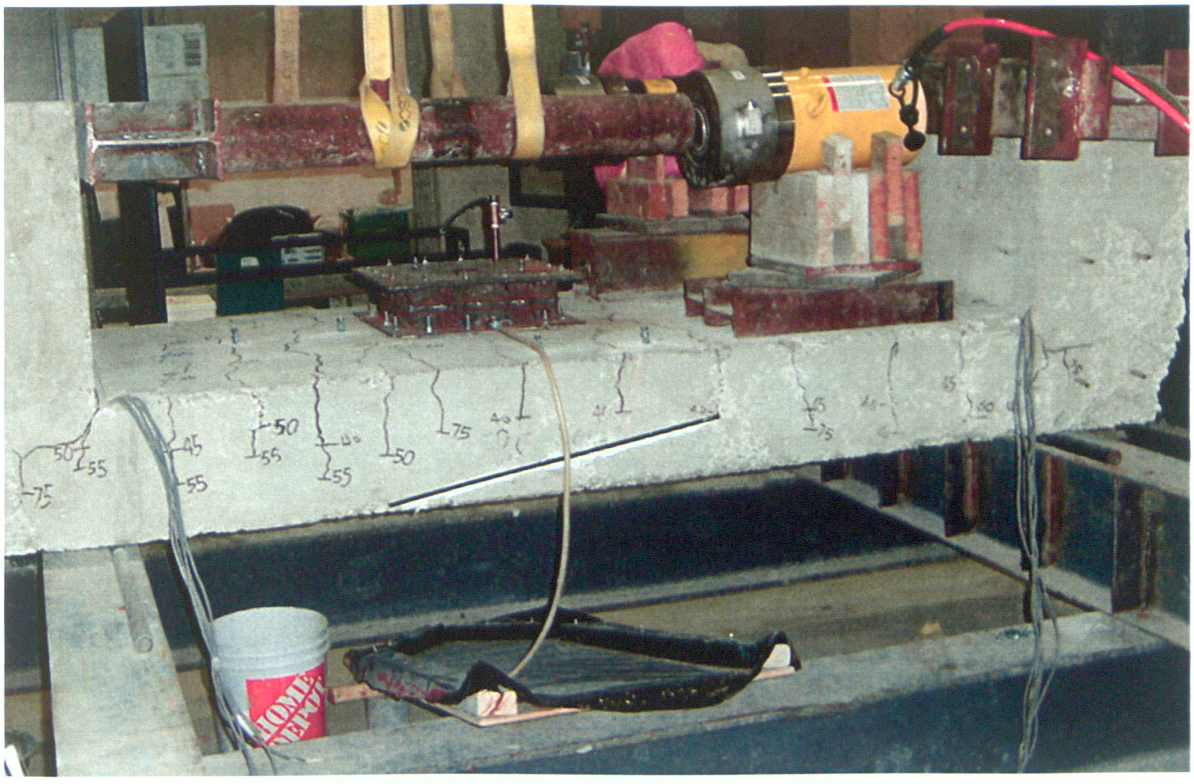

Figure 2.31 High eccentricity test final set-up

The applied tensile load was increased incrementally by means of two hydraulic pumps connected to the hydraulic jacks. While the load was gradually rising, the first crack occurred across the slab at a tensile load of 42 *kN*. The crack line was marked before continuing the test. The strain output results from the beginning of the test up to initial cracking are shown in Figures 2.32 and 2.33. The crack width was measured at the surface of the slab. It should be noted that the crack width reduces through the depth of slab for flexural induced cracks. Some crack models are giving the crack width at the reinforcement level. Thus, the effect of strain gradient must be taken into account in order to find the proper crack width at the surface of the member. It is because of this strain gradient that thicker concrete covers will result in formation of wider cracks. The wider the crack, the greater is the corrosion problem, because a greater portion of the bar has lost its passive protection. The influence of cracks on corrosion is not clearly known yet. It is believed that cracks transverse to reinforcement do not usually cause continuing corrosion of the reinforcement if the concrete has low permeability.

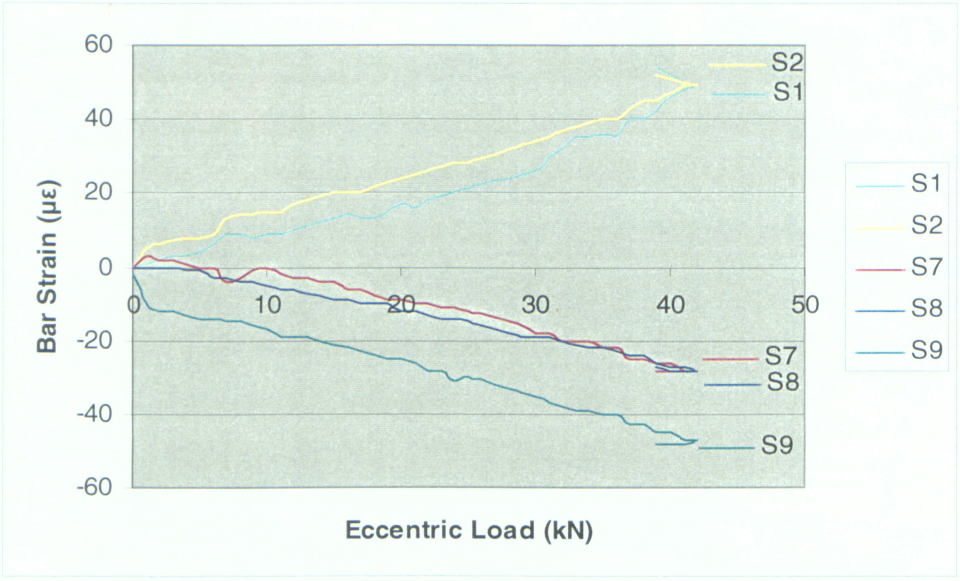

Figure 2.32 Bar strain versus eccentric load up to crack initiation for high eccentricity test

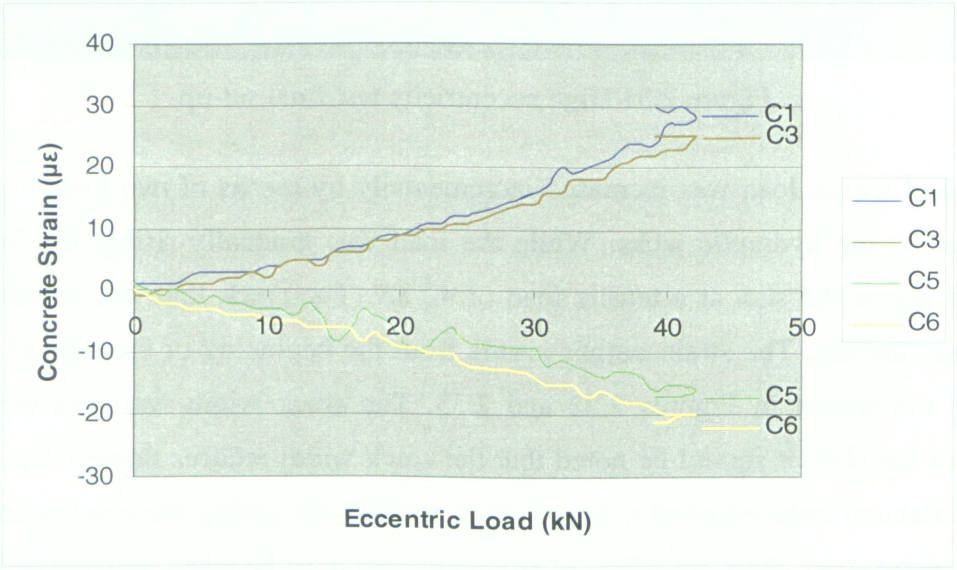

Figure 2.33 Concrete strain versus eccentric load up to crack initiation for high eccentricity test

After the crack initiation the specimen was unloaded, and the water chamber was placed and secured on top of the first crack. Again, the specimen was reloaded gradually up to the load of 51 *kN* at which some new cracks were developed and the previous cracks were grown deeper in to the slab. The strain history up to this load is presented in Figures 2.34 and 2.35.

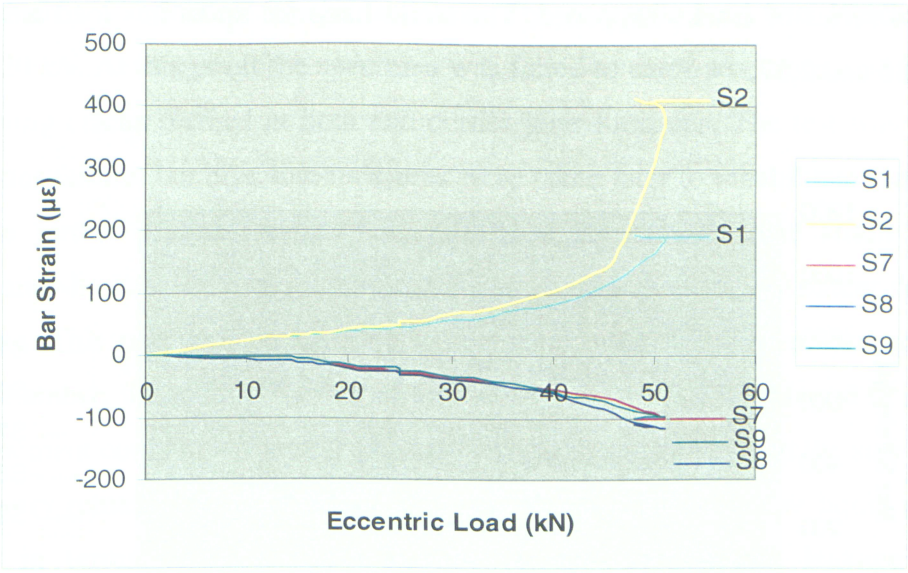

Figure 2.34 Bar strain versus eccentric load up to second crack formation for high eccentricity test

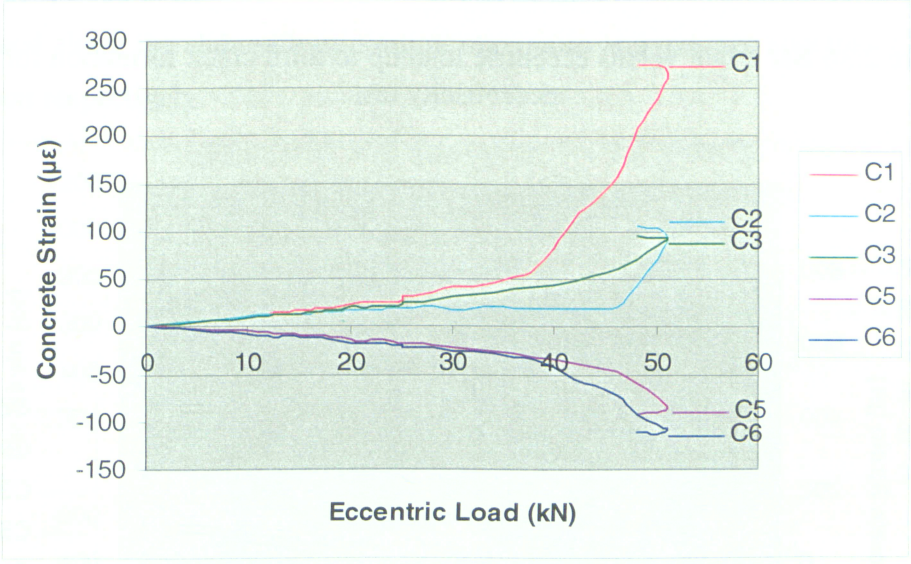

Figure 2.35 Concrete strain versus eccentric load up to second crack formation for high eccentricity test

Once again, the specimen was unloaded. Even though the specimen was completely unloaded, some of the strain was remained in place, which could be for some recoverability error in strain gauges or because of concrete and steel imperfect elastic behavior. Afterward, the tensile load was raised slowly up to the level of 79 *kN* upon

which third series of cracks happened. The strain histories up to this load are shown in Figures 2.36 and 2.37.

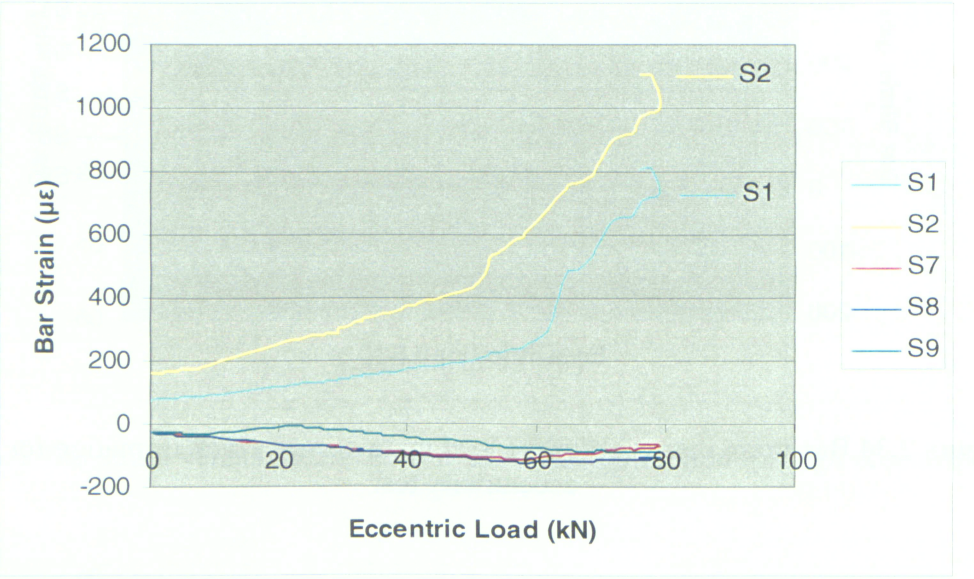

Figure 2.36 Bar strain versus eccentric load up to third crack formation for high eccentricity test

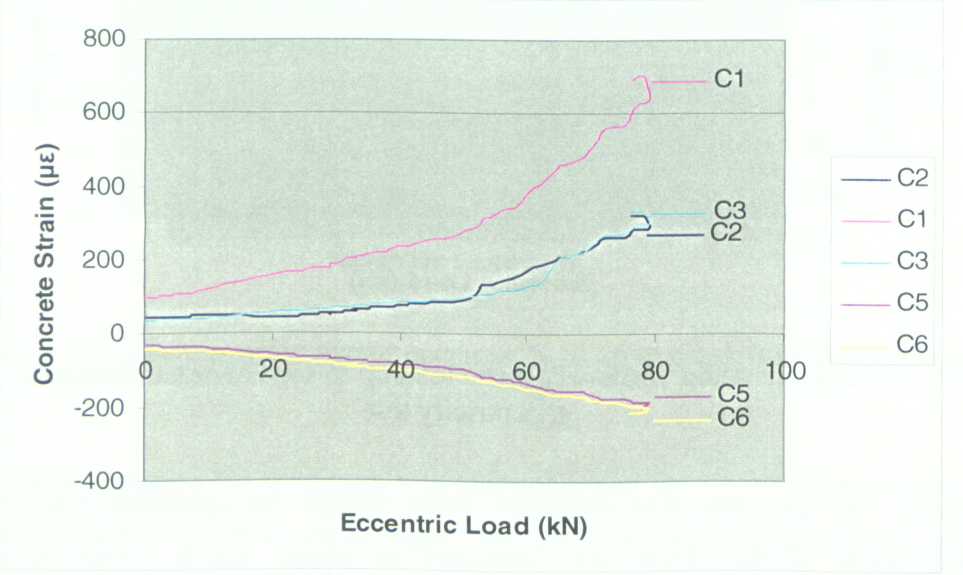

Figure 2.37 Concrete strain versus eccentric load up to third crack formation for high eccentricity test

The specimen was reloaded for the last time. The eccentric load was increased to the level of 120 *kN*. At this point the specimen was failed to carry any more load because of deep growing cracks formed at both end corner joint locations. The test was inevitably stopped after failure, but effective measures were taken later to rehabilitate the specimen to provide further loading capacity at the corner joints. The steel strain history is available and shown in Figure 2.38. No leakage was observed in any extent through the slab section. This means that nonetheless there were wide and deep cracks under water pressure chamber, the compression zone of the section that was developed as a result of bending moment could effectively stop water from penetrating through the slab thickness. This is a very remarkable phenomenon that can play a positive role in liquid containing structures in terms of reducing undesirable liquid loss through leakage problem. However, reinforcements are still exposed to liquid, and durability issue is yet an active problem to be considered. The crack width was recorded at the end of each load step, all of which are presented in Table 2.8 and drawn in Figure 2.39. During this test, 13 cracks were formed along the slab with minimum, maximum and average spacings of 100, 200 and 154 *mm* respectively.

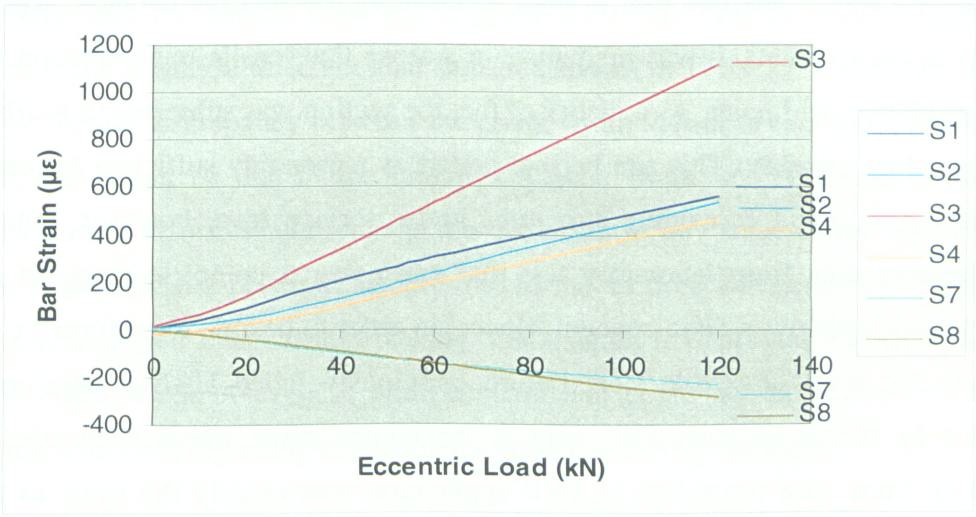

Figure 2.38 Bar strain versus eccentric load up to failure at corner joints for high eccentricity test

Table 2.8 Crack width at different loading levels for high eccentricity test

Eccentric Load (kN)	0	40	50	60	70	80	100	110	120
Average Crack Width (mm)	0.05	0.14	0.15	0.20	0.24	0.28	0.44	0.48	0.52

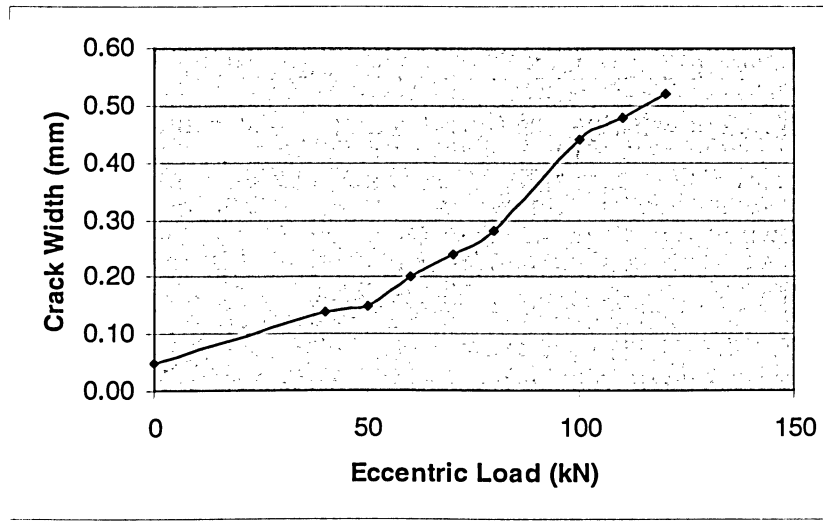

Figure 2.39 Crack width versus eccentric load for high eccentricity trial

2.3.2 FRP Retrofitted High Eccentricity Test

As mentioned earlier, the first trial of high eccentricity test was prematurely stopped due to failure at corner joints. It was premature in a sense that tensile reinforcement stresses did not reach the yield point. As a matter of fact the section was subjected to nearly 3/4 of its total loading capacity. This can be interpreted as reasonably sufficient for observing the behavior of liquid containing structures under service load, however, obtaining a comprehensive data from laboratory test that can cover a complete range of loading circumstances is always a main concern. Hence, in order to be able to perform a complete test up to the level of tensile steel failure, previously failed U-shape specimen was retrofitted by means of glass FRP only at the corner joints where deep cracks were originating from. The procedure of FRP application was exactly the same as the one explained earlier in the direct tension test. In addition to implementing a complete test, this phase could reveal the effectiveness of glass FRP application in recovering or strengthening structures loading capacity. As depicted in Figure 2.40, the FRP matte was placed orthogonal to the crack direction at corner joints. This would help to transmit the stresses from protruded arms to the slab across the crack. It should be noted that

specimen could only be reinforced at its surface by means of glass FRP and some discontinuity still remained deep inside the joint. As a result of this, although the application of FRP was beneficial in increasing the overall capacity, the risk of failure at corner joints inevitably remained crucial.

The test procedure was identical to what was performed in the first incomplete trial. Interestingly, this time the eccentric tensile load reached up to the level of 148 *kN* upon which the structure failed to carry any more load. This was nearly 30 *kN* more than previous maximum exerted load. Bar strain history is shown in Figure 2.41. It can be seen that while the strain at S5 exceeded the nominal yield strain 2000 με, the strain at other locations were not reached the yield level. The failure mechanism was again at corner joints and the objective of failure at slab section could not be achieved. However, this test has proved the outstanding efficiency of glass FRP in improving and strengthening damaged concrete structures. Concrete strain history is shown in Figure 2.42. All strain sensors attached to the bottom face of the slab and the bottom reinforcement layer were showing negative strain values, meaning that the bottom fiber of the section was under compression and the neutral axis was slightly above the bottom reinforcement layer. Recorded crack widths at different load steps are shown in Table 2.9 and drawn in Figure 2.43. The minute discrepancy between the crack width values of this test and that of the previous trial could be due to the remained plastic strain, measurement of dissimilar cracks or human errors. Water leakage did not occur at any stage of the test due to the fact that cracks did not penetrate deeply into to the section, and hence lower portion of the section remained intact from cracking. Once again it is proved that flexural cracks with the crack width of even as wide as 0.50 *mm* could not be a concern in liquid containing structures regarding the problems related to liquid tightness.

Figure 2.40 The final set-up for FRP retrofitted high eccentricity test

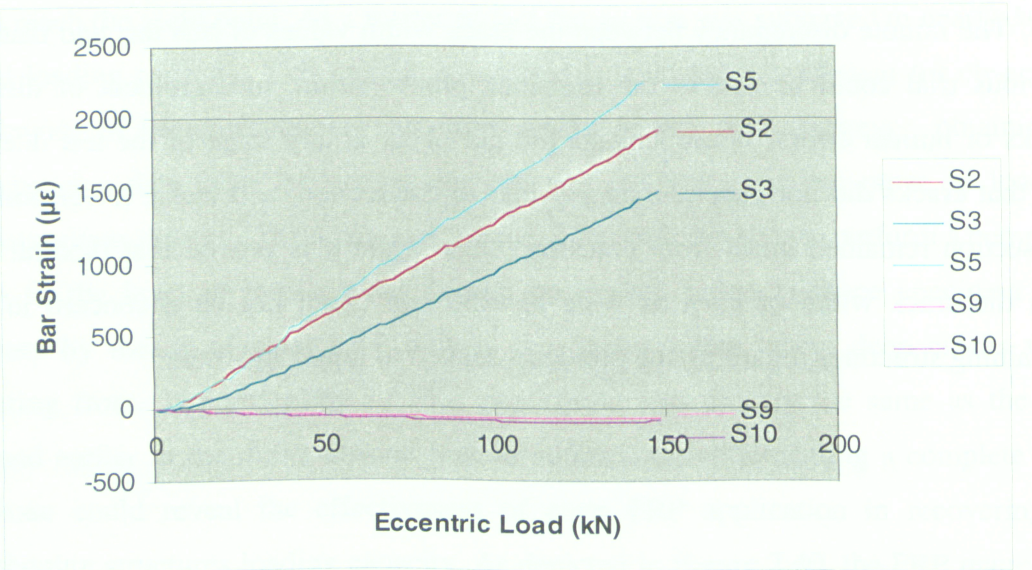

Figure 2.41 Bar strain versus eccentric load up to corner joint failure for FRP retrofitted high eccentricity test

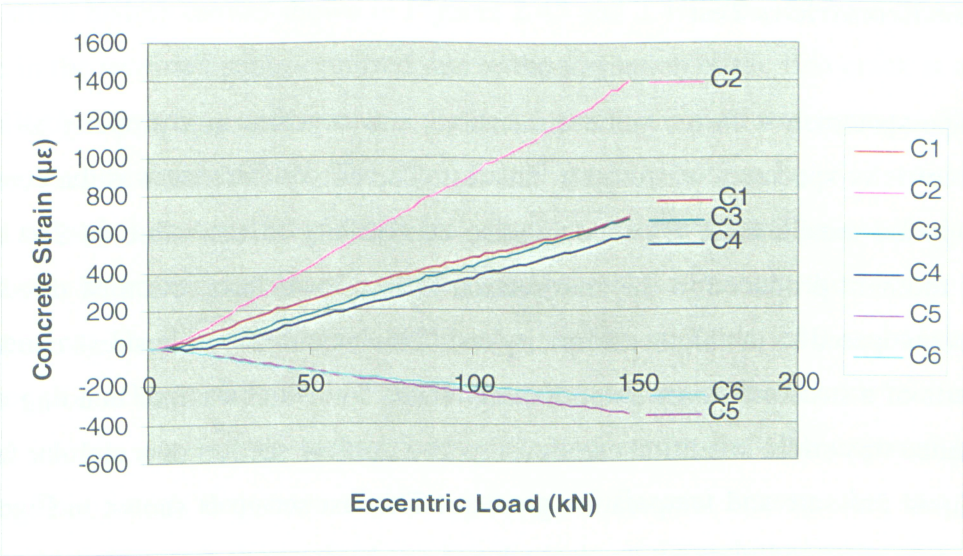

Figure 2.42 Concrete strain versus eccentric load up to corner joint failure for FRP retrofitted high eccentricity test

Table 2.9 Crack width for FRP retrofitted high eccentricity test

Eccentric Load (kN)	0	10	20	30	40	50	60	80	100	120	140	150
Crack Width (mm)	0.10	0.15	0.18	0.20	0.20	0.20	0.21	0.22	0.29	0.36	0.44	0.50

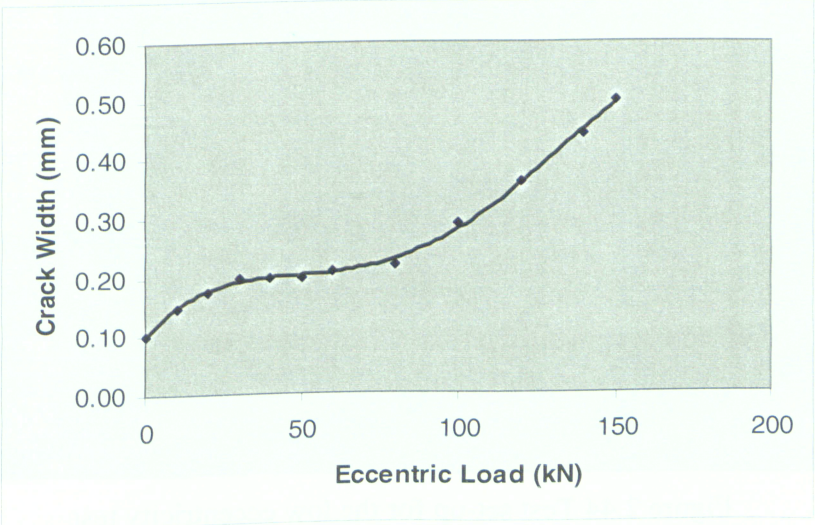

Figure 2.43 Crack width versus eccentric load for FRP retrofitted high eccentricity test

2.3.3 Low Eccentricity Test

A U-shape specimen with the same dimensions and concrete mix property as those of high eccentricity specimen was used in this test. The only difference was the eccentricity of the applied tensile load. By reducing the eccentricity to the value of 250 *mm*, the bending moment produced in the slab section is in a lower proportion of direct tensile forces as compared to the high eccentricity test. This would resemble stress conditions at some parts of a structure under a dominating tensile force and a minor bending moment. For instance this stress condition can develop in a vertical section of a circular tank wall under liquid pressure and temperature gradient. The test set-up is shown in Figure 2.44. The test was executed with similar procedure and objectives to that pursued in previous tests.

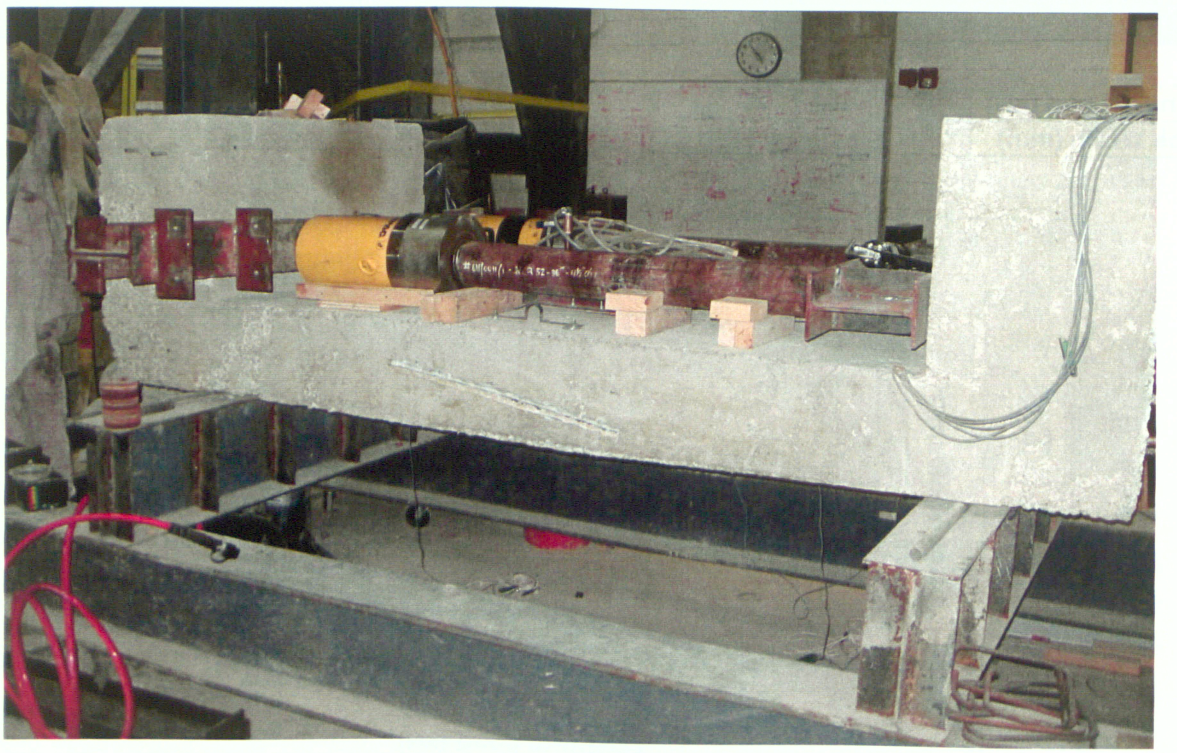

Figure 2.44 Test set-up for the low eccentricity test

In both strain history curves shown in Figures 2.45 and 2.46, it can be seen that a sudden increase in the recorded strain occurred due to the formation of the first crack at a load of about 110 *kN*. The steel reinforcements yielded at the location of strain gauges S2 and S5 under the load of about 250 *kN*. The sign of steel strain at bottom layer of reinforcement changed at loads between 150 and 200 *kN*, which means the neutral axis shifted down as the load was increased and the depth of existing cracks surpassed the bottom layer of reinforcement. The measured crack widths are shown in Table 2.10 and Figure 2.47. Even though cracks as wide as 0.52 *mm* and as deep as below the bottom reinforcement occurred in this test, yet no leakage was observed across the slab exposed to water pressure. This means that even slightest amount of flexural stresses that can produce compression field across the section, can prevent leakage through the crack.

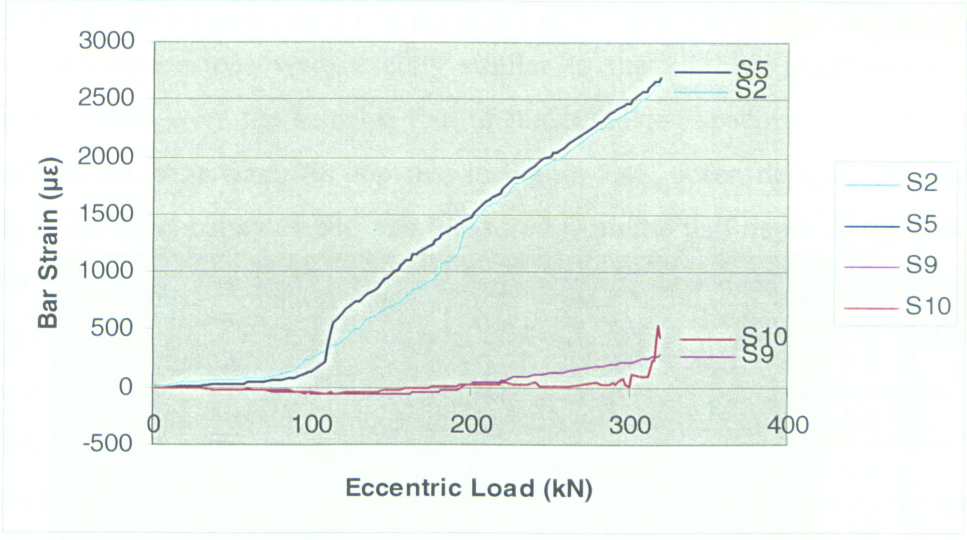

Figure 2.45 Bar strain versus eccentric load for low eccentricity test

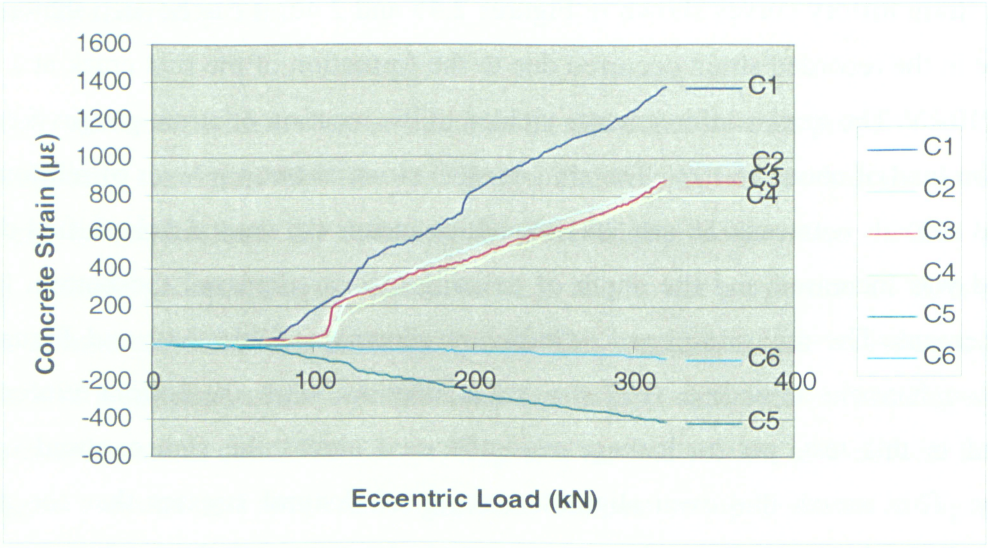

Figure 2.46 Concrete strain versus eccentric load for low eccentricity test

Table 2.10 Crack width for low eccentricity test

Eccentric Load (kN)	110	140	160	180	200	220	240	260	280	300	320
Crack Width (mm)	0.10	0.30	0.38	0.38	0.40	0.40	0.43	0.48	0.49	0.52	0.52

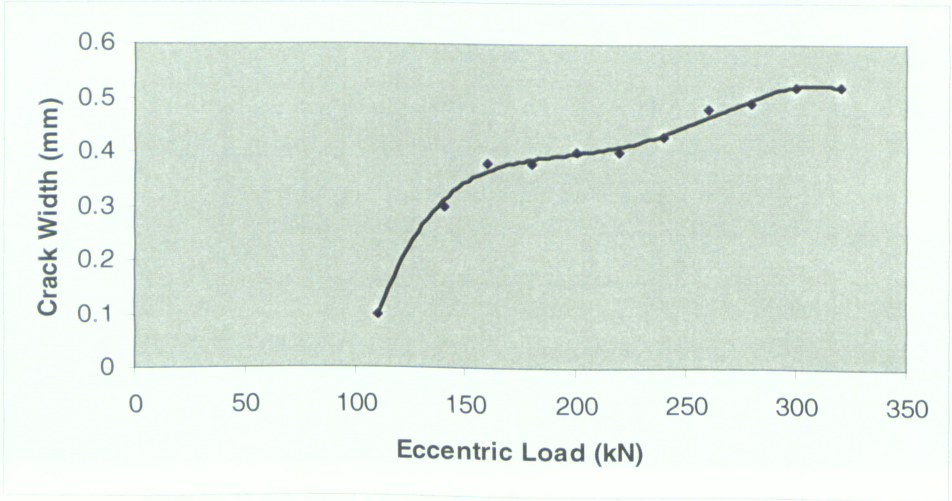

Figure 2.47 Crack width versus eccentric load for low eccentricity test

2.4 Combined Flexure, Tension and Shear

The main goal of this research study was to investigate the cracking behavior of concrete under variety of stress combinations. For this reason, another test was conducted under a different combination of stresses in an attempt to acquire further insight into the subject. This time internal shear forces were introduced in the slab section in addition to the previously applied tensile and flexural forces. At some parts of a liquid retaining tank, shear forces can be several times larger than any other type of forces. For instance very large shear stresses can exist at the base of a fixed base water tank especially in case of circular water tanks. However, as long as the section is adequately designed to carry the applied shear forces, shear cracks can hardly occur. Shear cracks are in the form of diagonal cracks that can penetrate in full depth of the section. Their prevention must be one of the priorities for a designer as they can be severely detrimental for the structure. The intention of this test is not to produce shear cracks but rather to see the influence of shear stresses on the formation of flexural cracks.

The specimen dimensions were exactly similar to that of high eccentricity test. The concrete properties were the same as that of direct tension specimen as both specimens were made at the same time. As depicted in Figure 2.48, eccentric hydraulic jacks were placed with the eccentricity of 540 *mm* measured from the half depth of the slab section. The shear load was introduced by means of a hydraulic jack placed underneath the slab at its mid-span. The test set-up can be seen in Figure 2.49. The specimen was seated on two I-beams at the end supports (roller pipes were used in-between to provide free to slide condition), and it was tightly secured to the top of the frame by means of two I-beams placed on top of protruded arms. All strain gauges were installed and connected to the data acquisition system.

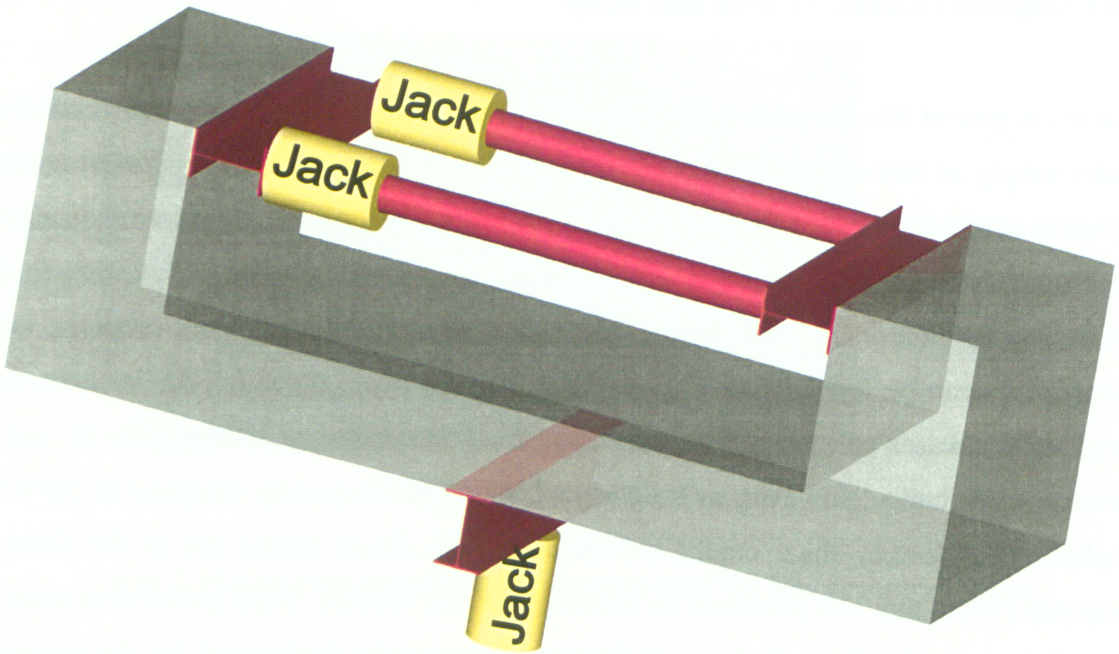

Figure 2.48 Combined test specimen and hydraulic jacks positioning

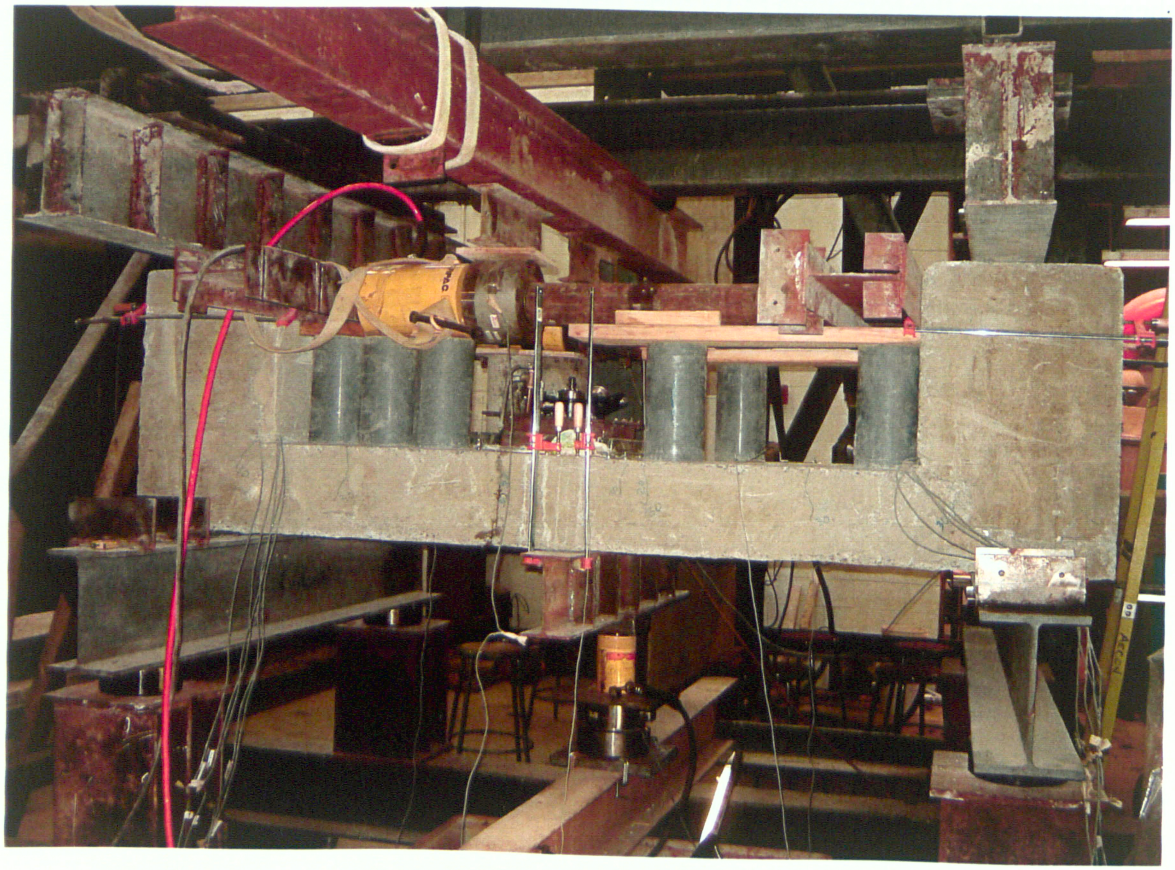

Figure 2.49 Combined test set-up

It was decided for the shear load and the eccentric load to be applied in proportion of 1 to 4. The eccentric load was increased in 10 *kN* increments, and the shear load increased in a constant proportion of eccentric load at all times. As the load was increased the first two cracks initiated simultaneously at an eccentric load of about 40 *kN* (a shear load of 10 *kN*) close to the mid-span on both sides of the shear load. They were labeled with north and south names and their width were measured with a crackscope the results of which are shown in Table 2.11. The eccentric load was raised up to the magnitude of 60 *kN*, upon which the specimen was unloaded for the installation of the water pressure chamber. Steel and concrete strain histories up to this point are shown in Figures 2.50 and 2.51 respectively. The sudden jump in strain readings can be evidently noticed at an eccentric load of about 40 *kN* due to the first crack initiation. Not a significant difference can be seen between the crack initiation load of this test and that of the high eccentricity test. This reveals the minor influence of mid-span load on the bending moment, as the load of this magnitude was mostly counteracted by the weight of specimen.

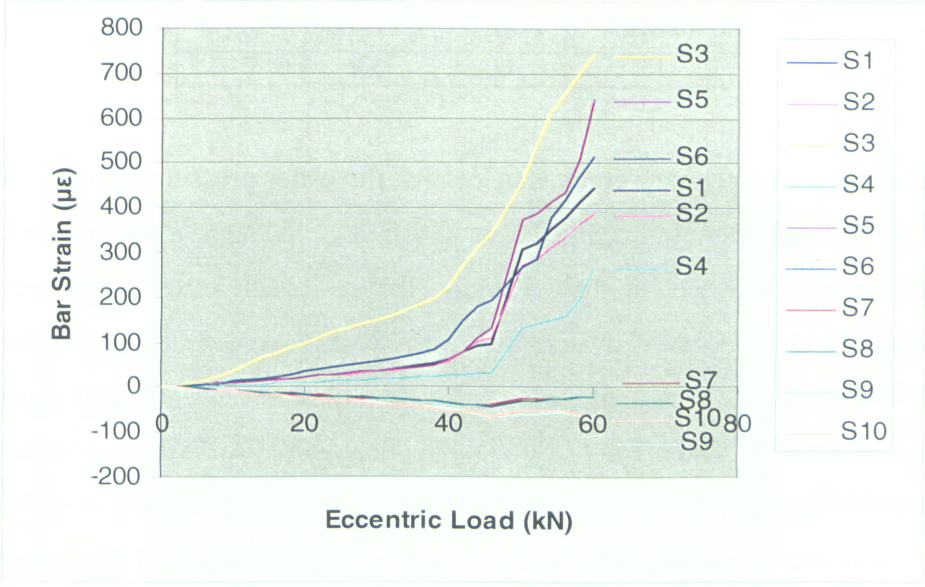

Figure 2.50 Bar strain versus eccentric load for combined test (initial part)

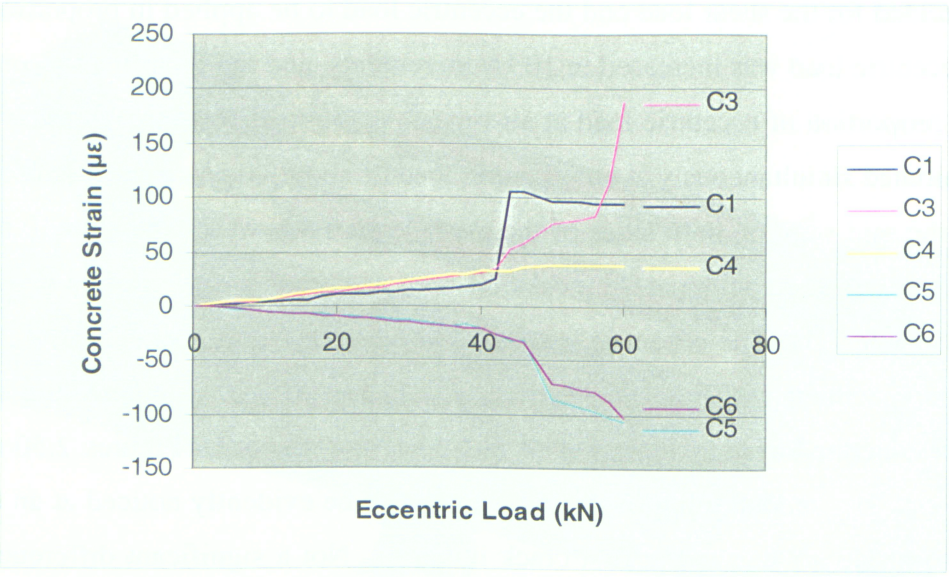

Figure 2.51 Concrete strain versus eccentric load for combined test (initial part)

Table 2.11 Crack width for initial part of combined test

Mid-span Load (kN)	Eccentric Load (kN)	Crack Width (mm)	
		North	South
10	40	0.1~0.15	0.1
15	60	0.2	0.15~0.2

When the location of a primary crack was known, the water pressure chamber was placed on top of it. The chamber was again sealed in the same manner as before, and after that the installation was finished, the test was ready to re-launch under water pressure. The load was applied in the same way as before. New cracks were developed as the load was increased. The steel reinforcement yielded at a load of about 160 *kN* as it can be seen in Figure 2.52. According to the bar strain history, the sign of steel strain at bottom layer of reinforcement changed at loads about 100 *kN*, which means the neutral axis shifted down as the load was increased and the depth of existing cracks surpassed the bottom layer of reinforcement. Concrete strain history is shown in Figure 2.53. Water leakage through the slab section was not observed even for a crack width as wide as 0.6 *mm*. The eccentric load was raised up to the magnitude of 170 *kN*. The test was stopped at this point due to the creation of wide cracks at the corner joints of specimen that would prevent the

structure from carrying any more loads. The widths of cracks were measured at each loading stage, the results of which are gathered in Table 2.12 and drawn in Figure 2.54. During this test, 13 cracks were formed along the slab with minimum, maximum and average spacings of 80, 275 and 154 *mm* respectively.

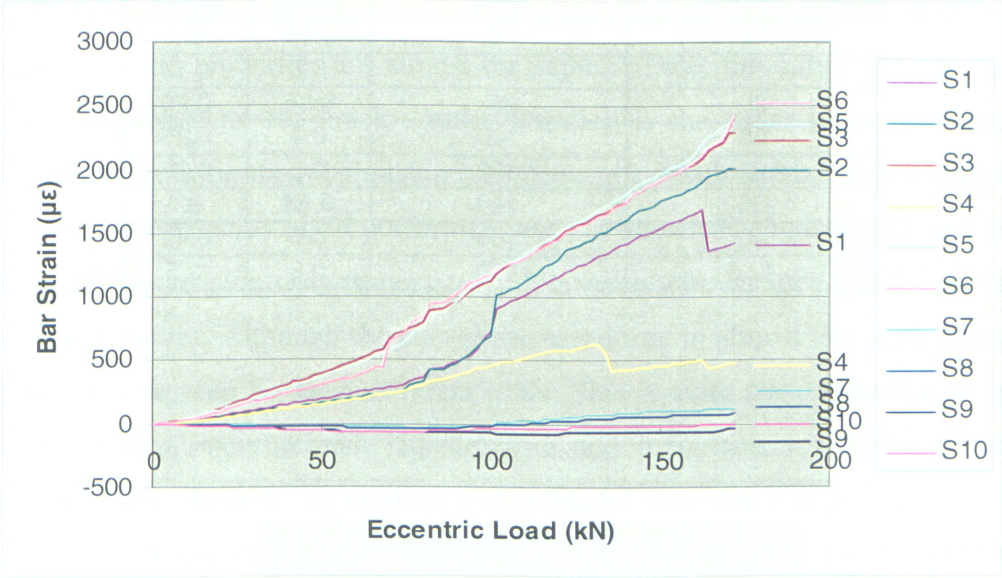

Figure 2.52 Bar strain versus eccentric load for combined test (second part)

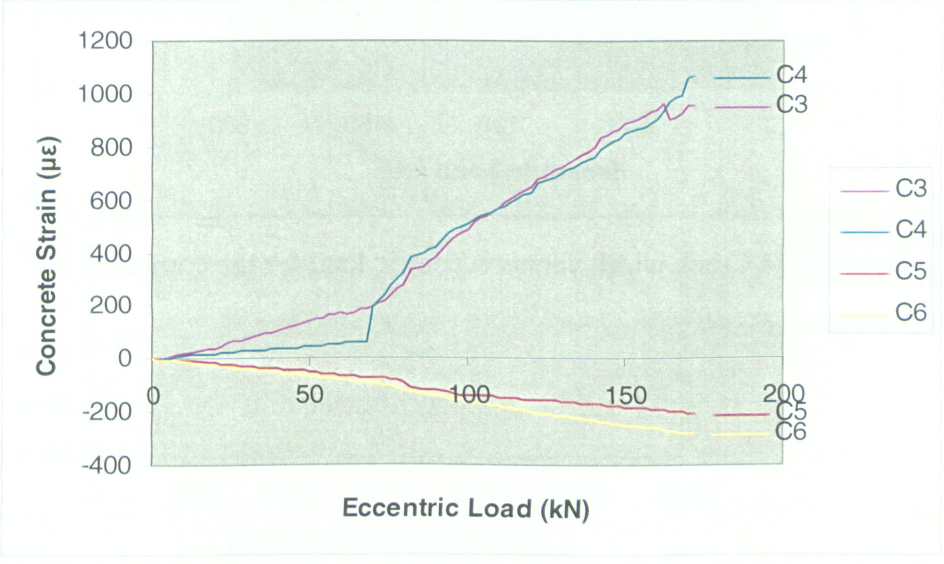

Figure 2.53 Concrete strain versus eccentric load for combined test (second part)

Table 2.12 Crack width for second part of combined test

Mid-span Load (kN)	Eccentric Load (kN)	Crack Width (mm)	
		North	South
10	40	0.15	0.1
15	60	0.2	0.15
20	80	0.35	0.25
25	100	0.4	0.35
30	120	0.5	0.35
35	140	0.56	0.4
40	160	0.6	0.45
42.5	170	0.6	0.5

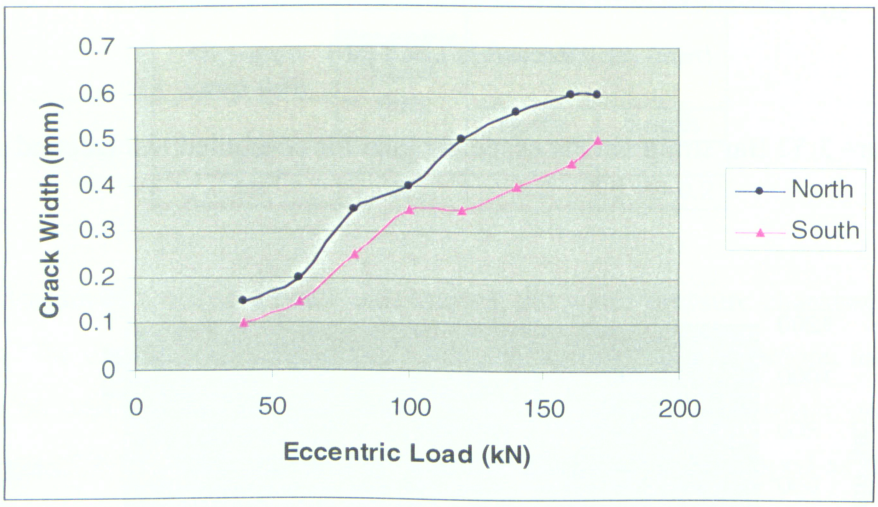

Figure 2.54 Crack width versus eccentric load for the combined test

2.5 Correlation between Crack Width and Steel Stress/Strain

According to the results of numerous experimental and analytical studies, the crack width is found to have a close relation with several factors, some of which are concrete cover, reinforcement spacing, bar diameter, bond stress and reinforcement stress. For all tests that are reported in this research study, the section dimensions, reinforcement ratio and layout and concrete properties are almost the same. Hence, the only parameter that can have major influence on the crack widths variation is the stress in reinforcement. To establish this correlation the relationship between crack width and bar strain must be first drawn based on the results of all performed tests, as shown in Figures 2.55 and 2.56 for flexural and direct tension tests respectively. The maximum detected bar strains are used to create these curves. Although the curves are ascending in almost the same trend, some discrepancy can be seen between different trials. This is quite reasonable due to possible human, equipment, measurement, construction and manufacturing errors or material property variations. In order to produce a meaningful data that can be used as a design guideline a best-fit line of the entire scattered values is drawn separately for each type of cracks, as shown in Figure 2.57. Although, the volume of data obtained from a few number of tests are small and a bigger scale of information is needed to produce a reliable design guideline, the final result is meaningful and can be expanded by including more relevant experimental data in this statistical computation.

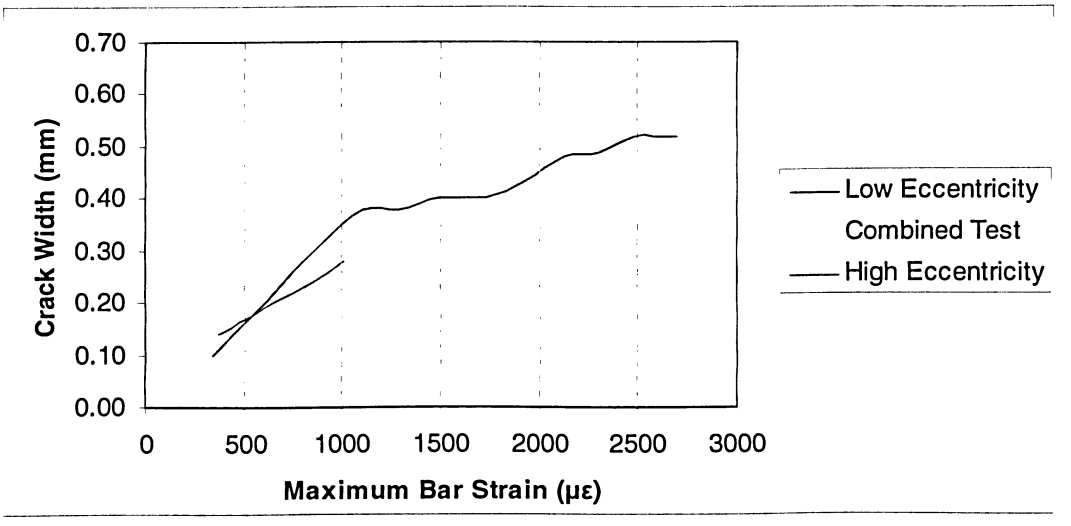

Figure 2.55 Crack width and maximum bar strain correlation for flexural cracks

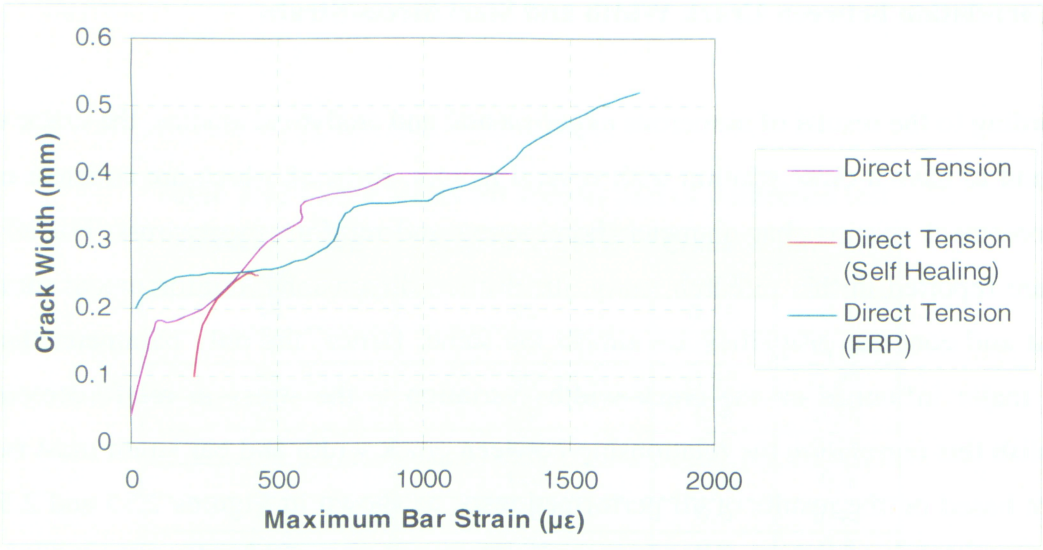

Figure 2.56 Crack width and maximum bar strain correlation for direct tension cracks

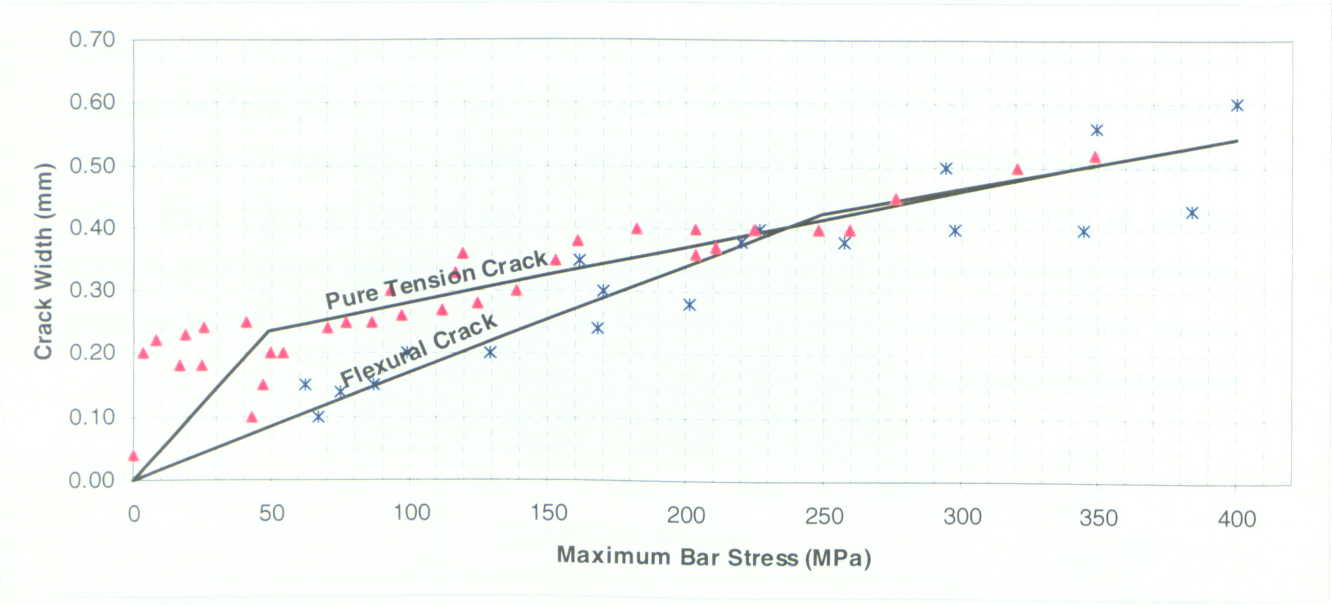

Figure 2.57 The crack width and the maximum bar stress correlation for sections with properties similar to those of tested slab

Tensile and flexural crack widths are used separately for drawing best-fit lines in Figure 2.57. These best-fit lines can be used to restrict the crack width to a certain limitation. For instance, to reduce the likelihood of cracks wider than 0.30 *mm* the stress in reinforcing steel at all times must be limited to the maximum of 180 *MPa* for flexural cracks under service load and to the maximum of 120 *MPa* for direct tension cracks. This means that

the steel stress limitation is more restrict for direct tensile induced cracks than for flexural cracks. The post-cracking stress in steel can be calculated based on the analytical analysis or the finite element modeling which will be explained in the following chapters. According to ACI 224R (2001), the crack width in water retaining structures should be limited to 0.10 *mm*. As it can be seen in Figure 2.57 this crack width limitation can be satisfied for the tested slab section if the stress in tensile reinforcement is limited to 60 and 10 *MPa* for flexural and pure tension cracks respectively. These are very low steel stresses as compared to the total capacity of the section, meaning that the specimen section was not properly designed to satisfy the crack width criterion. Thus, in order to take advantage of the full capacity of the section and limit the crack width at the same time the section attributes had to be modified. For instance the longitudinal reinforcement spacing could be reduced by using higher number of bars for the same reinforcement ratio. Although, ACI 224R does not specify the type of cracks, it is reasonable to use its recommended limitations for flexural cracks in water-retaining structures only and not for the direct tensile cracks. This is because even the smallest direct tensile induced cracks are full depth cracks that can provide a passage for liquid to the inside or outside of the structure. Therefore, the formation of this type of cracks can be critical and should be strictly limited in liquid containing structures. Even though, very narrow tensile cracks were shown to be able to seal themselves by autogenous healing process, the test was in laboratory condition and under steady tensile load. Therefore, it is possible that the healing may not occur in the real structure due to unsteady tensile forces or previously healed cracks re-open due to cyclic load effects.

2.6 Summary

Several experimental tests were performed and the results were reported in this chapter. The main goal of this experimental investigation was to explore the cracking behavior of concrete under different circumstances. Different stress combinations were introduced in the section and the responses of concrete specimens were closely monitored. The primary concern of the this study was related to crack control in liquid containing structures, thus,

the problem of water leakage was examined in each of these trials. Several valuable conclusions were arrived at in this exploration, and they are summarized as follows:

- The stress in steel reinforcement at cracked sections suddenly increases once the concrete cracks.
- Direct tensile cracks are full depth cracks that can raise water leakage problem even when their width is as low as 0.04 *mm*, and hence, their possible formation in the liquid containing structures must be avoided.
- A tensile crack as wide as 0.25 *mm* can partially heal itself through autogenous healing process, considering that the crack width is kept constant under a steady tensile load and there is a positive water flow through cracks at all times.
- The application of one layer of glass FRP on the concrete cracked surface can effectively stop water leakage under at least 0.5 *bar* $\left(5\times10^{4}\,Pa\right)$ water pressure and even after yielding of steel reinforcement.
- The presence of glass FRP has no significant influence in reducing the width of existing cracks at lower loads prior to yielding of reinforcement.
- Glass FRP can effectively be used to recover the strength of severely damaged members in a structure.
- Flexural cracks are not a major concern in regard to leakage problem, as the liquid can not pass through this type of cracks due to the presence of compression zone in the section. Therefore, a slightest amount of flexural stress that can produce compression zone across the section can prevent leakage through the crack.
- Crack width is very dependant on the stress in reinforcement. Providing that section properties are kept the same, the stress in reinforcement is the most important parameter with direct relation to the crack width.

CHAPTER 3

CRACK PREDICTION MODELS

3.1 General

As explained in section 1.2, several different formulations have been proposed by a number of researchers to predict the crack width and crack spacing. This diversity is an indication of the complex behavior inherent in concrete or any other composite material. The randomness in concrete cracking behavior was also experienced during the experimental investigation of this study. In this chapter, the more recent crack prediction analytical models proposed by Gilbert (2005) and Frosch (1999) and some earlier models such as Gergely and Lutz (1968), and Broms and Lutz (1965) are adapted for further investigation and assessment. Also the approaches of some design codes such as CEB-FIP (1990) and Euro EC2 (1997) toward crack control are examined.

3.2 Concrete Slab under Combination of Tension and Flexure

As reported in previous chapter, two similar U-shape specimens were tested under two different applied load eccentricities. In the following, crack widths and crack spacings are calculated analytically for each of these trials and a comparison is made with the experimental results.

3.2.1 High Eccentricity Test ($e = 525mm$)

The definition and specifications of this experimental test are provided in the previous chapter and will be used in the analytical calculation. The loading configuration and the specimen dimensioning are illustrated in Figure 3.1. The slab section properties and dimensioning are depicted in Figure 3.2. The same slab section was used in all empirical test specimens. The following calculation shows the step by step procedure of estimating the crack width.

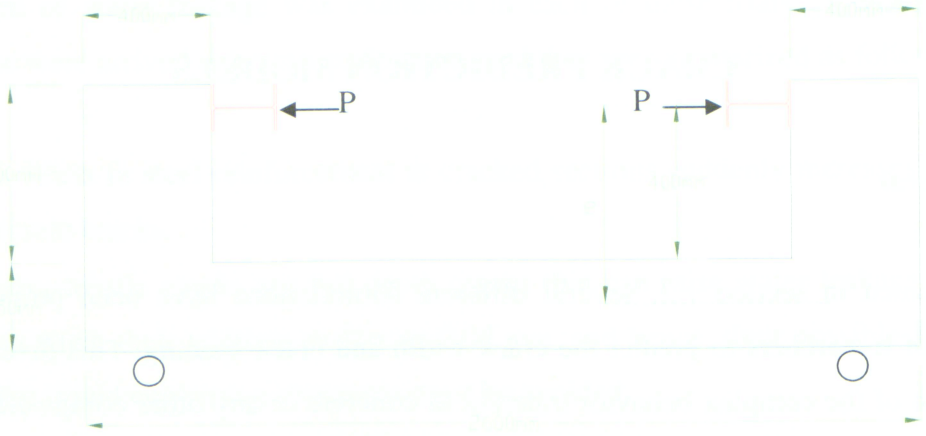

Figure 3.1 Loading configuration of high eccentricity test

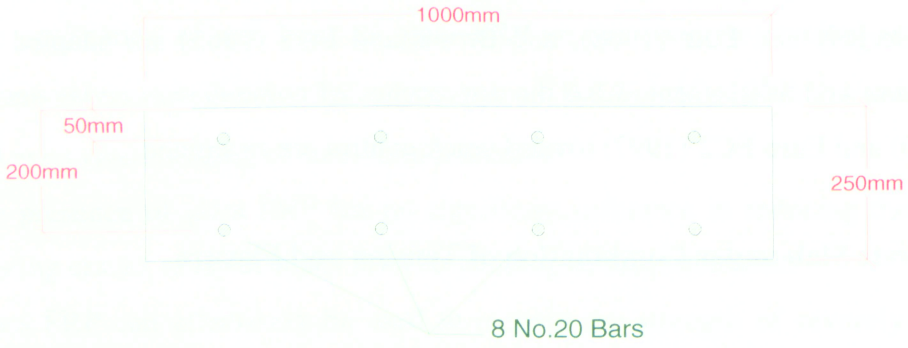

Figure 3.2 Slab section

In order to find the relationship between the crack width and the load, the first step is to determine the force at which the concrete slab will crack.

The modulus of elasticity of concrete can be estimated based on its compressive strength. According to ACI 209R (1992):

$$E_c = g_{ct}\left[\gamma_c^{\,3} f_c'\right]^{1/2} \tag{3.1}$$

in which E_c= modulus of elasticity of concrete; γ_c = unit weight of concrete (Kg/m^3); f_c' = compressive strength of concrete (MPa); and g_{ct} = 0.043.

Thus, $E_c = 0.043\left(2300^3 \times 25\right)^{1/2} = 23715 \quad MPa$

The modular ratio of steel and concrete will be:

$$n = \frac{E_s}{E_c} = \frac{200000}{23715} = 8.43$$

Based on the slab section shown in Figure 3.2, the transformed un-cracked section is drawn in Figure 3.3. The neutral axis lies at the mid-height of the section due to symmetry. Moment of inertia of the un-cracked section (I_{gt}) is calculated as:

$$I_{gt} = \frac{bh^3}{12} + (n-1)A_s d_1^2 \qquad (3.2)$$

$$\Rightarrow I_{gt} = \frac{1000 \times 250^3}{12} + (8.43-1) \times 8 \times 300 \times 75^2 = 1.4 \times 10^9 \quad mm^4$$

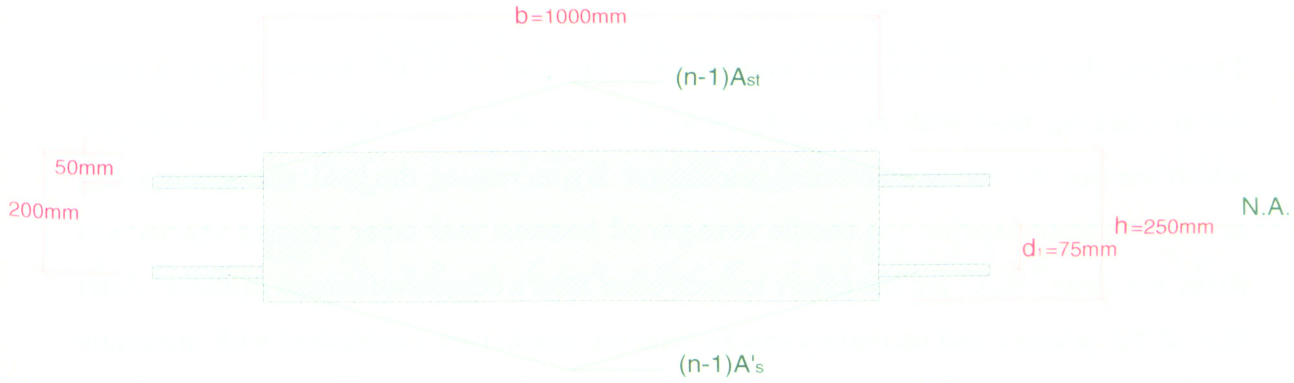

Figure 3.3 Transformed un-cracked section

Since the slab is carrying bending moments, the tensile strength of the concrete can be taken as its modulus of rupture (f_r), which according to ACI 209R (1992) can be approximated as follows:

$$f_r = g_r[wf_c']^{1/2} \tag{3.3}$$

in which $g_r = 0.012$ to 0.021 (the lowest value is used in here).

$$\Rightarrow f_r = 0.012\times[2300\times25]^{1/2} = 2.87 \quad MPa$$

The self-weight of the concrete slab produces some bending moment which is in favor of the crack closure. Therefore, the critical section for crack initiation is somewhere close to the end supports, where the bending moment caused by the slab self-weight is negligible. Stress at the extreme tension fiber of concrete section at a critical section can be found by combining flexural and tensile stresses as follows:

$$\sigma_{ct} = \frac{MY}{I} + \frac{P}{A} = \left[\frac{eh}{2I_{gt}} + \frac{1}{(n-1)(A_{st}+A_s')+bh}\right]\times P \tag{3.4}$$

$$\Rightarrow 2.87 = \left[\frac{525\times250}{2\times1.4\times10^9} + \frac{1}{(8.43-1)(1200+1200)+1000\times250}\right]\times P \;\Rightarrow\; P = 56709N = 56kN$$

Therefore, the first primary crack may occur at the load of 56 *kN*. Interestingly, a close initial cracking load with magnitude of 42 *kN* was observed during experimental test which verifies the above theoretical calculation. By increasing the load, the tensile stress at other sections reaches the tensile strength of concrete and other primary cracks will form, but these cracks are not closer to each other than a certain minimum distance. After that all the primary and secondary cracks (internal cracks) are established with minimum spacing, no more crack occurs, but the width of existing cracks still increases with the increase in the load. In order to find relationship between the crack width and the applied load, the stress in tensile reinforcement is needed. Accordingly, the compression chord depth (kd) at the cracked section, shown in Figure 3.4, must be determined first. Assuming a stress/strain distribution across a cracked section similar to that shown in

Figure 3.5, several equations can be written based on strain compatibility and internal force equilibrium as follows:

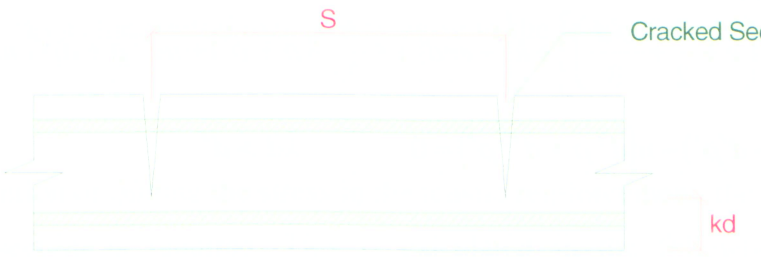

Figure 3.4 Schematic of crack spacing and the compression chord depth

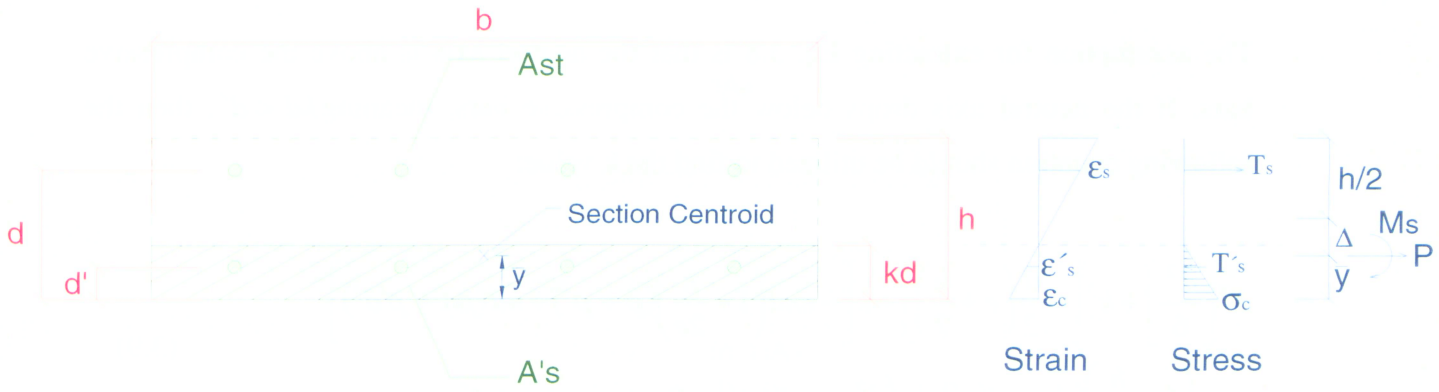

Figure 3.5 Stress/strain at the cracked section

$$\frac{\varepsilon_s}{d-kd}=\frac{\varepsilon_s'}{kd-d'}=\frac{\varepsilon_c}{kd}\ \rightarrow\ \frac{\varepsilon_s}{\varepsilon_c}=\frac{1-k}{k}\ ,\ \frac{\varepsilon_s'}{\varepsilon_c}=\frac{kd-d'}{kd} \tag{3.5}$$

$$T_s-T_s'-\sigma_c\left(\frac{kdb-A_s'}{2}\right)=P\ \rightarrow\ E_s\varepsilon_s A_{st}-E_s\varepsilon_s' A_s'-E_c\varepsilon_c\left(\frac{kdb-A_s'}{2}\right)=P \tag{3.6}$$

The eccentric load P is transmitted to the centroid of the cracked section as it is shown in Figure 3.5. Sum of internal moments about the mid-height of the section should be equal to the sum of external moments about the same point, therefore:

$$E_s\varepsilon_s A_{st}\left(d-\frac{h}{2}\right)+E_s\varepsilon_s' A_s'\left(\frac{h}{2}-d'\right)+E_c\varepsilon_c\left(\frac{kdb-A_s'}{2}\right)\times\left(\frac{h}{2}-\frac{kd}{3}\right) \tag{3.7}$$
$$=M_s-P\Delta=P(e+\Delta)-P\Delta=Pe$$

Solving equations (3.5), (3.6) and (3.7) simultaneously for the value of k results in a cubic equation in terms of k as follows:

$$k^3\left[\frac{d^2}{6}\right]+k^2\left[-\frac{d}{2}\left(e+\frac{h}{2}+\frac{\rho' d}{3}\right)\right]+k\left[-end\left(1+\frac{h}{2e}\right)(\rho+\rho')+nd^2\rho+d\rho'\left(nd'+\frac{h}{4}+\frac{e}{2}\right)\right]$$
$$+en\left(1+\frac{h}{2e}\right)(d\rho+d'\rho')-n(d^2\rho+d'^2\rho')=0 \qquad kd>d' \qquad (3.8)$$

in which $\rho=\frac{A_{st}}{bd}$; $\rho'=\frac{A_s'}{bd}$

The assumption for extracting Eq. 3.8 is that the neutral axis is above the compressive bars. If the neutral axis drops below the compressive bars, meaning $kd<d'$, then the following equation should be utilized to find the k value:

$$k^3\left[\frac{d^2}{6}\right]+k^2\left[-\frac{d}{2}\left(e+\frac{h}{2}\right)\right]+k\left[-end\left(1+\frac{h}{2e}\right)(\rho+\rho')+nd(\rho d+\rho' d')\right]$$
$$+en\left(1+\frac{h}{2e}\right)(d\rho+d'\rho')-n(d^2\rho+d'^2\rho')=0 \qquad kd<d' \qquad (3.9)$$

Solving the above cubic equation, the value for k can be determined. For the current experiment all parameters are defined as follows:

$d=200 \ \ mm$
$d'=50 \ \ mm$
$e=525 \ \ mm$
$n=8.43$
$\rho=\frac{4\times300}{1000\times200}=0.006$
$\rho'=\frac{4\times300}{1000\times200}=0.006$

From Eq. 3.8 the value for k is found to be 0.239, and $kd = 47.8mm$ which is not more than $d' = 50 \ mm$; therefore, the Eq. 3.9 must be used, from which the k value can be found as 0.237 and $kd = 47.4mm$. Not much difference is between the results of these two formulations as the neutral axis is very close to the level of the bottom reinforcement layer.

With the intention of finding the stress in the tensile reinforcement, the moment of inertia of cracked section is required. This is calculated in the following, based on the transformed cracked section depicted in Figure 3.6.

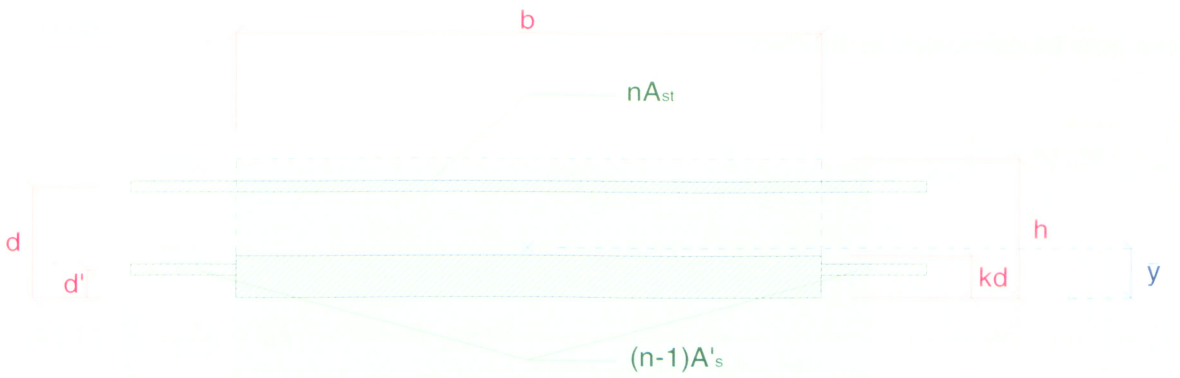

Figure 3.6 Transformed cracked section

The centroid of the cracked section is computed as:

$$\bar{y} = \frac{nA_{st}d + (n-1)A'_s d' + bk^2 d^2/2}{nA_{st} + (n-1)A'_s + bkd} \qquad kd > d' \tag{3.10}$$

Or,

$$\bar{y} = \frac{nA_{st}d + nA'_s d' + bk^2 d^2/2}{nA_{st} + nA'_s + bkd} \qquad kd < d' \tag{3.11}$$

Therefore, from Eq. 3.11, the centroid of the cracked section is found to be $\bar{y} = 54 \ mm$.

The moment of inertia of the cracked section can be expressed as:

$$I_{cr} = \frac{bk^3d^3}{12} + bkd\left(\bar{y} - \frac{kd}{2}\right)^2 + nA_{st}(d-\bar{y})^2 + (n-1)A_s'(\bar{y}-d')^2 \qquad kd > d' \qquad (3.12)$$

Or,

$$I_{cr} = \frac{bk^3d^3}{12} + bkd\left(\bar{y} - \frac{kd}{2}\right)^2 + nA_{st}(d-\bar{y})^2 + nA_s'(\bar{y}-d')^2 \qquad kd < d' \qquad (3.13)$$

Substituting the values into Eq. 3.13, the moment of inertia of cracked section is $I_{cr} = 2.682\times10^8 \ \ mm^4$. The force in the tensile reinforcement at the cracked section can now be calculated as follows:

$$T_s = \frac{M_s(d-\bar{y})}{I_{cr}} nA_{st} + \frac{P}{nA_{st} + (n-1)A_s' + bkd} nA_{st} \Rightarrow$$

$$T_s = \left[\frac{\left(e + \frac{h}{2} - \bar{y}\right)(d-\bar{y})}{I_{cr}} + \frac{1}{nA_{st} + (n-1)A_s' + bkd}\right] \times nA_{st}P \qquad kd > d' \qquad (3.14)$$

Or,

$$T_s = \left[\frac{\left(e + \frac{h}{2} - \bar{y}\right)(d-\bar{y})}{I_{cr}} + \frac{1}{nA_{st} + nA_s' + bkd}\right] \times nA_{st}P \qquad kd < d' \qquad (3.15)$$

Consequently, for this test, the tensile force in top reinforcement layer at the cracked section is related to eccentric tensile load P as follows:

$$T_s = \left[\frac{\left(525 + \frac{250}{2} - 54\right)(200-54)}{2.682\times10^8} + \frac{1}{8.43\times1200 + 8.43\times1200 + 1000\times0.237\times200}\right] \times 8.43\times1200\times P$$

$$T_s = 3.43P \qquad T_s < f_y A_{st}$$

As it has been shown, there exists a linear relation between the external load and the tensile force in the steel reinforcement as long as the concrete compression chord and the tensile reinforcement are in their elastic state. This is a reasonable assumption for liquid containing structures under service load, meaning the section should be adequately reinforced to prevent the yielding of reinforcement. Yielding can lead to formation of excessive crack width, which is not desirable in liquid containing structures. The comparison between the analytically calculated reinforcement strain and the empirical data is shown in Figure 3.7, while a good agreement can be observed between the two results.

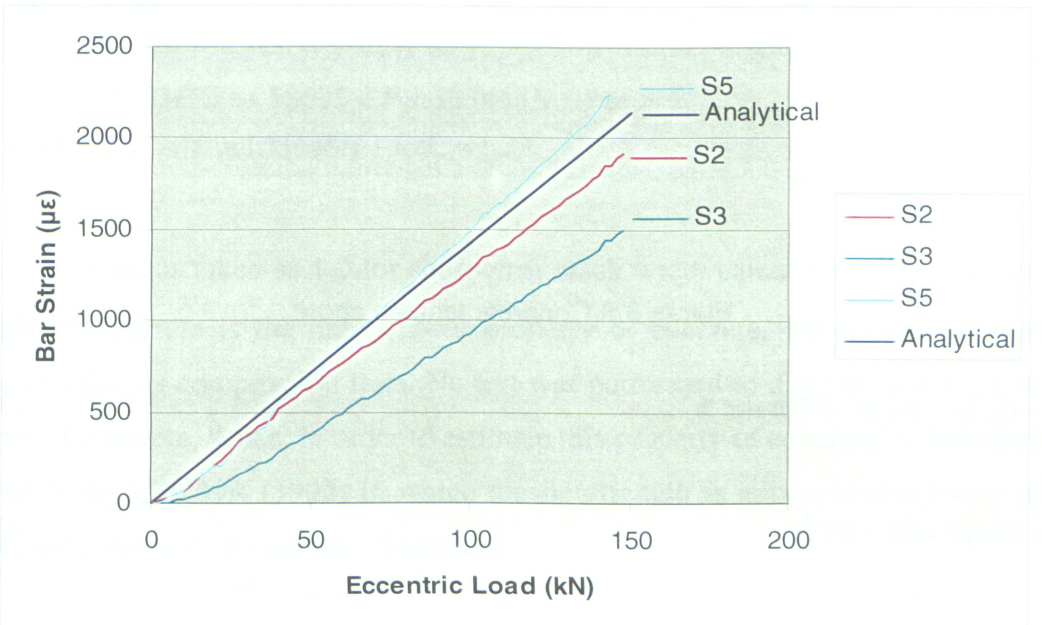

Figure 3.7 Comparison of analytical calculated steel strain and experimental data

Several analytical or statistical models are chosen here to estimate the crack width. These models are primarily based on the strain or stress in the tensile reinforcement which has been determined analytically so far. Therefore, the precision of the estimated crack width basically relies on the accuracy of calculated stress in reinforcement. In the next chapter finite element models (FEM) are shown to be capable of computing the stress or strain in

reinforcement. Compared to analytical results, The FE analysis can be more convenient, accurate and time saving in complex structures. Thus, a comprehensive attempt is made in this study to create an appropriate reinforced concrete FE model. In the following the crack width is estimated for the high eccentricity test according to some well-known flexural crack prediction models.

Gilbert model

According to Gilbert's model (Gilbert, 2005) the area of the concrete tension chord at any section between primary cracks (A_{ct}), as shown in Figure 3.8, is calculated as:

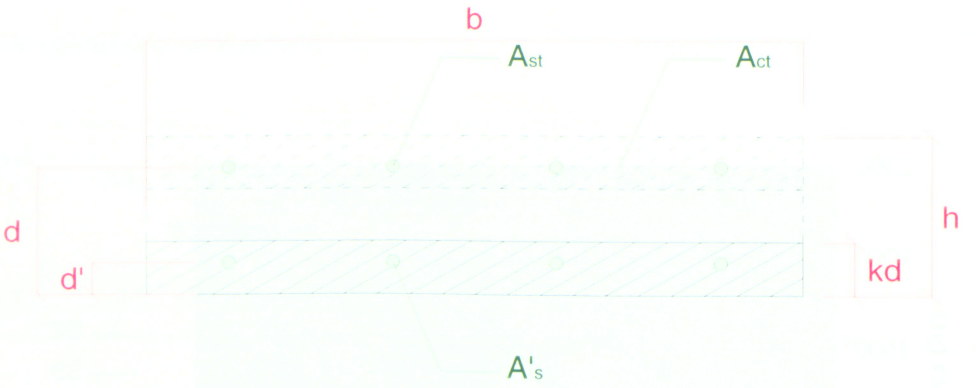

Figure 3.8 Concrete tension chord

$$A_{ct} = 0.5(h - kd)b^* \le 3(h - d)b^* \tag{3.16}$$

$$b^* = \min[b, m(h - kd)] \tag{3.17}$$

in which m is the number of tensile bars.

$$\Rightarrow b^* = \min[1000, 4(250 - 0.237 \times 200)] \rightarrow b^* = \min[1000, 810] \rightarrow b^* = 810 \quad mm$$

$$A_{ct} = 0.5 \times (250 - 0.237 \times 200) \times 810 = 82053 \quad mm^2$$

Bond stress τ_b between the steel and the surrounding tensile concrete is specified as:

$$\tau_b = \alpha_1 \alpha_2 f_{ct} \tag{3.18}$$

where α_1 depends on the steel stress at the crack ($\alpha_1 = 3.0$ when $\sigma_{st} \leq 170MPa$; $\alpha_1 = 2.0$ when $170 < \sigma_{st} < 300MPa$; and $\alpha_1 = 1.33$ when $\sigma_{st} \geq 300MPa$); α_2=1.0 for short-term calculations and α_2=0.5 for long-term calculations; and f_{ct}= direct tensile strength of concrete (MPa).

Therefore, the appropriate value for α_1 must be used in accordance with the stress in tensile bars, as follows:

$$\sigma_{st} = \frac{T_s}{A_{st}} = \frac{3.43P}{1200} = 0.0029P$$

$$\begin{cases} \sigma_{st} \leq 170MPa \rightarrow P \leq 58621N \rightarrow \alpha_1 = 3 \\ 170 < \sigma_{st} < 300MPa \rightarrow 58621 < P < 103448N \rightarrow \alpha_1 = 2 \\ \sigma_{st} \geq 300MPa \rightarrow P \geq 103448N \rightarrow \alpha_1 = 1.33 \end{cases}$$

The value of α_2 is taken as 1.0 for short-term crack width calculation. The compressive strength of concrete is the only known property of concrete, which was obtained by means of cylinder compression tests. No test was performed to directly obtain the tensile strength of concrete, hence, in order to estimate this property of concrete, a formulation is adopted from ACI209R (1992) in which tensile strength is approximated based on the compressive strength of concrete. Therefore:

$$f_{ct} = g_t [\gamma_c f_c']^{1/2} \tag{3.19}$$

in which $g_t = 0.0069$.

$$\Rightarrow f_{ct} = 0.0069[2300(25)]^{1/2} = 1.65 \quad MPa$$

Consequently, from Eq. 3.18 bond stresses at different loading levels are computed as:

$$\tau_b = 3\times1\times1.65 = 4.95 \quad MPa \quad , \quad P \le 58.6kN$$
$$\tau_b = 2\times1\times1.65 = 3.30 \quad MPa \quad , \quad 58.6 < P < 103.4kN$$
$$\tau_b = 1.33\times1\times1.65 = 2.19 \quad MPa \quad , \quad P \ge 103.4kN$$

The maximum crack spacing is twice the distance that is needed for stresses, transmitted from reinforcement through bond stress to the surrounding concrete, to reach the tensile strength of concrete. This can be calculated by integrating bond stresses over the length of tensile bars and set it equal to the tensile strength of concrete. The resulting formulas for the maximum and minimum crack spacing are found to be:

$$S_{max} = \frac{f_{ct}\phi}{2\tau_b\rho_{te}} \quad , \quad S_{min} = \frac{S_{max}}{2} \tag{3.20}$$

in which ϕ = bar diameter; and $\rho_{te} = \frac{A_{st}}{A_{ct}}$.

Therefore, the maximum and minimum crack spacing at each loading stage can be estimated as:

$$S_{max} = \frac{1.65\times19.5}{2\times4.95\times\frac{1200}{82053}} = 222 \quad mm \quad , \quad S_{min} = 111 \quad mm \quad , \quad P \le 58.6kN$$
$$S_{max} = \frac{1.65\times19.5}{2\times3.30\times\frac{1200}{82053}} = 333 \quad mm \quad , \quad S_{min} = 167 \quad mm \quad , \quad 58.6 < P < 103.4kN$$
$$S_{max} = \frac{1.65\times19.5}{2\times2.19\times\frac{1200}{82053}} = 502 \quad mm \quad , \quad S_{min} = 251 \quad mm \quad , \quad P \ge 103.4kN$$

The crack width associated with the maximum crack spacing is the maximum probable crack width. Generally, less crack spacing results in a higher number of cracks over the

full length of the slab. Hence, the overall strain is distributed between more cracks, resulting in smaller crack width for each of them. In other words, the elongation of tensile bars is larger over the maximum crack spacing resulting in the creation of wider cracks. It should be noted that when cracking initiates at the load less than 58.6 *kN* not all the final primary and secondary cracks occur at once because of the variability in tensile strength and flexural moment along the member. In this case it is decided that all cracks are established and stabilized at the loads between 58.6 and 103.4 *kN* and the corresponding maximum crack spacing of 303 *mm* will be used for the rest of calculations. In other words, all cracks have been established prior to the load of 103.4 *kN* and no more new cracks will occur in the range of loads higher than 103.4 *kN*.

According to Gilbert's model, the instantaneous crack width is the difference between the elongation of the tensile steel over the length S and the elongation of the concrete between the cracks. The final equation to find the maximum crack width is given by:

$$w_{\max} = \frac{S_{\max}}{E_s}\left[\frac{T_s}{A_{st}} - \frac{\tau_b S_{\max}}{\phi}(1+n\rho_{te})\right] \tag{3.21}$$

Substituting all parameters in Eq. 3.21 with their calculated values the maximum crack widths at each stage of loading are found to be:

$$w_{\max} = \frac{333}{200000}\left[\frac{3.43P}{1200} - \frac{4.95\times 333}{19.5}\left(1+8.43\times\frac{1200}{82053}\right)\right]$$

$$\rightarrow w_{\max} = 4.76\times 10^{-6}P - 0.16 \quad , \quad P \le 58621N$$

$$w_{\max} = \frac{333}{200000}\left[\frac{3.43P}{1200} - \frac{3.30\times 333}{19.5}\left(1+8.43\times\frac{1200}{82053}\right)\right]$$

$$\rightarrow w_{\max} = 4.76\times 10^{-6}P - 0.11 \quad , \quad 58621 < P < 103448N$$

$$w_{\max} = \frac{333}{200000}\left[\frac{3.43P}{1200} - \frac{2.19\times 333}{19.5}\left(1+8.43\times\frac{1200}{82053}\right)\right]$$

$$\rightarrow w_{\max} = 4.76\times 10^{-6}P - 0.07 \quad , \quad P \ge 103448N$$

The complexity of this method could be reduced by assuming a constant bond stress for all values of steel stresses. Although, the principle of this method is similar to that of some other models such as CEB-FIP (1990), the crack spacing and crack width are defined based on an exact integration of stresses, and hence, a more accurate result is expected from this model. Based on the result of preceding calculations, crack width versus load curve is drawn in Figure 3.10 for comparison with experimental observations as well as with other methods which are described in the following.

Frosch model

The second analytical model to be investigated is Frosch's model (Frosch, 1999). In this model, crack spacing basically depends on the maximum concrete cover which is shown in Figure 3.9. According to this model crack spacing can be estimated as:

$$S_c = \Psi_s d^* \tag{3.22}$$

where d^* = controlling cover distance; and ψ_s = crack spacing factor: 1.0 for minimum crack spacing; 1.5 for average crack spacing; and 2.0 for maximum crack spacing.

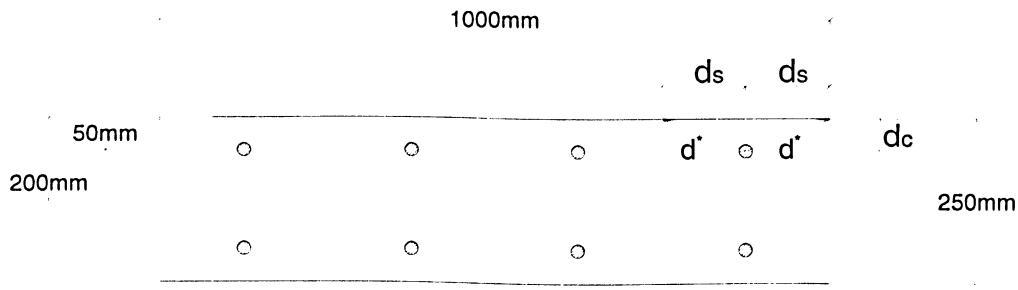

Figure 3.9 Controlling cover distance

According to Figure 3.9 controlling cover distance is calculated as:

$$d^* = \sqrt{d_c^2 + d_s^2} = \sqrt{50^2 + 125^2} = 134 \ \ mm$$

In order to find the maximum possible crack width a crack spacing factor (Ψ_s) of 2 must be used, thus:

$$S_{max} = 2 \times 134 = 268 \quad mm$$

The equation for estimating the crack width at the level of tensile reinforcement is given as:

$$w_s = \varepsilon_s S_c \tag{3.23}$$

In this model simplifications are made through several assumptions. It is assumed that the reinforcing steel is uniformly strained over the crack spacing. This implies that an average steel stress must be used in the formula, however, nothing is mentioned about this and no instruction is given for calculating the average steel stress. Normally, bond stress is needed to find the average steel strain. Since no assumption is made in the model for bond stress, the maximum steel stress that occurs at crack section is used here for simplicity. Additionally, the tensile strain in the concrete (tension stiffening) is neglected. As a result of this the crack width would be slightly overestimated and on the conservative side. Consequently, maximum crack width is calculated based on Eq. 3.23, as follows:

$$w_{s,max} = \frac{\sigma_{st}}{E_s} S_{max} = \frac{T_s}{E_s A_{st}} S_{max} = \frac{3.43P}{200000 \times 1200} \times 268 = 3.83 \times 10^{-6} P$$

Crack width at the slab tensile face can be estimated by taking the strain gradient into account. This is done by multiplying the crack width at the reinforcement level by the coefficient β which is the ratio of distance between neutral axis and tension face to distance between neutral axis and centroid of reinforcing steel. This coefficient is calculated based on Figure 3.5 for high eccentricity test as follows:

$$\beta = \frac{\varepsilon_2}{\varepsilon_1} = \frac{h - kd}{d - kd} = \frac{250 - 0.229 \times 200}{200 - 0.229 \times 200} = 1.32$$

Therefore, the maximum crack width at the surface of slab can be calculated as:

$$w_{t,\max} = \beta \times 3.83 \times 10^{-6} P = 5.05 \times 10^{-6} P$$

The estimated maximum crack width is very close to that has been resulted from Gilbert model, especially at larger eccentric loads, because the bond stress and consequently tension stiffening effect reduces at higher steel stresses. This implies that rigorous computational efforts in Gilbert model are unnecessary to obtain a reasonably accurate crack width.

Gergely and Lutz model

Gergely and Lutz model (1968) is one of the earliest models for crack prediction. They proposed a crack width prediction formula based on a computer statistical analysis of a large number of test results from different sources. A simplified version of their well-known equation is given as:

$$w_{t,\max} = 0.011 \beta f_s \sqrt[3]{c A_e} \times 10^{-3} \qquad (3.24)$$

in which A_e = effective stretched concrete area (area of concrete symmetric with reinforcing steel divided by number of bars) (mm^2); and c = thickness of cover from tension fiber to center of closest bar (mm). $w_{t,\max}$ is in mm, and f_s is in MPa.

Therefore, the maximum crack width at the face of concrete slab can be estimated as:

$$w_{t,\max} = 0.011 \times 1.32 \times \frac{3.43P}{1200} \sqrt[3]{50 \times \frac{2 \times 50 \times 1000}{4}} \times 10^{-3} = 4.47 \times 10^{-6} P$$

In spite of its simplicity, the result of this statistical model is showing a good agreement with experimental results as well as with other more complex analytical models. The maximum crack width is drawn versus load based on this model in Figure 3.10 along with the results of experiments and other models.

Eurocode EC2 1997 approach

The Eurocode EC2 (1997) stipulates that the design crack width be evaluated from the following expression:

$$w_k = \alpha S_{rm} \varepsilon_{sm} \tag{3.25}$$

where w_k = characteristic crack width; S_{rm} = average stabilized crack spacing; ε_{sm} = mean tensile reinforcement strain; and α = coefficient relating the average crack width to the design value (1.7 for load-induced cracking and for restraint cracking in sections with minimum dimension in excess of 800 *mm*).

The mean strain ε_{sm} is obtained from the following expression:

$$\varepsilon_{sm} = \frac{\sigma_s}{E_s}\left[1 - \beta_1 \beta_2 \left(\frac{\sigma_{sr}}{\sigma_s}\right)^2\right] \tag{3.26}$$

where σ_s = stress in the tension reinforcement computed on the basis of a cracked section (MPa); σ_{sr} = stress in the tension reinforcement computed on the basis of a cracked section under loading conditions that cause the first crack (MPa); β_1 = coefficient accounting for bar bond characteristics (1.0 for deformed bars and 0.5 for plain bars); β_2 = coefficient accounting for load duration (1.0 for single short-term loading and 0.5 for sustained or cyclic loading); and E_s = modulus of elasticity of the reinforcement (MPa).

Based on the theoretical calculation at the beginning of this section the first crack occurs at the load of 56 *kN*. Thus, the mean strain can be calculated as:

$$\varepsilon_{sm} = \frac{3.43P}{200000\times 1200}\left[1-1\times 1\times\left(\frac{3.43\times 56000}{3.43P}\right)^2\right] = 1.43P\left[1-\left(\frac{56000}{P}\right)^2\right]\times 10^{-8}$$

The average stabilized crack spacing S_{rm} is evaluated from the following expression:

$$S_{rm} = 50 + 0.25k_1k_2\phi/\rho_{s,eff} \tag{3.27}$$

in which $\rho_{s,eff}$ = effective reinforcement ratio = $\frac{A_{st}}{A_{c,eff}} = \frac{A_{st}}{b[2.5(h-d)]}$; k_1 = 0.8 for deformed bars and 1.6 for plain bars; and k_2 = 0.5 for bending and 1.0 for pure tension. S_{rm} is in *mm*.

Thus,

$$S_{rm} = 50 + 0.25\times 0.8\times 0.5\times 19.5\Big/\left(\frac{1200}{1000(2.5\times 50)}\right) = 253mm$$

From Eq. 3.25 the design crack width can be calculated as:

$$w_k = 1.7\times 253\times 1.43P\left[1-\left(\frac{56000}{P}\right)^2\right]\times 10^{-8} = 6.15P\left[1-\left(\frac{56000}{P}\right)^2\right]\times 10^{-6}$$

The resulting Eurocode EC2 design crack width curve is drawn along with other models in Figure 3.10.

CEB-FIP 1990 approach

According to CEB-FIP (1990) a characteristic crack width is defined for beams that must be limited to a certain value. The equation is expressed as follows:

$$w_k = l_{s,\max}(\varepsilon_{sm} - \varepsilon_{cm} - \varepsilon_{cs}) \tag{3.28}$$

where ε_{sm} = average reinforcement strain within segment length $l_{s,\max}$; ε_{cm} = average concrete strain within segment length $l_{s,\max}$; ε_{cs} = strain of concrete due to shrinkage; and $l_{s,\max}$ = the length over which slip occurs between the steel reinforcement and the concrete.

For stabilized cracking the segment length $l_{s,\max}$ is approximately the crack spacing and is given by:

$$l_{s,\max} = \frac{\phi}{3.6\rho_{s,eff}} \tag{3.29}$$

$\rho_{s,eff}$ is the same as that in Eq. 3.27. Thus the length $l_{s,\max}$ can be calculated as:

$$l_{s,\max} = \frac{19.5}{3.6 \times \dfrac{1200}{1000 \times 2.5 \times 50}} = 564mm$$

Based on the experimental observations this is an excessively overestimated maximum crack spacing and definitely will result in unjustifiably larger predicted crack widths. It is stated in the code that the average crack spacing is 2/3 of the length $l_{s,\max}$ which in this case would be 376 *mm* which is still a high value for the average stabilized crack spacing.

To evaluate crack width according to Eq. (3.28), it is necessary to evaluate the difference between the average steel and average concrete strains within the slip zone. This difference is approximated by the following:

$$\varepsilon_{sm} - \varepsilon_{cm} = \varepsilon_{s2} - \beta_1 \varepsilon_{sr2} \tag{3.30}$$

where ε_{s2}= steel strain at location of crack under service load; ε_{sr2}= steel strain at location of crack under load that causes cracking of the effective concrete area; and β_1= empirical factor to assess average strain within $l_{s,\max}$ (0.6 for short-term loading and 0.38 for long-term loading).

Steel strain at crack $\rightarrow \varepsilon_{s2} = \dfrac{T}{E_s A_{st}} = \dfrac{3.43P}{1200 \times 200000}$

Steel strain at crack under cracking load (56000 N) $\rightarrow \varepsilon_{sr2} = \dfrac{3.43 \times 56000}{1200 \times 200000}$

For short-term loading $\rightarrow \beta_1 = 0.6$

Substituting Eq. 3.30 and $l_{s,\max}$ into Eq. 3.28 and ignoring the concrete shrinkage strain the characteristic crack width is calculated as follows:

$$w_k = 564 \times \frac{3.43}{1200 \times 200000}(P - 0.6 \times 56000) = 8.06 \times 10^{-6} P - 0.27$$

The predicted maximum crack width is overestimated partly due to the wrong crack spacing value. Additionally, mean strain values and crack spacing are estimated based on a conceptual idea of a point with zero slip. This theory can be doubted especially at higher loading levels, as stabilized cracks can occur without a point of zero slip in between. In accordance with CEB-FIP code the above characteristic crack width must be used for design which is giving results much higher than what is observed in the experiment. This suggests that the provisions of CEB-FIP code for controlling crack

width are too conservative. The predicted crack width curve is drawn for this model along with other models in Figure 3.10 for comparison. Also, the results of all crack prediction models are summarized in Table 3.1.

Table 3.1 Crack prediction models results for high eccentricity test

	Crack Width (mm)					
Eccentric Load (kN)	Experiment	Gilbert	Frosch	Gergely & Lutz	EC2	CEB-FIP
40	0.14	0.03	0.20	0.18	-	0.05
50	0.15	0.08	0.25	0.22	-	0.13
60	0.20	0.18	0.30	0.27	0.05	0.21
70	0.24	0.22	0.35	0.31	0.15	0.29
80	0.28	0.27	0.40	0.36	0.25	0.37
100	0.44	0.37	0.51	0.45	0.42	0.54
110	0.48	0.45	0.56	0.49	0.50	0.62
120	0.52	0.50	0.61	0.54	0.58	0.70

Several comments can be made about the accuracy of investigated crack models based on their results shown in Figure 3.10 as follows:

- Frosch's model is giving reasonably accurate results for the maximum crack width. The predicted crack widths are somewhat higher than the actual crack widths, because the maximum steel strain at crack is used instead of mean steel strain. An overestimation in this scale is desirable in a model to be used as a basis for design codes.
- In spite of its simplicity, Gergely and Lutz model gives a close upper bound estimation of maximum crack width.
- The results of Gilbert's model are somewhat lower than the actual crack width especially at loading values less than 60 *kN*. This might be due to the assumption of slightly higher bond stress. Altogether, the model is providing a good crack width estimation, and with a little simplification it can be practically used for design purposes.
- EC2 method for evaluating the design crack width does not seem to be quite accurate as compared to the experimental results. Since the estimated crack

spacing was in a good range, the problem could be due to inapropriate mean reinforcement strain formulation.

- The CEB-FIP method overestimates the maximum observed crack widths. This indicates that a very conservative approach is used in this code.

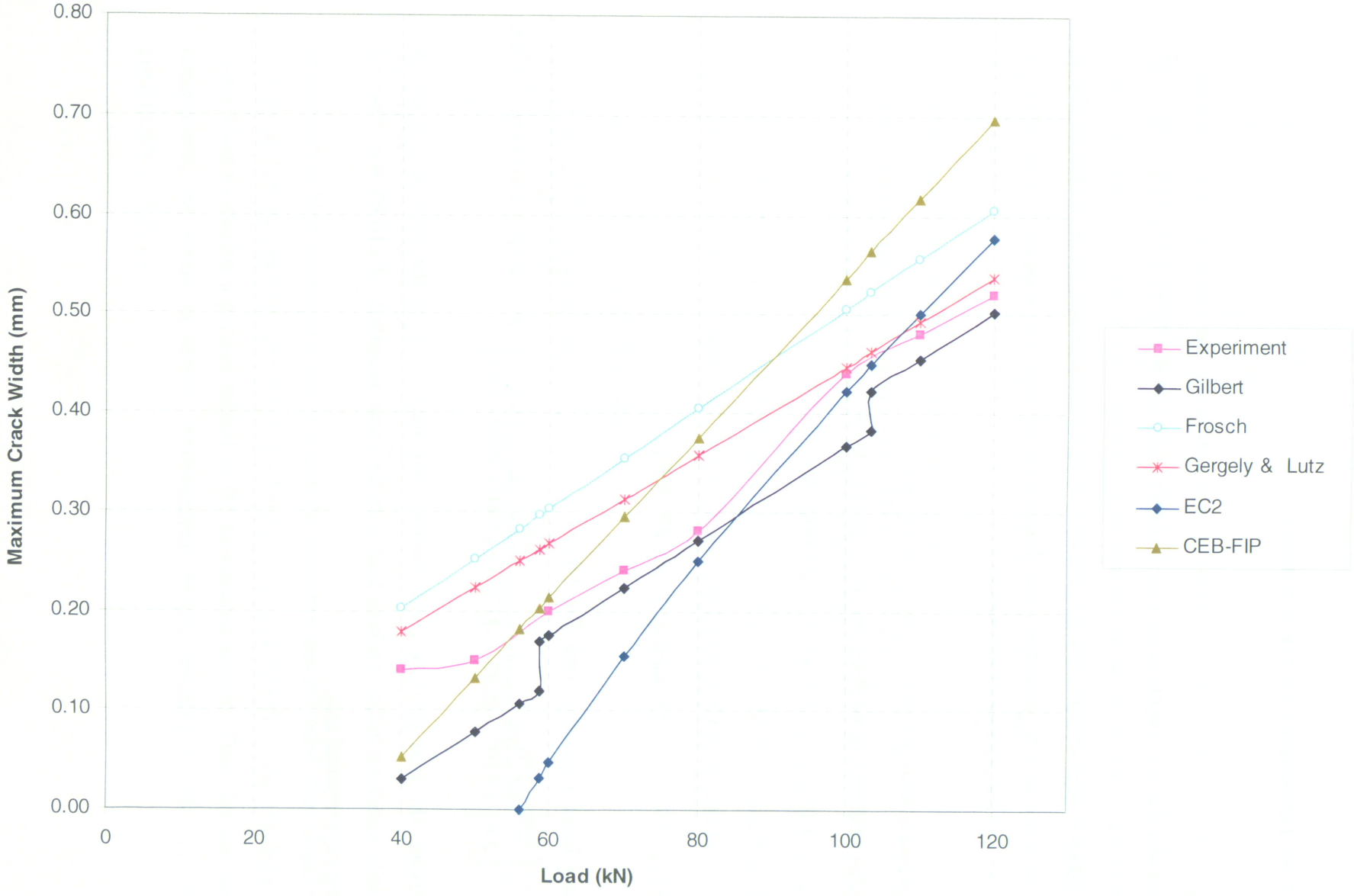

Figure 3.10 Crack width prediction models comparison for high eccentricity test

3.2.2 Low Eccentricity Test (e = 250*mm*)

Using previously discussed equations, in the following, the crack width is calculated analytically for low eccentricity test. Their final results are again compared to those of experimental observation. In an attempt of estimating crack width those steps that have been taken in high eccentricity case are exactly followed here and are presented briefly. It must be noted that all properties and dimensions are alike for high and low eccentricity trials, except the amount of eccentricity.

Compressive Strength of Concrete $f_c = 25 \ \ MPa$

Modulus of Elasticity of Concrete $E_c = 23715 \ \ MPa$

Modulus of Elasticity of Steel $E_s = 200000 \ \ MPa$

Modular Ratio $n = 8.43$

Moment of Inertia of Un-cracked Section $I_{gt} = 1.4 \times 10^9 \ \ mm^4$

Modulus of Rupture of Concrete $f_r = 2.87 \ \ MPa$

Finding Initial Cracking Load (Eq. 3.4) $\Rightarrow$

$$2.87 = \left[\frac{250 \times 250}{2 \times 1.4 \times 10^9} + \frac{1}{(8.43-1)(1200+1200)+1000 \times 250} \right] \times P \ \ \rightarrow \ \ P = 110151N = 110kN$$

Therefore, the first primary crack theoretically may occur at the load of 110 *kN*. A perfectly matching initial cracking load with the same magnitude of 110 *kN* was observed during experimental test.

Finding Compression Chord Depth (Eq. 3.9) $\Rightarrow$

$$k^3\left[\frac{200^2}{6}\right]+k^2\left[-\frac{200}{2}\left(250+\frac{250}{2}\right)\right]+$$

$$K\left[-250\times8.43\times200\left(1+\frac{250}{2\times250}\right)(0.006+0.006)+8.43\times200(0.006\times200+0.006\times50)\right]$$

$$+250\times8.43\left(1+\frac{250}{2\times250}\right)(200\times0.006+50\times0.006)-8.43(200^2\times0.006+50^2\times0.006)=0$$

$$\rightarrow 6666.67k^3-37500k^2-5058k+2592.23=0\rightarrow k=0.207 \qquad kd<d'$$

Computing the Centroid of the Cracked Section (Eq. 3.11) $\Rightarrow$

$$\bar{y}=\frac{8.43\times1200\times200+8.43\times1200\times50+1000\times0.207^2\times200^2/2}{8.43\times1200+8.43\times1200+1000\times0.207\times200}\rightarrow \bar{y}=55 \quad mm$$

Calculating Moment of Inertia of the Cracked Section (Eq. 3.13) $\Rightarrow$

$$I_{cr}=2.68\times10^8 \quad mm^4$$

Finding the Force in Tensile Bars (Eq. 3.15) $\Rightarrow$

$$T_s=\left[\frac{\left(250+\frac{250}{2}-55\right)(200-55)}{2.68\times10^8}+\frac{1}{8.43\times1200+8.43\times1200+1000\times0.207\times200}\right]\times8.43\times1200\times P$$

$$T_s=1.92P \qquad T_s<f_yA_s$$

In contrary to high eccentricity test in which the specimen was reloaded after cracks were stabilized, low eccentricity test was loaded only once, and therefore, the obtained steel strain history contains a portion related to the un-cracked section. Thus, for the sake of comparison, the stress in tensile reinforcement before cracking is also calculated analytically as follows:

$$\sigma_{st} = n\left(\frac{MY}{I} + \frac{P}{A}\right) = \left[\frac{e\left(h/2 - c\right)}{I_{gt}} + \frac{1}{(n-1)(A_{st} + A'_s) + bh}\right] \times nP \tag{3.31}$$

$$\sigma_{st} = \left[\frac{250(125-60)}{1.4\times10^{9}} + \frac{1}{(8.43-1)\times2400 + 250000}\right] \times 8.43 \times P = 1.29\times10^{-4} P$$

The comparison between the analytically calculated reinforcement strain and the empirical data is depicted in Figure 3.11. A good agreement can be seen between the theoretical calculated strain and experimental data.

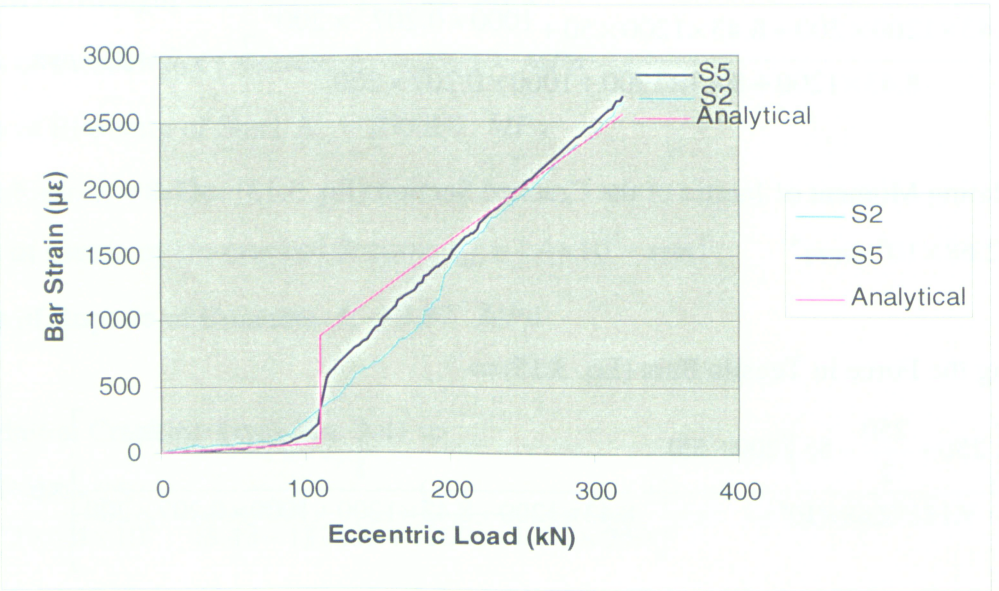

Figure 3.11 Comparison of analytical calculated steel strain and experimental data

Now that the force in tensile reinforcement is known in terms of external load, the crack width can be estimated based on crack prediction models as follows:

Gilbert model

Eq. 3.17 $\Rightarrow b^* = \min[1000, 4(250 - 0.207\times200)] \rightarrow b^* = \min[1000, 834] \rightarrow b^* = 834 \quad mm$

Eq. 3.16 $\Rightarrow A_{ct} = 0.5\times(250 - 0.207\times200)\times834 = 86986 \quad mm^2$

Finding Bond Stress $\Rightarrow$

$$\sigma_{st} = \frac{T_s}{A_s} = \frac{1.92P}{1200} = 0.0016P$$

$$\begin{cases} \sigma_{st} \le 170MPa \rightarrow P \le 106250N \rightarrow \alpha_1 = 3 \\ 170 < \sigma_{st} < 300MPa \rightarrow 106250 < P < 187500N \rightarrow \alpha_1 = 2 \\ \sigma_{st} \ge 300MPa \rightarrow P \ge 187500N \rightarrow \alpha_1 = 1.33 \end{cases}$$

$$\alpha_2 = 1$$

Direct Tensile Strength of Concrete $f_{ct} = 1.65 \ \ MPa$

Consequently, the bond stress at each level of applying load is given by Eq. 3.18 as:

$$\tau_b = 3 \times 1 \times 1.65 = 4.95 \ \ MPa \quad , \quad P \le 106kN$$
$$\tau_b = 2 \times 1 \times 1.65 = 3.30 \ \ MPa \quad , \quad 106 < P < 188kN$$
$$\tau_b = 1.33 \times 1 \times 1.65 = 2.19 \ \ MPa \quad , \quad P \ge 188kN$$

Maximum and Minimum Crack Spacing (Eq. 3.20) $\Rightarrow$

$$S_{max} = \frac{1.65 \times 19.5}{2 \times 4.95 \times \frac{1200}{86986}} = 236 \ \ mm \quad , \quad S_{min} = 118 \ \ mm \quad , \quad P \le 106kN$$

$$S_{max} = \frac{1.65 \times 19.5}{2 \times 3.30 \times \frac{1200}{86986}} = 353 \ \ mm \quad , \quad S_{min} = 177 \ \ mm \quad , \quad 106 < P < 188kN$$

$$S_{max} = \frac{1.65 \times 19.5}{2 \times 2.19 \times \frac{1200}{86986}} = 532 \ \ mm \quad , \quad S_{min} = 266 \ \ mm \quad , \quad P \ge 188kN$$

All cracks are assumed to be established and stabilized at the loads between 110 and 188 *kN* and the corresponding maximum crack spacing will be used for the rest of calculations.

The Maximum Crack Width (Eq. 3.21) $\Rightarrow$

$$w_{max} = \frac{353}{200000}\left[\frac{1.92p}{1200} - \frac{4.95\times353}{19.5}\left(1+8.43\times\frac{1200}{86986}\right)\right]$$

$$\rightarrow w_{max} = 2.82\times10^{-6}P - 0.18 \quad , \quad P \le 106000N$$

$$w_{max} = \frac{353}{200000}\left[\frac{1.92p}{1200} - \frac{3.30\times353}{19.5}\left(1+8.43\times\frac{1200}{86986}\right)\right]$$

$$\rightarrow w_{max} = 2.82\times10^{-6}P - 0.12 \quad , \quad 106000 < P < 188000N$$

$$w_{max} = \frac{353}{200000}\left[\frac{1.92p}{1200} - \frac{2.19\times353}{19.5}\left(1+8.43\times\frac{1200}{86986}\right)\right]$$

$$\rightarrow w_{max} = 2.82\times10^{-6}P - 0.08 \quad , \quad P \ge 188000N$$

Frosch model

Controlling Cover Distance $d^* = \sqrt{d_c^2 + d_s^2} = \sqrt{50^2 + 125^2} = 134 \ \ mm$

$\Psi_s = 2$ for maximum crack spacing.

Maximum Crack Spacing (Eq. 3.22) $\Rightarrow$ $S_{max} = 2\times134 = 268 \ \ mm$

Maximum Crack Width (Eq. 3.23) $\Rightarrow$ $w_{s,max} = \frac{1.92P}{200000\times1200}\times268 = 2.14\times10^{-6}P$

$$\beta = \frac{\varepsilon_2}{\varepsilon_1} = \frac{h-kd}{d-kd} = \frac{250-0.207\times200}{200-0.207\times200} = 1.32$$

Maximum Crack Width at the Tensile Face $\Rightarrow$ $w_{t,max} = \beta\times2.14\times10^{-6}P = 2.82\times10^{-6}P$

Gergely and Lutz model

Maximum Crack Width (Eq. 3.24) $\Rightarrow$

$$w_{t,max} = 0.011\times1.32\times\frac{1.92P}{1200}\sqrt[3]{50\times\frac{2\times50\times1000}{4}}\times10^{-3} = 2.50\times10^{-6}P$$

Eurocode EC2 1997 approach

Mean Reinforcement Strain (Eq. 3.26) $\Rightarrow$

$$\varepsilon_{sm} = \frac{1.92P}{200000\times 1200}\left[1-1\times 1\times\left(\frac{1.92\times 110000}{1.92P}\right)^2\right] = 0.8P\left[1-\left(\frac{110000}{P}\right)^2\right]\times 10^{-8}$$

The Average Stabilized Crack Spacing (Eq. 3.27) $\Rightarrow$

$$S_{rm} = 50+0.25\times 0.8\times 0.5\times 19.5\Big/\left(\frac{1200}{1000(2.5\times 50)}\right) = 253mm$$

The Design Crack Width (Eq. 3.25) $\Rightarrow$

$$w_k = 1.7\times 253\times 0.8P\left[1-\left(\frac{110000}{P}\right)^2\right]\times 10^{-8} = 3.44P\left[1-\left(\frac{110000}{P}\right)^2\right]\times 10^{-6}$$

CEB-FIP 1990 approach

The Slip Segment Length (Eq. 3.29) $\Rightarrow$ $l_{s,\max} = \dfrac{19.5}{3.6\times\dfrac{1200}{1000\times 2.5\times 50}} = 564mm$

Steel strain at crack $\rightarrow \varepsilon_{s2} = \dfrac{T}{E_s A_{st}} = \dfrac{1.92P}{1200\times 200000}$

Steel strain at crack under cracking load (110000 N) $\rightarrow \varepsilon_{sr2} = \dfrac{1.92\times 110000}{1200\times 200000}$

For short-term loading $\rightarrow \beta = 0.6$

The characteristic crack width (Eq. 3.30 into Eq. 3.28) $\Rightarrow$

$$w_k = 564\times\frac{1.92}{1200\times 200000}(P-0.6\times 110000) = 4.51\times 10^{-6}P-0.30$$

The results of crack prediction models are presented in Table 3.2 along with the experimental data. Additionally, the relevant crack width versus load curves are drawn in Figure 3.12 for comparison. Again, all models are giving results in almost the same range. EC2 and CEB-FIP curves are having a different trend with dissimilar slope to that of other curves. It also can be seen that the predicted crack widths are diverging from the experimental observation as the load increases. This kind of deviation is not observed in the high eccentricity test in which cracks developed under dominantly flexural stresses. This is probably due to the fact that all models considered here for crack prediction are adjusted for purely flexural cracks, and their accuracy is reduced as the section stresses deviate from purely flexural. For instance, the flexural calibrated tension chord depth or concrete effective area in some crack models is no longer valid for a section with dominating tensile stresses.

Table 3.2 Crack prediction models results for low eccentricity test

	Crack Width (mm)					
Eccentric Load (kN)	Experiment	Gilbert	Frosch	Gergely & Lutz	EC2	CEB-FIP
110	0.10	0.19	0.31	0.28	0.00	0.20
140	0.30	0.27	0.39	0.35	0.18	0.33
160	0.38	0.33	0.45	0.40	0.29	0.42
180	0.38	0.39	0.51	0.45	0.39	0.51
220	0.40	0.54	0.62	0.55	0.57	0.69
240	0.43	0.60	0.68	0.60	0.65	0.78
260	0.48	0.65	0.73	0.65	0.73	0.87
280	0.49	0.71	0.79	0.70	0.81	0.96
300	0.52	0.77	0.85	0.75	0.89	1.05
320	0.52	0.82	0.90	0.80	0.97	1.14

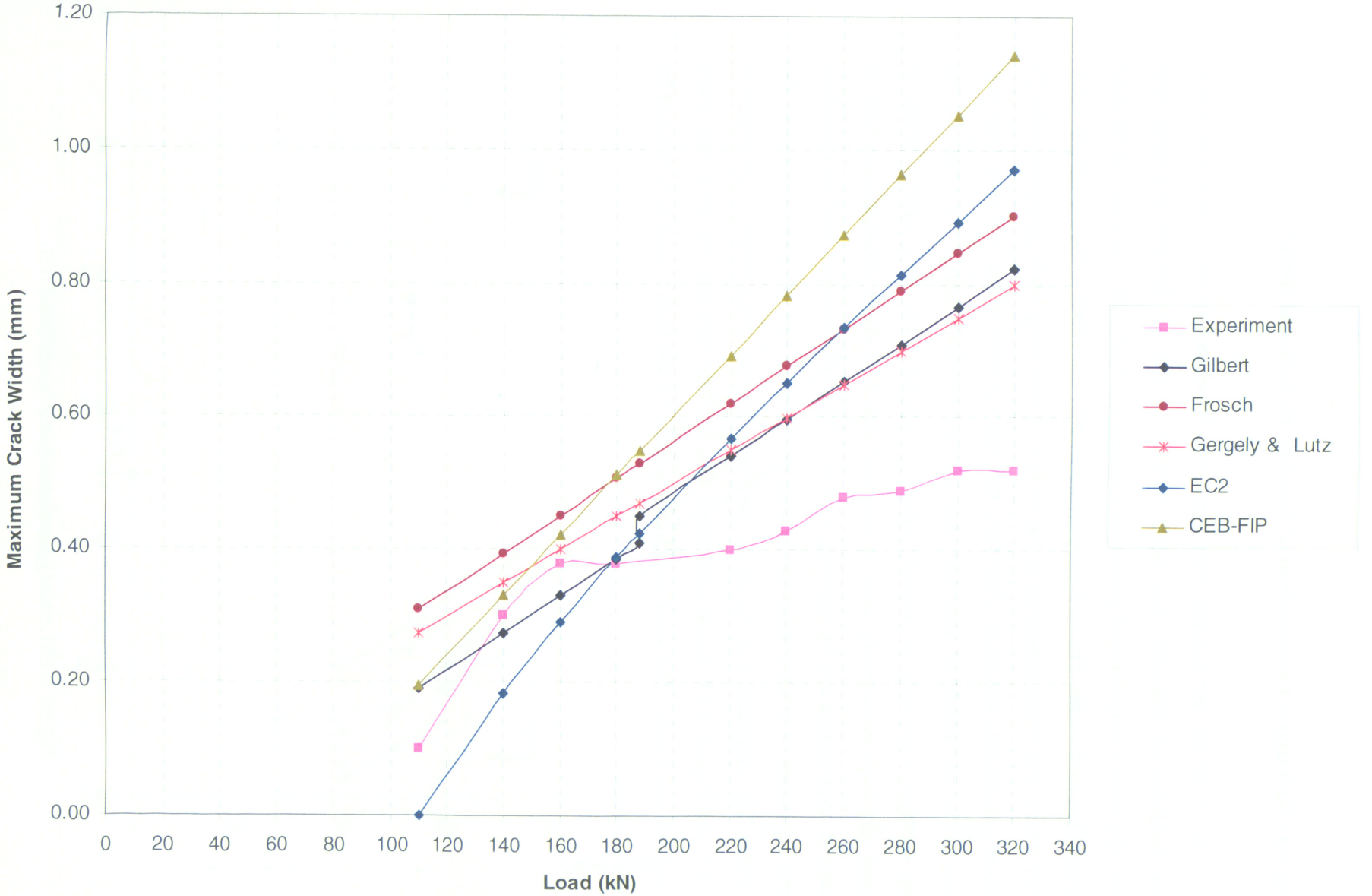

Figure 3.12 Crack width prediction models comparison for low eccentricity test

3.3 Concrete Slab under Combination of Tension, Flexure and Shear

Since, in the combined test internal shear force that developed in the section was small, cracking behavior of concrete was again similar to that of flexural cracking, and therefore, the same computational procedure explained for flexural cracking can be used to estimate the crack width. The mid-span load was only increased to the maximum value of 40 *kN* which was small compared to the weight of specimen itself (approximately 25 *kN* without equipments attached). Therefore, the major portion of the mid-span load was counteracted by the weight of structure, and it could not have significant effect on the bending moment especially at sections close to supports. The very similar result of combined and high eccentricity tests is verifying this fact. Here the mid-span load is neglected in computation and by ignoring a minute difference between load eccentricities the same equations of crack prediction in high eccentricity test are used to estimate the crack width. The comparison of theoretical and experimental crack widths is presented in Table 3.3 and Figure 3.14. Good agreement can be seen between the predicted crack width and the test results. The same conclusions made for the high eccentricity test can be drawn here again.

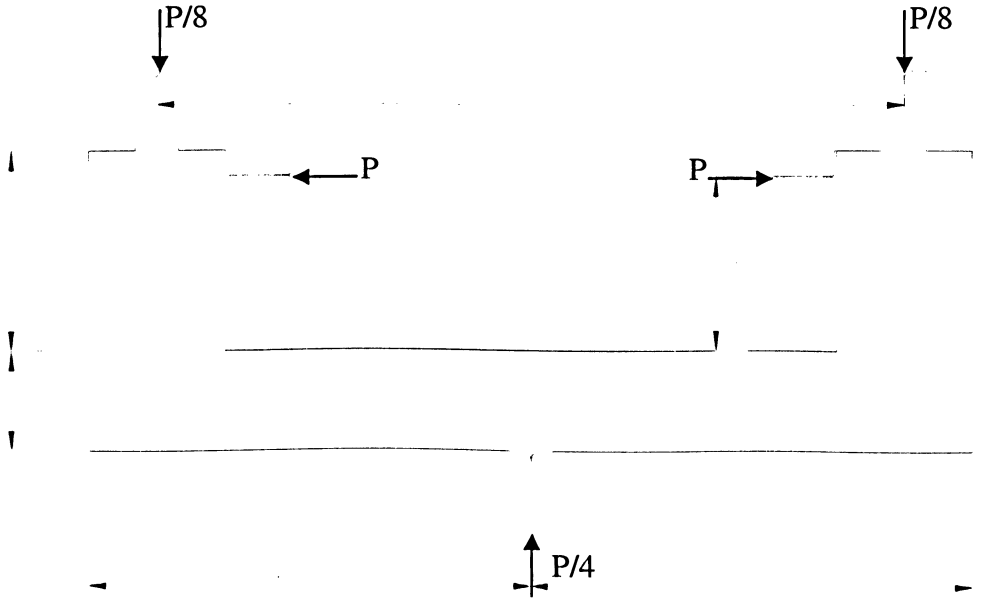

Figure 3.13 Loading configuration of combined test.

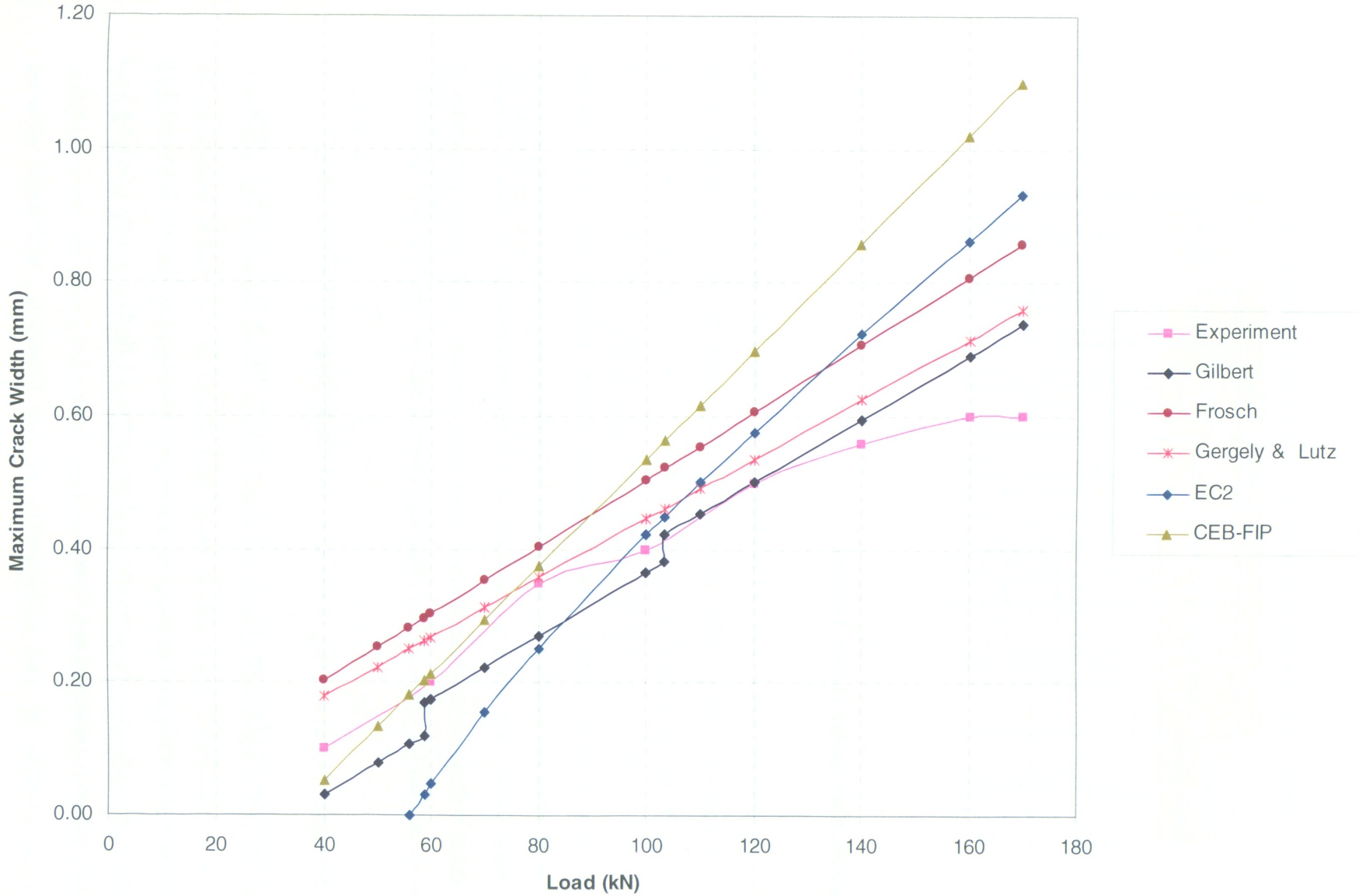

Figure 3.14 Crack width prediction models comparison for combined test

Table 3.3 Crack prediction models results for combined test

Eccentric Load (kN)	Crack Width (mm)					
	Experiment	Gilbert	Frosch	Gergely & Lutz	EC2	CEB-FIP
40	0.10	0.03	0.20	0.18	-	0.05
60	0.20	0.18	0.30	0.27	0.05	0.21
80	0.35	0.27	0.40	0.36	0.25	0.37
100	0.40	0.37	0.51	0.45	0.42	0.54
120	0.50	0.50	0.61	0.54	0.58	0.70
140	0.56	0.60	0.71	0.63	0.72	0.86
160	0.60	0.69	0.81	0.72	0.86	1.02
170	0.60	0.74	0.86	0.76	0.93	1.10

3.4 Concrete Slab under Direct Tension

The direct tension test that is reported in chapter 2 is analytically investigated here. The cracking mechanism is very simple in this case. Whenever, the tensile stresses in the section reach the tensile strength of concrete a through-crack occurs as a result of which all the internal tensile forces will be carried by reinforcements only. This will cause a sudden increase in reinforcement stress at cracked section. Moving away from cracked section the stresses are transferring from steel reinforcement to the surrounding concrete through bond stress, and when the stresses in concrete has reached its tensile strength another crack will occur at some distance away from the first crack. Some properties of concrete are needed for predicting its cracking behavior and are approximated as follows:

Tensile Strength of Concrete (Eq. 3.19) $\Rightarrow f_{ct} = 0.0069[2300(37)]^{1/2} = 2.01 \quad MPa$

Concrete Modulus of Elasticity (Eq. 3.1) $\Rightarrow E_{ct} = 0.043\left(2300^3 \times 37\right)^{1/2} = 28851 \quad MPa$

Slab section and transformed un-cracked section are illustrated in Figures 3.15 and 3.16 respectively. Accordingly, the computational procedure of finding tensile cracking load of the slab section is presented as follows:

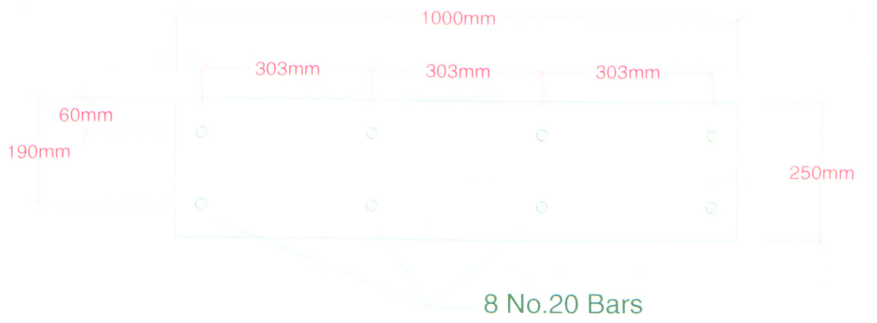

Figure 3.15 Slab section

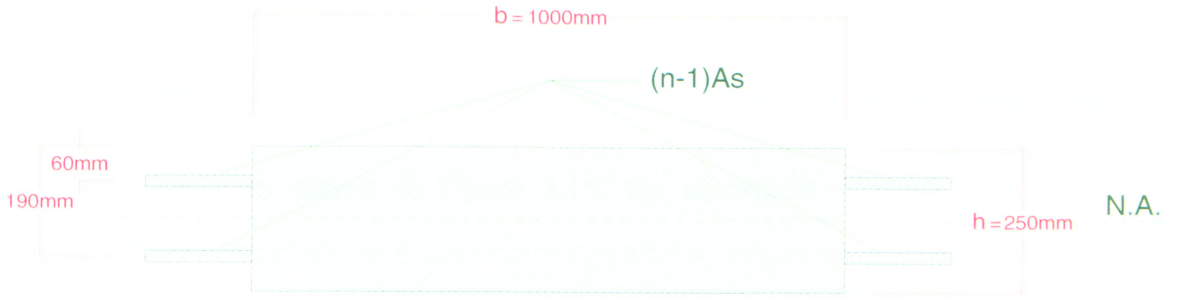

Figure 3.16 Transformed un-cracked section

$$\text{Modular Ratio } n = \frac{E_s}{E_c} = \frac{200000}{28851} = 6.93$$

$$\text{Concrete Tensile Stress } \sigma_{ct} = \frac{T}{A} = \frac{T}{(n-1)(A_s)+bh} \tag{3.32}$$

$$\Rightarrow 2.01 = \frac{T}{(6.93-1)(2400)+1000\times 250} \quad \rightarrow \quad T = 531 \ \ kN$$

Therefore, the predicted tensile load at which the section may crack is 531 *kN*, however, as mentioned before, not all cracks may occur at this level. Experimental observation indicated that cracks developed at various tensile loads between 480 and 540 *kN* due to variability in tensile strength along the length of the tension member. This load range suitably covers the above calculated cracking load, which indicates a good consistency between theoretical calculation and the experimental data. In addition, according to

experimental observation, tensile strain of reinforcement reached up to 0.001 right after cracking. Analytical calculation perfectly confirms this result as follows:

Steel Strain before Cracking (Initial Cracking)

$$\varepsilon_s = \frac{T}{E_c((n-1)A_s + bh)} = \frac{T}{28851((6.93-1)\times 2400 + 1000\times 250)} = 1.31\times 10^{-10} T$$

Steel Strain after Cracking (Reloading) $\varepsilon_s = \frac{T}{E_s A_s} = \frac{T}{200000\times 2400} = 2.08\times 10^{-9} T$

Steel Strain at Crack under Cracking Load $\varepsilon_s = 2.08\times 10^{-9} T_{cr} = 0.001$

A good agreement between these theoretical calculations and the experiment data is also depicted in Figure 3.17.

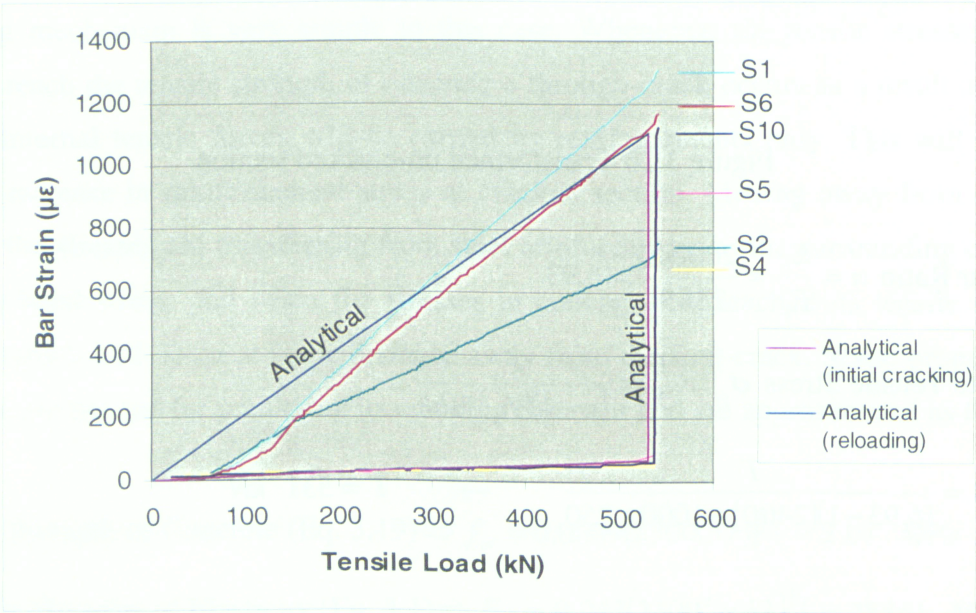

Figure 3.17 Comparison of analytical calculated steel strain and experimental data

Now that the steel strain is correctly found, crack prediction models can be used to evaluate the maximum probable crack widths. The available models for direct tensile induced cracks are not as broad as the flexural cracking models. Here a number of cracking models applicable to tensile cracks are used in the following.

Broms and Lutz model

As explained in chapter 1 the maximum tensile crack widths can be estimated by the following equations:

$$w_{max} = 4c_e\varepsilon_{s,ave} \tag{3.33}$$

$$c_e = d_c\sqrt{1+\left(\frac{s}{4d_c}\right)^2} \tag{3.34}$$

where w_{max} = maximum crack width; c_e = equivalent concrete cover; d_c = distance from center of bar to extreme tension fiber; and s = bar spacing.

Based on dimensions shown in Figure 3.15, the equivalent concrete cover can be calculated as follows:

$$c_e = d_c\sqrt{1+\left(\frac{s}{4d_c}\right)^2} = 60\sqrt{1+\left(\frac{303}{4\times 60}\right)^2} = 97 \quad mm$$

The maximum crack spacing is defined as 4 times the value of the equivalent concrete cover, therefore, by ignoring the concrete elongation between cracks and assuming a uniform steel strain over the crack spacing, the maximum crack width at each loading level is estimated by Eq. 3.33 as follows:

$$w_{max} = \frac{4f_s c_e}{E_s} = \frac{4T_s c_e}{E_s A_s} = \frac{4\times 97}{200000\times 2400}T = 8.08\times 10^{-7}T$$

Gilbert model

Although this model is basically developed for flexural cracks, the equation of crack spacing (Eq. 3.20) can still be used for pure tension cracks if only the effective reinforcement ratio is replaced by the actual reinforcement ratio. This is because the

effective tensile concrete area is almost equal to the entire section area for the tested slab. If a constant bond stress of $2f_{ct}$ is assumed, the maximum crack spacing can be found as:

$$S_{\max} = \frac{f_{ct}\phi}{2\tau_b \rho} = \frac{f_{ct}\phi}{2\tau_b\left(\frac{A_s}{A_c}\right)} = \frac{2.01\times 19.5}{2\times 2\times 2.01\times \frac{2400}{250\times 1000}} = 508mm$$

By ignoring the tension stiffening effect of concrete the Eq. 3.21 is simplified and the maximum crack width is calculated as:

$$w_{\max} = \frac{S_{\max} T_s}{E_s A_s} = \frac{508\times T}{200000\times 2400} = 1.06\times 10^{-6} T$$

The Eurocode EC2 is not used here because the model is capable of predicting crack width at loads higher than the cracking load, however, the experimental test was not continued that much beyond the cracking load, and therefore, the crack widths are not available for comparison. The results of crack prediction models are presented in Table 3.4 and Figure 3.18 for comparison with experimental data.

Table 3.4 Crack prediction models results for direct tension test

	Crack Width (mm)			
Tensile Load (kN)	Observation (phase 2)	Observation (phase 3)	Broms & Lutz	Gilbert
20	0.04	0.07	0.02	0.02
100	0.18	0.15	0.08	0.11
120	0.18	0.16	0.10	0.13
160	0.20	0.20	0.13	0.17
200	0.24	0.24	0.16	0.21
240	0.30	-	0.19	0.25
280	0.33	-	0.23	0.30
320	0.36	-	0.26	0.34
360	0.38	-	0.29	0.38
400	0.40	-	0.32	0.42
440	0.40	-	0.36	0.47
480	0.40	-	0.39	0.51
540	0.40	-	0.44	0.57

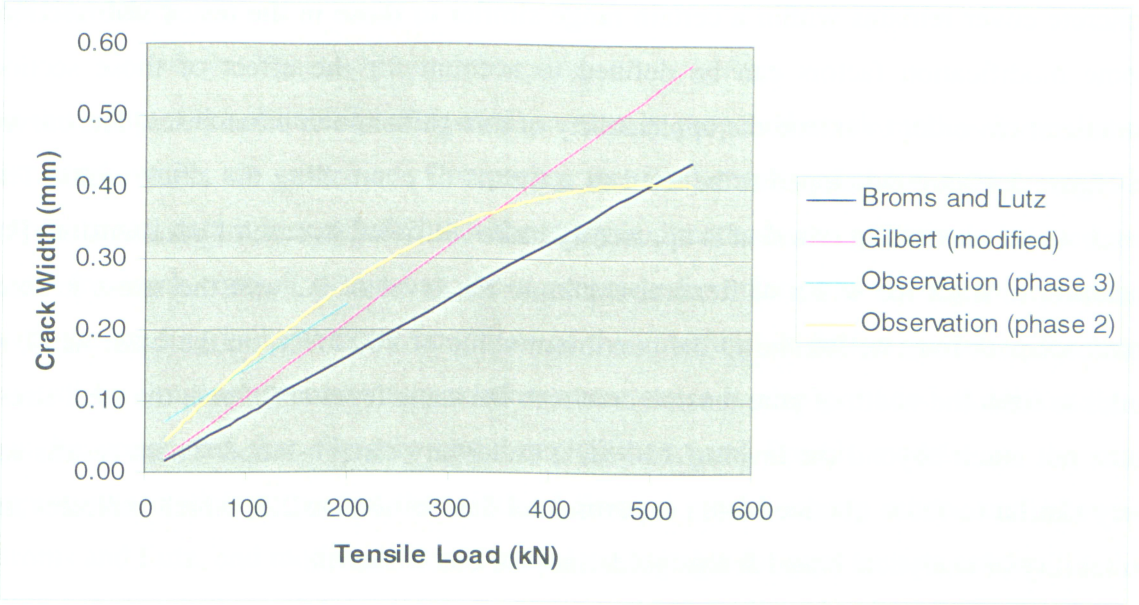

Figure 3.18 Crack width prediction models comparison for direct tension test

In spite of ignoring concrete strain between cracks, a good agreement can be seen between Gilbert model and the observation. This means that the tension stiffening is not a very significant phenomenon in case of purely tensile cracks. Broms and Lutz model is slightly underestimating the crack width. This is because the assumption for crack spacing is a little low in this model. However, by the time cracks are all fully established and the minimum crack spacing is achieved, a better estimation can be expected from this model.

3.5 Analytical Correlation between Crack width and Steel Strain

In section 2.5 of this thesis a correlation between crack width and steel strain has been established based on experimental data. Once again a similar correlation is created, but this time based on the results of analytical calculations and crack prediction models. With this intention, those models showing the best consistency with the experimental data are selected. Consequently, Gergely and Lutz model is chosen for flexural cracks as it is giving a close upper bound prediction providing a safety margin, and the modified Gilbert model is used for tensile cracks. The idea of controlling crack width by limiting the tensile stress in steel reinforcement is valid if other parameters such as bar spacing or

concrete cover remains within a certain range similar to those in the tested slab section. Some modification factors can be defined to account for the effect of those section parameters in order to extend the applicability of this guideline to other cases. The curves in Figure 3.19 are developed to be used as a means of controlling the crack width. The crack width controlling criterion is apparently more restricted in case of pure tension. For instance, to limit the width of flexural cracks to the level of 0.3 *mm* the stress in steel reinforcement must be limited to the maximum value of 200 *MPa*, on the other hand, in order to limit the width of pure tension cracks to the same level of 0.3 *mm* the steel stress must not reach beyond the level of 120 *MPa* under any circumstance. These results are very similar to those obtained from experimental data in section 2.5, which indicates the suitability of analytical based design guidelines for crack control.

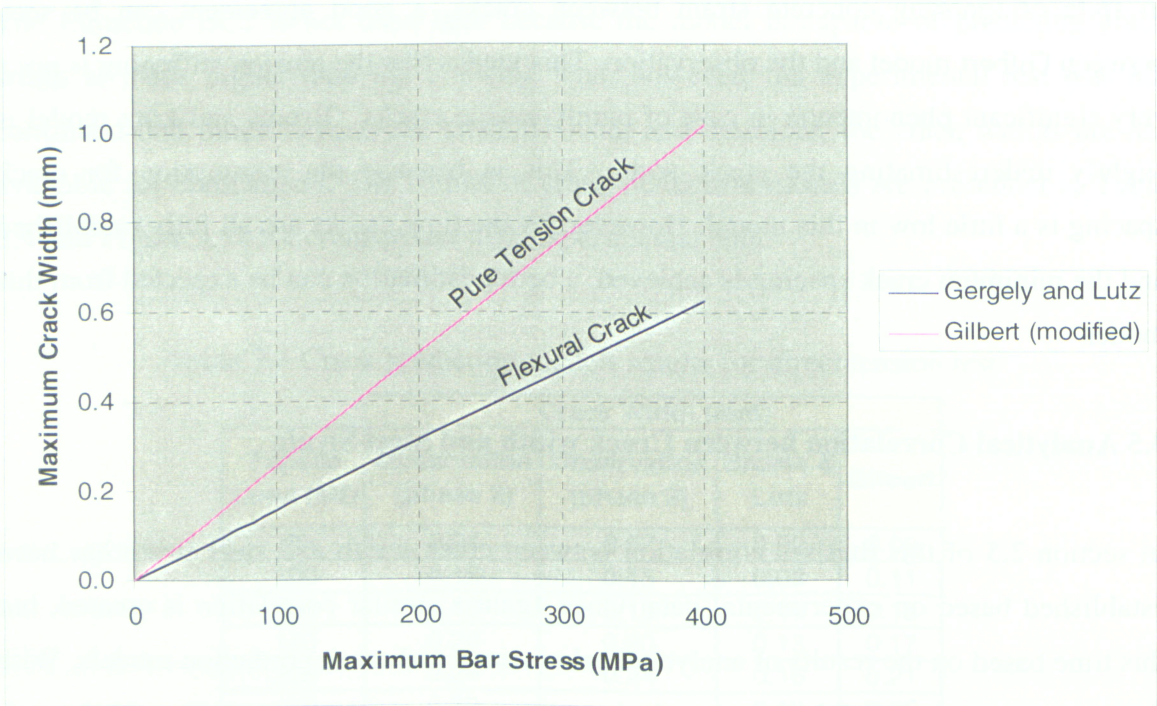

Figure 3.19 The maximum crack width and the maximum bar stress analytical correlation for sections with properties similar to those of tested slab

3.6 Summary

In this chapter the suitability of several previously proposed crack models in predicting the crack width are examined. Comparing the final results of these models with the experimental data it is concluded that the analytical methods can effectively be used as a basis for crack control, as long as, the appropriate formulation is chosen in accordance with the loading and geometry condition of the structure. A design guideline for crack control by limiting the maximum reinforcement stress is also provided. Additionally, it can be concluded that Gergely and Lutz, Gilbert, and Frosch models are the most appropriate models to predict the width of flexural cracks among others, and likewise, Broms and Lutz, and modified Gilbert model are suitable for pure tension cracks.

CHAPTER 4

FINITE ELEMENT MODEL

4.1 General

Reinforced concrete structures are commonly designed to satisfy the criteria of safety and serviceability. In order to ensure the serviceability requirement it is necessary to predict the cracking of RC structures under service loads. Thus far in this research study, the cracking behavior of concrete has been investigated experimentally and also with the aid of some analytical or statistical models. A good consistency is observed between crack prediction models and experiments, however, the precision of these models relies on the accurate determination of the stress in the steel reinforcement. Although the steel stresses can be determined by concrete cracking analysis, this may be quite tedious in case of the actual structure under a combination of different types of loadings and interactions. Furthermore, performing experimental tests for all kinds of loading and geometries is obviously not feasible. In addition to being time-consuming and costly, experiments can not always reflect the behavior of the actual structure due to difficulties in achieving the exact simulation of loading scale and support conditions. The finite element (FE) method has thus become a powerful computational tool, which allows complex analyses of the nonlinear response of RC structures to be carried out in a routine manner. Developing a reliable FE model can help to resolve many of difficulties and uncertainties that designers are dealing with for designing concrete structures. In the following, the efficiency of several reinforced concrete models provided in ABAQUS/6.5 (Hibbitt et al., 2004) in capturing the nonlinear behavior of RC structures is examined. The same structural geometries and properties as those of the previously explained experiments are used as an input. The output results are compared to the experimental observations.

4.2 Direct Tension Model

Several concrete models are available in ABAQUS/6.5 to capture the behavior of concrete under various stress conditions. In order to investigate concrete under purely

tensile load, the brittle cracking model seems to be the most appropriate one among others as it can simulate highly nonlinear behavior of concrete particularly under tension. This model is described in the following.

4.2.1 Brittle Cracking Model

Under different loading conditions, concrete exhibits two primary modes of behavior, namely, brittle mode and ductile mode. The ductile behavior is primarily observed under compression states of stress where microcracks develop more or less uniformly throughout the material, leading to nonlocalized deformation. It almost always involves hardening of the material, although subsequent softening is possible at low confining pressure. The brittle behavior is mainly observed under tension and tension-compression states of stress in which microcracks coalesce to form discreet macrocracks representing regions of highly localized deformation. The brittle mode is associated with cleavage, shear and mixed mode fracture mechanisms. The cracking model described here models only the brittle aspects of concrete behavior. Although this is a major simplification, in direct tension test only the brittle behavior of the concrete is significant, and therefore, the assumption that the material is linear elastic in compression is justified.

Crack models can be classified in two main categories: discreet and smeared. In discrete crack models cracks are modeled by separating the nodal points of the finite element mesh. With the change of topology and the redefinition of nodal points the narrow band of the stiffness matrix is destroyed and a greatly increased computational effort results in this model. Moreover, the lack of generality in crack orientation has made the discreet crack model unpopular. Here a smeared crack model is chosen to represent the discontinuous macrocrack brittle behavior. Rather than representing a single crack, the smeared crack model represents many finely spaced cracks perpendicular to the principle stress direction. This approximation of cracking behavior of concrete is quite realistic, since in concrete fracture is preceded by microcracking of material in the fracture process zone, which manifests itself as strain softening.

From three different types of crack direction theories, namely, fixed orthogonal, rotating, fixed multidirectional, ABAQUS/6.5 assumes fixed orthogonal cracks with a maximum number of cracks at a material point limited by the number of direct stress components present at that material point of the finite element model. That means the maximum number of cracks that can form are three cracks in three-dimensional, plane strain, and axisymmetric problems, two cracks in plane stress and shell problems, and one crack in beam or truss problems. In the fixed orthogonal crack model the direction normal to the first crack is aligned with the direction of maximum tensile principle stress at the time of crack initiation. The model has the memory of this crack direction, and subsequent cracks at the point under consideration can only form in directions orthogonal to the first crack. Crack closing and reopening can take place along the directions of the crack surface normals. The model neglects any permanent strain associated with cracking, that is, the cracks can close completely when the stress across them becomes compressive.

Some problems associated with the fixed orthogonal cracks, such as, numerical problems caused by the singularity of the material stiffness matrix and considerable deviations of predicted crack pattern from that observed in experiment, can be overcome by introducing a cracked shear modulus. This is discussed later in more detail.

In terms of crack detection, a simple Rankine criterion is used to detect crack initiation. This states that a crack forms when the maximum principle tensile stress exceeds the tensile strength of the brittle material.

4.2.2 Post-cracking Tensile Behavior

In a plain concrete when tensile stresses at a particular section reaches the tensile strength of concrete, a crack will form resulting to a sharp drop in stress/strain curve of the concrete. This cracking is so brittle that the tension softening can only be detected with special equipments. Consequently, the entire concrete body loses its stiffness at once. On the other hand, in reinforced concrete crack formation does not lead to a failure of entire concrete body but rather emerges as a local failure. In other words, the concrete between

cracks still has a stiffness which can be transmitted into the system through concrete/rebar bonding and have a considerable effect on the overall response of the structure. This phenomenon referred to as "tension stiffening", is of great importance in smeared crack modeling. Since ABAQUS/6.5 provides no direct modeling of the bond between rebar and concrete, tension stiffening must be simulated in the plain concrete part of the model. This generally can be done by manipulating the stress/strain or stress/displacement curve of the concrete.

Two approaches are proposed to define the post failure behavior of the concrete. In the first one the behavior of cracked concrete is represented by average stress/strain relations within the finite element. However, in parts with little or no reinforcement, this introduces mesh sensitivity in the results, in the sense that the finite element predictions do not converge to a unique solution as the mesh is refined. When large finite elements are used, each element has a large effect on the structural stiffness. When a single element cracks, the stiffness of the entire structure is greatly reduced. Higher order elements in which the material behavior is established at a number of integration points do not markedly change this situation, because, in most cases when a crack takes place at one integration point, the element stiffness is reduced enough so that a crack will occur at all other integration points of the element in the next iteration. Thus, a crack at an integration point does not relieve the rest of the material in the element, since the imposed strain continuity increases the strains at all other integration points. The overall effect is that the formation of a crack in a large element results in the softening of a large portion of the structure. The difficulty stems from the fact that a crack represents a strain discontinuity which can not be modeled correctly within a single finite element in which the strain varies continuously. Additionally, if it is accepted that concrete is a notch-sensitive material, it can be assumed that a cracking criterion which is based on tensile strength may be dangerously unconservative. In this case, the second approach which is based on fracture mechanics theory provides a more rational solution for the problem. It is generally accepted that Hilleborg's (1976) fracture energy proposal is adequate to allay the concern for many practical purposes. Hillerborg defines the energy required to open a unit area of crack in Mode I $\left(G_f^I\right)$ as a material parameter, using brittle fracture concepts.

With this approach the concrete's brittle behavior is characterized by a stress-displacement response rather than a stress-strain response. Under tension a concrete specimen will crack across some section, and its length after it has been pulled apart sufficiently for most of the stress to be removed (so that the elastic strain is small), will be determined primarily by the opening at the crack, which does not depend on the specimen's length.

In ABAQUS/6.5 this fracture energy cracking model can be invoked by specifying the postfailure stress as a tabular function of displacement across the crack, or alternatively by defining the failure stress, σ_{tu}^{I}, as a tabular function of the associated Mode I fracture energy. Here, the second alternative is chosen to characterize the postfailure behavior. This model assumes a linear loss of strength after cracking (Bazant and Oh 1983), as shown in Figure 4.1. G_f^I is the fracture energy which is dissipated in the formation of a crack of unit length per unit thickness and is considered a material property. The experimental study by Welch and Haisman (1969) indicates that for normal strength concrete the value of G_f^I / f_t is in the range of 0.005-0.01 *mm*. Here, in order to introduce some tension stiffening into postfailure behavior, an increased value of G_f^I, that is 0.09 *N/mm*, has been used. Higher tension stiffening also reduces the chance of instability in the analysis.

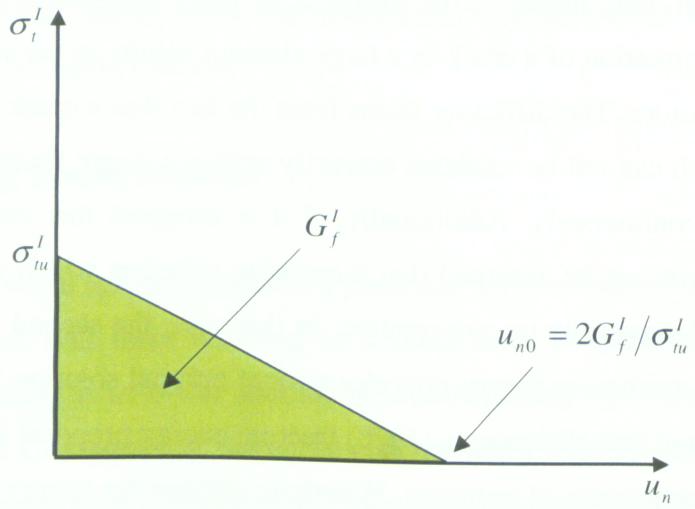

Figure 4.1 Postfailure stress-displacement curve based on fracture energy

4.2.3 Post-cracking Shear Behavior

As mentioned before, the problems of the fixed crack model can be overcome by introducing a cracked shear modulus, which eliminates most numerical difficulties of the model and considerably improves the accuracy of the crack pattern predictions. The results do not seem to be very sensitive to the value of the cracked shear modulus, as long as a value which is greater than zero is used, so as to eliminate the singularity of the material stiffness matrix and the associated numerical instability.

Based on the common observation, the cracked shear modulus is reduced as the crack opens. In ABAQUS/6.5 the cracked shear modulus is defined as a fraction of uncracked shear modulus, $\left(\frac{Shear\ \ Modulus_{\ Cracked}}{Shear\ \ Modulus_{\ Uncracked}} = Shear\ \ \text{Re}tention\ \ Factor \right)$. The shear retention factor can be defined as a function of crack opening strain. As shown in Figure 4.2 a linear assumption has been made for this function.

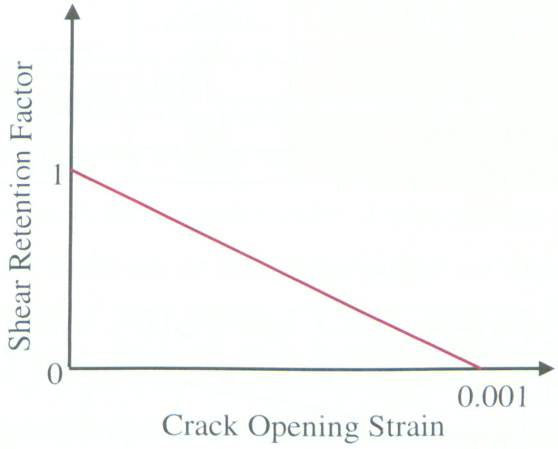

Figure 4.2 Postcracking shear behavior

4.2.4 Concrete and Steel Properties

The brittle cracking model assumes an elastic behavior for concrete in compression and in tension prior to cracking (post-cracking tensile behavior is explained earlier). The following shows assumptions made for concrete properties:

Modulus of Elasticity of Concrete = 28851 *MPa*

Tensile Strength of Concrete = 2.01 *MPa*

Concrete Poisson's Ratio = 0.18

Concrete Density = 2400 Kg/m^3 (2.4×10^{-9} $tonne/mm^3$)

An isotropic model has been used for steel. The assumptions for steel properties and strain/stress curve are given in Table 4.1 and Figure 4.3 respectively.

Table 4.1 Steel properties

Yield Stress (MPa)	400		
Modulus of Elasticity (MPa)	200000		
Poisson's Ratio	0.3		
Density (Kg/m^3)	7800 (7.8×10^{-9} tonne/mm^3)		
Stress (MPa)	400	400	600
Strain	0.002	0.005	0.050

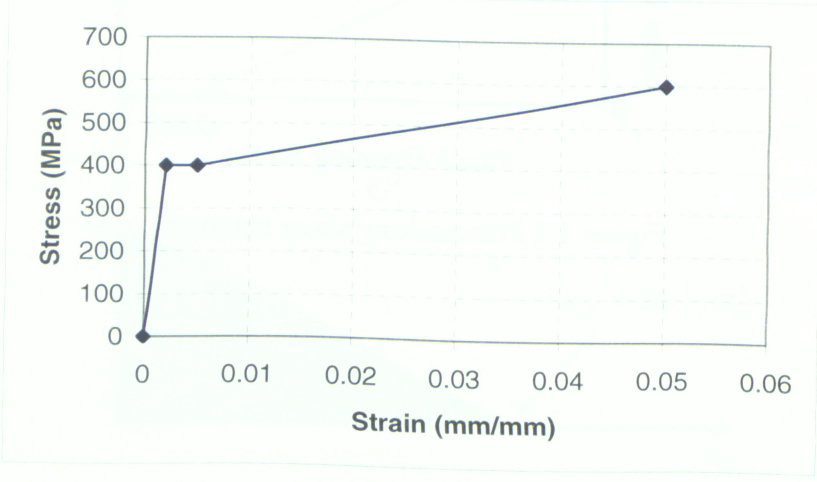

Figure 4.3 Steel assumed stress/strain curve

The above steel stress/strain data are in terms of nominal values (tensile test), however, in order to use them as input data for ABAQUS/6.5, these nominal values must be converted to equivalent true stresses and plastic strains. This conversion is done according to the following equations and results are shown in Table 4.2.

$$\sigma_{true} = \sigma_{nom}(1 + \varepsilon_{nom})$$
$$\varepsilon_{true} = \ln(1 + \varepsilon_{nom})$$
$$\varepsilon_{plastic} = \varepsilon_{true} - \frac{\sigma_{true}}{E}$$

Table 4.2 Converted steel stress/strain values

True Stress (MPa)	400.8	402.0	629.3
Plastic Strain	0	0.0030	0.0456

4.2.5 Three Dimensional Model with Solid Elements

Linear solid elements with 8 nodes are used for the concrete part of the structure, as shown in Figure 4.4, and a specific type of 3D planar shell element, so called surface element, is used for reinforcement, as depicted in Figure 4.5. Surface elements do not have any stiffness property themselves, but they have a built-in rebar layer option through which reinforcement can be defined intrinsically. These surface elements can then be embedded in concrete solid elements, so their deformation are imposed on or constrained by the displacement of concrete solid elements. Longitudinal reinforcement is defined in these rebar layers in direction of axis 1 with 300 mm^2 cross sectional area and 250 mm spacing. In addition to that, stirrups are defined in direction of axis 2 (normal to axis 1) with 200 mm^2 cross sectional area and 462.5 mm spacing. The program will use this data to produce a layer of reinforcement with certain thickness by dividing the total reinforcement cross sectional area by the width of rebar layer. As illustrated in Figure 4.6 boundary conditions are chosen carefully to create a stress state comparable to the actual test. In order to minimize the creation of stress concentration at supports, various degrees of freedom are set to zero at nodes located on certain edges and faces, as seen in Figure

4.6. This would allow the concrete section to freely shrink or expand in the vertical and transverse directions.

The test loading condition can be simulated in various ways, for instance by inducing displacement, velocity or external load. Because the ABAQUS/Explicit is performing a dynamic analysis, some disturbing inertial forces can exist in areas of high acceleration which are generated right at the start of concrete cracking. This can be more crucial in case of direct tension members, as the stresses are uniform across the member and can reach the tensile strength all at once causing a sudden instability in the analysis. In order to minimize the creation of these undesirable inertial forces and to achieve an accurate quasi-static analysis, in case of using direct load, the load must be increased very slowly over a quite long period of time. Alternatively, to reduce the time of analysis and to minimize the acceleration as much as possible, a velocity can be induced on one face of the slab, as shown in Figure 4.7. The application of a constant velocity would guarantee the elimination or reduction of unwanted acceleration caused by cracking. Also all concrete elements would not crack at once as the tensile load can reduce after each crack is occured. It should be noted that in the actual test, hydraulic jacks were inducing displacement on the specimen and not a direct load.

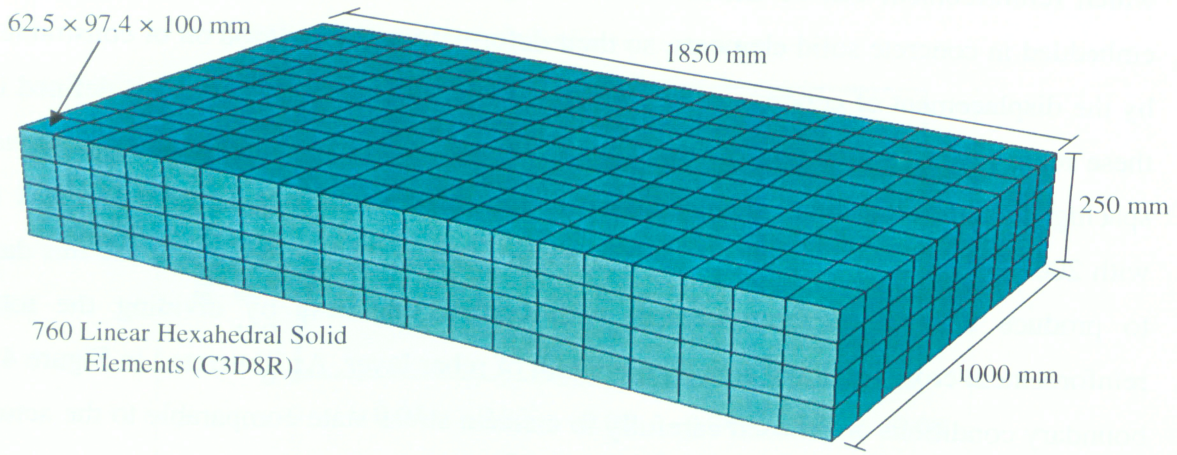

Figure 4.4 Slab geometry and meshing for direct tension 3D model

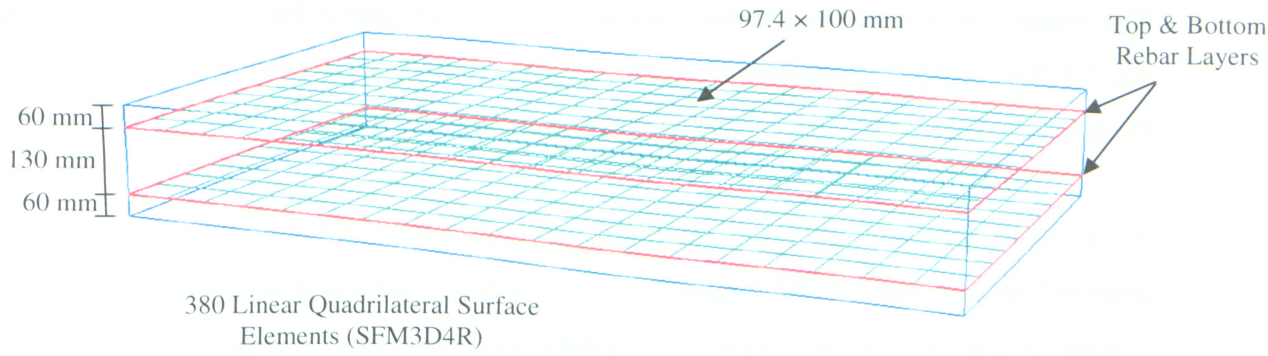

Figure 4.5 Reinforcement layers geometry and meshing

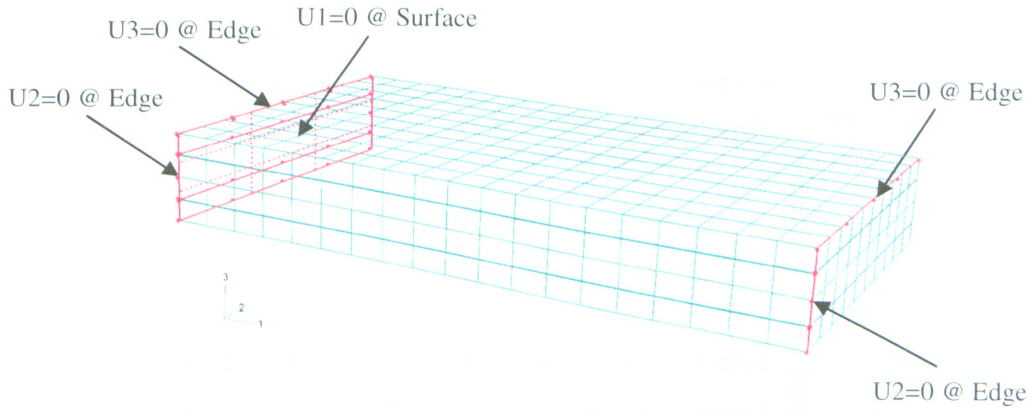

Figure 4.6 Boundary conditions

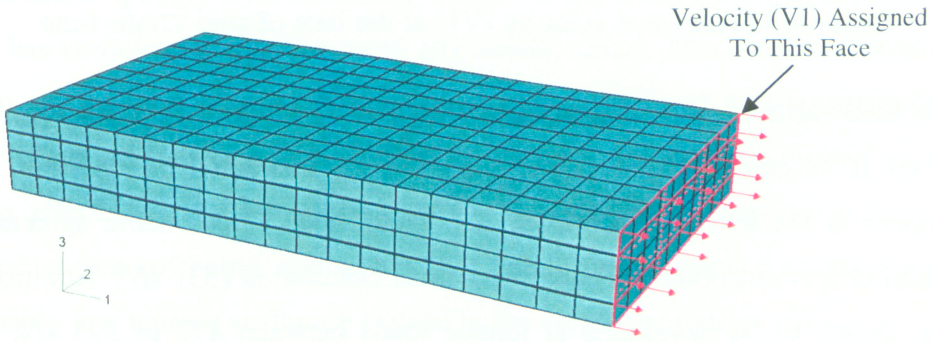

Figure 4.7 Velocity in direction of axis 1 assigned to one face of the slab

The model has been submitted to ABAQUS/Explicit processor for execution. The input file for this model is presented in section A.1 of Appendix. According to the results of analysis, the following information is obtained from the output.

As it can be seen in Figure 4.8, smoothly rising amplitude curve is defined for velocity assigned to one end of the concrete slab. A lower velocity is assigned during crack formation and once most of cracks are established, the velocity is raised smoothly to a higher value. The values for velocity are adjusted by trial and error to thoroughly capture the formation of cracks in the slab. A constant value could be used for velocity but this would increase the analysis time. The area under the velocity-time curve would be the overall elongation of the slab.

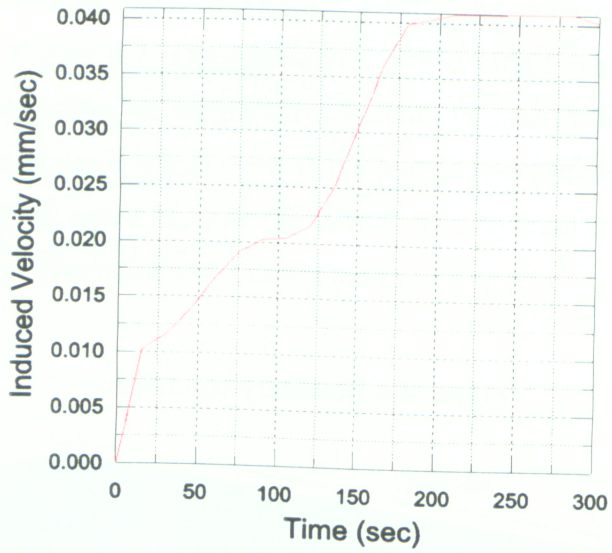

Figure 4.8 Predefined velocity (V1) at the face of slab versus time

The tensile load variation with analysis time is depicted in Figure 4.9. This is obtained by summing up all reactions in direction of axis 1 at the restrained face of slab. The first crack happens at the tensile load of 525 *kN* which is in a reasonable agreement with experimental observation (480 *kN*) and theoretical calculation (531 *kN*). Additionally, all cracks are shown to be developed at tensile loads between 477 to 595 *kN*, which is consistent with experimental observation (480 to 540 *kN*). Reinforcement has yielded at the tensile load of 956 *kN* in the model which is comparable to the calculated yield load

of $f_y \times A_s = 400 \times 2400 = 960 \ \ kN$. Unfortunately, no comparison can be made with experimental data as the test was not continued to the yielding of reinforcement.

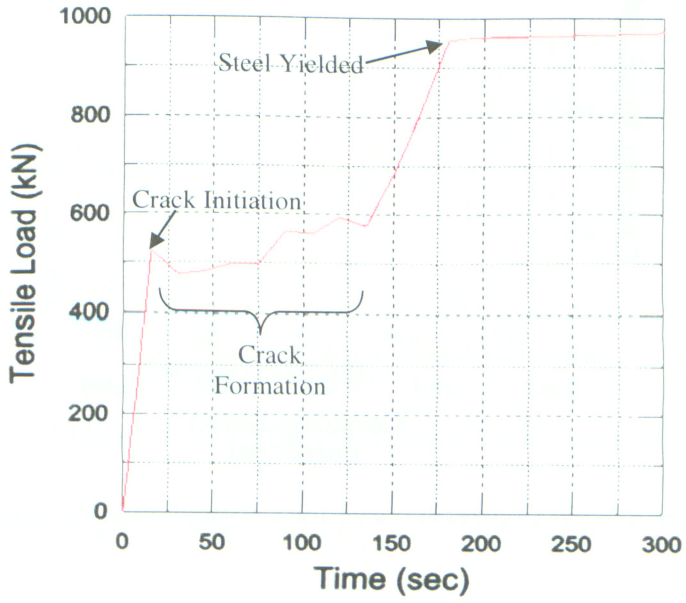

Figure 4.9 Tensile load history

Tensile stress/strain relation of the concrete was previously defined by using the fracture energy approach. For the sake of comparison, tension stress/strain curve of a typical concrete element is obtained from results of the analysis and is shown in Figure 4.10. Tension stiffening effect can be seen in the post failure behavior of the concrete element, i.e. the tensile stress in concrete element has not dropped sharply to zero after failure, but it has decreased quickly with increasing strain. At the strain of about 0.001 the concrete element has completely failed to carry any tensile stress. This strain value is computed based on the element size and the fracture energy defined earlier manually. Higher amount of fracture energy would increase the ultimate failure strain as well as the tension stiffening effect. The overall response of the structure is so sensitive to the predefined amount of tension stiffening, and an unstable condition can happen during the analysis if unreasonably low tension stiffening is used in the concrete model.

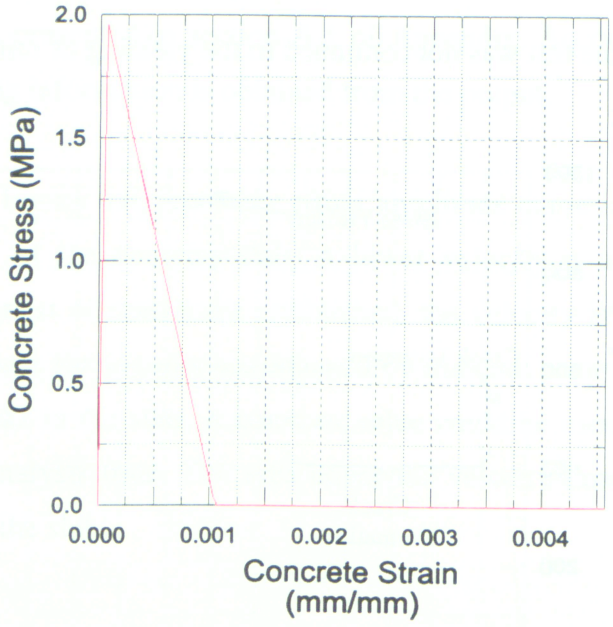

Figure 4.10 Stress/strain curve for a typical concrete element

Strain variation for a concrete element at different loads is shown in Figure 4.11. The experimental results are also drawn for comparison. In both cases, concrete strain suddenly increases after cracking. The amount of strain increase is less for experiment because during the experimental test the loading was not continued much beyond the cracking load. Additionally, a perfect bond condition is assumed in the model, however, some amount of bond slip always exists in the actual structure. This bond slip can reduce the amount of stresses transmitted from steel reinforcement at cracked section to the surrounding concrete, and hence, can result in lower stress/strain values in concrete than what are obtainable from a perfect bond model. The stress variation for a concrete element at different loads is shown in Figure 4.12. It can be seen that cracking occurs when the principle tensile stress in the element reaches the concrete tensile strength of about 2 *MPa* at a load of 525 *kN*.

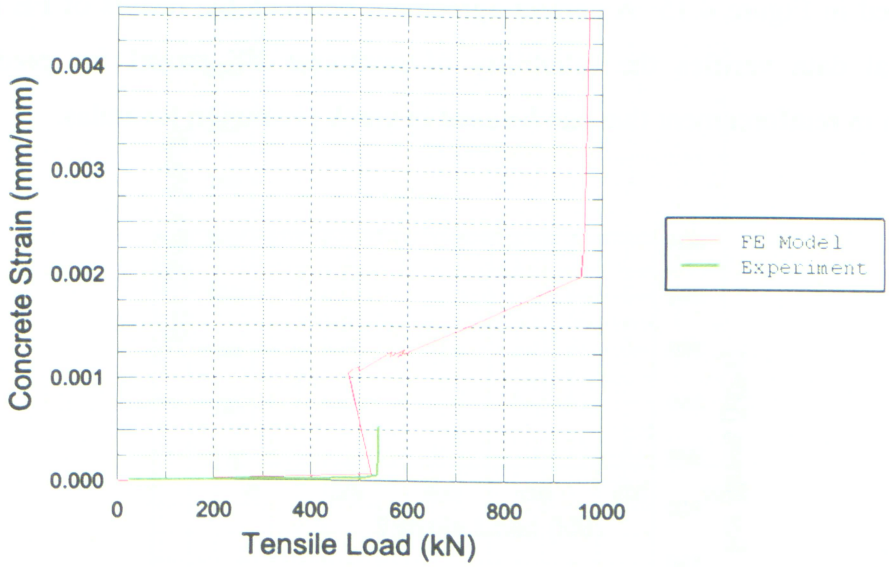

Figure 4.11 Strain versus tensile load comparison for a typical concrete element

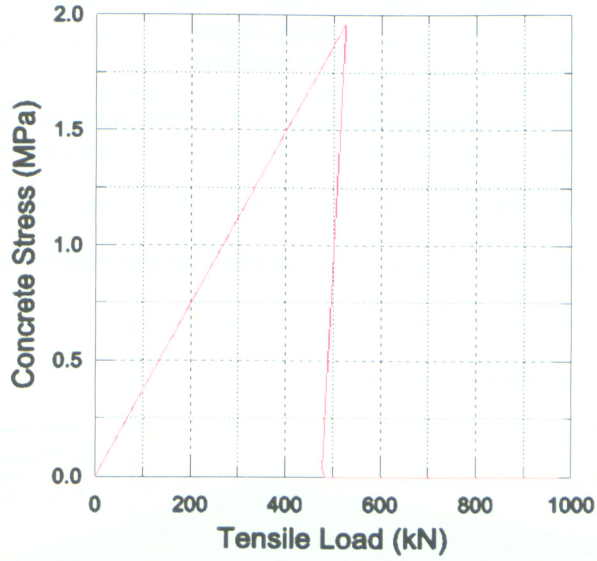

Figure 4.12 Stress versus tensile load for a typical concrete element

The same predefined steel stress/strain curve as in Figure 4.3 is obtained from a typical reinforcement element, as shown in Figure 4.13. A comparison is made in Figure 4.14 between the results of experiment and FE model for the steel strain at different loads. In both cases, at cracking load of 525 *kN*, the strain in reinforcement suddenly increases to the level of 0.001 after stresses are transferred from the concrete to the reinforcement at the cracked section. The same behavior can be seen for the stress in reinforcement versus

load depicted in Figure 4.15. A perfect agreement between the results of FE model and experimental data verifies the reliability of nonlinear FE model for predicting the stress/strain in reinforcement that can be used in crack prediction formulas.

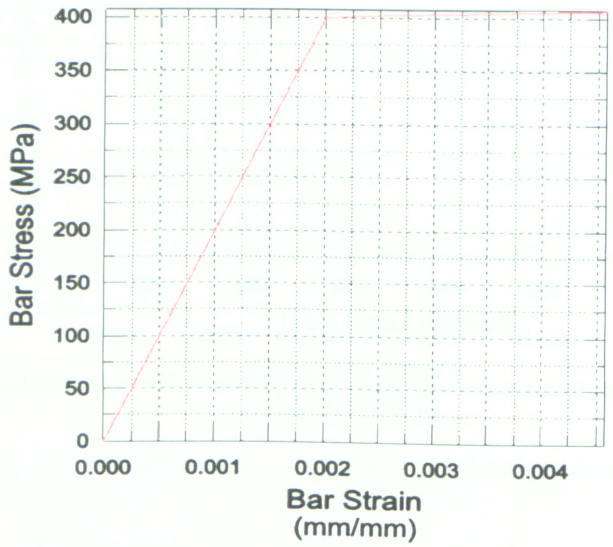

Figure 4.13 Stress/strain curve for a typical rebar element

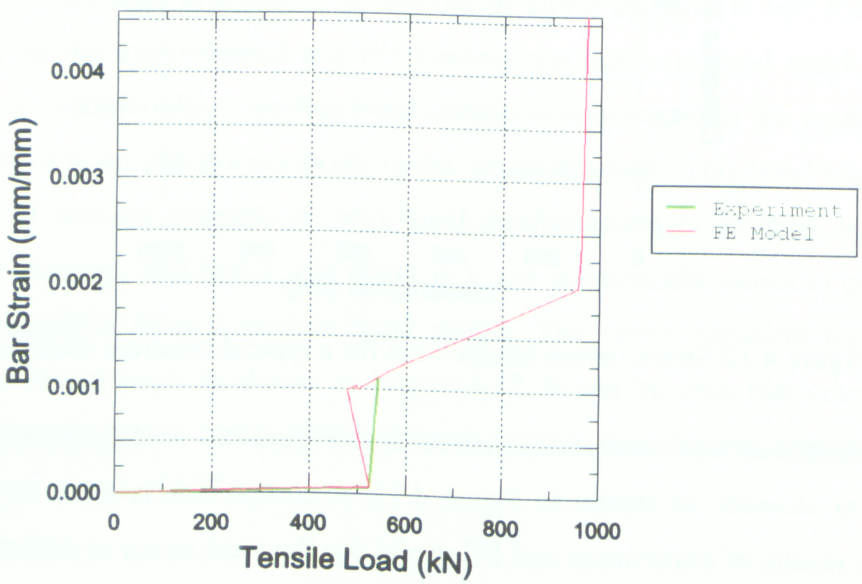

Figure 4.14 Strain versus tensile load comparison for a typical rebar element

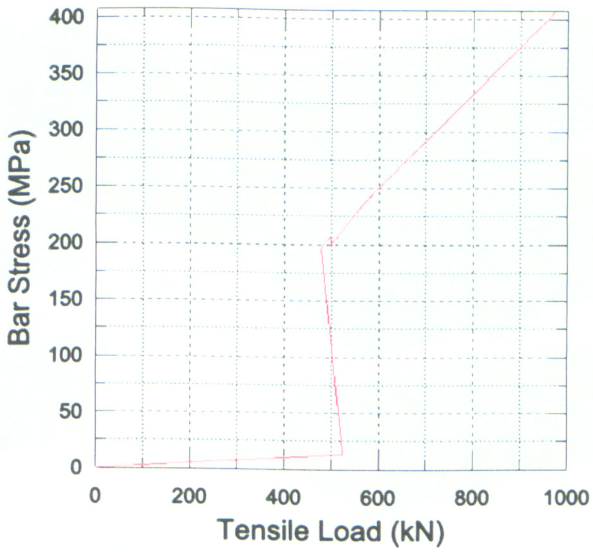

Figure 4.15 Stress versus tensile load for a typical rebar element

The formation of the first crack is illustrated graphically in Figure 4.16. This is obtained by drawing the strain contour for the slab. A strip of elements in red color which corresponds to the highest strained elements in the member represents the first crack. As the load increases the concrete stress at other sections again reaches the concrete tensile strength and other cracks form in the slab. The crack propagation in RC slab at different times in a loading step is depicted in Figure 4.17.

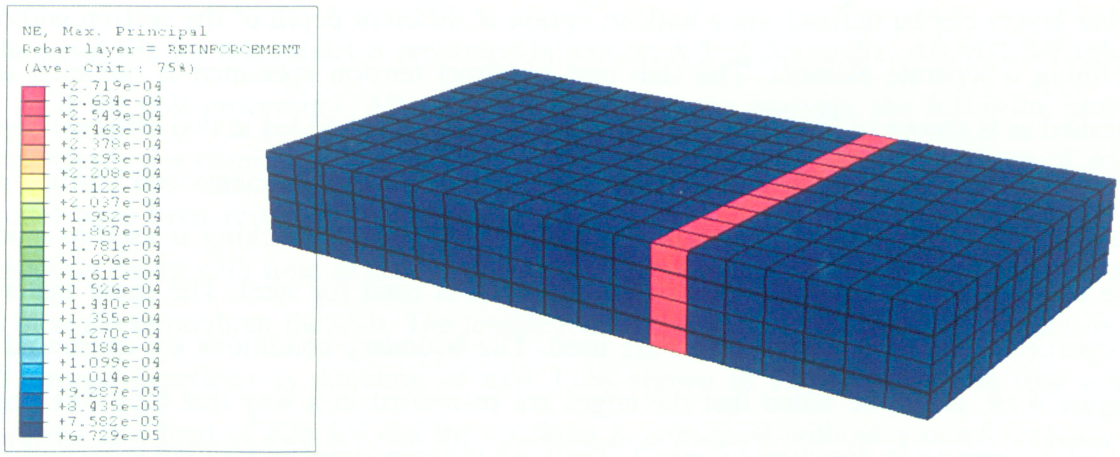

Figure 4.16 Graphical display of the first crack formed at step time = 15 sec

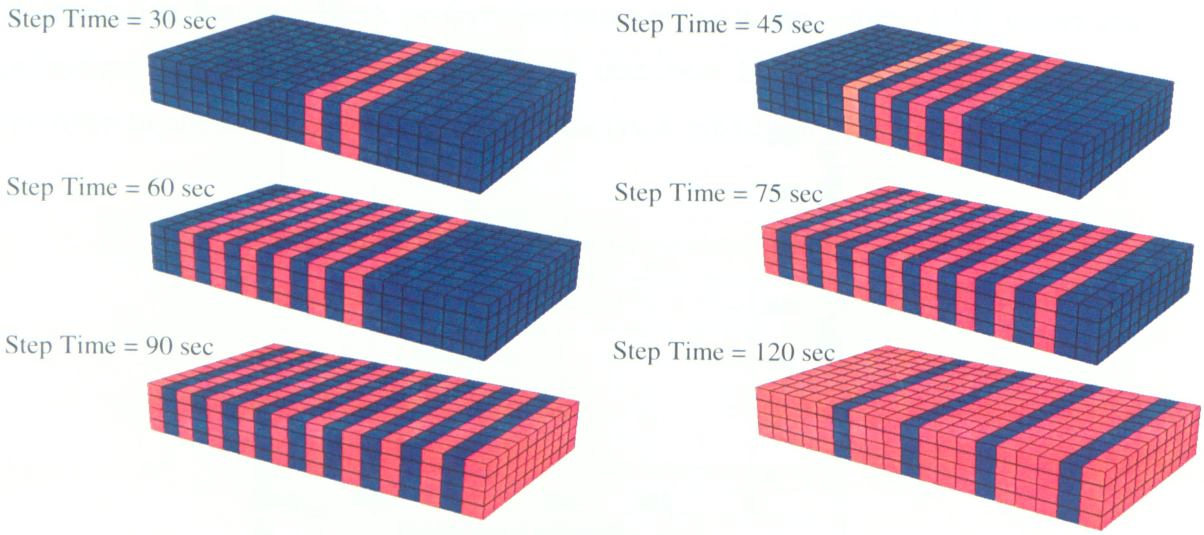

Figure 4.17 Graphical display of crack propagation at different time steps

4.2.6 Three Dimensional Model with Shell Elements

Although shell elements are graphically shown two dimensional, they are computationally three dimensional as they can have a number of integration points to render the stresses through their thickness. Apparently, defining the slab geometry is quite simple, and the overall analysis time is less than that of solid elements. Modeling the reinforcement is also much easier for this type of elements than for solid elements, as rebar layers can be defined via a built-in option at different depth of the section without defining a separate element. The slab part of direct tension specimen is modeled and meshed as is shown in Figure 4.18. Two rebar layers are embedded at two different depth of the section (60 and 190 *mm*), and both longitudinal reinforcements and stirrups are defined in the same manner as in the previous model. Brittle cracking is used to model the concrete and an isotropic elasto-plastic model is used for steel. The same material properties as in the previous model are used. The boundary conditions are illustrated in Figure 4.19. It can be noted that the edges are restrained in a way that they can freely shrink or expand in direction of axis 2. The load is again simulated by inducing velocity at one edge.

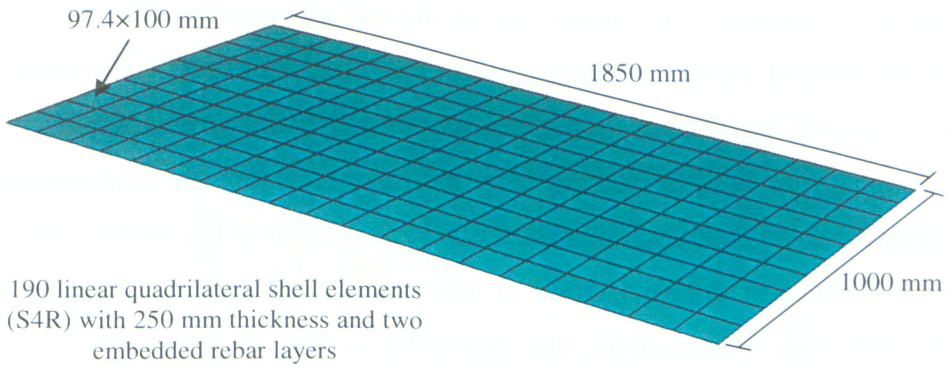

Figure 4.18 Slab geometry and meshing

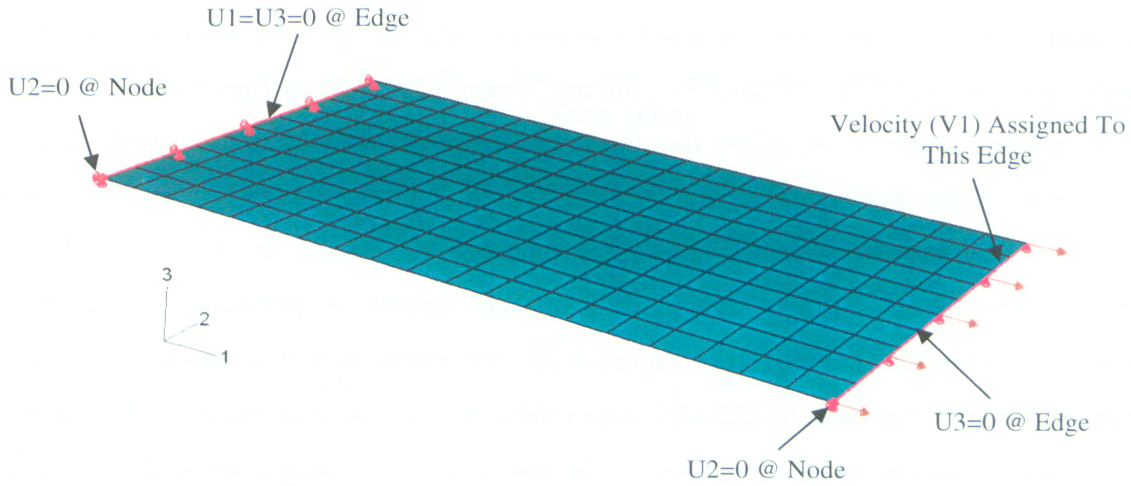

Figure 4.19 Boundary conditions and assigned velocity

The input file for this model is presented in section A.2 of Appendix. ABAQUS/Explicit is used for post-processing. After the completion of the analysis, the following graphs and figures are obtained from the output data. Almost similar results to those of solid model have been resulted from the shell model. The magnitude of induced velocity is smoothly rising with time as shown in Figure 4.20. This would cause the tensile stresses to increase throughout the slab. The tensile load history is obtained by the summation of all support reactions in direction of axis 1, as shown in Figure 4.21. The first crack happens at a load of 526 *kN* and the cracking is continued without a much increase in tensile load but with a large increase in tensile strain along the slab. As the slab stretches out, concrete elements along the slab fail one after each other till no more concrete

element remains un-cracked. This means that at the end all concrete elements have lost their stiffness because of a uniform stress condition throughout the slab. However, in the actual test the concrete can contribute to the structure stiffness by remaining un-cracked even at the ultimate load because of bond-slip that exists between the reinforcement and the surrounding concrete. Although a perfect bond is assumed in the model, this can not affect the maximum reinforcement strain at cracked sections which is needed for the crack width prediction. Furthermore, the bond-slip is less of a concern in case of structures under non-uniform stresses in which only few elements are highly strained. The ultimate capacity is achieved when the steel reinforcement yields at a load of 947 *kN*. Concrete stress/strain curve is shown in Figure 4.22. Again tension stiffening effect can be clearly seen in this curve. A good consistency can be seen between the results of model and the experimental data for concrete strain illustrated in Figure 4.23. Concrete stress history, Figure 4.24, shows that the stress in the cracked concrete sharply drops to zero value at the load of cracking. A stress/strain relation similar to predefined steel stress/strain curve is obtained for reinforcement as shown in Figure 4.25. The reinforcement strain history obtained from FE model is perfectly matching the experimental results as depicted in Figure 4.26. The stress in reinforcement at a cracked section suddenly increases to 225 *MPa* when the concrete cracks as shown in Figure 4.27. The crack formation and propagation in the slab is demonstrated graphically in Figures 4.28 and 4.29.

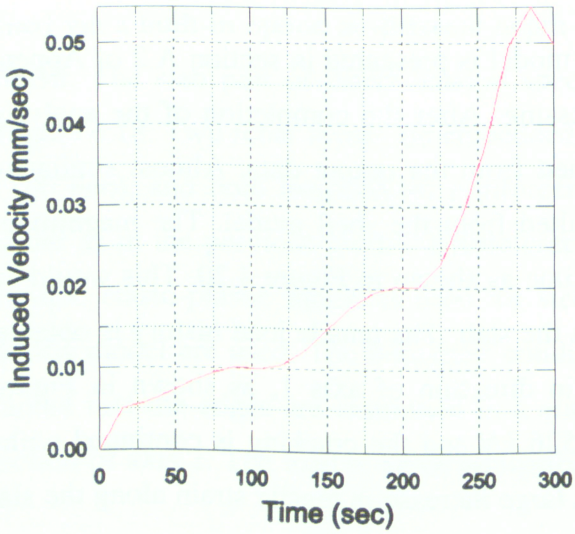

Figure 4.20 Predefined velocity (V1) at the edge of slab versus time

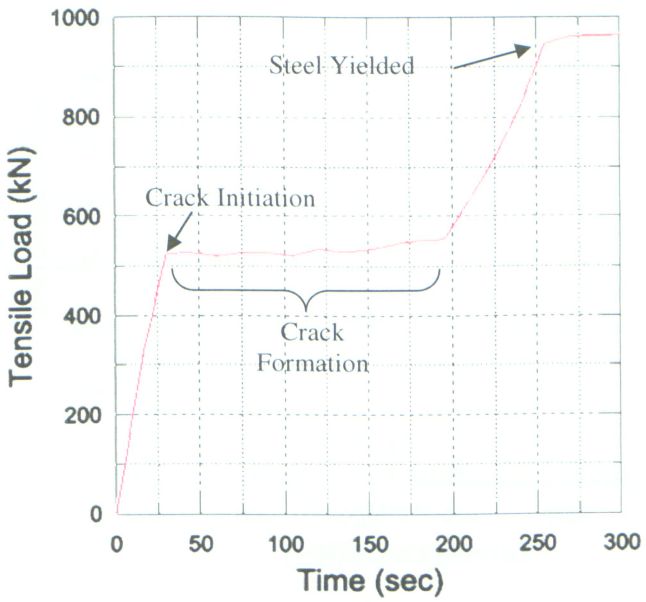

Figure 4.21 Tensile load history

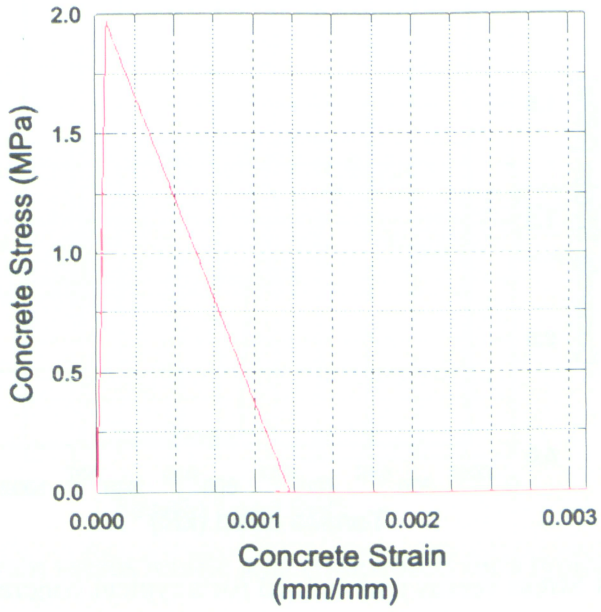

Figure 4.22 Stress/strain curve for a typical concrete element

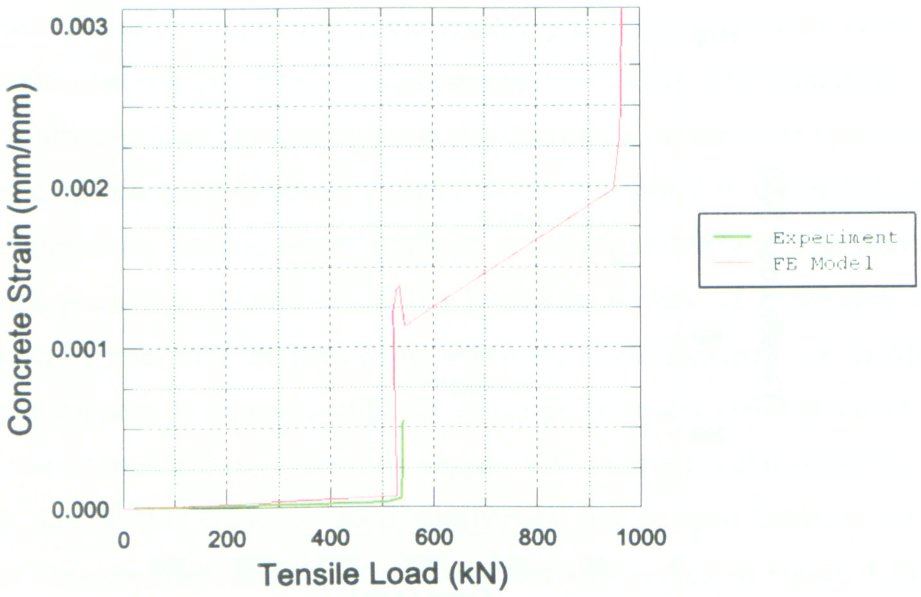

Figure 4.23 Strain versus tensile load comparison for a typical concrete element

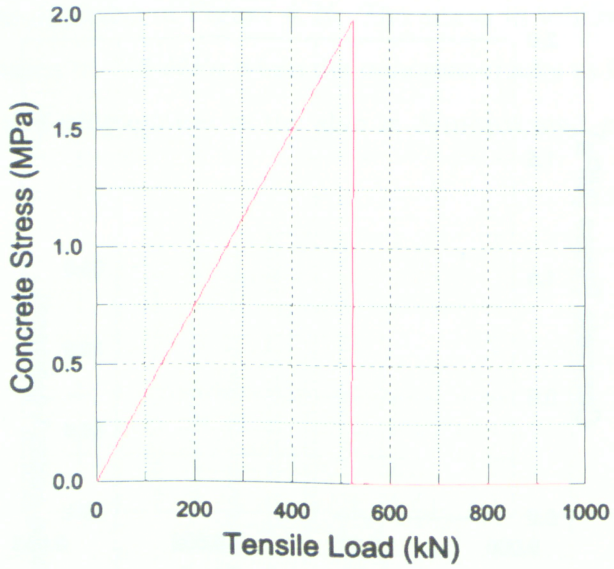

Figure 4.24 Stress versus tensile load for a typical concrete element

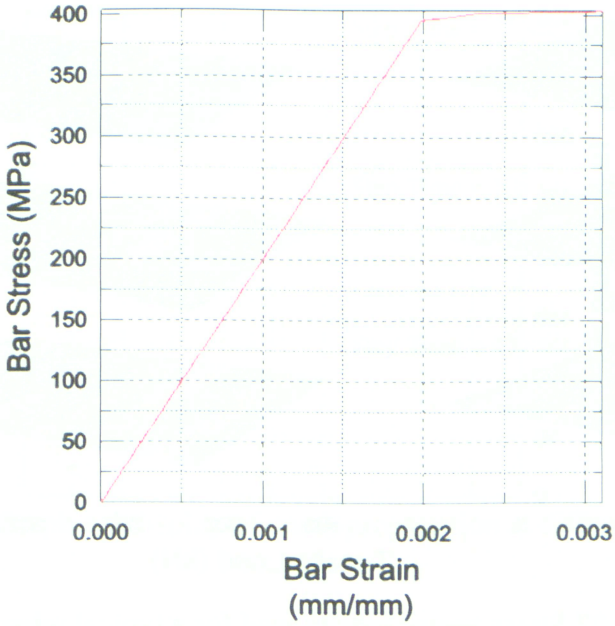

Figure 4.25 Stress/strain curve for a typical rebar element

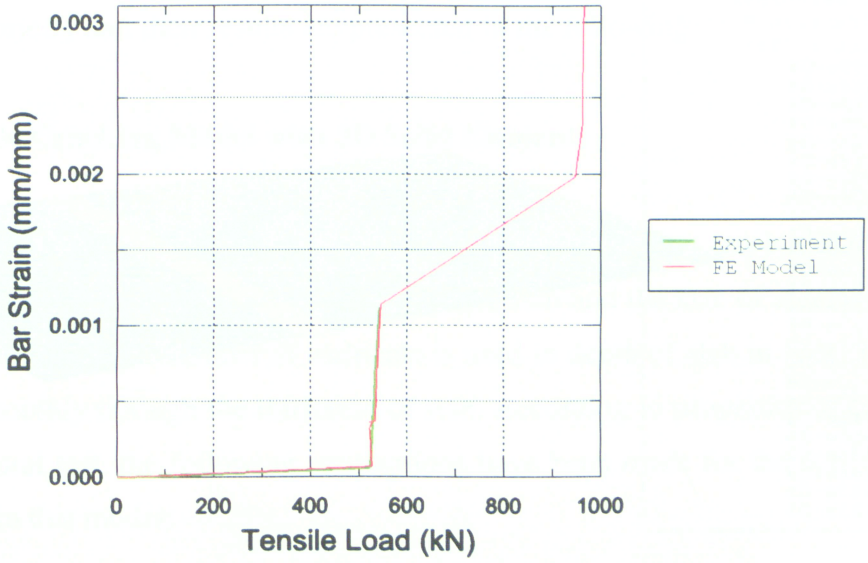

Figure 4.26 Strain versus tensile load comparison for a typical rebar element

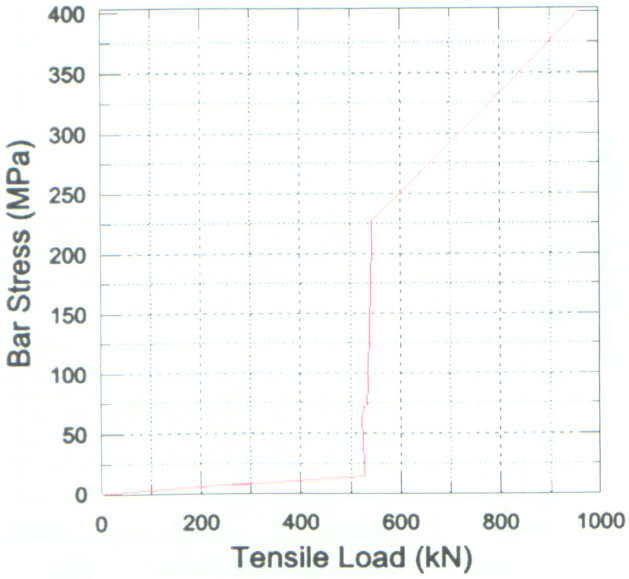

Figure 4.27 Stress versus tensile load for a typical rebar element

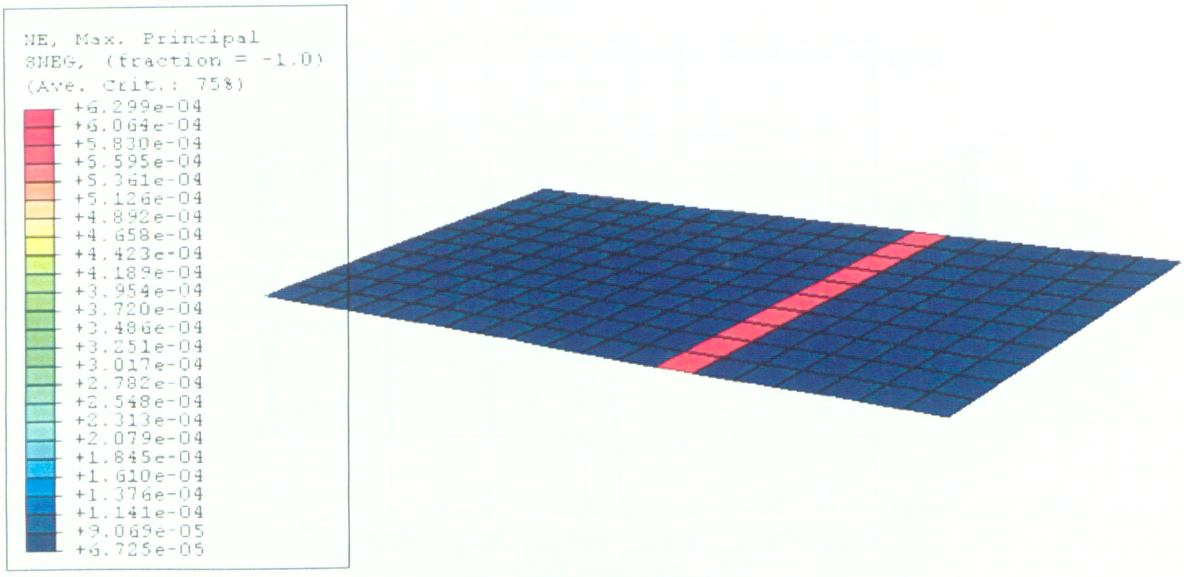

Figure 4.28 Graphical display of the first crack formed at step time = 30 sec

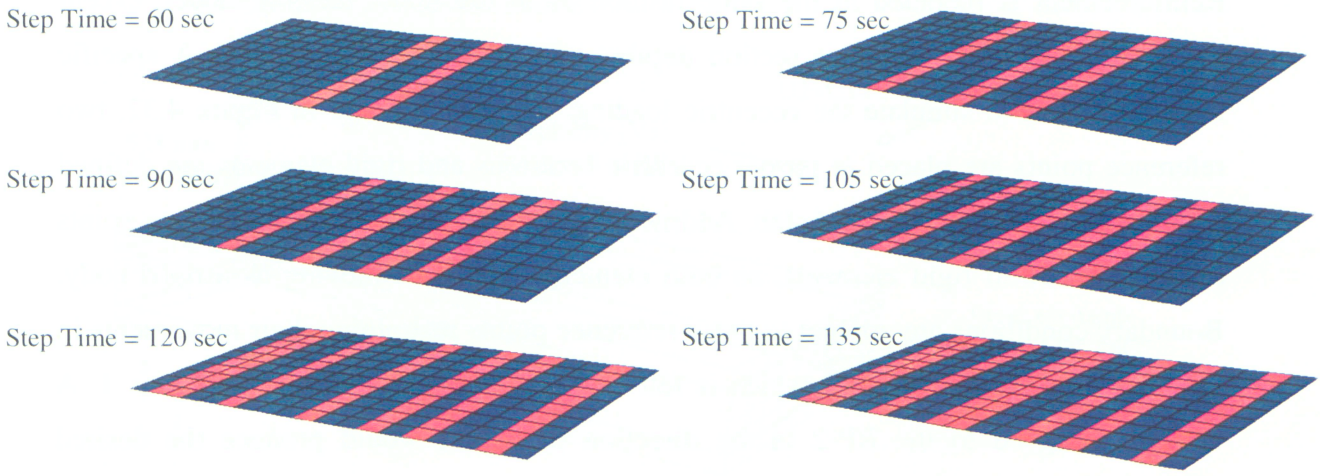

Figure 4.29 Graphical display of crack propagation at different step times

4.3 Flexural Model (High Eccentricity)

In this case in addition to previously explained brittle cracking model, the damaged plasticity model is also used for simulating the concrete behavior. These two models are described briefly and their results are presented in the following.

4.3.1 Brittle Cracking Model with 3D Solid Elements

There is not much difference between this model and the direct tension 3D solid model. A minute difference can be seen in the length of slab and the size of elements, as shown in Figure 4.30. Higher number of elements is used in depth of slab in order to render the stresses smoothly through the thickness of slab. According to properties of concrete used in the flexural test, the following assumptions have been made for the concrete material properties in this model:

Concrete Modulus of Elasticity = 23715 *MPa*

Concrete Tensile Strength = 1.65 *MPa*

Concrete Poisson's Ratio = 0.18

Concrete Density = 2400 Kg/m^3 (2.4×10^{-9} $tonne/mm^3$)

Reinforcement is modeled in the same fashion as in the direct tension model, except embedded at slightly different section depths, as depicted in Figure 4.31. A specific method is used to simulate the eccentric loading. As it is depicted in Figure 4.32, two reference points are placed at proper eccentric locations and rigid elements are defined and attached to the end faces of slab. Additionally, the movements of the reference points are constrained to rigid elements, so both elements would be moving as a rigid body. Boundary conditions are applied to these reference points restraining their movements in any direction except for RP-2 which is left free to move in the direction of axis 1. A velocity assigned to the RP-2 in the direction of axis 1 would produce the desired eccentric load. The input file for this model is presented in section A.3 of Appendix. The model is submitted to ABAQUS/Explicit post processing module for execution. The results of analysis are collected from the output module and presented briefly in the following.

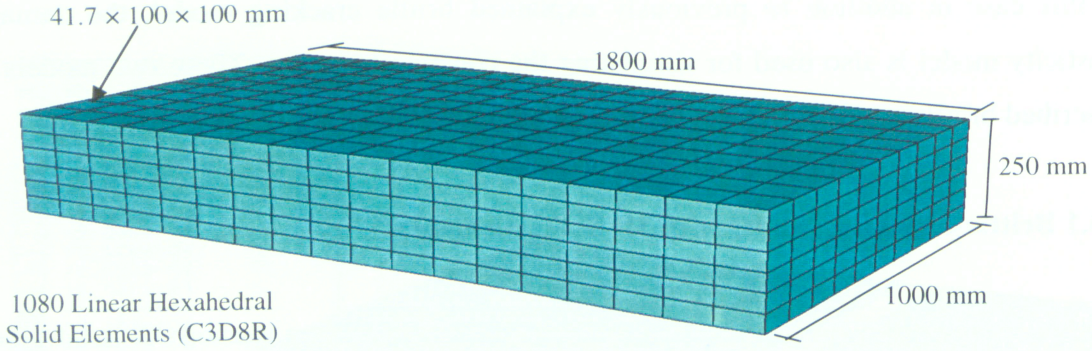

Figure 4.30 Slab geometry and meshing

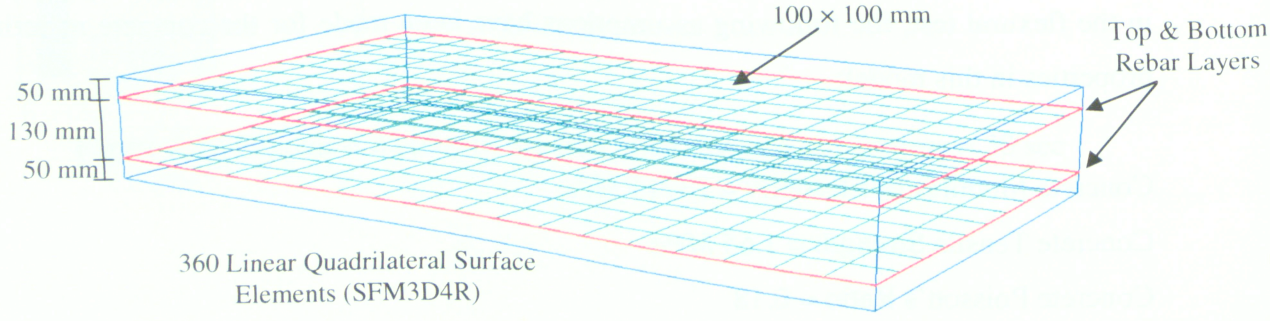

Figure 4.31 Rebar layers geometry and meshing

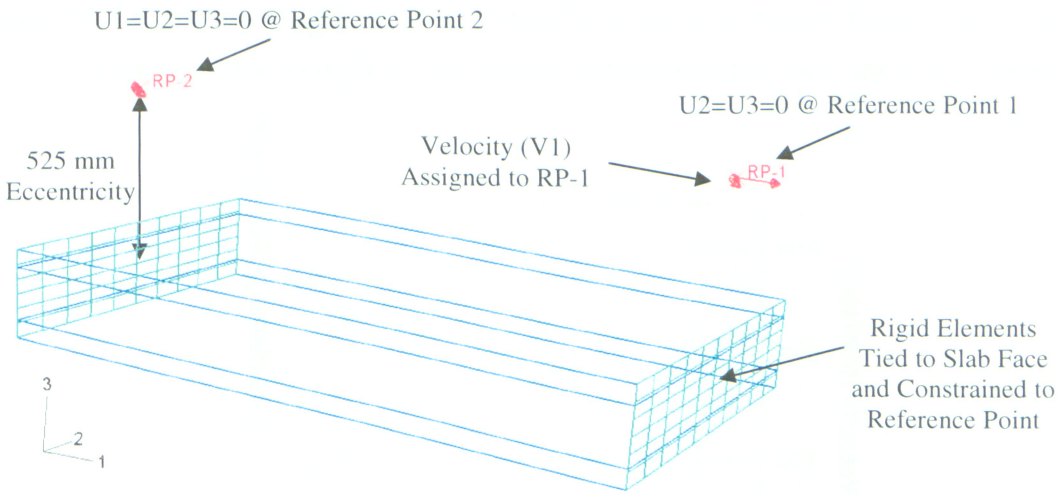

Figure 4.32 Boundary conditions and assigned velocity

The induced velocity at reference point 1 is raised to the value of 0.04 *mm/sec* over a short period of time at the beginning of the analysis as shown in Figure 4.33. The velocity is kept almost steady at this level for the rest of analysis. The first crack occurs at a load of 41 *kN* (Figure 4.34) which is analogous to the experiment initial crack load of 42 *kN*, and the tensile reinforcement has yielded at a load of 160 *kN*. As illustrated in Figure 4.35, a typical concrete element cracks when the principle tensile stress within the element reaches the value of about 1.6 *MPa*. As explained in brittle cracking model description a linear elastic behavior is assumed for concrete in compression (Figure 4.36). This is a reasonable assumption as the compressive stresses in concrete remain below 1/3 of its compressive strength. In the analysis, the strain values for concrete are higher than what was obtained from experiment (Figure 4.37). As explained earlier, this is due to the assumption of a perfect bond between the reinforcement and the surrounding concrete in the model. A drop in concrete stress at the cracking load can be seen in Figure 4.38. The obtained steel stress/strain curve in Figure 4.39 is perfectly matching with previously assumed steel stress/strain curve. An excellent agreement can be seen between the tensile steel strain obtained from FE model and the experimental data (Figure 4.40). Therefore, the results of this model for steel strain can effectively be used in crack prediction models. As it can be seen in the reinforcement stress history shown in Figure 4.41, when the eccentric load reaches to the level of cracking load the stress in reinforcement

increases at a cracked section to a value of about 75 *MPa*. The flexural crack formation and propagation in the slab is demonstrated graphically in Figures 4.42 and 4.43.

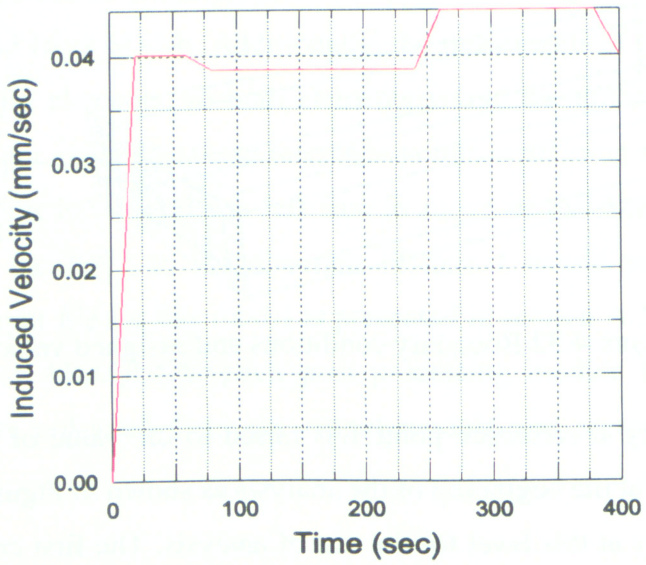

Figure 4.33 Predefined velocity (V1) at the reference point 1 versus time

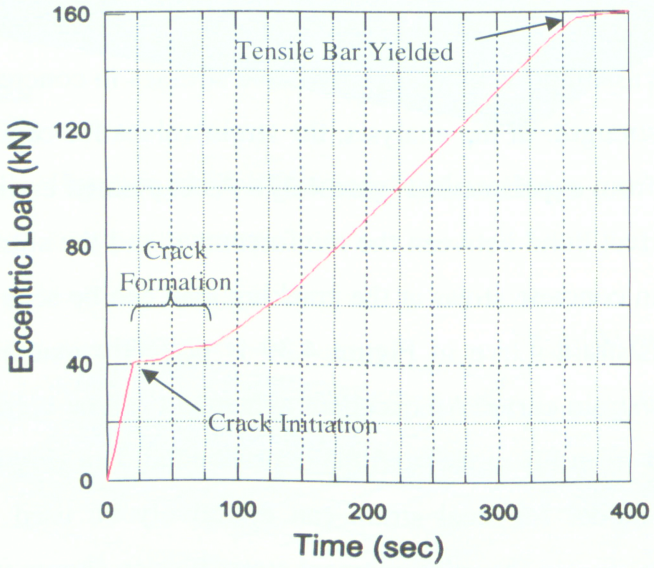

Figure 4.34 Tensile load history

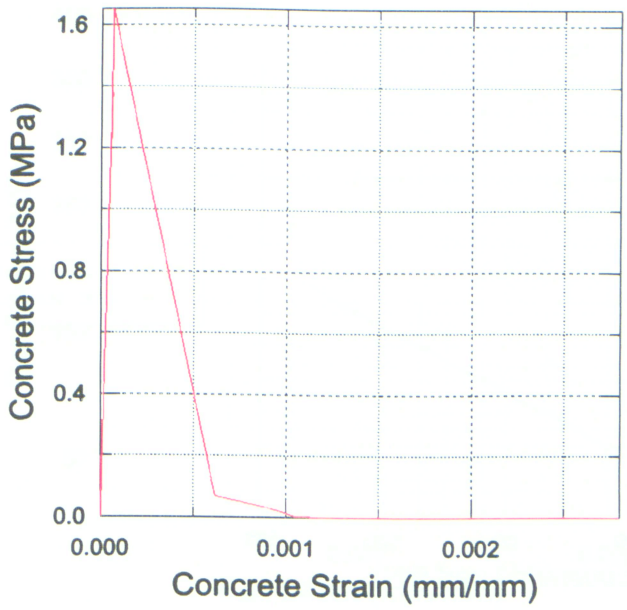

Figure 4.35 Tensile stress/strain curve for a typical concrete element at tension fiber of the section

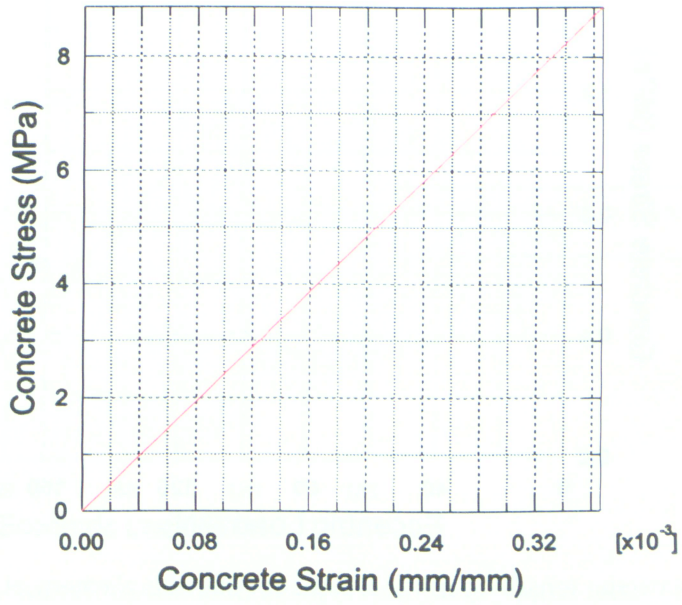

Figure 4.36 Compressive stress/strain curve for a typical concrete element at compression fiber of the section

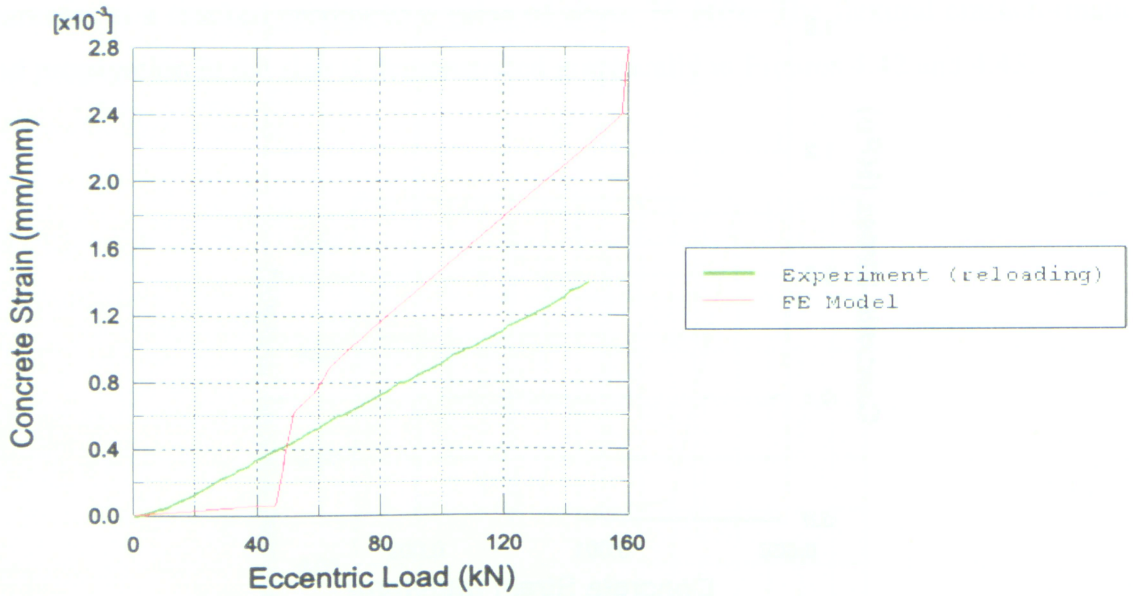

Figure 4.37 Strain versus tensile load comparison for a typical concrete element at tensile fiber of the section

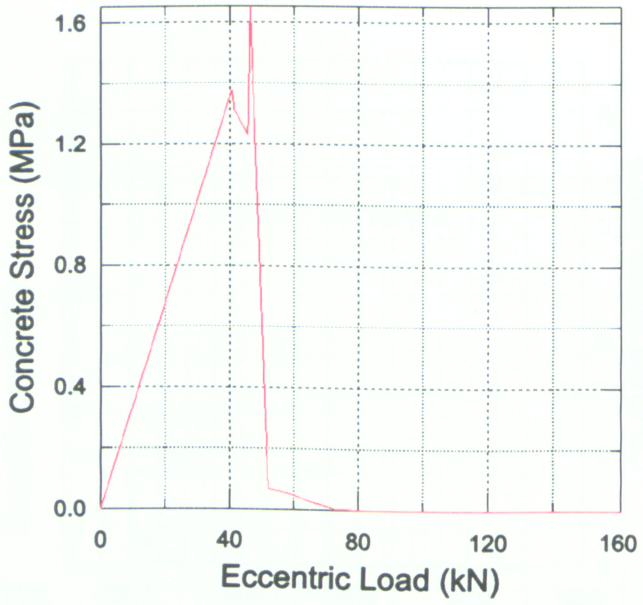

Figure 4.38 Stress versus tensile load for a typical concrete element at tensile fiber of the section

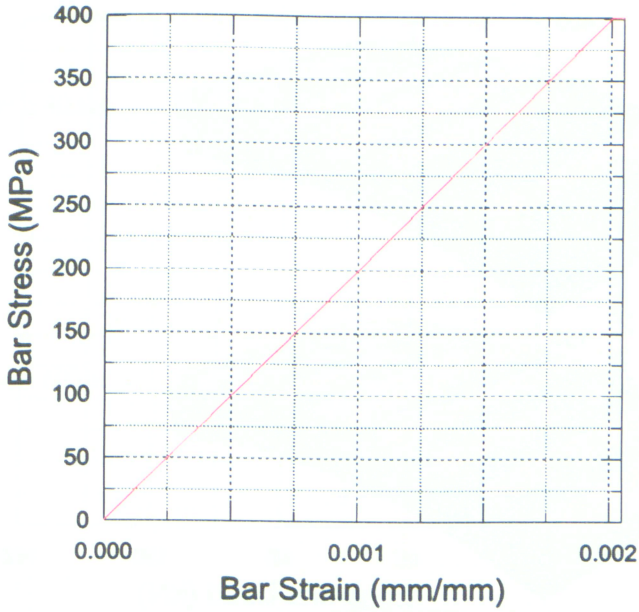

Figure 4.39 Stress/strain curve for a typical rebar element

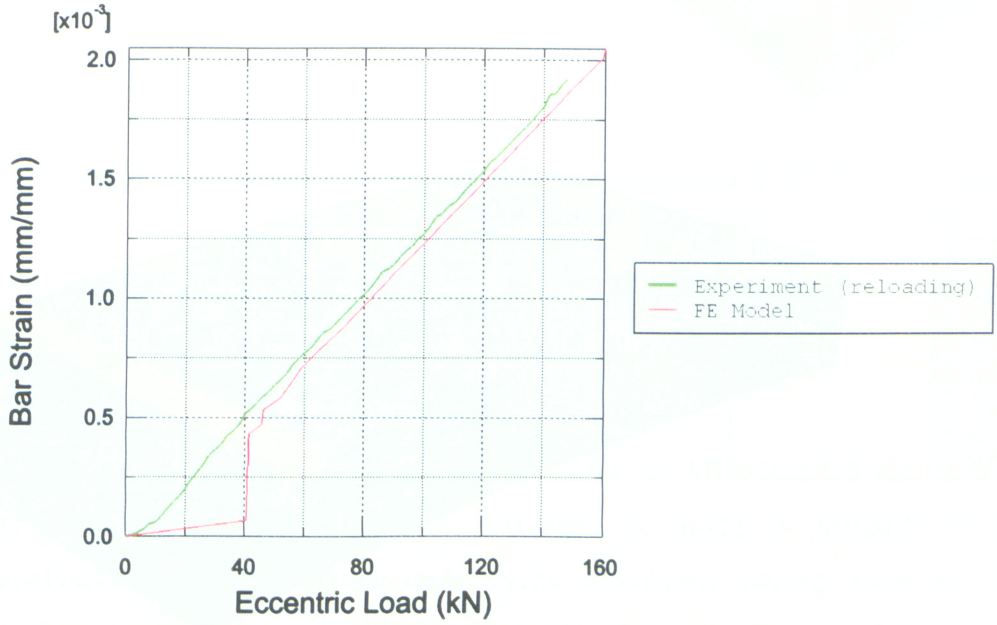

Figure 4.40 Strain versus tensile load comparison for a typical rebar element at top layer

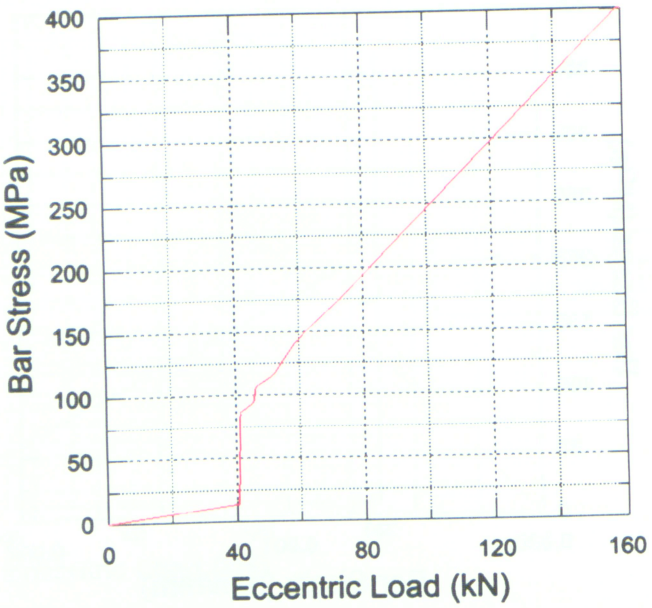

Figure 4.41 Stress versus tensile load for a typical rebar element at top layer

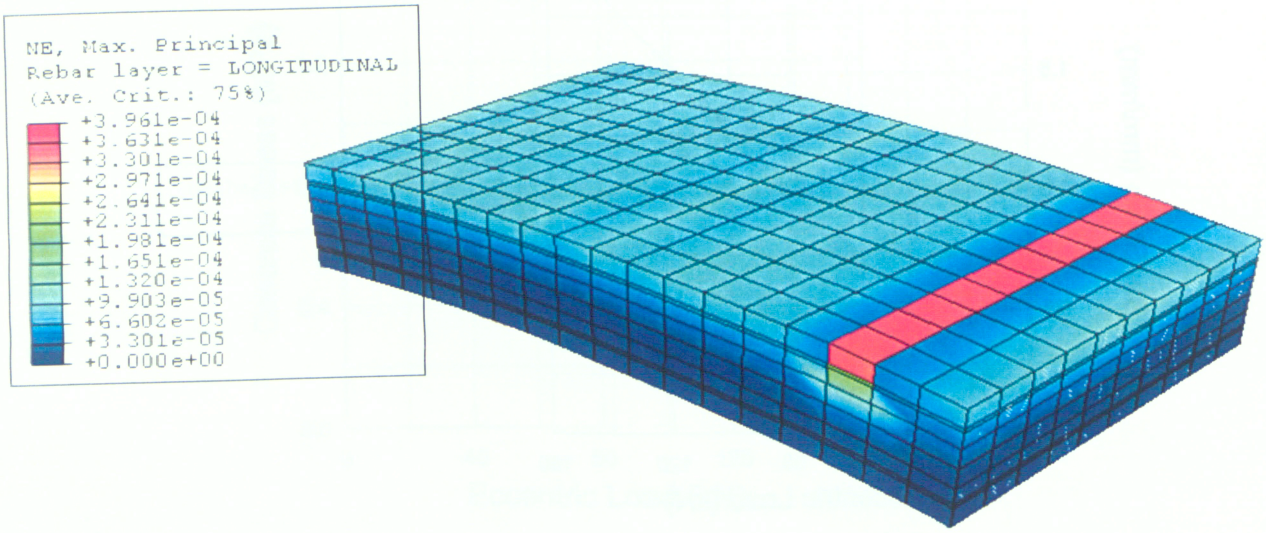

Figure 4.42 Graphical display of the first crack formed at step time = 20 sec

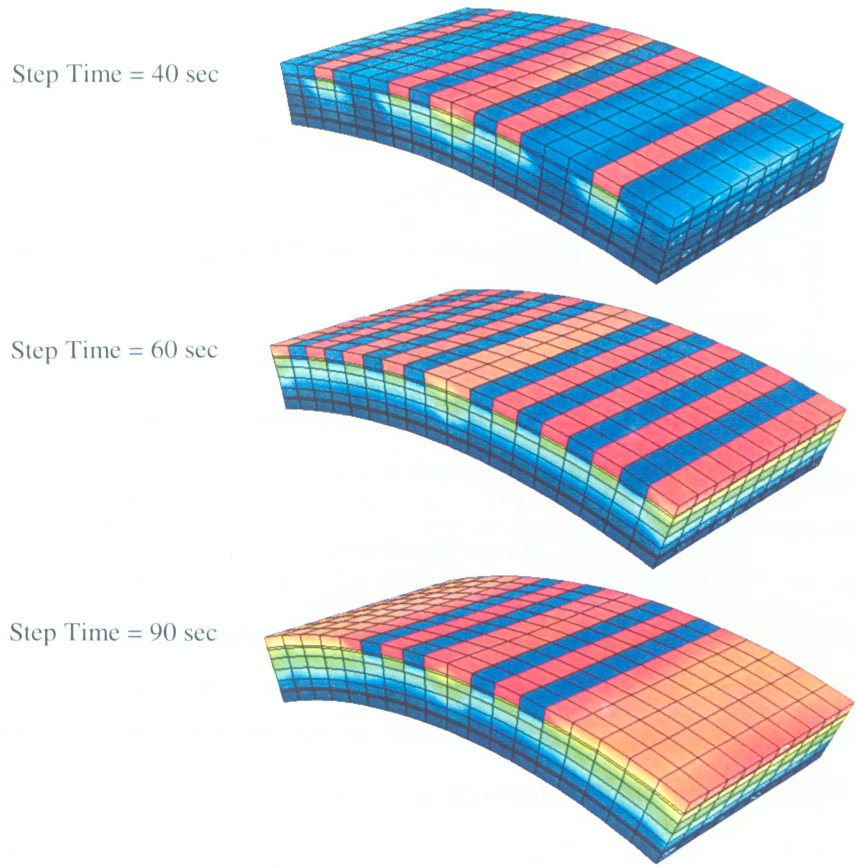

Figure 4.43 Graphical display of crack propagation at different step times with exaggerated deformed shape

4.3.2 Damaged Plasticity Model with 3D Solid Elements

Damaged plasticity is another model available in ABAQUS/6.5 for modeling a quasi-brittle material such as concrete. Although the model is primarily intended for the analysis of concrete structures under cyclic or dynamic loading, it can be efficiently used in the case of monotonic increasing loads. The failure mechanisms of concrete considered in this model include both the cracking in tension and crushing in compression. The post cracking tensile behavior of concrete can be defined in the same way as in brittle cracking. Since the compressive stresses remained relatively small in the tested slab section, the compressive behavior of concrete is not much influential on the overall

response of the structure, and is approximated by a trilinear curve as shown in Figure 4.44.

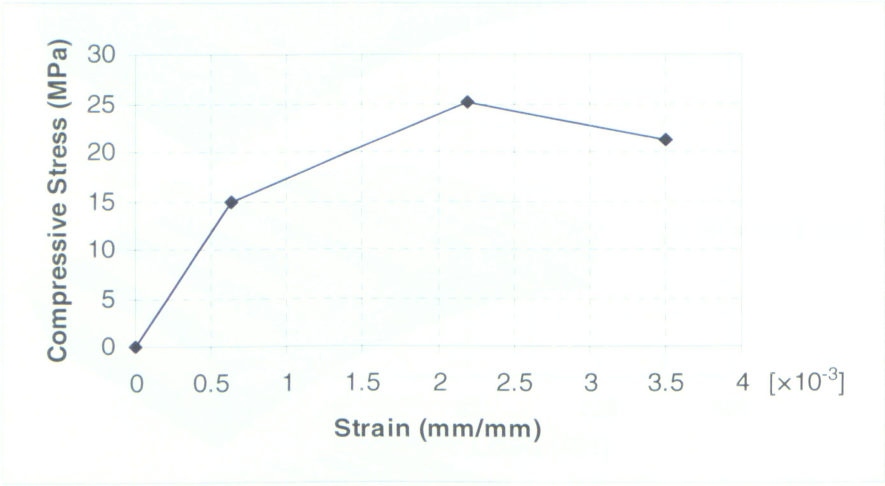

Figure 4.44 Concrete compressive stress/strain curve

The inelastic strain in Table 4.3 must be used as an input for ABAQUS/6.5 which is calculated based on the following equation:

$$\varepsilon_{inelastic} = \varepsilon_{total} - \frac{\sigma_c}{E_c}$$

Table 4.3 Concrete compressive stress/strain

Compressive Stress (Mpa)	Total Strain	Inelastic Strain
15	0.0006	0
25	0.0022	0.0011
21.25	0.0035	0.0026

Some other parameters must be determined for concrete material in damaged plasticity model. These parameters are more involved in compressive behavior of concrete and are not of much importance in monotonic flexural test which is failed in tensile cracking mode. Therefore, their default values are accepted here as described in the following:

Dilation Angle = 34 degrees

Flow Potential Eccentricity = 0.1

The ratio of initial equibiaxial compressive yield stress to initial uniaxial compressive yield stress = 1.16

The ratio of the second stress invariant on the tensile meridian, to that on the compressive meridian, at initial yield for any given value of the pressure invariant such that the maximum principal stress is negative = 0.666

Viscosity Parameter = 0 (ignored in ABAQUS/Explicit)

The rest of modeling procedure is exactly the same as what is described in brittle cracking flexural model. The input file for this model is presented in section A.3 of Appendix (considering the adjustment for damaged plasticity model on page A-16). The ABAQUS/Explicit module is used for post-processing, and the results are collected from the output data. The following graphs and figures are presented in the same previous manner based on the results of analysis. Nearly identical results to that of brittle cracking model are obtained from damaged plasticity model.

The velocity induced at reference point 1 is raised to the level of 0.05 *mm/sec* over the first 15 sec of the overall loading step time (Figure 4.45). This increase in velocity takes place before any crack occurs in the slab. The velocity is kept almost steady at this level to reduce the creation of undesirable acceleration due to cracking.

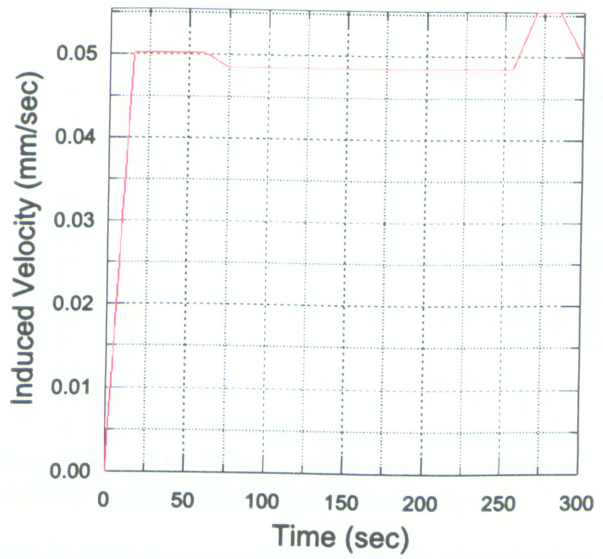

Figure 4.45 Predefined Velocity (V1) at the reference point 1 versus time

The first crack forms at a load of 44 *kN* as shown in Figure 4.46. The eccentric load history curve shows a fall and rise movement during the crack formation period. Tensile reinforcement is yielded when the eccentric load reaches the magnitude of about 160 *kN*.

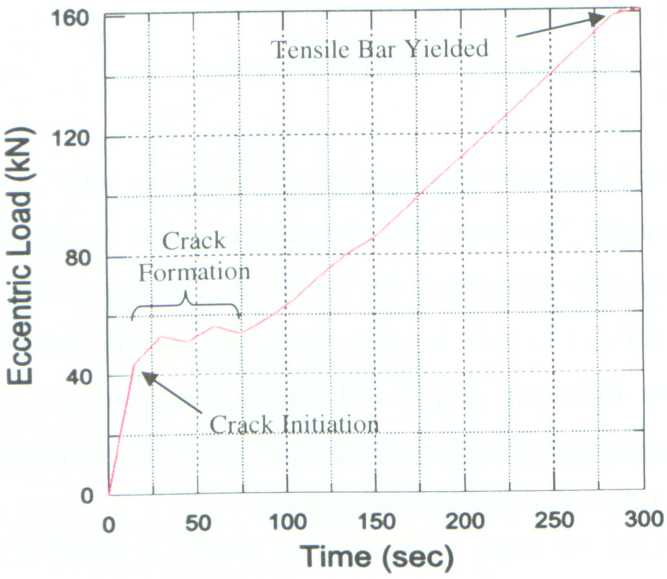

Figure 4.46 Tensile load history

An appropriate stress/strain curve with a sufficient amount of tension stiffening is obtained from a typical concrete element as illustrated in Figure 4.47.

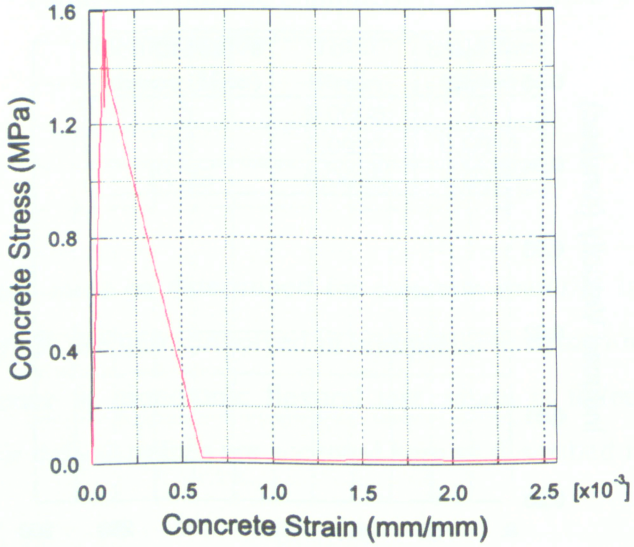

Figure 4.47 Tensile stress/strain curve for a typical concrete element at tension fiber of the section

The compressive stress at the compression fiber of the concrete section is in its elastic state with the maximum achieved stress of about 9 *MPa* as observed in Figure 4.48.

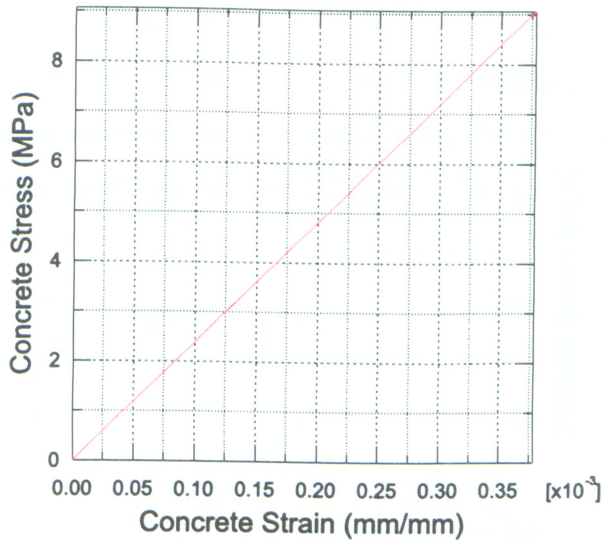

Figure 4.48 Compressive stress/strain curve for a typical concrete element at compression fiber of the section

The perfect bond assumption between the reinforcement and the surrounding concrete is again causing some discrepancy between the experimental and analytical data for strain in concrete as seen in Figure 4.49.

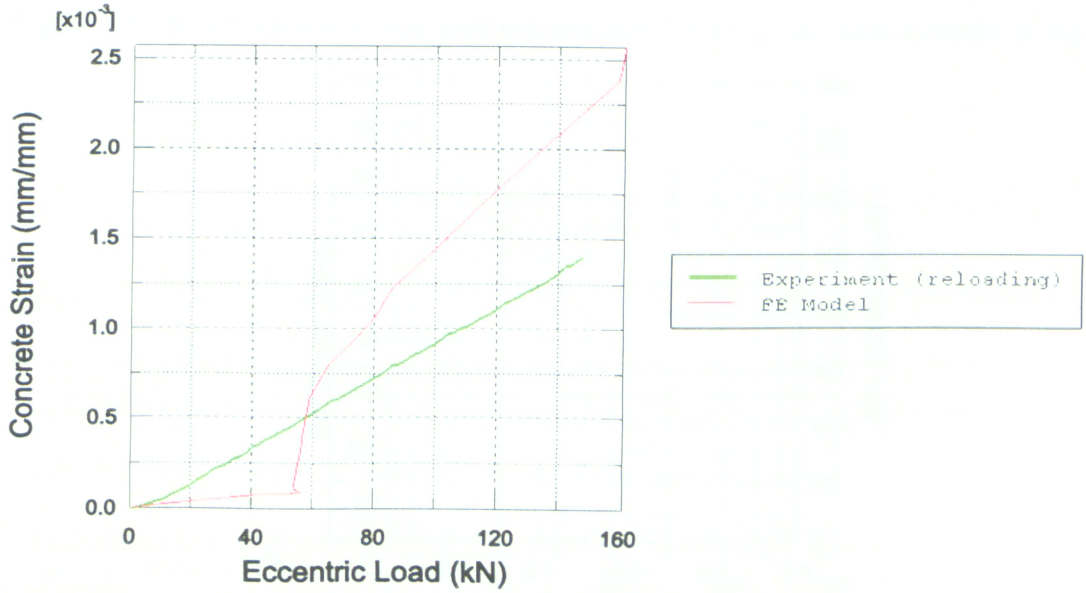

Figure 4.49 Strain versus tensile load comparison for a typical concrete element at tensile fiber of the section

At a cracking load of 44 *kN* the principle tensile stress in a typical concrete element reaches the tensile strength of concrete, upon which cracking occurs and the tensile stress in the concrete element sharply reduces to the lowest value of zero, as seen in Figure 4.50.

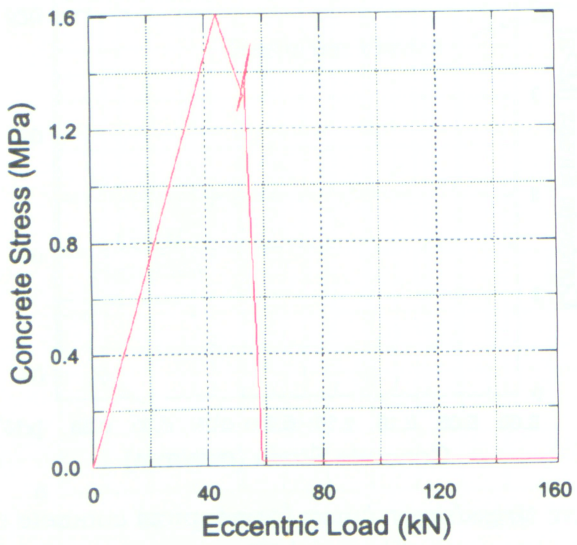

Figure 4.50 Stress versus tensile load for a typical concrete element at tensile fiber of the section

A suitable stress/strain curve similar to that is defined as an input for the steel material property is obtained from a typical rebar element, as presented in Figure 4.51.

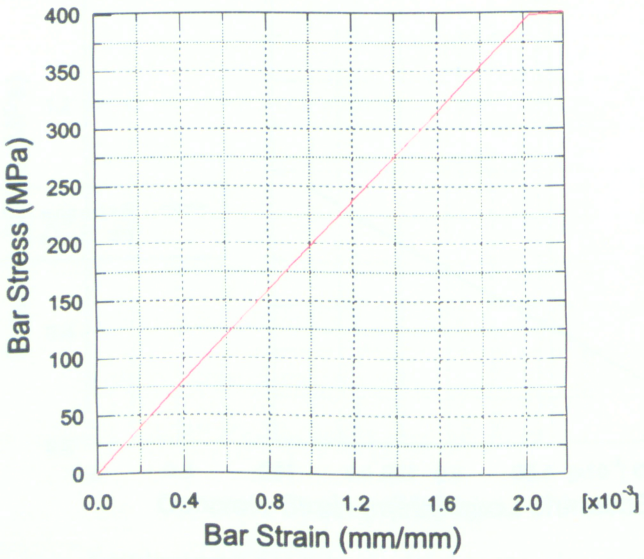

Figure 4.51 Stress/strain curve for a typical rebar element

A suitable agreement can be seen between the results of analysis and the experimental data for the strain in the reinforcement as depicted in Figure 4.52. This confirms the capability of this FE model in producing reliable results for the strain in reinforcement which then can be used in crack prediction models. The reinforcement stress history is obtained from a typical rebar element and is presented in Figure 4.53. An increase in reinforcement stress after cracking can be noticed in this figure. The crack formation and propagation in the slab is graphically shown in Figure 4.54.

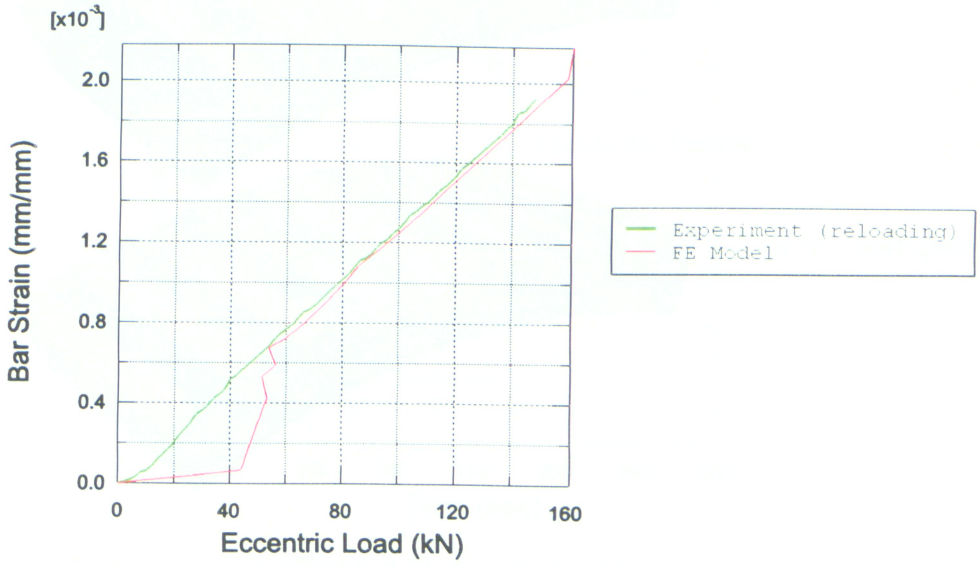

Figure 4.52 Strain versus tensile load comparison for a typical rebar element at top layer

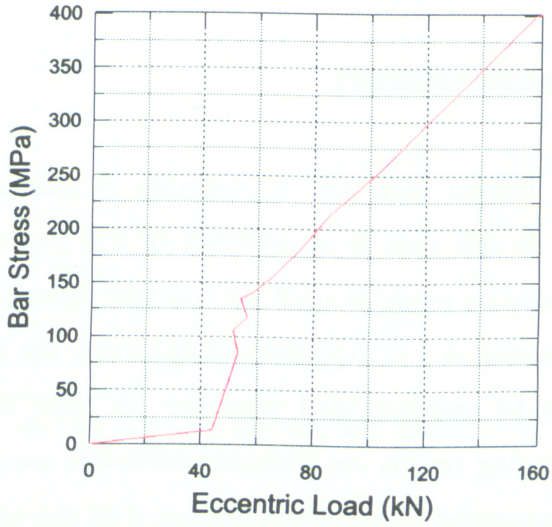

Figure 4.53 Stress versus tensile load for a typical rebar element at top layer

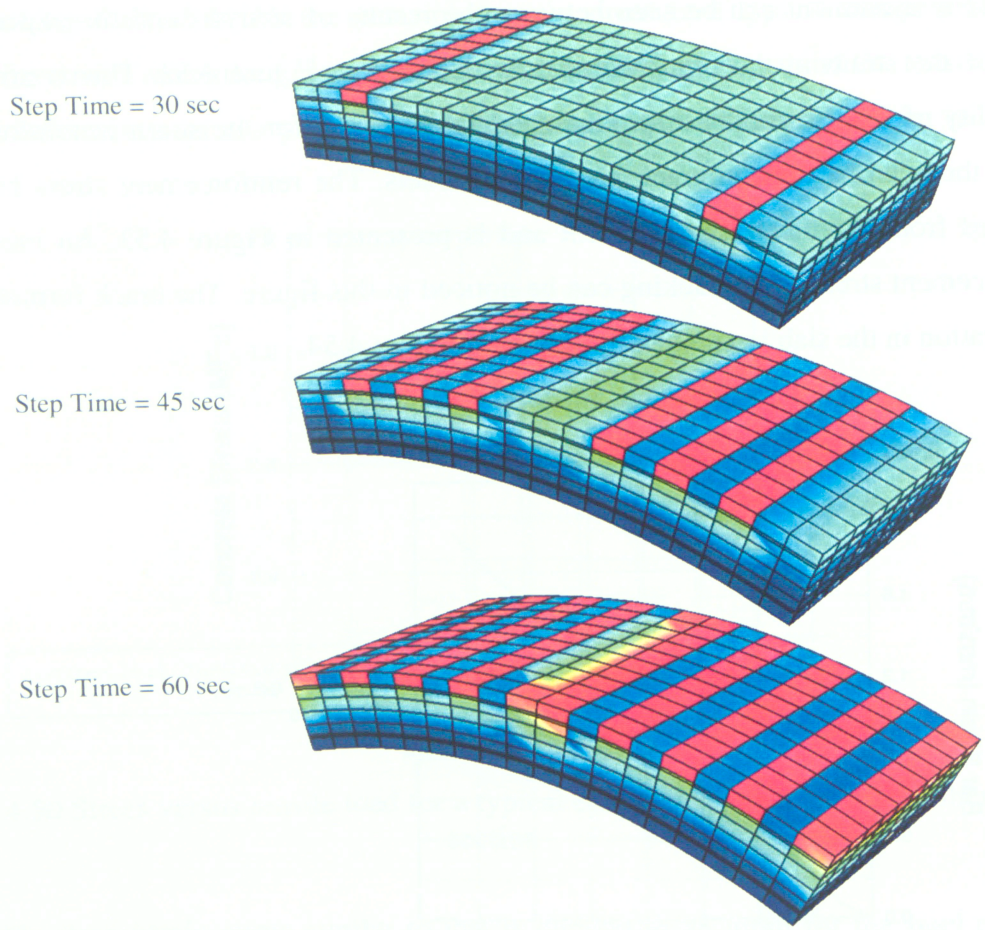

Figure 4.54 Graphical display of crack propagation at different step times with exaggerated deformed shape

4.4 Flexural Model (Low Eccentricity)

The modeling of slab loaded with low eccentricity is similar to that of the high eccentricity tested slab. In this case an eccentricity of 250 *mm* is defined for reference points. The damaged plasticity model is used for concrete material. The input file for this model is presented in section A.3 of Appendix (considering the adjustment for both low eccentricity on page A-14 and damaged plasticity on page A-16). Similar to other previous models, convincing results are obtained from this model. To avoid repetition only a few graphs are presented here for comparison with the experiment. Based on the

results of this model, the first crack occurs at the load of 95 *kN*, which is close to what was observed during experiment (110 *kN*), as depicted in Figure 4.55. The concrete strain comparison in Figure 4.56 is again highlighting some discrepancy between the results of the actual test and the FE model. This is due to the assumption of a perfect bond in the model. The results of the reinforcement strain are in good agreement with the experimental data as depicted in Figure 4.57.

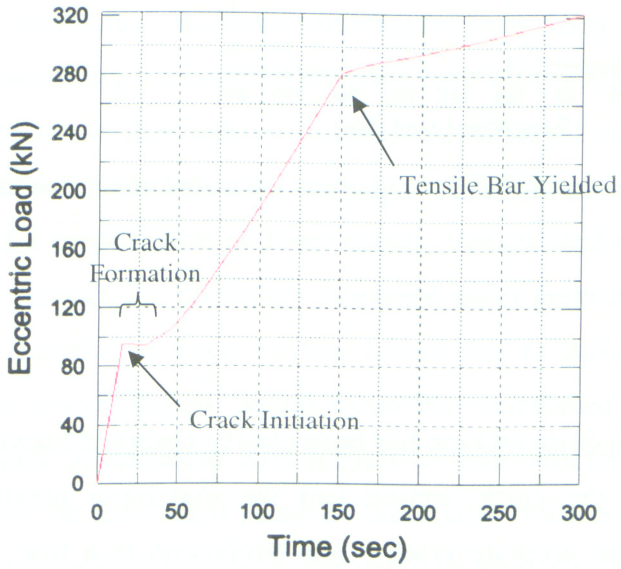

Figure 4.55 Tensile load history

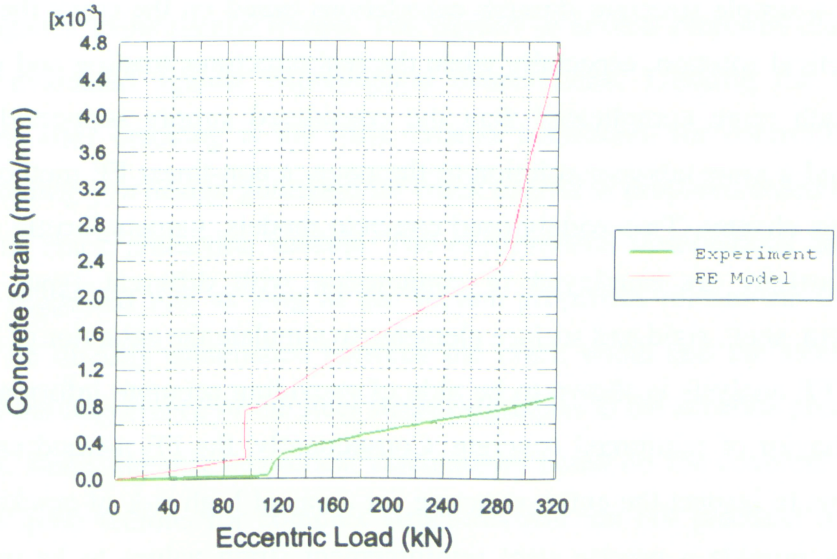

Figure 4.56 Strain versus tensile load comparison for a typical concrete element at tensile fiber of the section

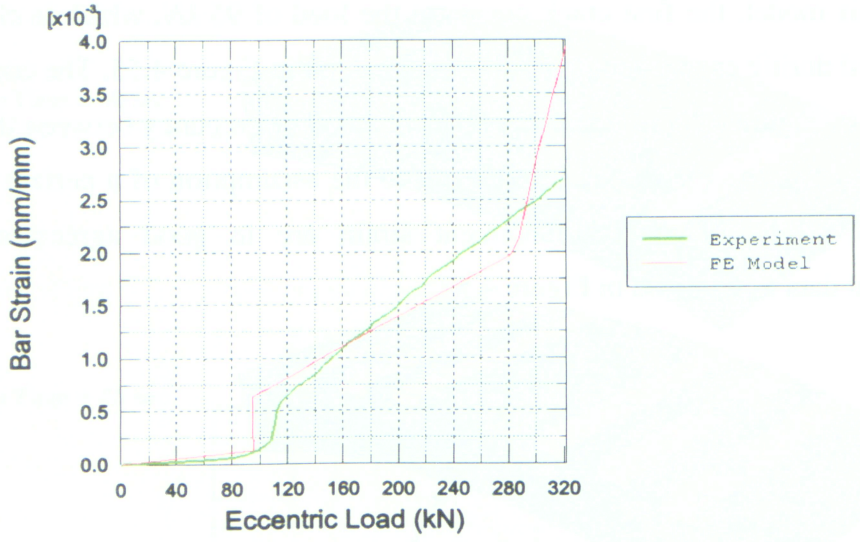

Figure 4.57 Strain versus tensile load comparison for a typical rebar element at top layer

4.5 Summary

In the previous chapter, a close relation has been clearly observed between the maximum reinforcement strain at the crack section and the maximum possible crack width. Therefore, essential to an accurate crack width prediction is a true estimation of the maximum steel strain after cracking. Although steel maximum strain values have been achieved for a simple structure through calculations based on the crack theory, this can not be a practical solution, especially when the real structures loading and geometry are normally much more complicated than the considered simply supported slab. In an attempt to find a more advance solution to the issue, a non-linear FE method of analysis is used in this chapter. Two widely-used concrete models, namely, brittle cracking and damaged plasticity are employed in conjunction with different types of elements including solid, shell, rigid and surface elements to simulate the behavior of RC structure. Finally, the FE analysis is shown to be able of providing accurate information on post-cracking behavior of reinforced concrete. Consequently, the FE method can effectively help designers to inspect the entire structure for areas of high risk of cracking problems, and also can provide a precise steel reinforcement strain values to be used for crack control.

CHAPTER 5

CONCLUSIONS

5.1 Summary

A study on the cracking behavior of reinforced concrete under monotonic increasing load is carried out. The main purpose of this study is to control cracking in reinforced concrete liquid containing structures. With this intention, various stress combinations are induced in specimens representing a reinforced concrete tank wall or slab. The cracking behavior and strain variations are thoroughly examined and reported in this thesis. The loading configurations include direct tensile load, two different combinations of tensile and flexural load, and a combination of direct tensile, flexural and shear load. In all of these cases the leakage through the cracks are examined under pressurized water. Additionally, the self-healing potential of direct tension cracks due to leakage is examined under a steady tensile load over a 30-hour period. Glass fiber reinforced polymers (FRP) are used as a means of crack remediation with respect to both structural strength recovery and leakage control. In the theoretical phase of this study, crack analyses are performed for the considered specimens from which the stress in steel reinforcement is obtained and used in crack prediction models. The accuracy of calculations is thoroughly verified by comparing against experimental results. The validity of several proposed crack prediction models are evaluated against experimental observations. Limiting the stress in the reinforcement after cracking is the main criteria considered for controlling the crack widths. Accordingly, a design guideline for crack control is proposed based on the results of the best fit crack prediction models. The experimental observations and theoretical calculations suggested that as long as the section properties remain the same, a direct relation can be directly established between the crack width and the steel strain. This would reveal the importance of the steel strain estimation in the accurate prediction of the crack widths. Realizing that theoretical calculations based on the concrete crack theory may become quite tedious for complex structures and are not practical unless several simplifications can be made, specific attention is given to the non-linear finite element (FE) analysis of the reinforced concrete. Comprehensive attempts are made on simulating

the reinforced concrete specimens with the aid of ABAQUS/6.5 (FE computer program). Several FE models are defined to capture the post-cracking behavior of the reinforced concrete, which are shown to be capable of providing quite accurate results for the strain in the steel reinforcement.

5.2 Conclusions

The main purpose of this study is to investigate the load induced cracking behavior of reinforced concrete. Specific attention is given to the extent of cracking problem in liquid containing structures. However, the results of this research study would be useful in similar applications as well. A number of experimental tests are conducted on a one-way reinforced concrete slab which represents a one-meter wide element of a tank wall. The following is the summary of several conclusions reached in the experimental investigation.

- Direct tensile cracks are full depth cracks that can raise water leakage problem even when their width is as low as 0.04 *mm*, and hence, their possible formation in liquid containing structures must be avoided.
- Tensile cracks as wide as 0.25 *mm* can partially heal themselves through autogenous healing process, considering that the crack width is kept constant under a steady tensile load and that there can be a positive water flow through cracks at all times.
- The application of one layer of glass FRP on the concrete cracked surface effectively prevents water leakage through the concrete slab under at least 5 m head of water pressure. In this case, even the yielding of reinforcing bars does not affect leakage.
- The presence of glass FRP has no significant influence on reducing the width of existing cracks at lower loading levels prior to the yielding of reinforcement.
- The FRP can effectively be used to recover the strength of severely damaged members in a structure.

- Flexural cracks are not of concern with regard to leakage, as the liquid can not pass through this type of crack due to the compression field presents in the section. Therefore, a slightest amount of flexural stress that can produce compression zone across the section can prevent leakage through the crack.
- The crack width is very dependant on the stress in the reinforcement. Provided that section properties are kept the same, the stress in the reinforcement is the most important parameter that has a close relation to the crack width.

In the theoretical part of this study, the initial cracking load and the steel strain relation to the applied load is successfully calculated. These findings are utilized in several well-known crack prediction models to estimate the crack width and the results are compared with the experimental observations. Subsequently, several comments are made on the precision of these models which are summarized as follows.

- The model proposed by Frosch gives reasonably accurate results for the maximum flexural crack width. The predicted crack widths will be somewhat higher than the actual crack widths if the maximum steel strain at crack is used instead of the mean steel strain. An overestimation in this scale is desirable for application of the model as a basis for design codes.
- In spite of its simplicity, Gergely and Lutz model gives a close upper bound estimation of maximum flexural crack widths.
- The model proposed by Gilbert yields crack widths somewhat lower than the actual flexural crack widths. This may be due to the assumption of slightly higher bond stress in his model. In general, the model provides a good crack width estimation, and with a little simplification it can be practically used for design purposes.
- The Eurocode EC2 approach for evaluating the design flexural crack width does not yield accurate results as compared to experiments. Since the estimated crack spacing by this code is within a good range, the problem may be due to the inappropriate formulation of the mean strain in the reinforcement .

- The CEB-FIP method overestimates the maximum observed flexural crack widths. This indicates that a very conservative approach is used in this code.
- The accuracy of flexural crack prediction models is reduced when the section stresses deviate from purely flexural to other types or combinations of stresses.
- A modified version of Gilbert model can be successfully used for estimating direct tensile cracks. In spite of ignoring concrete strain between cracks the model is reasonably accurate, meaning that, the tension stiffening is not a very significant phenomenon in case of pure tension cracks.
- Broms and Lutz model slightly underestimates the direct tensile crack width partly due to the use of small crack spacing. However, in case that all cracks are fully established and that the minimum crack spacing is achieved, a better estimation can be expected from this model.
- Authentic crack prediction models can be suitably used as the basis for crack control in a design guide.

Additionally, finite element models are shown to be able to predict concrete post-cracking behavior. Brittle cracking and damaged plasticity models available in ABAQUS /6.5 can efficiently simulate the highly non-linear properties of concrete. Reasonably accurate crack initiation loads and steel stress/strain relations are obtained from these FE models. However, the concrete strain values after cracking are overestimated, which is due to a perfect bond condition assumed for the interaction of the steel and the surrounding concrete.

5.3 Suggestions for Further Research

Although an extensive research is performed in this study on the cracking behavior of reinforced concrete in liquid containing structures, the subject is very broad and there are many areas that still need to be investigated. The following are some suggestions for future study based on the outcome of the current research study.

- All specimens that are tested in this study have the same section dimensions and the reinforcement ratio. The effect of other parameters such as bar spacing, bar size, concrete cover, reinforcement ratio, etc. can be investigated by testing specimens with various section geometries and reinforcement layouts.
- From all different types of cracks, only external load induced cracks are investigated in this study. The behavior of other types of cracks such as shrinkage or temperature cracks and their influence on the water tightness of the member can be inspected.
- The crack widths are mostly measured under short-term loading condition during the experiments. The experimental data can be expanded by including long-term loading effects in the experimental tests.
- The self-healing capacity of the concrete is examined for a certain crack width of 0.25 *mm*. This phenomenon can be inspected again to see the extent of healing for various crack widths.
- To certify the application of glass FRP in liquid containing tanks, the possible reaction of glass FRP with various liquids can be a subject of investigation.
- In all FE models, a perfect bond condition is assumed between the reinforcement and the surrounding concrete. The overall response of the reinforced concrete slab and the crack pattern can be improved by including the bond slip effect into these models.
- A finite element model can be developed to consider the effect of the glass FRP on the cracking behavior of a retrofitted member. For instance, the model for FRP retrofitted direct tension test can be built by adding extra elements simulating the behavior of a layer of glass FRP on top of the same concrete elements used for modeling the direct tension specimen.

REFERENCES

ACI Committee 207, 1995, "Effect of Restraint, Volume Change, and Reinforcement on Cracking of Mass Concrete", (ACI 207.2R-95), American Concrete Institute, Farmington Hills, Mich.

ACI Committee 209, 1992, "Prediction of Creep, Shrinkage and Temperature Effects in Concrete Structures", (ACI 209R-92), American Concrete Institute, Farmington Hills, Mich.

ACI Committee 224, 2001, "Control of Cracking in Concrete Structures", (ACI 224R-01), American Concrete Institute, Farmington Hills, Mich.

ACI Committee 224, 2007, "Causes, Evaluation, and Repair of Cracks in Concrete Structures", (ACI 224.1R-07), American Concrete Institute, Farmington Hills, Mich.

ACI Committee 224, 1992, "Cracking of Concrete Members in Direct Tension", (ACI 224.2R-92), American Concrete Institute, Farmington Hills, Mich.

ACI Committee 318, 2002, "Building Code Requirements for Structural Concrete (ACI 318-02) and Commentary (ACI 318R-02)", American Concrete Institute, Farmington Hills, Mich.

ACI Committee 350, 2006, "Code Requirements for Environmental Engineering Concrete Structures and Commentary", American Concrete Institute, Farmington Hills, Mich.

Aldea, C., Shah, S.P., and Karr, A., 1999, "Permeability of Cracked Concrete", Materials and Structures, Paris, Vol. 32, No. 219, pp. 370–376.

Aldea, C., Song, W., Popovics, J.S., and Shah, S.P., 2000, "Extent of Healing of Cracked Normal Strength Concrete", Journal of Materials in Civil Engineering, Vol. 12, No.1, pp. 92-96.

Barzegar, F., and Schnobrich, W.C., 1986, "Nonlinear Finite Element Analysis of Reinforced Concrete under Short Term Monotonic Loading", Civil Engineering Studies SRS No. 530, Univ. of Illinois at Urbana, Illinois.

Bazant, Z.P., and Oh, B.H., 1983, "Spacing of Cracks in Reinforced Concrete", Journal of the Structural Engineering, American Society of Civil Engineers, Vol. 109, No. 9, pp 2066-2085.

Becker, J.M., and Bresler, B., 1974, "FIRES-RC-A Computer Program for the Fire Response of Structures-Reinforced Concrete Frames", Report No. UCB/FRG 74-3, Department of Civil Engineering, University of California, Berkeley.

Beeby, A.W., 1970, "An Investigation of Cracking in Slabs Spanning One Way", Cement and Concrete Association, Technical Report 42.433, London.

Beeby, A.W., 1971, "Prediction and Control of Flexural Cracking in Reinforced concrete Members", Cracking, Deflection and Ultimate Load of Concrete Slab Systems, SP-20, American Concrete Institute, Farmington Hills, Mich., pp. 55-75.

Beeby, A.W., 1971, "An Investigation of Cracking on the Side Faces of Beams", Cement and Concrete Association, Technical Report 42.466, London.

Beeby, A.W., 1979, "The prediction of Crack Widths in Hardened Concrete", The Structural Engineer, Vol. 57A, No. 1, pp. 9-17.

Bresler, B., and Bertero, V.V., 1968, "Behavior of Reinforced Concrete Under Repeated Load", Journal of the Structural Division, ASCE, Vol. 94, No. ST6, pp. 1567-1590.

British Standard Institute, 1997, "Structural Use of Concrete: Code of Practice for Design and Construction", BS 8110: Part 1, British Standard Institute.

Broms, B.B., 1965, "Crack Width and Crack Spacing in Reinforced Concrete Members", ACI Journal, Proceedings, Vol. 62, No. 10, pp. 1237-1255.

Broms, B.B., 1965, "Stress Distribution in Reinforced Concrete Members with Tension Cracks", ACI Journal, Proceedings, Vol. 62, No. 9, pp. 1095-1108.

Broms, B.B., 1965, "Technique for Investigation of Internal Cracks in Reinforced Concrete Members", ACI Journal, Proceedings, Vol. 62, No. 1, Jan. 1965, pp. 35-44.

Broms, B.B., and Lutz, L.A., 1965, "Effects of Arrangement of Reinforcement on Crack Width and Spacing of Reinforced Concrete Members", ACI Journal, Proceedings, Vol. 62, No. 11, pp. 1395-1410.

CEB-FIP Model Code, 1990, "Model Code for Concrete Structures", Comite Euro-International due Beton/Federation Internationale de la Precontrainte, Paris 1990.

Cervenka, V., 1970, "Inelastic Finite Element Analysis of Reinforced Concrete Panels", Ph.D. Dissertation, University of Colorado, Boulder.

Chi, M. and Kirstein, A.F., 1958, "Flexural Cracks in Reinforced Concrete Beams", ACI Journal, Proceedings, Vol. 54, No. 10, pp. 865-878

Chowdhury, S.H., and Loo, Y.C., 2001, "A New Formula for Prediction of Crack Widths in Reinforced and Partially Prestressed Concrete Beams", Advances in Structural Engineering, Vol. 4, No. 2, pp. 101-109.

Clark, A.P. 1956, "Cracking in Reinforced Concrete Flexural Members", ACI Journal, Proceedings, Vol. 52, No. 8, pp. 851-862.

Clear, C. A., 1985, ''The Effects of Autogenous Healing upon the Leakage of Water Through Cracks in Concrete'', Technical Report 559, Cement and Concrete Association, London.

Cope, R.J., Rao, P.V., Clark, L.A., and Norris, R., 1980, "Modeling of Reinforced Concrete Behavior for Finite Element Analysis of Bridge Slabs", Numerical Methods for Nonlinear Problems , C. Taylor, E. Hinton and D.R.J. Oden, eds., Pineridge Press, Swansea, pp. 457-470.

Dotroppe, J.C., Schnobrich, W.C., and Pecknold, D.A., 1973, "Layered Finite Element Procedure for Inelastic Analysis of Reinforced Concrete Slabs", IABSE Publication, Vol. 33-11.

Edvardsen, C., 1999, "Water Permeability and Autogenous Healing of Cracks in Concrete", ACI Materials Journal, Vol. 96, No. 4, pp. 448-454.

Eurocode 2, 1997, "Design of Concrete Structures - Part 1: General Rules and Rules for Buildings", Paris.

Franklin, H.A., 1970, "Non-Linear Analysis of Reinforced Concrete Frames and Panels", Ph.D. Dissertation, Division of Structural Engineering and Structural Mechanics, University of California, Berkeley, SEMM 70-5.

Frosch, R.J., 1999, "Another Look at Cracking and Crack Control in Reinforced Concrete", ACI Structural Journal, Vol. 96, No. 3, pp. 437–442.

Frosch, R.J., 2001, "Flexural Crack Control in Reinforced Concrete," Design and Construction Practices to Mitigate Cracking, SP-204, American Concrete Institute, Farmington Hills, Mich., pp. 135-154.

Gergely, P., and Lutz, L. A., 1968, "Maximum Crack Width in Reinforced Concrete Flexural Members", Causes, Mechanism, and Control of Cracking in Concrete, SP-20, American Concrete Institute, Farmington Hills, Mich., pp. 87–117.

Gilbert, R.I., and Warner, R.F., 1978, "Tension Stiffening in Reinforced Concrete Slabs", Journal of Structural Division, ASCE, Vol. 104, No. ST12, pp. 1885-1900.

Gilbert, R.I., 2005, "Time-Dependent Cracking and Crack Control in Reinforced Concrete Structures", Serviceability of Concrete, SP-225, American Concrete Institute, Farmington Hills, Mich., pp. 223–240.

Gilbert, R.I., 2006, "Design for Flexural Crack Control - Recent Amendments to the Australian Standard AS3600", 1st International Structural Specialty Conference, Canadian Society of Civil Engineers, Calgary, Canada.

Granger, S., Loukili, A, Pijaudier-Cabot, G., and Chanvillard, G., 2006, "Experimental Characterization of the Self Healing of Cracks in an Ultra High Performance Cementitious Material: Mechanical Tests and Acoustic Emission Analysis", Cement and Concrete Research, doi: 10.1016/j.cemconres.2006.12.005

de Groot, A.K., Kusters, G.M.A., and Monnier, T., 1981, "Numerical Modeling of Bond-Slip Behavior", Heron, Concrete Mechanics, Vol. 26, No. 1B.

Hearn, N., and Morley, C.T., 1997, "Self-Sealing Property of Concrete – Experimental Evidence", Materials and Structures, Vol. 30, pp. 404-411.

Hearn, N, 1998, "Self–Sealing, Autogenous Healing and Continued Hydration: What is the Difference?", Materials and Structures, Vol. 31, pp. 563-567

Hibbitt, H.D., Karlson, B.I., and Sorenson, E.P., 2004, "ABAQUS version 6.5, Finite Element Program", Hibbit, Karlson & Sorenson, Inc, Providence, R.I.

Hillerborg, A., Modeer, M. and Petersson, P.E., 1976, "Analysis of Crack Formation and Growth in Concrete by Means of Fracture Mechanics and Finite Element", Cement and Concrete Research, Vol. 6, No. 6, pp. 773-782.

Jacobsen, S., Marchand, J., and Hornain, H., 1995, "SEM Observations of the Microstructure of Frost Deteriorated and Self Healed Concrete", Cement and Concrete Research, Vol. 25, No. 8, pp. 55-62.

Jacobsen, S., and Sellevold, E., 1996, "Self Healing of High Strength Concrete after Deterioration by Freeze/Thaw", Cement and Concrete Research, Vol. 26, No. 1, pp. 55-62.

Jofriet, J.C., and McNeice, G.M., 1971, "Finite Element Analysis of RC Slabs", Journal of Structural Division, ASCE, Vol. 97, No. ST3, pp. 785-806.

Kaar, P.H., and Mattock, A.H., 1963, "High Strength Bars as Concrete Reinforcement-Part 4: Control of Cracking", Journal of Portland Cement Association Research and Development Laboratories, Vol. 7, No. 1, pp. 42-53.

Keuser, M., and Mehlhorn, G., 1987, "Finite Element Models for Bond Problems", Journal of Structural Engineering, ASCE, Vol. 113, No. 10, pp. 2160-2173.

Kwak, H.G., and Filippou, F.C., 1990, " Finite Element Analysis of Reinforced Concrete Structures Under Monotonic Loads", Report 90-14, Department of Civil Engineering, University of California, Berkeley, Calif., Nov. 1990.

Lan, Z., and Ding, D., 1992, "Crack Width in Reinforced Concrete Members", International Journal of Structures, Vol. 12, No. 2, pp. 137-163

Lin, C.S., and Scordelis, A.C., 1975, "Nonlinear Analysis of RC Shells of General Form", Journal of Structural Division, ASCE, Vol. 101, No. ST3, pp. 523-538.

MacGregor, J.G., Bartlett, F.M., "Reinforced Concrete Mechanics and Design", First Canadian Edition, Prentice Hall Canada Inc., Scarborough, Ontario, 2000.

Marti, P., Alvarez, M., Kaufmann, W., and Sigrist, V., 1998, "Tension Chord Model for Structural Concrete", Structural Engineering International, 4/98, pp. 287-298.

Munday, J.C.L., Sangha, C.M., and Dhir, R.K., 1974, "Comparative Study of Autogeneous Healing of Different Concretes", Proc., 1st Australian Conf. on Engrg. Mat., Sydney, pp. 177–189.

Nayak, G.C., and Zienkiewicz, O.C., 1972, "Elasto-Plastic Stress Analysis", International Journal of Numerical Methods in Engineering, Vol. 5, pp. 113-135.
Neville, A., 2002, "Autogenous Healing – A concrete miracle?", Concrete International, Vol. 24, No. 11, pp. 76-82.

Ngo, D., and Scordelis, A.C., 1967, "Finite Element Analysis of Reinforced Concrete Beams", ACI Journal, Vol. 64, No. 3, pp. 152-163.

Nilson, A.H., 1972, "Internal Measurement of Bond Slip", ACI Journal, Vol. 69, No. 7, pp. 439-441.

Park, R., and Paulay, T., 1975, "Reinforced Concrete Structures", John Wiley & Sons, Inc., New York.

Pimienta, P., and Chanvillard, G., 2004, "Retention of the Mechanical Performances of Ductal® Specimens Kept in Various Aggressive Environments", Fib - Symposium 2004, April 26-28, Avignon, France

Piyasena, R., 2002, "Crack Spacing, Crack Width and Tension Stiffening Effect in Reinforced Concrete Beams and One-Way Slabs", Ph.D. Dissertation, Faculty of Engineering and Information Technology, Griffith University, Australia, Nov. 2002.

Rajagopal, K.R., 1976, "Nonlinear Analysis of Reinforced Concrete Beams, Beam-Columns and Slabs by Finite Elements", Ph.D. Dissertation, Iowa State University.

Rashid, Y.R., 1968, "Analysis of Prestressed Concrete Pressure Vessels", Nuclear Engineering and Design, Vol. 7, No. 4, pp. 334-344.

Reinhardt, H.W., and Joos, M., 2003, "Permeability and Self-healing of Cracked Concrete as a Function of Temperature and Crack Width", Cement and Concrete Research, Vol. 33, No. 7, pp. 981-985.

R.J. Watson, Inc., Bridge & Structural Engineering Systems, 78 John Glenn Drive, Amherst, NY 14228, www.rjwatson.com

Scanlon, A., and Murray, D.W., 1974, "Time Dependent Reinforced Concrete Slab Deflections", Journal of the Structural Division, ASCE, Vol. 100, No. ST9, pp. 1911-1924.

Scordelis, A.C., Ngo, D., and Franklin, H.A., 1974, "Finite Element Study of Reinforced Concrete Beams with Diagonal Tension Cracks", Proceedings of Symposium on Shear in Reinforced Concrete, ACI Publication SP-42.

Selna, L.G., 1969, "Creep, Cracking and Shrinkage in Concrete Frame Structures", Journal of the Structural Division, ASCE, Vol. 95, No. ST12, pp. 2743-2761.

Suidan, M.T., and Schnobrich, W.C., 1973, "Finite Element Analysis of Reinforced Concrete", Journal of the Structural Division, ASCE, Vol. 99, No. ST10, pp. 2109-2122.

Ter Heide, N, 2005, "Crack Healing in Hydrating Concrete", M.Sc. Thesis, Delft University of Technology, May 2005.

Transportation Research Circular E-C107, 2006, "Control of Cracking in Concrete: State of the Art", Washington, DC, Oct. 2006.

Vecchio, F., and Collins, M.P., 1982, "The Response of Reinforced Concrete to In-Plane Shear and Normal Stress", Publication No. 82-03, Department of Civil Engineering, University of Toronto, Toronto, Canada.

Venkateswarlu, B., and Gesund, H., 1972, "Cracking and Bond Slip in Concrete Beams", Journal of the Structural Division, Proceedings, American Society of Civil Engineers, Vol. 98, No. ST11, pp. 2663-2885.

Watsein, D., and Parsons, D.E., 1943, "Width and Spacing of Tensile Cracks in Axially Reinforced Concrete Cylinders", Journal of Research, National Bureau of Standards, Vol. 31, No. RP1545, pp. 1-24.

Welch, G.B. and Haisman, B., 1969, "Fracture Toughness Measurements of Concrete", Report No. R42, University of New South Wales, Sydney, Australia.

APPENDIX A

A.1 Direct Tension Model with Solid Elements Input File

```
*Heading
** Job name: Direct-Tension-Solid Model name: Model-1
*Preprint, echo=NO, model=NO, history=NO, contact=NO
**
** PARTS
**
*Part, name=b-rebar
*Node
     1,       -925.,        500.,          0.
     2,       -925.,        400.,          0.
     .
          .
          .
   220,        925.,       -500.,          0.
*Element, type=SFM3D4R
 1,  1,  2, 13, 12
 2,  2,  3, 14, 13
 .
 .
 .
190, 208, 209, 220, 219
*Nset, nset=_PickedSet2, internal, generate
  1, 220,   1
*Elset, elset=_PickedSet2, internal, generate
  1, 190,   1
** Region: (rebar:Picked), (Controls:Default)
*Elset, elset=_PickedSet2, internal, generate
  1, 190,   1
** Section: rebar
*Surface Section, elset=_PickedSet2
*Rebar Layer
reinforcement, 300., 250., , steel, 0., 1
stirrups, 200., 462.5, , steel, 90., 1
*End Part
**
*Part, name=slab
*Node
     1,         925.,       -500.,         250.
     2,   827.631592,       -500.,         250.
     .
          .
```

```
        .
  1100,      -925.,       500.,         0.
*Element, type=C3D8R
 1, 101, 102, 122, 121,   1,   2,  22,  21
 2, 102, 103, 123, 122,   2,   3,  23,  22
 .
 .
 .
760, 1079, 1080, 1100, 1099,  979,  980, 1000,  999
*Nset, nset=_PickedSet2, internal, generate
   1, 1100,    1
*Elset, elset=_PickedSet2, internal, generate
  1, 760,   1
** Region: (slab:Picked), (Controls:EC-1)
*Elset, elset=_PickedSet2, internal, generate
  1, 760,   1
** Section: slab
*Solid Section, elset=_PickedSet2, controls=EC-1, material=concrete
1.,
*End Part
**
*Part, name=t-rebar
*Node
     1,       -925.,       500.,         0.
     2,       -925.,       400.,         0.
     .
          .
          .
   220,        925.,       -500.,         0.
*Element, type=SFM3D4R
 1,  1,  2, 13, 12
 2,  2,  3, 14, 13
 .
 .
 .
190, 208, 209, 220, 219
*Nset, nset=_PickedSet2, internal, generate
  1, 220,   1
*Elset, elset=_PickedSet2, internal, generate
  1, 190,   1
** Region: (rebar:Picked), (Controls:Default)
*Elset, elset=_PickedSet2, internal, generate
  1, 190,   1
** Section: rebar
*Surface Section, elset=_PickedSet2
*Rebar Layer
```

```
reinforcement, 300., 250., , steel, 0., 1
stirrups, 200., 462.5, , steel, 90., 1
*End Part
**
**
** ASSEMBLY
**
*Assembly, name=Assembly
**
*Instance, name=slab-2, part=slab
      0.,       0.,      -125.
*End Instance
**
*Instance, name=b-rebar-1, part=b-rebar
      0.,       0.,       65.
*End Instance
**
*Instance, name=t-rebar-1, part=t-rebar
      0.,       0.,      -65.
*End Instance
**
*Nset, nset=_PickedSet26, internal, instance=b-rebar-1, generate
  1,  220,   1
*Nset, nset=_PickedSet26, internal, instance=t-rebar-1, generate
  1,  220,   1
*Elset, elset=_PickedSet26, internal, instance=b-rebar-1, generate
  1,  190,   1
*Elset, elset=_PickedSet26, internal, instance=t-rebar-1, generate
  1,  190,   1
*Nset, nset=_PickedSet27, internal, instance=slab-2, generate
   1, 1100,    1
*Elset, elset=_PickedSet27, internal, instance=slab-2, generate
  1,  760,   1
*Nset, nset=_PickedSet101, internal, instance=slab-2, generate
  20,  1100,   20
*Nset, nset=_PickedSet101, internal, instance=b-rebar-1, generate
 1,  11,   1
*Nset, nset=_PickedSet101, internal, instance=t-rebar-1, generate
 1,  11,   1
*Elset, elset=_PickedSet101, internal, instance=slab-2, generate
 19,  760,   19
*Elset, elset=_PickedSet101, internal, instance=b-rebar-1, generate
1, 10,  1
*Elset, elset=_PickedSet101, internal, instance=t-rebar-1, generate
1, 10,  1
*Nset, nset=_PickedSet102, internal, instance=slab-2, generate
```

```
 20, 1020,  100
*Elset, elset=_PickedSet102, internal, instance=slab-2, generate
 19, 703,  76
*Nset, nset=_PickedSet103, internal, instance=slab-2, generate
20, 100, 20
*Nset, nset=_PickedSet103, internal, instance=b-rebar-1
11,
*Nset, nset=_PickedSet103, internal, instance=t-rebar-1
11,
*Elset, elset=_PickedSet103, internal, instance=slab-2, generate
19, 76, 19
*Nset, nset=_PickedSet105, internal, instance=slab-2, generate
  1, 1001,  100
*Elset, elset=_PickedSet105, internal, instance=slab-2, generate
 1, 685,  76
*Nset, nset=_PickedSet106, internal, instance=slab-2, generate
 1, 81, 20
*Nset, nset=_PickedSet106, internal, instance=b-rebar-1
220,
*Nset, nset=_PickedSet106, internal, instance=t-rebar-1
220,
*Elset, elset=_PickedSet106, internal, instance=slab-2, generate
 1, 58, 19
*Nset, nset=_PickedSet107, internal, instance=slab-2, generate
  1, 1081,  20
*Nset, nset=_PickedSet107, internal, instance=b-rebar-1, generate
210, 220,  1
*Nset, nset=_PickedSet107, internal, instance=t-rebar-1, generate
210, 220,  1
*Elset, elset=_PickedSet107, internal, instance=slab-2, generate
 1, 742,  19
*Elset, elset=_PickedSet107, internal, instance=b-rebar-1, generate
181, 190,  1
*Elset, elset=_PickedSet107, internal, instance=t-rebar-1, generate
181, 190,  1
** Constraint: Constraint-1
*Embedded Element, host elset=_PickedSet27
_PickedSet26
*End Assembly
**
** ELEMENT CONTROLS
**
*Section Controls, name=EC-1, hourglass=ENHANCED
1., 1., 1.
*Amplitude, name=Amp-1
0., 0., 30., 1.
```

```
*Amplitude, name=Amp-2, definition=SMOOTH STEP
0., 0., 1., 0.002, 100., 0.004, 200., 0.008, 300., 0.01
**
** MATERIALS
**
*Material, name=concrete
*Density
 2.4e-09,
*Elastic
28851., 0.18
*Brittle Cracking, type=GFI
2.01,    .09
*Brittle Shear
 1,    0.
  0., 0.001
*Material, name=steel
*Density
 7.8e-09,
*Elastic
200000., 0.3
*Plastic
 400.8,    0.
  402.,  0.003
 629.3, 0.0456
**
** BOUNDARY CONDITIONS
**
** Name: BC-1 Type: Displacement/Rotation
*Boundary
_PickedSet101, 1, 1
** Name: BC-2 Type: Displacement/Rotation
*Boundary
_PickedSet102, 3, 3
** Name: BC-3 Type: Displacement/Rotation
*Boundary
_PickedSet103, 2, 2
** Name: BC-5 Type: Displacement/Rotation
*Boundary
_PickedSet105, 3, 3
** Name: BC-6 Type: Displacement/Rotation
*Boundary
_PickedSet106, 2, 2
** ----------------------------------------------------------------
**
** STEP: Step-1
**
```

```
*Step, name=Step-1
loading
*Dynamic, Explicit
, 300.
*Bulk Viscosity
0.06, 1.2
** Mass Scaling: Semi-Automatic
**               Whole Model
*Fixed Mass Scaling, factor=100.
**
** BOUNDARY CONDITIONS
**
** Name: BC-7 Type: Velocity/Angular velocity
*Boundary, amplitude=Amp-2, type=VELOCITY
_PickedSet107, 1, 1, 5
**
** OUTPUT REQUESTS
**
*Restart, write, number interval=1, time marks=NO
**
** FIELD OUTPUT: F-Output-1
**
*Output, field
*Node Output
A, RF, U, V
*Element Output, directions=YES
E, LE, NE, PE, PEEQ, PEEQT, PS, S, VE, VEEQ, VS
*Element Output, rebar, directions=YES
E, LE, NE, PE, PEEQ, PEEQT, PS, S, VE, VEEQ, VS
*Contact Output
CSTRESS,
**
** HISTORY OUTPUT: H-Output-1
**
*Output, history, variable=PRESELECT
*End Step
```

Mass scaling is used to reduce the overall analysis time by virtually increasing the mass of structure.

A.2 Direct Tension Model with Shell Elements Input File

```
*Heading
** Job name: Direct Tension Shell Model name: Model-1
*Preprint, echo=NO, model=NO, history=NO, contact=NO
**
** PARTS
**
*Part, name=Slab
*Node
     1,       -925.,        500.,          0.
     2,       -925.,        400.,          0.
     .
          .
          .
   220,         925.,       -500.,          0.
*Element, type=S4R
  1,   1,   2,  13,  12
  2,   2,   3,  14,  13
  .
  .
  .
190, 208, 209, 220, 219
*Nset, nset=_PickedSet2, internal, generate
  1,  220,    1
*Elset, elset=_PickedSet2, internal, generate
  1,  190,    1
** Region: (slab sec:Picked), (Controls:EC-1)
*Elset, elset=_PickedSet2, internal, generate
  1,  190,    1
** Section: slab sec
*Shell Section, elset=_PickedSet2, controls=EC-1, material=concrete
250., 7
*Rebar Layer
"top long", 300., 250., 65., Steel, 0., 1
"bottom long", 300., 250., -65., Steel, 0., 1
"top stirrup", 200., 462.5, 65., Steel, 90., 1
"bottom stirrup", 200., 462.5, -65., Steel, 90., 1
*End Part
**
**
** ASSEMBLY
**
*Assembly, name=Assembly
**
*Instance, name=Slab-1, part=Slab
```

```
*End Instance
**
*Nset, nset=_PickedSet4, internal, instance=Slab-1, generate
 1,  11,  1
*Elset, elset=_PickedSet4, internal, instance=Slab-1, generate
 1, 10,  1
*Nset, nset=_PickedSet5, internal, instance=Slab-1
 11,
*Nset, nset=_PickedSet6, internal, instance=Slab-1, generate
 210,  220,  1
*Elset, elset=_PickedSet6, internal, instance=Slab-1, generate
 181,  190,  1
*Nset, nset=_PickedSet7, internal, instance=Slab-1
 220,
*Nset, nset=_PickedSet8, internal, instance=Slab-1, generate
 210,  220,  1
*Elset, elset=_PickedSet8, internal, instance=Slab-1, generate
 181,  190,  1
*End Assembly
**
** ELEMENT CONTROLS
**
*Section Controls, name=EC-1, hourglass=ENHANCED
1., 1., 1.
*Amplitude, name=Amp-1, definition=SMOOTH STEP
0., 0., 1., 0.001, 100., 0.002, 200., 0.004
300., 0.01
**
** MATERIALS
**
*Material, name=Steel
*Density
 7.8e-09,
*Elastic
200000., 0.3
*Plastic
 400.8,    0.
  402.,  0.003
 629.3, 0.0456
*Material, name=concrete
*Density
 2.4e-09,
*Elastic
28851., 0.18
*Brittle Cracking, type=GFI
2.01,    .05
```

```
*Brittle Shear
 1,    0.
  0., 0.001
**
** BOUNDARY CONDITIONS
**
** Name: BC-1 Type: Displacement/Rotation
*Boundary
_PickedSet4, 1, 1
_PickedSet4, 3, 3
** Name: BC-2 Type: Displacement/Rotation
*Boundary
_PickedSet5, 2, 2
** Name: BC-3 Type: Displacement/Rotation
*Boundary
_PickedSet6, 3, 3
** Name: BC-4 Type: Displacement/Rotation
*Boundary
_PickedSet7, 2, 2
** ----------------------------------------------------------------
**
** STEP: Step-1
**
*Step, name=Step-1
loading
*Dynamic, Explicit
, 300.
*Bulk Viscosity
0.06, 1.2
** Mass Scaling: Semi-Automatic
**            Whole Model
*Fixed Mass Scaling, factor=100.
**
** BOUNDARY CONDITIONS
**
** Name: BC-5 Type: Velocity/Angular velocity
*Boundary, amplitude=Amp-1, type=VELOCITY
_PickedSet8, 1, 1, 5.
**
** OUTPUT REQUESTS
**
*Restart, write, number interval=1, time marks=NO
**
** FIELD OUTPUT: F-Output-1
**
*Output, field
```

```
*Node Output
A, RF, RT, U, V
*Element Output, directions=YES
LE, NE, PE, PEEQ, PS, S, VE, VEEQ, VS
*Element Output, rebar, directions=YES
LE, NE, PE, PEEQ, PS, S, VE, VEEQ, VS
**
** HISTORY OUTPUT: H-Output-1
**
*Output, history, variable=PRESELECT
*End Step
```

A.3 Flexural Model Input File

```
*Heading
** Job name: Bend Model name: Model-1
*Preprint, echo=NO, model=NO, history=NO, contact=NO
**
** PARTS
**
*Part, name="Bottom Rebar"
*Node
     1,       -900.,        500.,          0.
     2,       -900.,        400.,          0.
          .
          .
          .
   209,        900.,       -500.,          0.
*Element, type=SFM3D4R
 1,  1,  2, 13, 12
 2,  2,  3, 14, 13
 .
 .
 .
180, 197, 198, 209, 208
*Nset, nset=_PickedSet2, internal, generate
  1, 209,   1
*Elset, elset=_PickedSet2, internal, generate
  1, 180,   1
** Region: (Rebar:Picked), (Controls:Default)
*Elset, elset=_PickedSet2, internal, generate
  1, 180,   1
** Section: Rebar
*Surface Section, elset=_PickedSet2
*Rebar Layer
Longitudinal, 300., 250., , Steel, 0., 1
Stirrups, 200., 462.5, , Steel, 90., 1
*End Part
**
*Part, name=Slab
*Node
     1,        900.,       -500.,        250.
     2,        800.,       -500.,        250.
     .
          .
          .
  1463,       -900.,        500.,          0.
*Element, type=C3D8R
```

```
  1,  134,  135,  154,  153,    1,    2,   21,   20
  2,  135,  136,  155,  154,    2,    3,   22,   21
  .
  .
  .
1080, 1443, 1444, 1463, 1462, 1310, 1311, 1330, 1329
*Nset, nset=_PickedSet2, internal, generate
   1,  1463,    1
*Elset, elset=_PickedSet2, internal, generate
   1,  1080,    1
** Region: (Slab:Picked), (Controls:EC-1)
*Elset, elset=_PickedSet2, internal, generate
   1,  1080,    1
** Section: Slab
*Solid Section, elset=_PickedSet2, controls=EC-1, material=Concrete
1.,
*End Part
**
*Part, name="Top Rebar"
*Node
     1,       -900.,        500.,          0.
     2,       -900.,        400.,          0.
     .
          .
          .
   209,        900.,       -500.,          0.
*Element, type=SFM3D4R
  1,  1,  2, 13, 12
  2,  2,  3, 14, 13
  .
  .
  .
180, 197, 198, 209, 208
*Nset, nset=_PickedSet2, internal, generate
  1,  209,    1
*Elset, elset=_PickedSet2, internal, generate
  1,  180,    1
** Region: (Rebar:Picked), (Controls:Default)
*Elset, elset=_PickedSet2, internal, generate
  1,  180,    1
** Section: Rebar
*Surface Section, elset=_PickedSet2
*Rebar Layer
Longitudinal, 300., 250., , Steel, 0., 1
Stirrups, 200., 462.5, , Steel, 90., 1
*End Part
```

```
**
*Part, name=rigid1
*Node
      1,       -900.,       -500.,        250.
      2,       -900.,       -400.,        250.
      .
           .
           .
     77,       -900.,        500.,          0.
*Element, type=R3D4
 1,  1,  2, 13, 12
 2,  2,  3, 14, 13
 .
 .
 .
60, 65, 66, 77, 76
*End Part
**
*Part, name=rigid2
*Node
      1,        900.,       -500.,        250.
      2,        900.,       -400.,        250.
      .
           .
           .
     77,        900.,        500.,          0.
*Element, type=R3D4
 1,  1,  2, 13, 12
 2,  2,  3, 14, 13
 .
 .
 .
60, 65, 66, 77, 76
*End Part
**
**
** ASSEMBLY
**
*Assembly, name=Assembly
**
*Instance, name=Slab-1, part=Slab
*End Instance
**
*Instance, name="Bottom Rebar-1", part="Bottom Rebar"
        0.,          0.,         50.
*End Instance
```

```
**
*Instance, name="Top Rebar-1", part="Top Rebar"
       0.,          0.,         200.
*End Instance
**
*Instance, name=rigid1-1, part=rigid1
*End Instance
**
*Instance, name=rigid2-1, part=rigid2
*End Instance
**
*Node
     1,        900.,          0.,        650.
*Node
     2,       -900.,          0.,        650.
*Nset, nset=_PickedSet12, internal, instance="Bottom Rebar-1", generate
  1,  209,    1
*Nset, nset=_PickedSet12, internal, instance="Top Rebar-1", generate
  1,  209,    1
*Elset, elset=_PickedSet12, internal, instance="Bottom Rebar-1", generate
  1,  180,    1
*Elset, elset=_PickedSet12, internal, instance="Top Rebar-1", generate
  1,  180,    1
*Nset, nset=_PickedSet13, internal, instance=Slab-1, generate
   1,  1463,     1
*Elset, elset=_PickedSet13, internal, instance=Slab-1, generate
   1,  1080,     1
*Nset, nset=_PickedSet18, internal
 2,
*Nset, nset=_PickedSet19, internal
 1,
*Nset, nset=_PickedSet20, internal
 1,
*Nset, nset=_PickedSet25, internal
 2,
*Nset, nset=_PickedSet26, internal, instance=rigid1-1, generate
  1,  77,   1
*Elset, elset=_PickedSet26, internal, instance=rigid1-1, generate
  1,  60,   1
*Nset, nset=_PickedSet27, internal
 1,
*Nset, nset=_PickedSet28, internal, instance=rigid2-1, generate
  1,  77,   1
*Elset, elset=_PickedSet28, internal, instance=rigid2-1, generate
  1,  60,   1
*Nset, nset=_PickedSet30, internal, instance=Slab-1, generate
```

375 mm for low eccentricity model

```
  19,  1463,   19
*Nset, nset=_PickedSet30, internal, instance="Bottom Rebar-1", generate
  1,  11,  1
*Nset, nset=_PickedSet30, internal, instance="Top Rebar-1", generate
  1,  11,  1
*Elset, elset=_PickedSet30, internal, instance=Slab-1, generate
  18,  1080,   18
*Elset, elset=_PickedSet30, internal, instance="Bottom Rebar-1", generate
 1, 10,  1
*Elset, elset=_PickedSet30, internal, instance="Top Rebar-1", generate
 1, 10,  1
*Nset, nset=_PickedSet32, internal, instance=Slab-1, generate
   1,  1445,   19
*Nset, nset=_PickedSet32, internal, instance="Bottom Rebar-1", generate
 199,  209,   1
*Nset, nset=_PickedSet32, internal, instance="Top Rebar-1", generate
 199,  209,   1
*Elset, elset=_PickedSet32, internal, instance=Slab-1, generate
   1,  1063,   18
*Elset, elset=_PickedSet32, internal, instance="Bottom Rebar-1", generate
 171,  180,   1
*Elset, elset=_PickedSet32, internal, instance="Top Rebar-1", generate
 171,  180,   1
*Elset, elset=__PickedSurf29_SNEG, internal, instance=rigid1-1, generate
  1,  60,  1
*Surface, type=ELEMENT, name=_PickedSurf29, internal
__PickedSurf29_SNEG, SNEG
*Elset, elset=__PickedSurf31_SPOS, internal, instance=rigid2-1, generate
  1,  60,  1
*Surface, type=ELEMENT, name=_PickedSurf31, internal
__PickedSurf31_SPOS, SPOS
*Surface, type=NODE, name=_PickedSet30_CNS_, internal
_PickedSet30, 1.
*Surface, type=NODE, name=_PickedSet32_CNS_, internal
_PickedSet32, 1.
** Constraint: Constraint-2
*Rigid Body, ref node=_PickedSet25, elset=_PickedSet26
** Constraint: Constraint-3
*Rigid Body, ref node=_PickedSet27, elset=_PickedSet28
** Constraint: Constraint-4
*Tie, name=Constraint-4, adjust=yes
_PickedSet30_CNS_, _PickedSurf29
** Constraint: Constraint-5
*Tie, name=Constraint-5, adjust=yes
_PickedSet32_CNS_, _PickedSurf31
** Constraint: embed
```

```
*Embedded Element, host elset=_PickedSet13
_PickedSet12
*End Assembly
**
** ELEMENT CONTROLS
**
*Section Controls, name=EC-1, hourglass=ENHANCED
1., 1., 1.
*Amplitude, name=Amp-1, definition=SMOOTH STEP
0., 0., 1., 1.
**
** MATERIALS
**
*Material, name=concrete
*Density
 2.4e-09,
*Elastic
23715., 0.18
*Brittle Cracking, type=GFI
1.65,    .02
*Brittle Shear
 1,    0.
  0., 0.001
*Material, name=Steel
*Density
 7.8e-09,
*Elastic
200000., 0.3
*Plastic
 400.8,    0.
  402.,  0.003
 629.3, 0.0456
**
** BOUNDARY CONDITIONS
**
** Name: BC-1 Type: Displacement/Rotation
*Boundary
_PickedSet19, 2, 2
_PickedSet19, 3, 3
** Name: BC-2 Type: Displacement/Rotation
*Boundary
_PickedSet18, 1, 1
_PickedSet18, 2, 2
_PickedSet18, 3, 3
** ----------------------------------------------------------------
**
```

For Damaged Plasticity Model

```
*Concrete Damaged Plasticity
34.,   0.1,  1.16, 0.666,    0.
*Concrete Compression Hardening
   15.,      0.
   25., 0.00114
 21.25,  0.0026
*Concrete Tension Stiffening, type=GFI
 1.65, 0.03
```

```
** STEP: Step-1
**
*Step, name=Step-1
loading
*Dynamic, Explicit
, 400.
*Bulk Viscosity
0.06, 1.2
** Mass Scaling: Semi-Automatic
**                Whole Model
*Fixed Mass Scaling, factor=100.
**
** BOUNDARY CONDITIONS
**
** Name: displc Type: Velocity/Angular velocity
*Boundary, amplitude=Amp-1, type=VELOCITY
_PickedSet20, 1, 1, 0.04
**
** OUTPUT REQUESTS
**
*Restart, write, number interval=1, time marks=NO
**
** FIELD OUTPUT: F-Output-1
**
*Output, field
*Node Output
A, RF, RM, RT, U, V
*Element Output, directions=YES
E, LE, NE, PE, PEEQ, PS, S, VE, VEEQ, VS
*Element Output, rebar, directions=YES
E, LE, NE, PE, PEEQ, PS, S, VE, VEEQ, VS
*Contact Output
CSTRESS,
**
** HISTORY OUTPUT: H-Output-1
**
*Output, history, variable=PRESELECT
*End Step
```